155

283 p.

# TELSTAR I, VOLUME 3

N64 11079* – N64 11089*

CODE-1

(NASA SP-32, Pt. 3)

VOLUME 3

JUNE 1963

283 p refa

Corp. author:
NATIONAL AERONAUTICS AND SPACE ADMINISTRATION.
GODDARD SPACE FLIGHT CENTER,
Greenbelt, Md.

Contents:
Part 3

## Contents, Part 3

# Components for the *Telstar* Project

By W. C. HITTINGER

(Manuscript received March 5, 1963)

*The Telstar project required a variety of components and structures of high reliability. The program for obtaining these components was essentially that originated for submarine cable devices, in which designs of proven integrity were manufactured under controlled conditions, screened and aged to remove defectives, and then life tested and certified using techniques for selecting the most stable components. This program summary illustrates in principle the techniques described in detail in the body of this components section of the issue.*

## I. INTRODUCTION

The papers comprising Part 3 of this issue describe the design, performance, and reliability considerations of the major components utilized in the Telstar spacecraft and certain of the unique electronic components of the earth station. Those papers pertaining to components of the spacecraft were presented orally at Bell Telephone Laboratories, Murray Hill, New Jersey, on November 14, 1962, to representatives of the National Aeronautics and Space Administration, Department of Defense, and many electronics and space companies. Particular emphasis was placed on the reliability requirements of spacecraft components and the means taken to ensure satisfactory life of the communications satellite. This issue highlights reliability by describing those steps taken to design, fabricate, test, and certify components to ensure reasonable certainty of operation for the communications satellite experiment. Companion papers presenting descriptions of the Telstar system are contained elsewhere.[1]

This paper is devoted to a broad description of component reliability as related to the design of the system. Consideration is given to the means for obtaining highly reliable components within a time schedule which precluded highly specialized manufacture and long term life testing.

## II. COMPONENT RELIABILITY REQUIRED FOR PROJECT TELSTAR

The reliability requirements of components for communication satellites have been stated previously.[2] This earlier study described the three periods of satellite life, namely pre-launch, launch, and orbit, and showed how the orbit period dominates the reliability design. The Telstar experiment was undertaken with an objective of two years operating life in orbit. Because of the large launch cost penalty of increased weight and size, excessive component and circuit redundancy was considered prohibitive. The system therefore depended critically upon the use of highly reliable components which must survive a wide variety and range of thermal, electrical, mechanical, and radiation stresses. These stresses arise in particular during the launch and orbit phases when replacement of defectives is impossible. Certain of the components, such as the traveling-wave tube, are used singly or in small numbers, and thereby present a challenging design and reliability assurance problem. Other components are used in quantity and, to meet the objectives of the system, require maximum failure rates in the range of 1 to 20 failures per $10^9$ component hours (0.0001 to 0.002 per cent per 1000 hours). This degree of reliability had been observed in the field and therefore gave confidence that the system objective could be met. When one considers that Project Telstar was accomplished in 15 months from start of the program to launch, and that design changes involving the addition of component types were made during a significant part of this period, the task of assuring this level of reliability became imposing indeed.

The decision was made at the onset that only components of proven integrity could be used. The environmental conditions during the launch phase, involving large mechanical stresses, and the orbit phase, involving Van Allen belt radiation and temperature cycles, were defined. Component designs were evaluated to ensure that they had the capability of meeting environmental conditions with margin. Where time allowed, devices were manufactured under engineering surveillance to ensure the highest possible integrity. All devices were carefully screened to expected environmental conditions and pre-aged to eliminate defectives. The survivors were then life tested under simulated system conditions and then the best were certified using statistical analysis and engineering judgment. Finally, the components were used in circuits of conservative design where they operated well within maximum ratings.

## III. COMPONENT RELIABILITY ACHIEVEMENT

The program used to provide Telstar components was essentially that originated for submarine cable devices.[3] The major steps of this program are shown in Fig. 1.

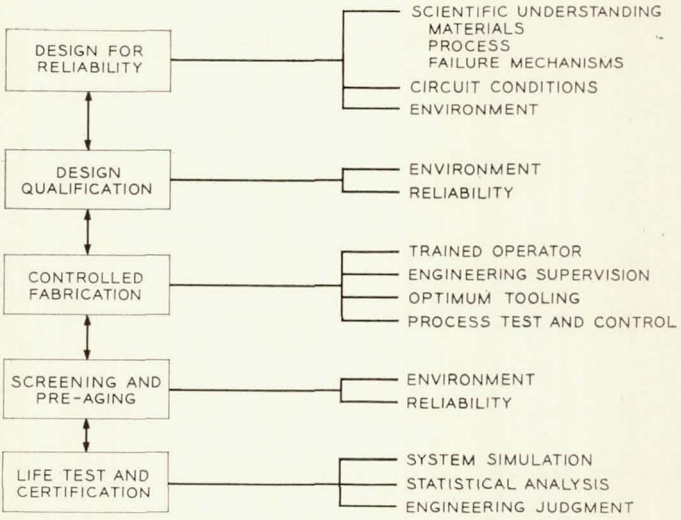


Fig. 1 — Major steps of component reliability program.

### 3.1 *Design for Reliability*

Satellite components must operate over a wide variety and range of mechanical, electrical, thermal, chemical, and radiation stresses. Device types intended for use were first examined for compatibility with these environments. In general only those which had demonstrated a consistent history of minimum manufacturing difficulty and outstanding field performance were considered. Specific details of design choices, such as diffused silicon semiconductor devices and nonadjustable passive components, are described in the companion papers of this part of issue.

Fig. 2 shows a failure distribution for a manufacturing lot of a component type in which failure rate is plotted as a function of time under expected system conditions. The distribution has two regions of relatively high failure rate, one early in life attributable to manufacturing "freaks," one later in life attributable to "wear-out," separated by a region of low failure rate. Device types were chosen in which the designer, through his knowledge of structure and mechanisms of change, could place the onset of wear-out well beyond the required useful life. Specific instances of wear-out were the deactivation of cathode life in the traveling-wave tube used in the satellite transmitter and the degradation of solar cells by energetic bombardment in the Van Allen belt. In cases like these, lengthening the onset of wear-out could only be achieved by understanding the mechanisms and then designing the devices to minimize or eliminate the effect.

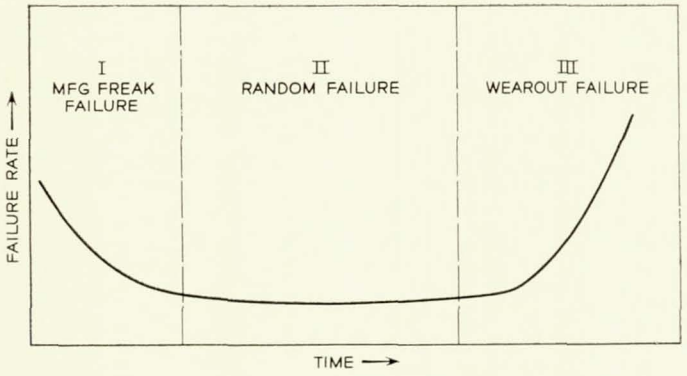


Fig. 2 — Failure distribution curve for components from one manufacturing lot.

### 3.2 *Design Qualification*

After the question of wear-out was settled, the next step was to ensure that the design was capable of meeting the variety of environmental conditions encountered during launch and orbit. Samples of each device type were subjected to qualification tests, many of which greatly exceeded the expected system conditions. Of particular note were gamma ray bombardment studies designed to simulate long periods of exposure expected in the Van Allen belt. Many tests were extended to destruction to obtain a measure of the design margins obtainable under actual operating conditions.

### 3.3 *Controlled Fabrication*

Because of the short Telstar program schedule, most of the devices were selected from manufacturing lines already producing standard products; only in a few cases were new lines established for special controlled production runs. In all cases, reliance was placed on the use of trained operators working on stable product lines in which quality control procedures were well established. These lines normally produce product in which the occurrence of manufacturing "freaks" (Fig. 2) is kept to a low level.

### 3.4 *Screening and Pre-Aging*

Remaining "freaks" were carefully removed from the manufactured product through the use of environmental screening and pre-aging tests. All devices were given environmental tests, many of which exceeded the

expected system levels. For example, short-term aging at highly elevated temperatures was used to eliminate devices that normally would have exhibited early failure. Samples from each manufacturing lot were subjected to step-stress aging,[4] in which the median stress for failure and the failure distribution with stress were compared to previous lot history. This latter test is a rapid means to determine whether the lot is similar to preceding lots.

Controls applied during the manufacturing phase and the screening and pre-aging tests were designed to eliminate the "freaks." The remaining product should then exhibit the low and almost constant failure distribution of the "random failure" portion of Fig. 2.

### 3.5 *Life Test and Certification*

For this last step, a larger number of devices than needed for the system was put on life test under circuit and temperature conditions expected in service. Every effort was made to continue the life test for the longest possible time. Parameter data were taken periodically using automatic testing and recording techniques. Only those devices were chosen for satellite assembly which showed the minimum change and closest behavior to design predictions. Final certification was done after the use of statistical analysis and engineering knowledge and judgment by experienced personnel.

## IV. CONCLUSIONS

The Telstar experiment required a large number and variety of components, the reliability of which, for satellite use, had to be in the range of 1 to 20 failures per $10^9$ component hours for success of the mission. This need called for the same approach to component reliability that was first used for submarine cable devices, in which devices of proven integrity are used in a conservative design. Fig. 1 lists the major steps in the program. Devices with proven design were manufactured under controlled conditions, screened and aged to remove manufacturing "freaks," and then life tested and certified using statistical techniques and engineering judgment.

Detailed descriptions of each major class of device used in the Telstar project are given in the papers to follow. Each paper describing components used in the satellite illustrates the application of these reliability principles in detail. Although components used in the earth station did not require the same degree of reliability assurance as those in the satellite, they were also designed for reliable, high performance service.

REFERENCES

1. B.S.T.J., this issue, Parts 1 and 2.
2. Ross, I. M., Reliability of Components for Communication Satellites, B.S.T.J., **41,** March, 1962, p. 635.
3. McNally, J. O., Metson, G. H., Veazie, E. A., and Holmes, M. F., Electron Tubes for the Transatlantic Cable System, B.S.T.J., **36,** January, 1957, p. 163.
4. Dodson, G. A., and Howard, B. T., High Stress Aging to Failure of Semiconductor Devices, Proc. Seventh National Symposium on Reliability and Quality Control, Philadelphia, Pa., Jan., 1961.

# Component Design, Construction and Evaluation for Satellites

By D. S. PECK and M. C. WOOLEY

(Manuscript received March 11, 1963)

*Components for a high-reliability system such as the Telstar project are obtained by:*

*(a) design of the component for the required environment,*

*(b) careful control of manufacturing processes,*

*(c) elimination of potential early failures by screening tests, and*

*(d) selection of the most stable components.*

*For passive components, these methods could be applied by using design parameters, suppliers and screening techniques established in the earlier submarine cable program, with consideration being given to the additional effects of the satellite launch and orbit environments.*

*Semiconductor component designs were selected by qualification tests using accelerated electrical and environmental stress conditions. Screening tests were applied to eliminate early failures, and resulting components were aged from two to six months before selection for the satellite. The recognition of the effect of ionizing radiation on transistors caused the addition of a radiation qualification test, or a screening to assure selection of the least sensitive devices. Tests have shown this screening to be effective for the radiation intensity expected.*

*Experience with the passive components, and evaluation of the accelerated test results and aging data of the semiconductor devices, indicate that the reliability objective was obtained.*

## I. INTRODUCTION

The importance of component reliability in the production of a successful electronic equipment of the complexity and with the reliability requirements of the Telstar satellite is well appreciated. Small systems and those of less complexity can be designed and built with special care, at reasonable cost, to have long life; large systems are subject to the laws of large numbers, which increase the probability of the malfunction-

ing of at least one component part. Normal maintenance of large earth-bound systems may be economical, however, and system performance may be acceptable if malfunctions are not too frequent. In an orbiting satellite, on the other hand, the first failure must be at sufficiently great time to provide an economical system, and the component failures must therefore be sufficiently distant in time, or at a sufficiently low rate, to allow a practical design. This does not ignore the requirement that the circuit and equipment designs use the component characteristics to best advantage, and also protect themselves as much as possible against the probable modes of component failure.

Considerable experience has been built up in the Bell System on the use of parts of high reliability, a most easily recognized example being the long submarine telephone cable systems which at this date have had no failures in over $10^9$ passive component hours and $5 \times 10^7$ electron tube hours of service.

The submarine cable repeaters, however, use specially designed and manufactured electron tubes and passive components. The design and selection of these were based upon many years of experience and life testing.[1,2] In contrast to this situation, the limited power available in an orbiting satellite and the severe limitation on total weight dictate the use of transistors as the active components, and in this case there is no extensive experience in a system of limited maintainability such as that of the submarine cable. Evidence is rapidly mounting, however, regarding the low failure rates obtainable with transistors in large systems, even without the use of special selection techniques. Transistors in large military systems have recorded replacement rates of 25 to 35 failure units,* and subsequent improvements in manufacturing processes show promise of failure rates appreciably below this figure. The sample calculations by I. M. Ross,[3] however, show that failure rates in the order of 10 failure units would be required even for a satellite system using only 140 transistors and 160 diodes in order to achieve a satisfactory probability of success for times appreciably beyond one year. Since the Telstar satellite circuitry requires a complement of about 1100 transistors and 1500 diodes, it can be recognized that failure rates better than 10 failure units would be desirable even for an experimental system. Similarly, since there are approximately 4700 passive components, capacitors, inductors, resistors and transformers in the satellite, these components must have an over-all failure rate of the order of 1 in $10^9$ component hours if there is to be a high probability of success for a two-year experiment.

* A failure unit is defined as one failure per $10^9$ component hours.

The immensity of the testing required to measure such low failure rates is difficult to comprehend and all but impossible to achieve in a limited time. For example, to provide 90 per cent confidence that none of the passive components in the satellite would fail in less than two years would have required that components of the same quality be tested until they had accumulated over $2 \times 10^9$ component hours without a failure. Even with the use of accelerated tests which, in the extreme case, might compress time by a 1000:1 ratio for some types of components, this amount of testing is prohibitive. Fortunately, other avenues are available which provide a basis for obtaining a high degree of reliability but with less assurance of its numerical value.

1.1 *Principles of Achievement of Satellite Component Reliability*

The principles and techniques originated for submarine cable components and now being applied to some of the complex missile systems were recently reviewed by J. A. Morton at the Eighth National Symposium on Reliability and Quality Control. These are, briefly:

(*a*) *Design of the component for the required environment.* This requires consideration of the possibility of actual "wear-out" of the component because of the environmental or life conditions. Even with the best design knowledge and perfect manufacture there may be fundamental limitations to the usefulness of a given material in its environment. Examples are the eventual evaporation of the oxide cathode in an electron tube and the limitation on the life of silicon solar cells due to radiation bombardment in space. If possible, with a proper knowledge of the operating and environmental requirements and of the capabilities of materials and processes, the designer should place this wear-out point well beyond the required useful life of the component.

(*b*) *Careful control of manufacturing process.* The relationship of quality control in manufacture to resulting uniformity of product and hence uniformity of response to operating environment can be readily acknowledged. This process control should be used to control all three phases of product life response: (1) it should prevent marginal product from extending the period of early failures due to manufacturing defects far into the useful life region, (2) it should assure low failure rates during the useful life, and (3) it should assure that wear-out failures do not occur prematurely, in the region of normally useful life.

(*c*) *Weed-out of potential early failures by screening tests.* It may be recognized that even in a product under careful quality control in manufacture there may be a certain percentage subject to early failure because of some defect not recognizable by the normal testing processes. Such

defective units can usually be eliminated by means of rigorous environmental tests and by operating tests under conditions similar to that expected in use.

(*d*) *Selection of the most stable components of the population.* Even with careful quality control of the manufacturing process and with rejection of defective units through screening tests, there may still be expected a distribution of stability among the remaining units in the product. The state of the art of a given process required to obtain suitable operating characteristics may possibly result in variations of initial electrical parameters or in drifts or variations of these parameters with time. The careful observation of such parameters during the life test period may then allow the use of various selection techniques, more or less sophisticated as the requirements indicate, to obtain for actual satellite use those components least likely to fail in operation or to cause circuit performance changes.

The techniques of application of the principles of achieving reliable components will vary somewhat, depending upon the state of knowledge of design and processing, of testing and life evaluation methods and of circuit application factors. Because of the wide disparity of system experience with passive components and semiconductor devices, the following material will treat each of these separately.

## II. PASSIVE COMPONENTS

Experience with passive components in submarine telephone cable repeaters has shown that this philosophy when applied to the selection, construction and testing of those components resulted in a highly reliable product. (Since in the systems made with such tightly controlled components there have been no component failures, for the present we can only say that there is a 70 per cent probability that the failure rate of the passive components does not exceed 1 in $10^9$ per hour.) Similarly, experience and performance records with other Bell System and military projects has shown that some other types of components not used in submarine cable repeaters, when carefully manufactured and screened, are capable of this kind of performance. In a satellite these failure rates may be increased by unknown environmental factors, particularly the effects of Van Allen belt radiation and extreme shock or vibration during launch. Another liability for Telstar was a short schedule which required that screening tests, intended to eliminate potential failures, be limited to short-time tests, generally 100 hours or less. A further complication was the wide range of component types and values required.

These liabilities are offset to some extent by the fact that operating

conditions of voltage, power dissipation and temperature are mild for the vast majority of the passive components. Thus the most likely causes of component malfunction are an occasional mishap in construction or some unforeseen effect of the environment or application. Consequently, with adequate derating to minimize the deteriorative processes resulting from load or voltage, the problem becomes primarily one of

(a) careful choice of components to minimize the effects of the environment,

(b) thorough inspection and screening to eliminate all components which may be subnormal in any way and thereby potential failures, and

(c) care in the physical application of the components to avoid compromising their integrity.

### 2.1 *Selection of Component Types*

The choice of the component types to be used was governed by a number of factors. One of the most basic and restrictive of these was that no new or untried types could be used. In other words, only those types which have been in widespread use for a period long enough and under a sufficient range of conditions to prove by field performance that they were capable of reliable operation, were considered for use. This restriction was also applied to the materials used in the construction of the components and to the details of construction so that both materials and the type of construction were well established and proven by field experience.

It is generally recognized that, especially under conditions of severe vibration or mechanical shock, adjustable components are less stable than their fixed counterparts. Consequently a strenuous effort was made to avoid the use of adjustable types. In most cases this was accomplished by selection from "post office" bins which covered the required range in suitably small fixed steps. Where this was inadequate, the over-all stability was enhanced by limiting the range of adjustable components to cover only the range between closely-spaced fixed steps.

It is easy to visualize the increased hazard of failure when conductors are made very small or dielectrics are unusually thin. Thus for extreme values of resistance the resistive film may be made so tenuous that at some points it is practically nonexistent, or for very low values the heavy deposit required to produce low resistance may be mechanically unstable. Similarly in capacitors, in an effort to crowd the maximum capacitance into a given space, factors of safety may be reduced, clearances may be made smaller, and physical damage to critical parts may even result. In addition to this degradation of reliability at the extremes of compo-

nent values, it is not uncommon to find that characteristics such as temperature coefficient and stability with time or frequency are also degraded at extreme values. For these reasons the range of values, in a given physical size, was severely limited for the satellite components. This affected capacitors and resistors particularly, and in some cases limited the range of usable values to less than 15 per cent of the range of commercially available values.

Although the anticipated cumulative exposure to electron and proton radiation appeared to be well within the acceptable limit for most components, only the most resistant types were used. Thus hermetically sealed components filled with oils or electrolytes were avoided because such materials gas and build up destructive pressures under severe radiation. Structural and housing materials and coatings were also examined and chosen for their resistance to deterioration under radiation. These choices were based on the reported results of many studies, both within and outside Bell Laboratories, and on supplementary tests made in a $Co^{60}$ cell on the specific types of components used in the satellite. Most of these were tests in which the components were subjected to load or voltage during radiation, and they were continued until the exposure exceeded by several times the maximum expected in service. From these tests it was concluded that radiation would not be the limiting factor in the life of the components, at least in a two-year experiment.

It was expected that, because of being sealed in the canister, the majority of the components would not be exposed to the extreme vacuum of space. All of the types, however — resistors, capacitors and power transformers — on which low pressure might have an effect were tested under such conditions. Furthermore, such components were rated so that they would operate under extremely low pressure without abnormal temperature rise or other harmful effects.

Even with these restrictions there were very few instances where suitable standard components were not available.* Table I lists the types of components used and their typical uses.

### 2.2 *Selection of Components for Specific Applications*

As mentioned above, the most likely causes of malfunction of components are misapplication and deviations from design intent during manufacture of the components. The term "misapplication" in this case

* Approximately 95 per cent of the passive components used were purchased outside the Bell System.

TABLE I—TYPES AND TYPICAL USES OF PASSIVE COMPONENTS

| Use | Type | Number Used |
|---|---|---|
| | **Capacitors** | |
| General purpose, temperature compensation | Ceramic | 814 |
| Precision in low values | Glass | 47 |
| Precision in high values | Mylar* | 18 |
| High values, small size | Tantalum solid | 444 |
| Precise tuning | Glass and quartz tubular trimmers | 20 |
| | **Resistors** | |
| General purpose, low precision | Carbon composition | 1325 |
| General purpose, moderate precision | Pyrolytic carbon film | 1414 |
| High precision, high frequency | Metal film | 136 |
| High precision | Wire wound | 44 |
| Power dissipation | Vitreous enameled wire wound | 30 |
| | **Inductors** | |
| High frequency, general purpose | Nonmagnetic core, fixed<br>Nonmagnetic slug, adjustable | 140 |
| Power frequency | Permalloy dust core toroid | 2 |
| Memory coils | Ferrite core | 230 |
| | **Transformers** | |
| Narrow-band high frequency (tuned) | Nonmagnetic core, adjustable inductance<br>Magnetic core toroid | 43 |
| Broadband high frequency | Closed ferrite core<br>Ferrite cup core<br>Laminated magnetic core | 15 |
| Power frequency | Magnetic tape core toroid<br>Permalloy dust core toroid | 6 |

* Registered trademark, E. I. DuPont DeNemours & Co.

is used in a broad sense to include improper voltage, temperature or wattage, or failure to meet circuit or ambient conditions, as well as the actual physical mishandling or incorrect mounting of the component. Since the components used were types known to be capable of reliable operation, the major problems were to assure their reliability by careful handling and use and to eliminate by thorough testing or screening those individuals which were abnormal in any way. An essential ingredient in any project requiring reliability in components is the care and perspicacity with which these factors of selection and use are examined. In these respects Project Telstar differed from other Bell System projects in

degree only. Component engineers recommended types on the basis of circuit engineers' requirements and also prescribed conditions of use (handling, mounting, etc.). Subsequently the application was independently checked by a reliability engineer, who compared operating conditions with component ratings which were established especially for the Telstar program. In general, all components were derated at least 50 per cent from commercial ratings. During fabrication of all development, preproduction and final models of the Telstar spacecraft, all cases of malfunction which were in any way related to the components were examined and appropriate measures taken to avoid future difficulties. This procedure was particularly effective in eliminating misapplications and physical mishandling.

### 2.3 *Screening and Final Selection*

The testing or screening of components varied from type to type, but in general the bases for the tests were standard Bell System high-reliability specifications, which were supplemented by restrictions on materials and in some instances by additional requirements. In addition the suppliers were asked, and willingly agreed, to apply any additional tests or requirements which in their opinion would enhance the reliability of the product. Several such additions to normal processing were made, ranging from special handling to the imposition of short-time life tests or special electrical tests. Chief of the requirements added to the Bell System specifications was the assignment of an identifying number to each component and the recording of data for each numbered component at various stages of the test program. These data were delivered by the supplier with the components. On receipt of the components they were subjected to additional tests which ranged from a check of electrical characteristics to voltage or power aging supplemented by "before" and "after" measurements of all critical characteristics. All of the data, both the supplier's and the Bell Telephone Laboratories', were then analyzed either manually or by machine. The components to be used were selected by this analysis. Three criteria were used in this selection:

(1) fixed limits on critical attributes,

(2) stability of characteristics throughout the test period, and

(3) conformance with normal behavior.

Many of the requirements applied to conventional components have no direct relation to the performance of the circuits in which the components are used but are instead applied to control the quality, i.e., to insure the integrity of the materials and proper processing of the component. The same is true to an even greater extent when extreme re-

liability is required, so that every property which might have an effect on, or be a measure of, reliability is controlled. Table II lists the major kinds of requirements applied to capacitors and resistors. Some of these were applied only to certain types: for example, the X-ray requirement was used only on hermetically sealed designs where internal clearances and positioning could not be checked visually. Similarly the requirement for change under load was applied only to resistors intended to dissipate significant amounts of power. As shown in this table, the requirements for the Telstar satellite components covered much more than those attributes which were of importance from a circuit performance standpoint. An example of this is the application of requirements for ability to withstand atmospheric moisture. At no time during shipment, assembly into equipment, or use were the components subjected to severe humidity conditions, but tests were made to measure their ability to withstand such conditions. Since the normal product is capable of meeting these requirements, failure of the Telstar satellite components to do so would have indicated that the product was inferior to normal product either in its moisture protection or in contamination with moisture-sensitive materials. Similarly, voltage aging tests on capacitors and power aging tests on resistors were made at stress levels chosen to insure that the component quality was consistent with capability rather than just adequate for the stresses in service. Furthermore, these tests were made on 100 per cent of the product, and entire lots which had more than a few per cent of failures were rejected.

In the final selection of the components to be used the record of each one was scanned. Where there was a large margin between the component capability and operating conditions or requirements, practically all components which met the fixed requirements were considered qualified for use. In other cases where the margin between capability and use was

TABLE II—TYPES OF REQUIREMENTS APPLIED TO CAPACITORS AND RESISTORS

| Resistors | Capacitors |
|---|---|
| Resistance | Capacitance |
| Aging resulting from load | Power factor |
| Aging resulting from temperature cycling | Insulation resistance (or leakage current) |
| Moisture resistance (sampling) | Dielectric strength |
| Change under load | Capacitance-temperature characteristic |
| Temperature coefficient of resistance | Voltage aging (100%) |
| | Life test (sampling) |
| | X-ray |

smaller, only those components with characteristics near the norm and showing a high degree of stability were considered acceptable. Even when deviations from normal behavior were in the direction of better performance, those which showed abnormal deviations were rejected since this might be the compensatory result of two mechanisms, one of which could ultimately cause failure. As a result, the yield of acceptable components ranged from nearly 100 per cent of those received of some types to approximately 50 per cent of other types.

While the foregoing applies specifically to purchased components, the procedure for those few components made by the Bell Telephone Laboratories or Western Electric Company differed mainly in that their construction was under direct engineering supervision and inspection. This close supervision and detailed inspection is particularly important for some types of components, such as inductors and transformers, where tests to accentuate and uncover weaknesses are either destructive or nonexistent. In addition to this factor, manufacture of some components by Bell Telephone Laboratories or Western Electric was undertaken because of the need for special characteristics, unusually close tolerances on electrical parameters or unusual operating conditions. Examples are: very stable inductors with a narrow (2 to 3 per cent) adjustment range, others with inductance tolerances measured in millimicrohenries and unimpregnated capacitors for use at high voltages. The manufacture and testing of many of these were essentially laboratory operations, but even with this close control the components were screened by appropriate tests before being released for use. For example, the high-voltage capacitors used in the dc supply for the traveling-wave tube were screened by applying an overvoltage of 150 per cent of rating for eight weeks.

While these measures do not permit or lead to any quantitative calculation of the reliability of the components, past experience, coupled with engineering judgment of the effect of the special handling, leads to the belief that the passive components will achieve the low failure rate needed for successful conclusion of the Telstar experiment.

### III. SEMICONDUCTOR DEVICES

As indicated previously, the number of semiconductors to be used in the Telstar experimental satellite dictated that the failure rate should be in the order of 10 failure units or less to provide assurance of reasonable life even for experimental purposes. The achievement of such reliability would require close attention to the principles outlined previously, and a program was established along these lines for selecting the necessary devices. In contrast to the situation on passive components,

very limited experience was available regarding the specification of suitable procedures for manufacture or selection to the desired reliability. The reliability principles described in Section 1.1 can be applied, however, and the particular techniques of application are indicated in the following description of the semiconductor program.

### 3.1 *Component Design*

Table III shows the numbers of diodes and transistors required per satellite, the total number required for all satellite models and the number actually processed in the program. The total number of transistors and diodes was divided into 41 different basic types or prototypes, from which a total of 93 individual codes were selected to match the specific requirements of the many circuits. Although two types of diffused germanium transistors and three types of diffused silicon diodes were designed and manufactured for the Telstar satellite, the large number of other types and the total numbers required dictated that existing types in production be used where possible for this system, provided each had the basic design features necessary for reliability[3] and could also qualify for use in the specific intended environment.

A basic requirement of design-for-reliability is that there should not be any feature of the design which contributes the possibility of wear-out failure within the usable lifetime or which prevents the achievement of low failure rate during that time. Most of the types were selected from those previously designed for either military or Bell System use. The designs had already received consideration of possible wear-out failures and they had also met such design requirements as (a) high internal element resonant frequencies, (b) capability of withstanding storage temperature extremes and soldering temperatures and (c) adequate resistance to vibration or shock of typical applications.

Beyond these normal design considerations, it was additionally necessary to review the capability of each candidate type for operation in the satellite environment. This was accomplished by a number of design

TABLE III—*Telstar* SEMICONDUCTOR REQUIREMENTS

| | Number per Satellite | Number of Types | Total Number Required | Total Number Processed |
|---|---|---|---|---|
| Diodes | 1,521 | 18 | 12,526 | 28,525 |
| Transistors | 1,119 | 23 | 9,996 | 29,644 |
| Total | 2,640 | 41 | 22,522 | 58,169 |

qualification tests, as shown in Table IV. The requirements for these tests were established to exceed the specific conditions resulting from the satellite design or, as with some of the mechanical tests, to reconfirm the normal device design capability. For example, the temperature cycling extremes for the devices to be used in the electronics package were established by typical device capability even though the mechanical design of the package is such as to maintain its internal temperature at or near normal room temperature. The diodes used to isolate groups of solar cells, however, were to be mounted near the outer shell or skin and would be subjected to much more extreme temperatures; the temperature limits were established, therefore, to assure that no feature of the design would prevent proper performance at these temperatures.

Similarly, the vibration tests for most of the designs were established to assure performance in the electronics package at the low frequency of resonance determined by its mounting, using considerable margin in the acceleration level. The blocking diode design, however, was actually tested on a mechanical model of the Telstar satellite design in order to assure achieving the mechanical environment of the exact mounting location. The other conditions of centrifuge, shock and temperature-humidity cycling conform to typical requirements of handling, since the corresponding requirements of the satellite would be very mild.

The qualification of device types for reliability depended heavily upon the step-stress techniques[4,5] which determine the distribution of failures with increasing stress for a given time of application of stress. With this distribution obtained for several different times of application, a plot can be made of a relationship between time and the stress value at

TABLE IV—DESIGN QUALIFICATION TESTS

| | |
|---|---|
| **Mechanical** | |
| Temperature cycling | |
| −65 C to +85 C for devices in electronics package | |
| −120 C to +40 C for devices on skin | |
| Temperature-humidity cycling | |
| Shock | 2,000g, 0.2 msec |
| Centrifuge | 5,000–10,000g |
| Vibration | 100g, 80 cycles for devices in electronics package |
| | 100g, 100–2,000 cycles for devices on skin |
| **Reliability** | |
| Accelerated tests | |
| Field experience | |
| **Radiation** | |
| Proton, electron and $\gamma$-ray exposure | |

median failure. Either temperature or power, or both were used as the stress for each transistor or diode type in order to achieve extrapolations to the expected condition of use and to provide estimates of the failure rates to be expected. Generally the results were significant and satisfactory. One diode type was rejected from the program because of the very short median life indicated by the extrapolation of the step-stress data. Some of the microwave diodes, however, were not capable of accelerated stress testing because of their construction, and dependence was therefore placed upon the long history of satisfactory experience with these diode types in other transmission systems.

To qualify the designs for resistance to radiation, samples were exposed to proton and electron radiation, with electrical tests being made before and after exposure. No adverse response was indicated here except for germanium alloy transistors for power regulation, which showed degradation due to permanent damage in the germanium. These tests were augmented with $\gamma$-ray exposure (correlated to proton exposure) and sufficient data were obtained to establish the alloy transistor degradation rate. A shielding of about 0.120 inch of aluminum was used to reduce this rate to an acceptable value for the system life.

In addition to the design qualification testing, consideration was given to circuit application factors and to the effect of the environment on device capability as described for passive components in Sections 2.1 and 2.2.

### 3.2 *Control of the Manufacturing Process*

Most of the semiconductor devices were obtained as early as possible in order to provide a suitable time period for certification life testing. They were therefore taken from product already manufactured under normal quality control and inspection techniques. A sample of each lot of product obtained, however, was subjected to step-stress testing where applicable to assure that the failure pattern would match that expected from the design qualification tests or from previous experience. Some of the diffused germanium high-frequency transistors, however, and three types of special diffused silicon diodes were manufactured specifically for the Telstar program and were made under direct engineering control with careful scrutiny of each step of the processing.

### 3.3 *Screening and Pre-Aging*

Table V shows the list of the various screening and pre-aging conditions used to eliminate early failures from the product. Each condition was considered for at least one of three reasons: (1) general applicability

TABLE V—SCREENING CONDITIONS

| |
|---|
| Mechanical |
| Centrifuge |
| Temperature-humidity cycle |
| Tap, shock or vibration |
| X-ray inspection |
| Temperature cycle |
| Reliability |
| High-temperature processing |

of the testing condition for quality control, (2) knowledge of the design which would cause concern about capability of every individual device to withstand the environmental condition or (3) specific requirements of the application. In addition, when prior experience was not available, tests were made to obtain assurance that the environmental screening condition would not induce additional incipient failures into the product and would, in fact, eliminate devices which were distinctly weaker than the normal population. Not all conditions were used for each type, and the choice of conditions for each type was determined, at least in part, by results of the qualification tests.

Results of the mechanical screening operations are presented in Table VI. The low rejection rate of the diffused germanium high-frequency transistors, in comparison to that of the silicon transistors having a generally similar structure, is felt to represent the improvement due to the careful attention given them during fabrication. On the other hand, the high rejection rate of the alloyed germanium types for power use reflects marginal capability of meeting screening conditions for which these particular types were not originally intended.

Reliability screening, or pre-aging by the application of high temperatures, was used only in one case where the qualification testing indicated early failure rates could be improved. In most cases such proc-

TABLE VI—MECHANICAL SCREENING RESULTS

| | Number Processed | Per Cent Rejects |
|---|---|---|
| Diodes | | |
| Microwave | 774 | 2.3 |
| Rectifier | 3,292 | 3.0 |
| Small Signal | 24,109 | 0.27 |
| Transistors | | |
| Power (Ge) | 635 | 9.5 |
| High Frequency (Ge) | 4,780 | 0.3 |
| Amplifiers (Si) | 24,229 | 2.8 |

essing was included in the normal production sequence and was not repeated in this program.

In addition to these results of the planned program, additional mechanical screening was required later for two diode types when molded into a module. The molding flash removal operation was apparently causing damaging shocks to be transmitted down the diode leads. Although alteration of the flash-removal process appeared to eliminate the problem, diodes were also given a very severe tap test which caused rejection of 25 per cent of the diodes for that application.

Subsequent to the initial radiation evaluation it was recognized that devices held under electrical bias while being exposed to ionizing radiation could suffer degradation at a much lower dose than that necessary to produce permanent damage in the semiconductor material.[6] This effect occurs in quite varying degrees in transistors of different types and among individuals of a sensitive type. It apparently results from ionization of the gas ambient in the device and the effect of such ionization on the semiconductor surface. All types were therefore exposed to ionizing gamma radiation from a $Co^{60}$ source for short periods at an accelerated dose rate of about $10^6$ rads per hour and for long periods at a dose rate of 5 rads per hour, simulating the exposure expected in the Telstar satellite orbit, according to data available prior to launch. Those types showing no degradation under either exposure were considered qualified for this environment. Those types showing degradation were given additional radiation screening, consisting of exposure while under bias in normal transistor operation, for one minute in a $\gamma$-ray dose of $8.5 \times 10^5$ rads per hour. This provided a total dose of $1.4 \times 10^4$ rads, the equivalent in ionization energy to that dose expected in three months in the satellite orbit for devices shielded in the electronics canister. Such screening was necessary for two types of silicon mesa transistors. Fig. 1 shows an example of the distribution (on a normal probability scale) of the increase in collector reverse current ($I_{CBO}$) of one of the transistor codes after screening, indicating the percentage selectable at any stated screening limit for three months in orbit. (The measurements prior to radiation were in the $10^{-10}$ to low $10^{-9}$ ampere range.) Since for these types the $I_{CBO}$ increases beyond this value approximately as the $\frac{1}{2}$ power of total dose, a selection for two-year operation (eight times the equivalent of the screening dose) is made by setting the $I_{CBO}$ limit for screening a factor of 2.8 tighter than the circuit limit. Some additional safety factor is desirable because of the lack of perfect correlation between screening dose and dose in orbit. The knowledge of this response to radiation and the distribution thereof allows careful matching of screening limits and circuit use requirements, if necessary to obtain maximum screening yield.

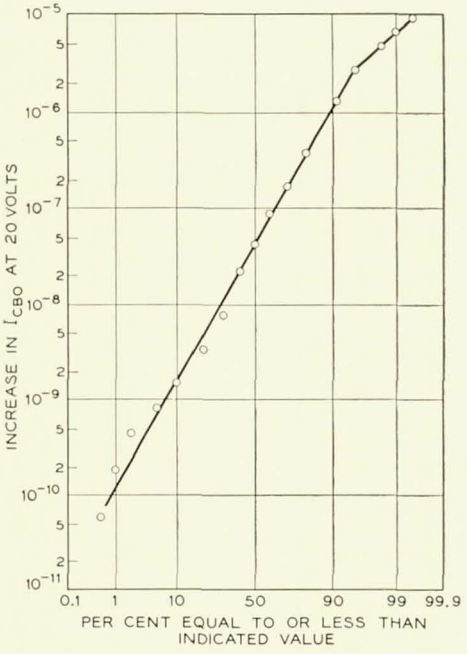


Fig. 1 — Distribution of reverse current degradation resulting from radiation screening.

Suitable selection was made of these types, without allowing more than two orders of magnitude increase for use in the most lenient circuit.

Subsequent low-level exposure tests[6] have confirmed the effectiveness of this screening procedure through equivalence of its results to those expected in orbit. Fig. 2 shows the distribution, on a normal probability scale, of the ratio of $h_{FE}$ of one of the transistors after the screening dose to that before screening. This shows that, in the total population screened, 10 per cent suffered degradation to below 30 per cent of the original measurement. Since increases in gain were not of concern, the screening selection affected most strongly the units degrading most. The units with highest initial gain suffered the greatest percentage of degradation in screening, while those with lower initial gains degraded less or tended to increase, so that the problem of selecting units with sufficiently high gain after radiation was not severe.

### 3.4 *Selection of the Most Stable Components*

In order to select the best devices from the available product, all devices were subjected to a life testing period of an intended six-month

duration or for as long as possible between the time of availability and the deadline for shipment. (For the devices selected for the Telstar satellite, the average life test was about fifteen weeks.) During this life test period all pertinent parameters were measured on each device at regular intervals, generally of the order of two weeks. Up-to-date listings were kept of the data on each device so that the life history could be examined readily for drifts of characteristics, unusual variations in measurements, proximity to critical circuit limits or the existence of wild and unexplainable readings.

All the devices were operated at electrical conditions close to those at which they would be used in the satellite or close to the most severe condition for those types used in several circuit applications. On this basis, the operating condition was typically in the order of 10 per cent of the normal device rating. Although this does not take advantage of the acceleration of changes which might be induced by higher power levels, it was considered to be the safest approach. Furthermore, this resulted in some of the transistor types operating at quite low currents, at which the gain measurements are more sensitive to changes, and differences in stability between individuals may have tended to show up even more readily than at the higher power levels. Most of the devices were installed in modules which could be inserted into the aging equipment or into the test equipment without additional handling of the device itself.

The selection process consisted of obtaining the most stable units on the basis of the recorded life data and electrical measurements before

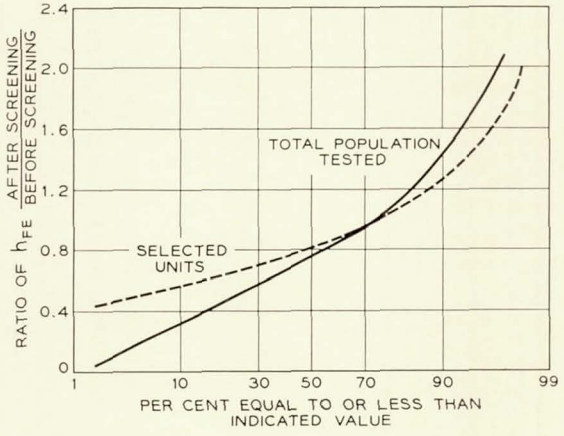


Fig. 2 — Distributions of $h_{FE}$ degradation, of total group screened and of selected units, resulting from radiation screening.

and after the various screening procedures. Whereas many of the lots were sufficiently small that this could be done readily by observation of the data listings, other lots were sufficiently large that the initial selection was done by machine as much as possible. A computer was programmed to estimate the time at which each device would exceed an established limit for any parameter, considering drift, variations, and the initial values. The individuals were then ranked according to these time estimates and a listing was prepared from which selections could readily be made.

The final certification of each device chosen for use consisted of a complete review of all electrical measurements, X-ray photographs and similar data by qualified technical personnel, stamping of the proper code number to identify the circuit application intended and final inspection and electrical test. Many of the general considerations were similar to those described for passive components in Section 2.3.

### 3.5 *Evaluation of Life Testing and Selection*

It is of interest to review the life testing data and the results of selection, in order to observe the effectiveness and the degree of discrimination of selection and to obtain some estimate, if possible, of the probable reliability of the selected units.

Fig. 3 shows one example of the selection sensitivity for one parameter of a silicon mesa transistor. This plot, on a normal probability scale, shows the distribution of the rate of change of $h_{FE}$ , or transistor current gain, in per cent change per month, averaged over the life test period (six months in this case). Silicon transistors typically experience a slight increase in gain early in life, becoming quite stable thereafter, and the total population on this life test shows, for most of the units, this typical increase. About 4 per cent of the total, however, evidence a negative drift, indicating degradation of the order of 1 to 2 per cent per month or more, this portion of the product also deviating from the Gaussian distribution indicated by the straight line of the rest of the product. The distribution of the selected units shows the complete elimination of the degrading units. Those having the expected increase in gain during life test have stabilized during the latter part of the test and are stable at the time of selection. It is felt important that the life testing period be sufficient to provide the data necessary to distinguish such a distribution and such a deviation from it.

Another means of evaluating life test results consists of assigning "defect" limits to the electrical parameters being measured for each

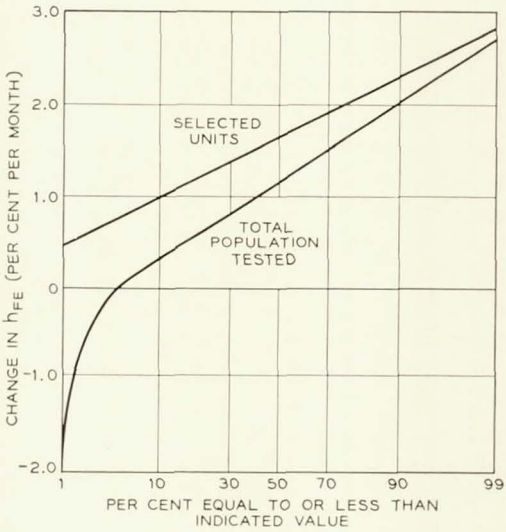


Fig. 3 — Distribution of $h_{FE}$ degradation rate on life test, for total group life tested and for selected units.

transistor or diode type and noting the frequency of occurrence of units exceeding these limits. Such limits were defined for the major types on life test, and Fig. 4 shows the resulting plot of defect rates for a typical transistor and a typical diode. The defect rate, in defects per $10^9$ component hours, is calculated for life test intervals and is plotted with time on test, on a log scale, showing the decreasing "failure" rate typically reported for semiconductor life tests. The shape and general position of the curves are also typical of most of the types on life test and show the marked gain which can be achieved in defect rate of the product through such a life test period.

It is also noted that the defect rate of about 1000 defects per $10^9$ component hours for transistors, or 100 for diodes, at the selection time of about fifteen weeks is appreciably above the 10 failure units set as the maximum objective for Telstar satellite semiconductors. In order to estimate probable failure rate of Telstar components from the life test data, however, certain factors must be considered. A large factor is that the spacecraft components are selected as the most stable ones, whereas the life defects represent generally the least stable. Most of the defects occur by degradation of a measured parameter to the defect limit, this degradation being recognizable early in life. The certified units are those with no definite degrading trend and hence should not be subject to such

failures. The only indication of possible failures from among the selected units is the frequency of catastrophic life test defects, a measurable rate much below that of the total defect rate. Additionally, since most of such sudden changes occur in units showing some tendencies which would otherwise prevent their selection, the measurable estimate of improvement from total defect rate to estimated catastrophic failure rate of the selected units is considered quite conservative.

Many of the device types are used in several circuits, some of which have requirements for device parameter limits which are relatively severe compared to the majority of circuits using that type. The life defect limits correspond to the most severe requirements, and the calculated defect rate is therefore much greater than that which would be representative of the major portion of that product. The average failure rate is therefore additionally reduced by as much as a factor of ten for some types for this reason. The frequent testing is another factor which may have more bearing on some types than on others, but may always be present. Consideration of all these factors for each type, to the degree measurable, indicates conservative ratios of from 10 to 200 between life defect rates and estimated circuit failure rates.

Table VII shows a summary of the defect rates by device classes taken from such plots as in Fig. 4 for the time of shipment of Models 1 and 2 of the satellite and of Models 3 and 4. These data include over 90 per cent of the types, excepting those for which the numbers on life test were too small to develop meaningful statistics — among these being the germanium alloy types for power control use. Among all types, the lower defect rate for the second shipment time shows the effect of the decreas-

TABLE VII—LIFE TEST AND SELECTION RESULTS

| | Number per Satellite | Defect Rate at Shipment Time, Defects per $10^9$ Component Hours | | Conservative Failure Rate in Satellite, Failures per $10^9$ Component Hours | |
|---|---|---|---|---|---|
| | | Models 1 & 2 | Models 3 & 4 | Models 1 & 2 | Models 3 & 4 |
| Diodes | | | | | |
| Microwave | 14 | 4,500 | 3,000 | 45 | 30 |
| Rectifier | 83 | 30 | 20 | 3 | 2 |
| Small signal | 1,424 | 70 | 35 | 3.5 | 2 |
| Transistors | | | | | |
| High frequency (Ge) | 94 | 550 | 400 | 13 | 10 |
| Amplifiers (Si) | 1,011 | 4,000 | 3,000 | 30 | 20 |
| Weighted average | | | | 14.2 | 9.3 |

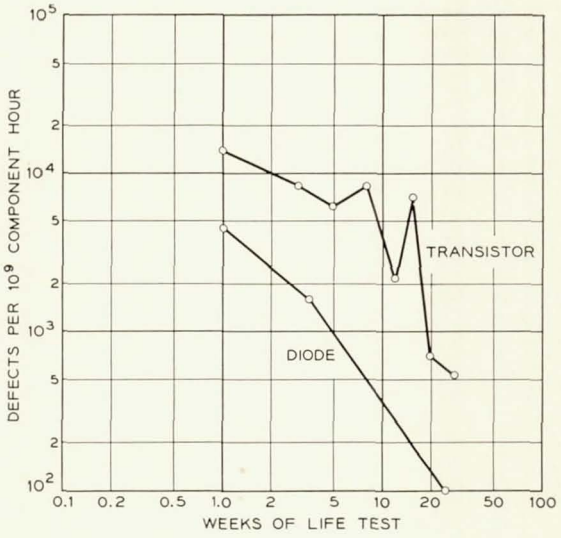


Fig. 4 — Defect rates through life test for typical transistor and diode.

ing defect rate as shown in Fig. 4. The relatively high defect rate of the silicon transistors for general amplifier use comes about largely through the contribution of one type which had a defect limit on collector reverse current, $I_{CBO}$, of $10^{-8}$ ampere, a much lower figure than that normally used for life test limits. Also shown for each class of product are the failure rate estimates for the selected devices, taking into account the factors mentioned above.

With these failure rate estimates weighted according to the number of each class of device used per satellite, an over-all average can be calculated, indicating about 14 failure units for the Telstar satellite semiconductors, with an expected improvement to 9 failure units for Models 3 and 4. Since these estimates are conservative, as indicated above, it is felt with considerable confidence that the screening and life testing program has resulted in devices meeting the initial objective of less than 10 failure units.

REFERENCES

1. McNally, J. O., Metson, G. H., Veazie, E. A., and Holmes, M. F., Electron Tubes for the Transatlantic Cable System, B.S.T.J., **36,** January, 1957, p. 163.
2. Gleichmann, T. F., Lince, A. H., Wooley, M. C., and Braga, F. J., Repeater Design for the North Atlantic Link, B.S.T.J., **36,** January, 1957, p. 69.
3. Ross, I. M., Reliability of Components for Communication Satellites, B.S.T.J., **41,** March, 1962, p. 635.

4. Dodson, G. A., and Howard, B. T., High Stress Aging to Failure of Semiconductor Devices, Proc. Seventh National Symposium on Reliability and Quality Control, Philadelphia, Pa., January, 1961.
5. Peck, D. S., The Uses of Semiconductor Life Distributions, *Semiconductor Reliability*, Vol. II, ed. W. Von Alven, Engineering Publishers, Elizabeth, New Jersey, 1962.
6. Peck, D. S., Blair, R. R., Brown, W. L., and Smits, F. M., Surface Effects of Radiation on Transistors, B.S.T.J., **42**, January, 1963, p. 95.

# Nickel-Cadmium Cells for the Spacecraft Battery

By D. C. BOMBERGER and L. F. MOOSE

(Manuscript received January 31, 1963) 11082

*The storage battery for the Telstar satellite must undergo frequent charge-discharge cycles; in addition, it is subject to overcharge during a substantial portion of its life. Nickel-cadmium cells were chosen as best capable of satisfactory long-time operation under these conditions. A design and selection program was undertaken to ensure that Ni-Cd cores would meet objectives imposed by battery service conditions, and the cell enclosure was designed to minimize electrolyte leakage. Selection, qualification, and life tests indicated that a storage battery using the cell design would perform satisfactorily. To date, the only failures occurring during continuing life tests have been among cells subjected to 100 per cent discharge daily; this operation is far in excess of the expected duty cycle of satellite cells.*

AUTHOR

## I. BATTERY DESIGN OBJECTIVES

Since the peak power required during the communications experiment exceeds that available from the solar cells, the storage battery will undergo many charge-discharge cycles (to depths of discharge as great as 40 per cent of capacity) during the lifetime of the satellite. On the other hand, several times each year the satellite is in continuous sunlight for long periods, during which the daily average solar cell power exceeds the average power used during visible passes. Thus the battery will receive overcharge current for a substantial fraction of its life.

Design objectives for the storage battery thus include high overcharge capability and long cycle life; additionally, high recharge efficiency is of importance in minimizing electrical losses, and a nonfailing hermetic seal is required to prevent the loss of electrolyte. The nickel-cadmium storage cell, in principle, can meet these objectives. It has a theoretical capability of long cycle life; also, if there is an excess of capacity in the negative electrode of the cell, no hydrogen will be evolved during normal overcharge, and the oxygen which does form will recombine at moderate



Bell Sys. Tech. J. Telstar 1, Vol. 3 Jun. 1963
P. 1687–1702 0 refs
(See N64-11079 02-01)

pressures so that the cell can be sealed. However, commercial sealed nickel-cadmium cells available at the beginning of the satellite program did not appear to meet all objectives. Most cells leaked, their electrical characteristics were not uniform, and there were no data to indicate a life expectancy adequate for the Telstar experiment.

## II. CELL DEVELOPMENT PROGRAM

The sealed nickel-cadmium cells in the storage battery are the result of a development program intended to effect improvements in two general areas:

(*i*) Production controls on active element manufacture
  (a) Adequate excess capacity of negative electrode
  (b) Individual cell electrode measurements before assembly.
(*ii*) Container enclosure with high integrity
  (a) Corrosion-resistant seal
  (b) Improved welding techniques.

Activity in the first area of the above program was made effective through the cooperation of a nickel-cadmium battery manufacturer, who provided special active elements (cores) in accordance with detailed specifications presented below. For the second area, a special container was developed within Bell Laboratories, full advantage being taken of knowledge and processes resulting from experience in enclosing and sealing electron tubes. After assembly, the cells were subjected to a series of selection and qualification tests; on the basis of the results of electrical measurements made during these tests, satellite batteries were assembled of cells with well-matched characteristics.

## III. ACTIVE ELEMENTS

Special active elements for nickel-cadmium cells, manufactured in accordance with the specifications in Table I, were purchased.

Cores were made according to these specifications in the research laboratory facilities of the battery manufacturer, with careful attention paid to each process used. The weight increase of plaques due to addition of active material was held within narrow limits; the edges of plates were treated to minimize the possibility of puncture of the separator. Positive and negative plates were assembled into cores, in pairs matched with respect to the results of open-cell capacity measurements. The quantity of electrolyte to be used was specified on the basis of core weight, which was closely controlled.

TABLE I—SPECIFICATIONS FOR F-SIZE CORES

| | |
|---|---|
| Positive plate thickness: | $0.0249 \pm 0.0005$ inch |
| Positive plaque porosity: | $79.8 \pm 0.4$ per cent |
| Negative plate thickness: | $0.0200 \pm 0.0007$ inch |
| Negative plaque porosity: | $78.2 \pm 0.6$ per cent |

Positive plate capacity in open cell test: 9.5 ampere hour minimum at approximately 1.35 ampere discharge rate after a charge of 700 milliamperes for 16 hours.

Ratio of the negative plate capacity to positive plate capacity: greater than 1.5 for each cell.

Short-circuit test: all cores to be tested for internal shorts by measuring the resistance between the positive and negative terminals, before the addition of electrolyte.

Separator: Pellon (nylon) individual sheets to be visually examined for flaws.

Copper contamination: no material or equipment, including welding tips, which contains copper to be used in any operation involved in preparing the cells.

Electrolyte: the supplier to provide a recommendation with regard to the quantity and concentration of electrolyte to be added to the cells.

Axial length of core: $3.250 \begin{smallmatrix} +0.000 \\ -0.015 \end{smallmatrix}$ inches.

## IV. CELL CONTAINERS

With one exception, the requirements for the cell container and seal were comparable with the requirements for envelopes used to contain electron tubes. The exception was that the enclosure must be resistant to the potassium hydroxide electrolyte. In order to determine the effect that the electrolyte would have on structural materials, the reaction rates between potassium hydroxide and various metals and insulating materials were measured. Because of time limitations, the majority of these measurements were made at elevated temperatures in order to accelerate the reaction rates. A low reaction rate was observed between the electrolyte and components of the high-alumina ceramic, iron-nickel-cobalt alloy* sealing system, and this system was chosen for the insulator assembly. The remaining design parameters were selected so that the reaction would not cause failure during the time of the Telstar experiment. In addition to the insulator, the enclosure consisted of a cylindrical nickel can and a small nickel-iron alloy tube used for testing and filling purposes. The general appearance of the structure is shown in Fig. 1.

The seal was designed by the Laboratories and fabricated on contract at other locations. Details of the seal are shown in Fig. 2. In order to provide suitable stress balance in the seal and to minimize tolerance problems in fabrication, a configuration was chosen which allowed the metal member to surround conical segments of the ceramic on both the small diameter and the large diameter seal. The bond between the

* Common trade names for this alloy are Kovar and Rodar.

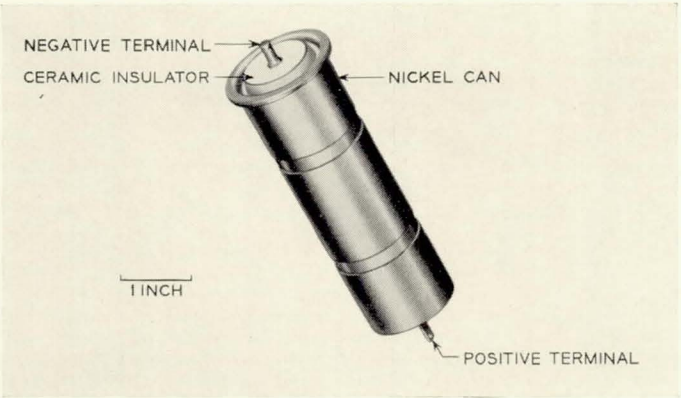


Fig. 1 — Nickel-cadmium cell for spacecraft battery.

ceramic and metal members was made by first metallizing the ceramic with a finely divided mixture of molybdenum and manganese sintered at 1525°C in a wet hydrogen atmosphere. The surfaces were then prepared for brazing by adding approximately 30 milligrams per square inch of electroplated nickel. A nickel-gold alloy requiring a brazing

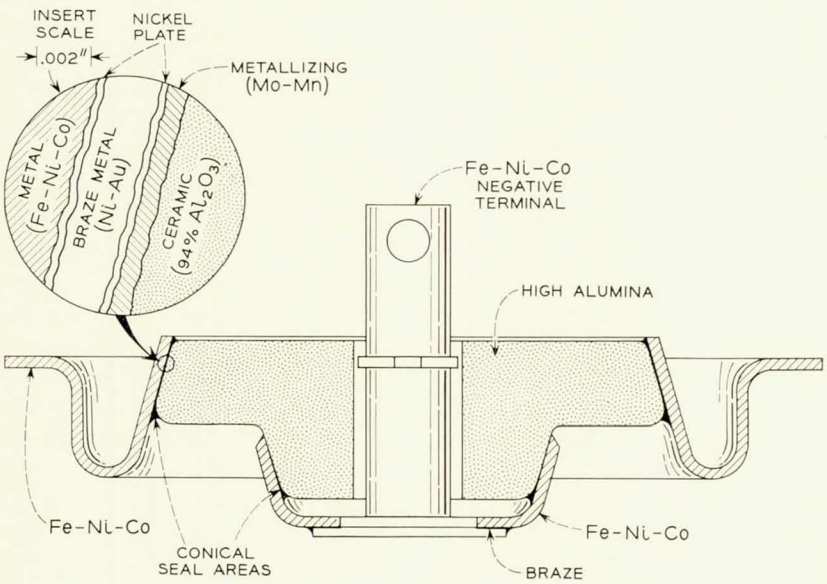


Fig. 2 — Details of ceramic seal.

temperature of approximately 1000°C was used to bond the metallized ceramic to the iron-nickel-cobalt alloy. An additional part later to serve as the negative terminal of the cell was attached to the smaller metal member at the time of the braze. The nickel-gold brazing alloy was chosen in order to avoid copper. Copper, common in other conventional brazing alloys, was considered to be an undesired electrolyte contaminant in cells designed for long life.

The remainder of the container consisted of a cylindrically drawn nickel shell having a flange at the open end with a cylindrical projection coined on the outer surface of the flange. The center of the closed end of the can was pierced to accommodate the tubulation. The tubing was attached to the can by means of a gold braze made in a resistance welder.

The sequence of assembly, as shown in Table II, was initiated by inserting the electrode assembly into the cylindrical can. Then the connector from the positive plate was spot welded to the can as shown in Fig. 3, and the negative connection from the assembly was spot welded to the center terminal of the insulator assembly. The insulator assembly was welded to the flange of the cylindrical can by a resistance weld, using the projection that had been previously formed. A resistance weld was chosen because it provided a positive means of attachment that could be accomplished with a minimum of deformation and with only local heating, thereby eliminating the use of temporary heat sinks and minimizing the chance of damage to the electrode assembly. This weld was performed using a 175-kva welder and a time setting of approximately 1/10 second. If more power had been available, a shorter time cycle would have

TABLE II—SEQUENCE OF ASSEMBLY

| |
|---|
| Preliminary assembly |
| (a) Fabricate seal assembly<br>(b) Fabricate can and tubulation assembly<br>(c) Fabricate electrode assembly |
| Insert electrode assembly in can and tubulation assembly |
| Spot weld electrode connectors to terminals |
| Projection weld seal assembly to flange of can and tubulation assembly |
| Add electrolyte through tubulation |
| Seal tubulation and form positive terminal |
| Compress can to contact electrode assembly |
| Charge and selection test |

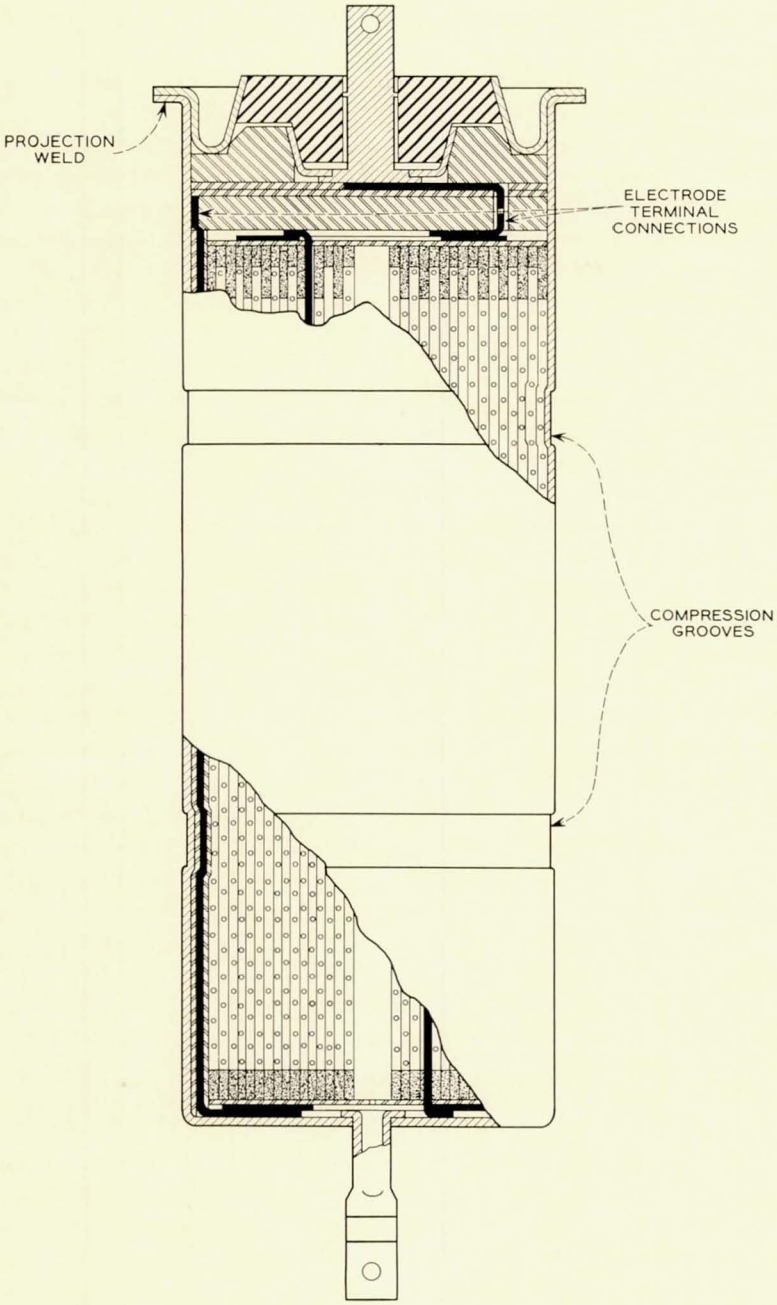


Fig. 3 — Section of completed cell.

been chosen. Cylindrical electrodes were mounted in a die set, and adequate pressure was used to prevent local expulsions.

Next, a carefully metered amount of electrolyte was inserted through the small diameter tubing using a needle type filler. The tubing had an integral gold-clad liner, which was wiped clean after application of electrolyte. Next, the tubing was squeezed flat and sealed by a resistance weld. Thus the final closure was accomplished. By shearing and drilling, the end of the tubulation was formed into a usable positive terminal. Radial compression was applied by a spinning operation to assure a snug fit of the core to the can. The snug fit was used to prevent core motion in the can during the vibration and acceleration of the launch period. Deformation resulting from the compression may be seen as two cylindrical grooves in Fig. 3.

The quality of all closure parts, of the welding operations, and the brazing operations, was evaluated by inspection of metallurgical sections made of sample assemblies. In addition, hydrostatic pressure tests were made to determine the strength of the welds. Each seal assembly and can and tubulation assembly was individually checked for leaks, using helium as a tracer gas and a mass spectrometer as a detector. Similarly, the complete assembly was checked for leaks before the electrolyte was added. The cells were finally sealed with a 50 per cent helium, 50 per cent oxygen atmosphere, with the expectation that tracer techniques could be used on the completed cell. However, after the electrolyte was added, the sensitivity of all types of tracer gas techniques proved to be erratic. It is hypothesized that this behavior is due either to a liquid or solid plug of the electrolyte, or to a compound containing electrolyte that prevented the flow of gas while selectively permitting a seepage of potassium hydroxide liquid. The most sensitive method for detecting leaks after seal-in proved to be the use of hydroxyl ion detectors on external surfaces adjacent to the seal. Tests on the completed container showed that no plastic deformation occurred for internal pressures below 500 pounds per square inch, and that rupture would occur only at appreciably higher pressures. In the event such pressures were generated, no provision was made to prevent destructive rupture.

In life tests of batteries similar to those installed in the satellite, evidence of leakage has been found on some cells. In all cases this leakage appeared to take place in the vicinity of the ceramic-to-metal seal. The design of this seal took into account actual rates of chemical reaction of alkali solutions with the materials used and, while corrosion was expected, the seals were designed so that failure was not anticipated in a two-year interval. Examination of sectional microphotographs of leaking

seals indicated that more rapid attack had taken place in this area than had been anticipated. It was observed that the thickness of the brazing material used in the ceramic-to-metal seal varied from the desired thickness of 2–3 mils to less than 1 mil and to greater than 6 mils. In addition, void areas were found where brazing material was present at both surfaces of the leaking seals. In some instances blisters were discovered between the metallizing and the plating. Leakage observed may have been due to a combination of the expected corrosion of the interface material coupled with fast creepage of electrolyte in void areas internal to the seal. As the voids appreciably reduced the seal length susceptible to corrosion, the time to failure was shorter than anticipated. The completed metal ceramic seals cannot be inspected for continuity of internal interfaces; hence, prevention of internal defects must be established by tolerance control and process inspection.

Experience indicated that when leaks did occur they were small. The dimensions of the material subject to attack were limited by the small circular area of the metal-ceramic interface adjacent to the void, and they were further diminished by the plugs of electrolyte. In most cases the appearance of a carbonate which forms when potassium hydroxide reacts with carbon dioxide in air has been so slight that leaks could not be detected by visual examination even though pH tests of the surface showed the presence of potassium hydroxide. Since the plugging effects observed in the leak-detection experience appeared to limit the flow of gases, it is believed that little gas has been lost from the leaking cells.

## V. SELECTION TESTS

The following tests were performed on each completed cell, in the order shown:

(*i*) Capacity test — At an ambient temperature of 77°F, the cells were charged at 0.6 ampere for a period of 16 hours, then discharged at about the one-ampere rate. This cycle was repeated a minimum of 8 times. The end-of-charge voltage, cell temperature, and cell capacity were measured.

(*ii*) Continuous overcharge test — At an ambient temperature of 77°F the discharged cells were charged for a period of 64 hours at 0.6 ampere. The end-of-charge voltage and cell temperature were measured. The cells were then discharged and capacity was determined.

(*iii*) Self-discharge test — At an ambient temperature of 77°F the cells were again charged at 0.6 ampere for 16 hours. At the end of this period the cells were placed on open circuit for a period of 48 hours.

The cell voltage was measured continuously and the cell capacity determined by a discharge at the one-ampere rate.

(*iv*) Internal resistance test — At an ambient temperature of 77°F the cells were again charged at 0.6 ampere for 16 hours. Following this charge the cells were discharged at the one-ampere rate for 2 hours, after which a 2-ampere, 3-second pulse discharge was performed. The cell voltage was monitored on an oscilloscope to observe the instantaneous voltage change.

(*v*) Capacity test — Test (*i*) was repeated for two cycles at an ambient temperature of 30°F.

(*vi*) Vibration test — The cells were vibrated in the axial direction as shown in Table III. Total time for this test was 4.3 minutes.

(*vii*) Capacity test — Test (*i*) was repeated for 4 cycles at an ambient temperature of 77°F.

(*viii*) Leak test — All cells were tested for leakage using pH indicator paper, which was moistened with distilled water and rubbed over seal and weld.

(*ix*) Selection — For each test, distribution curves were plotted of the test variable (i.e., end-of-charge voltage, capacity, etc.) versus the number of cells. Only those cells which fell into a tight grouping around the variable mean were selected for satellite use.

## VI. QUALIFICATION TESTS

A small sample of cells which passed the selection tests was given the following qualification tests, and then retested electrically:

(*i*) Vibration tests — Selected cells were subjected to 40g vibration in two planes between 5 and 2000 cps for 1.5 hours.

(*ii*) Acceleration tests — After vibration tests, the cells were subjected to 30-g acceleration in two planes for $\frac{1}{2}$ hour.

## VII. CELL CHARACTERISTICS

Of 513 nickel-cadmium cells constructed and tested as described above, only two were found to be defective. One of these had an ob-

TABLE III

| Frequency Range, cps | Test Duration, Seconds | Acceleration, g, 0 to Peak |
|---|---|---|
| 7–25 | 30 | 1.5 |
| 25–60 | 40 | 14.0 |
| 60–2000 | 75 | 7.0 |
| 550–650 | 30 | 14.0 |

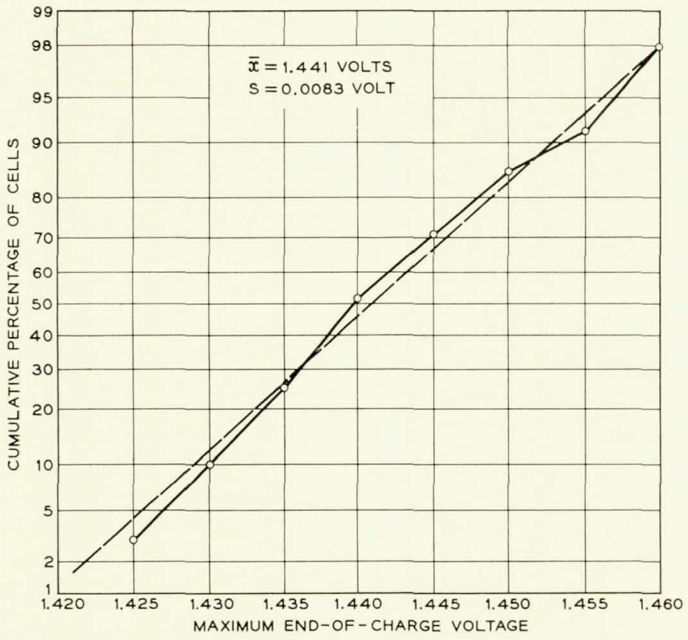


Fig. 4 — End-of-charge voltage distribution, 200 nickel-cadmium cells. Temperature 77°F, 0.6-ampere charge current.

viously cracked seal which caused a leak. The second developed a short circuit during the selection tests, and was considered to be the sole operational failure during selection testing. Only the 391 cells produced in the later stage of seal development were considered suitable for satellite batteries. The first 122 had seals of an earlier design which was considered to be less satisfactory.

Electrically, all cells (except the two noted above) showed adequate uniformity in the important measured quantities. The distribution charts showed normal distribution with satisfactory central values, which changed only slightly from test to test of the selection sequence. An example of a cumulative distribution chart for end-of-charge voltage of 200 cells is shown in Fig. 4. The ordinate scale on this figure is one for which a normal distribution plots a straight line.

A summary of the results of the electrical measurements of all cells at 77°F ambient temperature is as follows:

| | |
|---|---|
| Capacity | 6.2 ± 0.7 ampere hours |
| End-of-charge voltage at 0.6 ampere | 1.45 ± 0.025 volts |

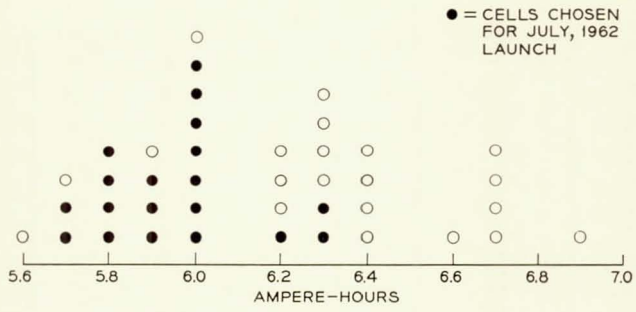


Fig. 5 — Capacity distribution, 40 nickel-cadmium cells.

| | |
|---|---|
| Capacity loss on open circuit | 0.8 ± 0.2 ampere hours (48 hours) |
| Internal resistance | 28.0 ± 4.0 milliohms |

Fig. 5 shows a typical chart of capacity measurements for the 40 cells from which the Telstar spacecraft battery was selected. The cells chosen for use were those whose capacities had the tightest grouping around a central value, while also showing reasonably tight grouping around central values of the other electrical quantities measured.

Fig. 6 presents what are commonly known as Tafel curves, for typical cells. These show the end-of-charge voltage as a function of overcharge current at various temperatures between −15°F and 120°F. The curve for 0°F has been extended to show the typical rapid rise of cell voltage which occurs when the overcharge current exceeds the safe value for the temperature at which the cell is operating. The limit to overcharge current is shown, for other temperatures, by the upper ends of the curves. Even at a temperature as low as 30°F the cells can accept the full output current of the solar cell power plant, although they never receive this full amount, nor are they expected to operate at this low temperature.

Ampere-hour charge efficiency of the cells is of general interest for two kinds of operation: (a) charging a completely discharged cell and (b) replacing a partial discharge removed from a fully charged cell. However, only the second of these operations is of importance to spacecraft operation, since the satellite's battery normally is only partially discharged. Representative data from significant efficiency measurements are presented in Table IV.

These data are believed to be descriptive of spacecraft battery performance. The sequence of measurement operations for each test was as follows:

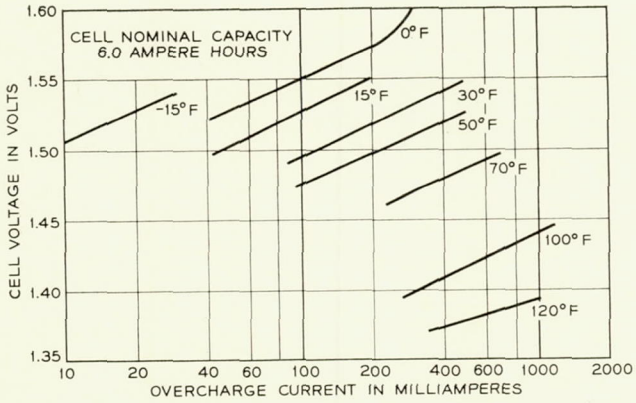


Fig. 6 — Nickel-cadmium cell Tafel characteristics.

(a) Charge, then discharge, all cells to measure normal capacity
(b) Charge all cells fully
(c) Discharge all cells at 1 ampere for 2.5 hours
(d) Recharge all cells at 0.200 ampere for time indicated
(e) Repeat (c), (d) nine times
(f) Discharge all cells to measure remaining capacity.

The above procedure divided capacity-measurement uncertainties among ten charge-discharge cycles, and resulted in efficiency data which had a spread of only a few per cent among all cells measured. Further, the procedure simulated (except for a difference in the time scale) a 2.5-ampere-hour discharge occurring during several successive orbits, followed by recharge during subsequent nonvisible orbits, at about the spacecraft's normal charge current.

The high efficiency noted in the 12-hour charge is actually an incremental efficiency; at the end of this charge-discharge sequence the battery was no longer fully charged. The lower efficiencies of the other tests reflect extra ampere-hours required to recharge the battery more

TABLE IV — AMPERE-HOUR CHARGE EFFICIENCY (REPLACING A PARTIAL DISCHARGE)

| Test No. | Temp. °F | Charge, Amperes | Charge Time, Hours | Average Charge Efficiency |
|---|---|---|---|---|
| 1 | 60 | 0.200 | 12 | 97% |
| 2 | 60 | 0.200 | 14 | 88% |
| 3 | 60 | 0.200 | 15 | 82% |
| 4 | 60 | 0.200 | 16 | 77% |

nearly completely. Full charge was obtained only after about 14 hours of recharge time. For this reason, a charge efficiency of 85 per cent is a conservative value to use in calculating the charge-discharge balance of the battery.

## VIII. LIFE TESTS

At the time of launch of the Telstar satellite, many thousands of cell-hours of operation had been accumulated as a result of both selection tests of many cells and many experimental studies with a limited number of cells. However, the failure mechanisms of the spacecraft sealed nickel-cadmium cells are not yet known, so that significant life estimates will require data from operation over extended periods of time. Such data will be obtained from several batteries on life test.

One battery of 20 cells was placed on a simulated orbital cycle at room temperature in November, 1961. The cells of this battery had early seals, not used for satellites, but otherwise they were identical with those used for all models of the satellite, including that in orbit. This battery receives approximately 9 charge-discharge cycles per day, as shown in the load profile of Fig. 7. The three deep discharges represent use of the communications equipment during eclipse; the five shallow discharges represent subsequent eclipses when the beacon and telemetry constitute the loads on the power system.

A second battery of 22 cells with later, improved, seals was placed

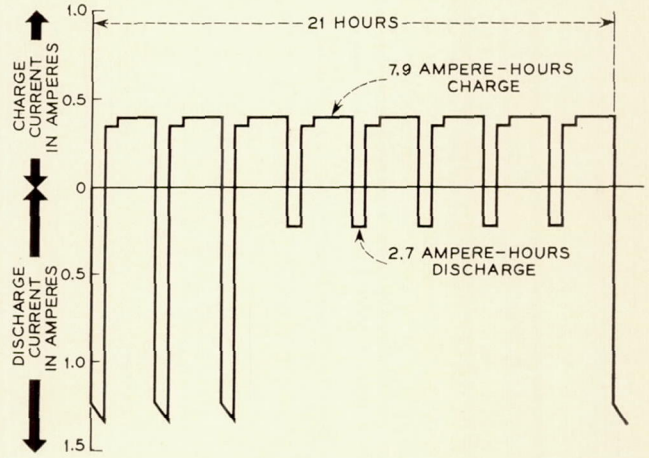


Fig. 7 — Load profile — simulated orbital cycle.

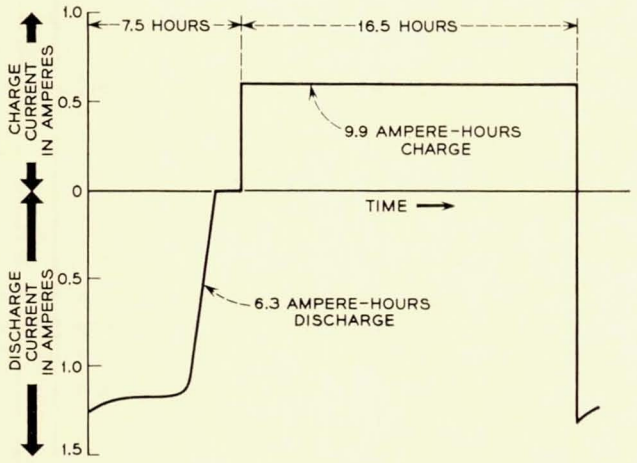


Fig. 8 — Load profile — accelerated life cycle.

on cycle test in April, 1962. This battery receives daily a complete discharge followed by a substantial overcharge, as shown in Fig. 8. This cycle was intended to provide an accelerated life test, and is identical to those of the selection tests; cells of this battery had received 22 selection-test cycles before being placed on life test.

During June, 1962, the battery on the simulated orbital cycle was removed from cycle test for measurements to answer questions raised during the spacecraft tests. Before being returned to the life test cycle all cells were examined for leaks, as had been done periodically since the life test was initiated. An indication of leakage of potassium hydroxide was found around the seals of 5 of the cells. Similar leak tests were made on the cells of the battery on accelerated life test, and two indications of leakage were found. These circumstances are summarized in Table V.

Both batteries were given several deep discharge cycles, after which several other indications of leak were found in cells on orbital life cycle,

TABLE V—JUNE, 1962, RESULTS

| 20 Cells, Orbital Life cycle | | 22 Cells, Accelerated Life Cycle |
|---|---|---|
| 217 | Test days | 43 |
| 1753 | Cycles | 65 |
| 5 | No. cells with indication of leak | 2 |

TABLE VI

| Group No. | Depth of Discharge | Charge Time, Hours | Discharge Time, Hours* |
|---|---|---|---|
| 1 | 100% | 16.5 | 7.5 |
| 2 | 75% | 12 | 4 |
| 3 | 25% | 4 | 1.5 |
| 4 | Continuous overcharge at 0.6 ampere | | |

* Discharge through 1-ohm resistor.

and one other in a cell on the accelerated life cycle. Capacity measurements made during these discharges showed no loss of capacity from that measured on the cells during selection tests.

After the finding of indications of leakage in June, the battery on accelerated life cycle was divided into 4 cell groups, to determine, if possible, the effects of different modes of operation. These 4 groups were operated as shown by Table VI.

New cells previously subjected only to the selection test cycling were added to these groups as shown in Table VII.

In October, 1962, all the above cells were discharged to measure capacity. All yielded the capacity measured during their selection tests. The original cells had 6 months of operation, the new ones four months, all in addition to the selection tests. Eight of the original cells gave a positive indication to leak test, as did seven of the new cells. These seven were distributed among the four groups with no clear correlation between mode of operation and tendency to leak.

Most of the leaks discussed above have not resulted in visual evidence of the effect of potassium hydroxide reaching the open air. Thus the loss of electrolyte by these cells is quite small, although it is enough to cause a blue coloration of the indicator paper used in the leak test. As discussed in connection with the cell enclosure, it is believed that loss of evolved gas is also small.

In December, 1962, after more than one year of operation, all cells on

TABLE VII

| Group No. | Depth of Discharge | Original Cells | New Cells | Total |
|---|---|---|---|---|
| 1 | 100% | 5 | 7 | 12 |
| 2 | 75% | 5 | 5 | 10 |
| 3 | 25% | 5 | 5 | 10 |
| 4 | Continuous overcharge, 0.6 ampere | 5 | 8 | 13 |

simulated orbital cycle, with their early seals, showed indications of leak. Less than half of the cells with later seals showed indications of leak. However, three of the cells in group 1 (Table VI) were found to have distorted seal assemblies, indicating that internal pressure had built up to dangerously high levels. End-of-charge voltages on these, as well as on several nondistorted cells of group 1, had risen to 1.5 volts. It has been determined that these cell failures were coincident with the evolution of hydrogen gas, although the cause of this evolution is not yet known.

Thus the first cell failures have occurred on the accelerated life cycle (100 per cent discharge daily). All cycle tests are being continued, and it is anticipated that useful data on both length of life and mechanism of failure will eventually be acquired. As yet, however, there are no significant data on which to estimate cell life in a satellite environment. Telemetry data from the satellite continued to show normal battery performance through January, 1963.

# The Satellite Traveling-Wave Tube

By M. G. BODMER, J. P. LAICO, E. G. OLSEN, and A. T. ROSS

(Manuscript received March 5, 1963)

*The traveling-wave tube amplifier described provides a minimum output power of 3.5 watts at 4.0 to 4.2 gc. Design aspects that lead to lifetimes in excess of 10 years and to tube efficiencies between 35 to 40 per cent are discussed. The tube is focused by an improved version of the single-reversal magnetic circuit. Performance data pertinent to this particular satellite operation are shown. Highlights from the final production run and the subsequent life test serve to illustrate the care with which this TWT has been built.*

## I. INTRODUCTION

The output power amplifier in the Telstar spacecraft microwave repeater operates near 4 gc; the amplifier is required to accept a fractional milliwatt signal distributed over approximately 100 megacycles bandwidth and amplify it some 4000 times to provide an output of several watts. In the satellite, this power amplifier is the major power utilizing device, and its efficiency is controlling in the design of the satellite and of the system. Of the possible microwave devices which might be considered, the traveling-wave tube is outstandingly well suited to the application. The broad bandwidth and high gain is such that only a single tube is necessary. The efficiency is as high as or higher than that of competitive devices, and a considerable history exists to suggest that very long life and high reliability can be achieved.

This paper describes the development of the M4041 traveling-wave tube for this application. The design methods for traveling-wave tubes for radio relay applications are well known and can be found in such texts as Ref. 1; therefore, discussion will be limited to those aspects which are peculiar to this application. Since reliability is the most important aspect in the Telstar experiment, considerable attention will be paid to this aspect of the design. The development of the tube was carried on in five phases. Initially, there was a design phase in which close interaction with the systems area produced a final amplifier specification



Bell Sys. Tech. J., Vol. 3 Jan. 1963
p 1703-1748 refer (See N64-11079 02-09)

which was compatible with other parts of the system. This was followed by a qualification period, during which development models of the tube were subjected to extensive electrical and mechanical tests at levels in excess of the environment anticipated in the application. Next, a group of tubes was fabricated under the best available clean-room conditions, which included extensive engineering checks on the details of the fabrication. These tubes were tested and placed on aging racks at the established nominal operating conditions. Finally, from this group of tubes, those showing the most uniform and stable characteristics were selected and married to their final power supplies for incorporation into actual satellites. Each of these phases will be discussed in the text.

In considering the design and qualification phases of the development, it must be remembered that this amplifier is a relatively complex package, and it is therefore not possible to fabricate a sufficient number of models to permit extensive use of statistical methods and stress aging. It was therefore necessary to place great emphasis on design integrity: that is, upon the use of techniques which had been established as reliable in previous devices. While nearly every one of the electron tubes which have been developed by the Laboratories has contributed in some way to our knowledge, three developments are peculiarly related to the Telstar spacecraft application. The earliest of these was the development of the 175HQ, the pentode used in the present submarine cable repeaters. During this development, a large number of controlled laboratory experiments were carried out, some extending to 100,000 hours of real-time testing. These tests have given us a great deal of information concerning the effect of impurities and processing on cathode life. It was during the development of this tube that many of the techniques of building superclean tubes for applications requiring high reliability were developed. In particular, the concepts of aging and selection to avoid manufacturing freaks appeared. There are currently 1608 such tubes in underwater applications, and these have accumulated over 60,000,000 tube hours of operation without failure. The second development which is of specific interest is that of the M1789 traveling-wave tube. This is a 5-watt amplifier developed for a 6-gc transcontinental radio relay. This tube is currently in production, and field experience has given us a great deal of information concerning failure mechanisms in traveling-wave amplifiers. Towards the end of the development, a group of final design tubes were fabricated, under what were then considered clean conditions; and from these, 12 tubes were selected on the basis of cathode activity for a life experiment. After some six years of operation, 11 of these tubes are still operating satisfactorily. (The twelfth tube was accidentally lost during

a modification of the laboratory building.) This experiment suggests that our selection techniques can be successfully applied to a traveling-wave amplifier. These tube developments show that it is possible to develop tubes with extremely long life and with high reliability. The third development relates to the rigors of the launch environment. The M1958 traveling-wave amplifier is a 9-gc tube developed for a missile guidance system. In this system, the tube is mounted in the missile-borne equipment and must not only survive, but also operate satisfactorily, during the shock and vibration of the launch. In more than 100 launches, no failures of this device have been observed. In the design of the M4041 traveling-wave tube, the techniques developed for these previous devices have been employed wherever possible. Where the specialized application required new design approaches, these have been extensively qualified during this development.

## II. SYSTEM REQUIREMENTS

Table I lists the final requirements placed upon the performance of the M4041 traveling-wave amplifier. The table lists not only specific maximum or minimum values for parameters, but also indicates other design constraints necessary to the application.

## III. TUBE DESIGN PARAMETERS

Previous experience has established the practical range of a number of tube parameters. From this experience in using conventional traveling-wave tube analysis, a three-dimensional set of tube designs was computed using the following three parameter ranges:

$$\gamma a = 1.0\text{–}1.6$$

$$V_{helix} = 1000\text{–}2500 \text{ v}$$

$$I_0 = 5.0\text{–}20 \text{ ma.}$$

In these designs, a number of restrictions were imposed, based on past experience and on engineering judgment. These restrictions are listed in Table II and will be discussed in detail in subsequent sections. From this field of designs, a final set of parameters was chosen as the optimum, and this is summarized in Table III, where $\gamma$ = radial propagation constant; $a$ = helix radius; $K = 2\pi/\lambda_0$ and $\lambda_0$ = free-space wavelength; $C$ = gain parameter from Pierce; and $QC$ = space charge parameter from Pierce.

TABLE I — SYSTEM REQUIREMENTS FOR M4041 TWT

| | |
|---|---|
| Life (average before failure) | In excess of 10 years |
| Operating frequency band<br>Beacon at 4.08 gc<br>Signal at 4.17 gc ± 25 mc | 4.0–4.2 gc |
| Output power (saturated) | $P_0$ = 3.5 w minimum |
| Input drive available | $P_{in}$ = 0 dbm maximum |
| Total dc power available | $P_{dc}$ = 16 w |

Weight of TWT
To be minimized along with its associated equipment — like the solar plant with its support structure, storage batteries, power supply, etc.

Hot matches at optimized $V_{helix}$ and $I_0$
Input better than 18-db return loss in band (VSWR = 1.3)
Output better than 10-db return loss in band (VSWR = 1.9)
Output better than 5-db return loss over a 20% band (VSWR = 3.5)

Short circuit stability with $V_{helix}$ reduced 75 volts from operating point*

Tube must operate with all voltages ±3% from set nominal value (because of long time drift in regulated 16-v supply)

Noise figure better than 30 db

AM to PM conversion less than 12°/db

Cooling of collector by conduction to housing and through waveguide to remainder of electronics canister

Completed package to withstand environmental conditions during launch, in orbit, and eclipse

Vibration — tube inoperative; 15-50-15 cps, 0.3-inch displacement 50-2000-50 cps at 20 g in all 3 directions at a sweep rate of one octave per minute

Thermal cycling ±15°F to 90°F to 15°F.

* The operating point for best efficiency was chosen at helix overvoltage ($\Delta V_{helix} \approx 150$ volts) where amplifier gain is considerably reduced from the low-level synchronous condition. Reducing the helix voltage from the operating point automatically increases the over-all gain and reduces short circuit stability.

TABLE II — DESIGN PARAMETERS FOR M4041 TWT

| | |
|---|---|
| Cathode current density | <85 ma/cm² |
| Beam area convergence | <25 |
| Beam perveance | <0.3 microperv |
| Voltages | <2000 volts |
| Magnetic flux density | <550 gauss |
| Saturated output power at output flange | >3.5 watts |
| Computed depressed efficiency (not including heater) | >35% |
| Intercept currents | <1% |

TABLE III — SUMMARY OF M4041 DESIGN

Helix Dimensions

| | |
|---|---|
| Mean diameter | 90 mils |
| Wire diameter | 10 mils |
| Turns per inch | 49 |
| Pitch | 20.4 mils |
| Active length | 5.75 inches |

Voltages and Currents

| | Voltage | Current |
|---|---|---|
| At 4.0 watts output cathode | 0 | 17.4 ma |
| Beam forming electrode | 0 | 0 |
| Accelerator | 1800 | <0.1 ma |
| Helix (overvoltage) | 1550 | <0.15 ma |
| Collector | 750 | >17.15 ma |
| Heater power | | 1.4 watts (730°C true at cathode) |

TWT Parameters at Midband (4.1 gc)

$\gamma a = 1.33$
$Ka = 0.098$
$C = 0.063$
$QC = 0.25$
$N$ (number of λ's on helix) 26
Dielectric loading factor 0.86
Impedance reduction factor 0.4

Electron gun:

Gun type — converging Pierce gun
Cathode type — high purity nickel with 0.1% zirconium; base coating low-density double carbonate
Cathode current density 85 ma/cm² ($I_k$ = 17.4 ma)
Cathode diameter 0.192 inch
Convergence half-angle 12° 45′
Cathode radius of curvature ($\bar{r}_c$) 0.435 inch
Anode radius of curvature ($\bar{r}_a$) 0.176 inch
$\bar{r}_c/\bar{r}_a = 2.48$.

## IV. DESIGN OF THE TRAVELING-WAVE TUBE

From the foregoing specification, it is apparent that the M4041 is, as might be expected from the reliability required in the application, a conservative design. On the other hand, if the goals in life and efficiency are met, the tube will represent the state-of-the-art in these parameters.

Fig. 1 shows a photograph of the completed traveling-wave tube amplifier. The functional parts — the TWT, the magnets with their respective pole-pieces, and the RF couplers — are displayed in their relative positions. The magnetic design used is a single-reversal circuit. It consists basically of two cylindrical magnets charged with the same polarity at the center plane and separated by a septum, the field reversal pole-piece. The tube is held in alignment with the magnets through

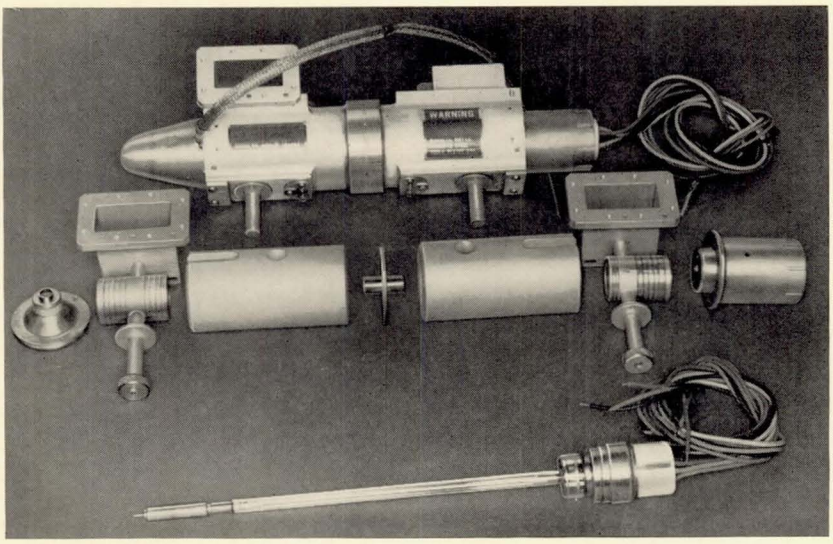


Fig. 1 — Packaged TWT amplifier with a layout of its major functional components.

reference surfaces in both gun and collector pole-pieces. RF connections to the TWT are established by externally tuned reentrant coaxial couplers which, in turn, are matched to the rectangular waveguide.

In this section, the tube is broken down into its individual parts of gun, helix, collector, envelope and focusing circuit, and each part with its major design parameters is discussed separately.

### 4.1 *The Gun*

The basic Pierce-type gun is characterized by three major parameters: perveance, convergence, and cathode current density. To maintain the concept of "proven integrity," these parameters were limited to the corresponding values of the 6-gc radio relay tube, our main source of life test data. The limiting values are 0.3 microperv for perveance and 25 for the area convergence. The choice of the cathode current density limit warrants a separate discussion which follows this paragraph.

Life tests on 12 M1789, 5-watt TWT's, developed for a 6-gc radio relay, had in 1960 exceeded without failure an individual accumulated life of 35,000 hours at a cathode current density of 210 ma/cm$^2$. Analyses of the life test data compiled over the past six years showed a slow, but steady, increase in accelerator and helix interception with constant cathode current in the majority of the 12 M1789 TWT's on life test, by a

factor of as much as five. This has been interpreted as a small degradation of the beam profile within the gun, caused by small areas of lowered activity on the cathode. Their effect is an increase of the transverse velocities of the electrons, producing crossovers and consequently an increase of the final beam diameter. This type of beam degradation is aggravated by increasing the area convergence and perveance to higher values. Either increase results in a gun which is inherently less stable and more sensitive to aberration in the beam formation.

The cathode current density chosen has a first-order effect on the life capability of the TWT. From our past life tests on TWT's, we have observed that the average life is highly dependent on the actual cathode temperature; a decrease of 25°C will, in general, double the life of the cathode. Similar data have been obtained with microwave triodes, using a considerably larger universe for testing. The cathode temperature, in turn, is dependent on cathode current density and the work function of the coating. In Fig. 2, these relations are approximated by a line of constant slope; a lower work function moves the line to the right, a higher work function to the left. We cannot measure the work function in completed tubes, but we have a point which represents our tube art of several years ago. In our final life test, all M1789 TWT's had exceeded 35,000 hours in 1960. This point is plotted at the proper cathode current density in Fig. 2 and a line with the proper constant slope drawn through it. This curve was used as our design basis and is quite conservative, since not all tubes will fail at one time. For a ten-year life, the current density should be less than 85 ma/cm$^2$. Since that time, most of these same tubes have passed 50,000 hours (however, one envelope broke due to an interruption of the cooling air). The graph has been revised accordingly (1962). It must be pointed out that our area of experience is limited and that, in the interest of conservatism, the extrapolations indicated by the dashed part of the line should be used with caution at the present time.

In choosing the cathode base material for the M4041, a number of factors must be considered. Most important in this application are questions of rate of activation, sublimation and coating adherence. Of the 12 M1789 TWT's in the life test mentioned earlier, several exhibited internal arcing, usually between 5000 and 20,000 hours of operating life. This arcing is attributed to a build-up of a conducting film on the electrode insulators. The film is believed to be due in part to sublimation of the additive from the base nickel of the cathode. This problem is distinct from those encountered in gridded tubes like the submarine cable pentode, just as interface resistance does not influence the choice in this case. Several alloys were considered for the cathode base. The final choice was a pure nickel with a single 0.1 per cent Zr additive. It is produced

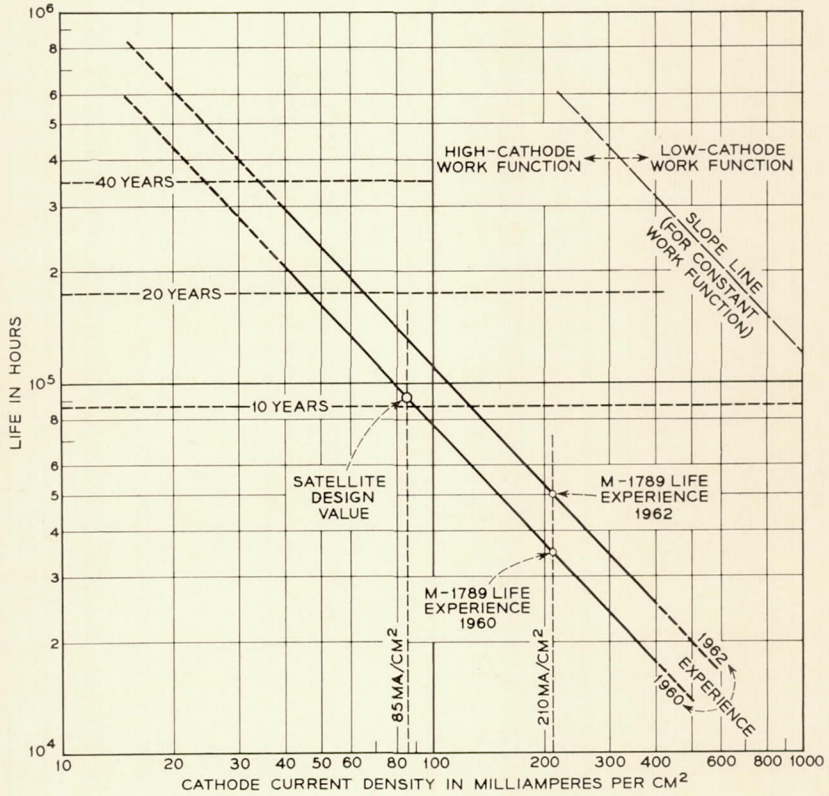


Fig. 2 — Average life expectancy vs cathode current density.

in this Laboratory[2] under conditions in which impurities, particularly carbon, are held to less than 0.005 per cent. The Zr additive as a reducing agent has the advantage of producing little or no sublimation. In addition, the production of donors is not limited by the diffusion of the reducing agent, but by the chemical reaction rate of the coating. The thickness of the alloy was chosen as 0.040 inch, which should give at 730°C a 100 per cent depletion of the coating with an 89 per cent depletion of the Zr after 19 years,[3] as shown in Fig. 3. This represents a safety margin of nine years over the expected tube life, a needed guarantee, since a tube will fail long before complete exhaustion of the cathode coating. As the coating becomes thin, the emission becomes nonuniform and the beam transmission is impaired. This results in excessive heating of the helix and subsequent further deactivation of the cathode through

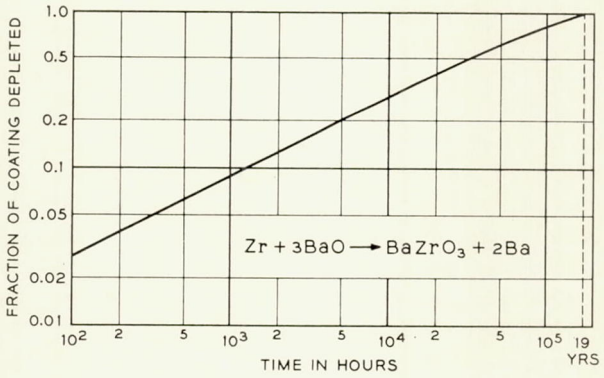


Fig. 3 — Calculated depletion of oxide coating on 0.1 per cent Zr-nickel base. Calculations are based on the following numbers, corresponding to values for M4041 tube:

| | |
|---|---|
| thickness of nickel base | 0.040 inch |
| thickness of coating | 0.0015 inch |
| density of coating | 1.1 gm/cm³ |
| cathode temperature | 730°C, true. |

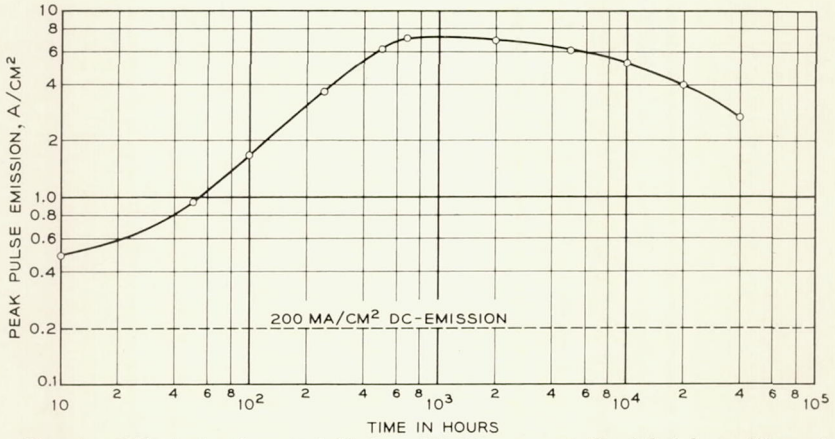


Fig. 4 — Life tests of control diodes with 0.1 per cent Zr-nickel base. Normal operating condition 200 ma/cm² dc, cathode temperature 740°C true. Activity measured by superimposing pulse directly over dc.

the released gases. It is predicted that uniform emission will be maintained at least to the design figure of ten years. This estimate is supported by tests with diodes constructed with this alloy, which have been operating close to six years without noticeable decreases in emission. Fig. 4 gives the average peak pulse emission versus elapsed time which has been

obtained in diode testers with this alloy in recent tests.[2] Beyond choosing a low sublimation rate base nickel, a maximum voltage limit of 2000 volts per electrode was imposed and all possible leakage paths were lengthened and shielded. These steps were taken because some of the leakage may be due to the deposition of barium from the coating.

The emitter is physically in the form of a button, machined precisely to shape. The surface on which the cathode coating is to be applied is liquid-honed with calcium oxide powder to provide a roughened area to facilitate adherence. Calcium oxide is used because it is chemically compatible with the cathode coating materials, should any particles be embedded. A combined coating of barium and strontium carbonates is machine sprayed on the roughened surface. The density of the coating is held to $1.10 \pm 0.1$ gm/cm$^3$, equivalent to a thickness of $1.5 \pm 0.10$ mils.

Structurally, the gun is designed in two sections, as shown in Fig. 5. One section, which might be considered a chassis, consists of two molybdenum focusing electrodes — the beam-forming electrode and the accelerating electrode — plus the molybdenum cathode-support sleeve, all of which are concentrically aligned and supported from a cupped molybdenum base. Support for the focusing electrodes from the base is obtained by glazing to three Alsimag 475 (zircon body) ceramic tubes,

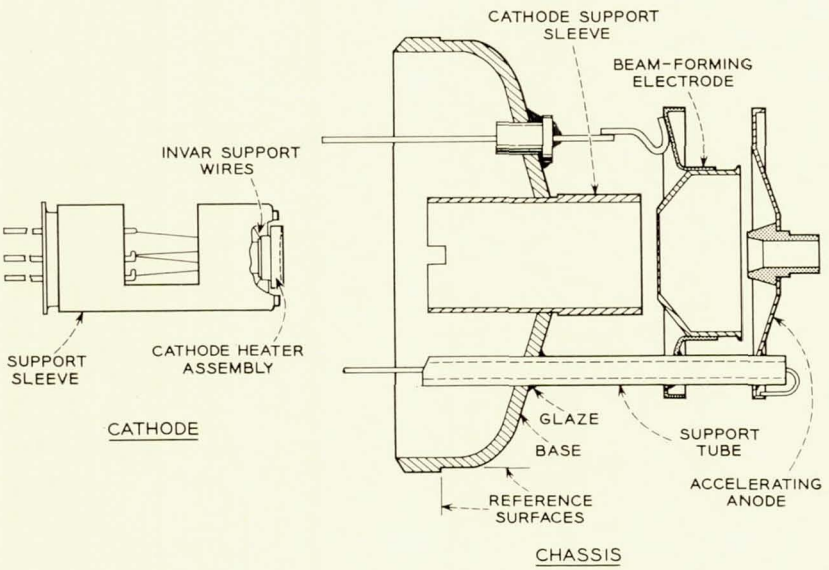


Fig. 5 — Gun assembly.

which also serve to insulate these electrodes. The cathode support sleeve is brazed concentric to the reference surface machined on the base. Tolerances in tenths of mils are readily held in concentricity, squareness and axial dimensions (see Fig. 5). These materials have compatible thermal expansions, are structurally stable, and are capable of withstanding thermal shock, rigorous cleaning, high-temperature outgassing, and vigorous vibrating.

The inner section consists of a cathode and heater mounted in a sleeve. The sleeve serves a double purpose. Its inside diameter encloses and supports the cathode heater assembly by means of fine Invar wires, while its outside diameter is machined to slide snugly, by selection, within the cathode support sleeve of the chassis.

The heater is one of the principal power consuming elements of the tube. It is therefore important to minimize this power, or else the over-all efficiency will be degraded. By virtue of the unique design,* in which the cathode is suspended by fine wires, and a minimized radiating area of the cathode body, a power of 1.4 watts is sufficient to heat the 0.192-inch diameter emitting surface of the cathode to an operating temperature of 730°C.

### 4.2 *The Helix*

The interaction efficiency of the TWT depends to a large degree on the helix itself, even if the beam parameters are optimized. In early prototypes, the depressed collector efficiency averaged around 27 to 30 per cent. In the final series of tubes, this value had climbed to 36–40 per cent. The only changes made were: the reduction of the cold loss, the increase of the dielectric loading factor and, finally, the optimization of the shape and length of the sprayed loss pattern. The cold loss of the 6-inch helix averaged 4.2 db; this value was reduced to 2.7 db with careful copper plating of the helix and subsequent sintering.

The original helix support was provided by three round F66 steatite rods. They were replaced by grooved rods of the same material, as illustrated in Fig. 6. Most of the dielectric material has been removed from the vicinity of the helix wire, where the RF fields are the strongest. The dielectric loading factor, which is computed from the low-current synchronous helix voltage, increased from 0.81 to 0.86. As a consequence, the helix turns-per-inch (TPI) was increased from 46 to 49 to maintain the same helix voltage.

The original loss section was about 2 inches long, with a 1.5-inch section where no net gain could be obtained, and started 1.5 inches from

* To be described in a subsequent paper.

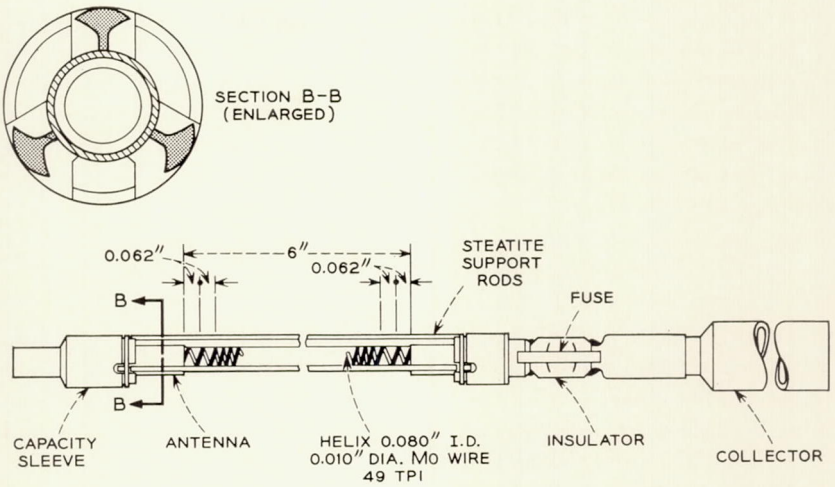


Fig. 6 — Helix assembly, showing cross section with special undercut F66 ceramic support rods.

the input coupler. It was found that the efficiency continued to improve as this section was shortened and moved closer to the input, as long as enough gain was maintained in the input section to establish the slow wave. The final loss pattern, as measured on a completed helix, is shown in Fig. 7. Moving the loss section towards the input and shortening it led to a considerable increase in the gain of the output section, where a maximum low-level gain of 46 to 49 db is produced. Since the tube must be short-circuit stable, this imposes a tremendous requirement on the return loss of the output edge of the loss pattern and the uniformity of the helix near this edge. A return loss of 52 db or more would have been desirable. It proved to be extremely difficult to maintain a return loss of better than 46 db. The short-circuit stability test was the most serious shrinkage factor on otherwise acceptable tubes for flight. Fig. 8 shows the hot and cold output match for an acceptable and a rejected tube, measured when the voltages are adjusted for maximum low-level gain.

The physical embodiment of the helix consists of a winding of 10-mil diameter molybdenum wire, wound with an inside diameter of 80 mils and a length of 6 inches at 49 TPI, except for two turns at each end which are at 66 TPI. Each turn of the winding is glazed to each of the three F66 steatite ceramic rods (spaced 120° apart) and then it is copper plated. After this, attenuation in the form of the aquadag is sprayed on. Fig. 9 shows schematically the means for applying and controlling this deposit.

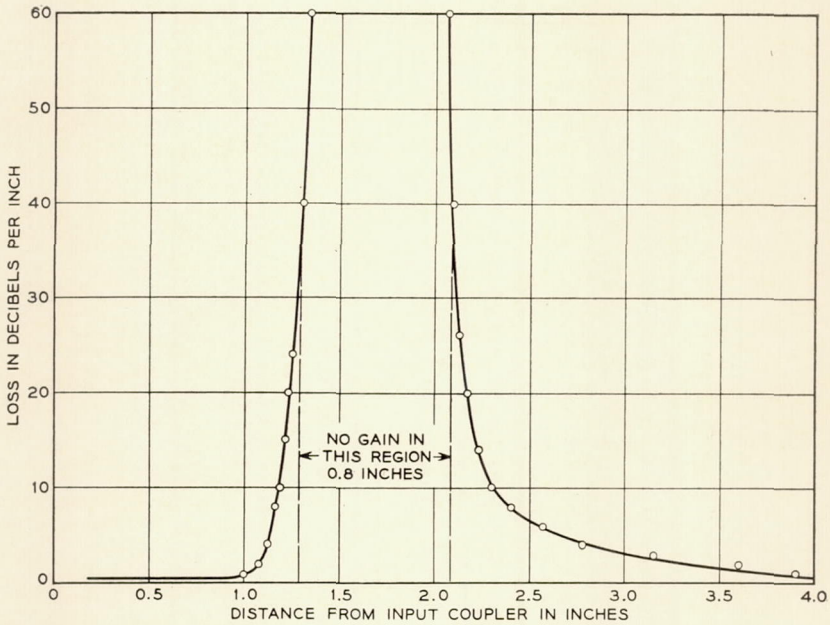


Fig. 7 — Final helix loss patterns of sprayed aquadag (intrinsic loss with Cu plating 2.78 db; total loss 83 db).

The glazed helix structure is shown in Fig. 6. The helix wire is wound to a maximum pitch variation of ±1 per cent (±0.0002 inch). Techniques developed at these Laboratories for fabricating glazed helices[4] make it possible to hold the outside diameter of the helix structure, defined by the outside of the ceramic support rods, to ±0.00075 inch. This is a maximum of 1.4 mils smaller than the inside bore diameter of the glass envelope within which it will be assembled later on. This close fit not only precisely aligns the helix, but also provides a support that enhances its resistance to shock and vibration. The helix structure is capable of withstanding thermal shock, extensive cleaning procedures, and outgassing in vacuum. The outgassing temperature is limited by the vapor pressure of the copper plating to 650°C.

### 4.3 *The Collector*

The collector in a high-efficiency TWT plays an important part. To improve the efficiency, the collector voltage is depressed below that of the helix until the maximum tolerable helix or accelerator interception is reached. For long-life tubes, it is desirable to keep this interception at

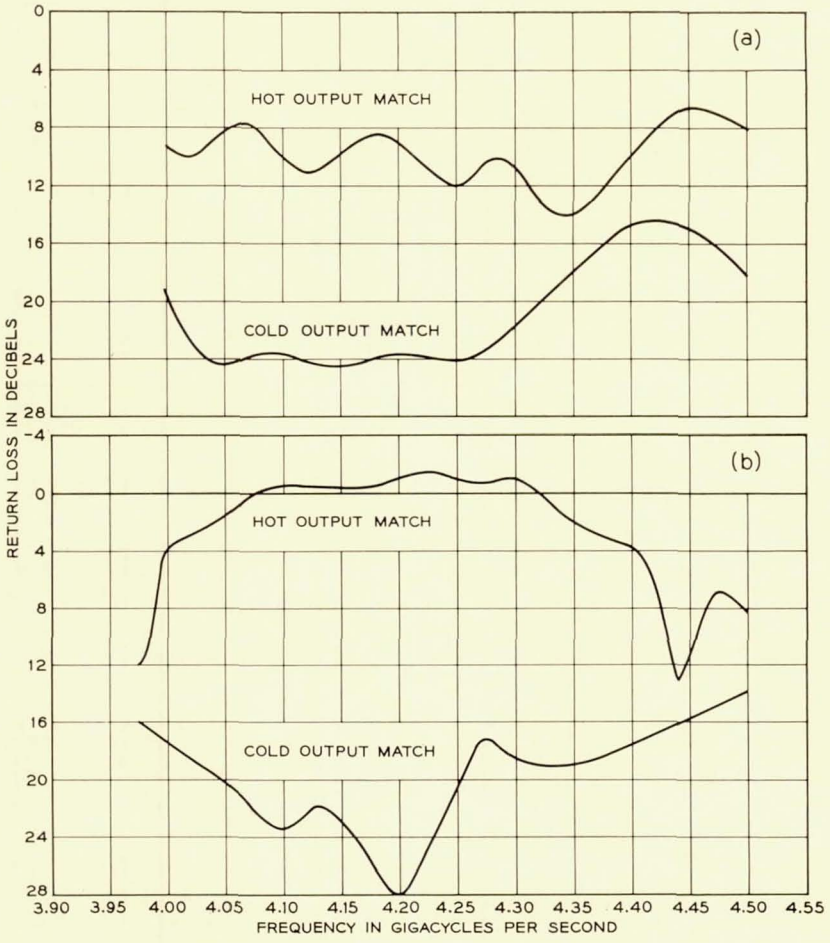


Fig. 8 — M4041, output matches measured at waveguide flange: (a) acceptable tube, (b) rejected tube (note return gain in band center).

the beginning of life to a maximum of 1 per cent of the beam current, since this interception increases slowly but steadily throughout life.

In Fig. 10, the helix current is shown as a function of collector voltage with no RF drive and with a drive to saturate the output power. When the collector voltage is depressed below the helix, the helix interception rises rapidly until it reaches a plateau. This current, called back-streaming, consists largely of secondary or reflected electrons, which finally terminate on the helix or accelerator. In addition, RF feedback that can

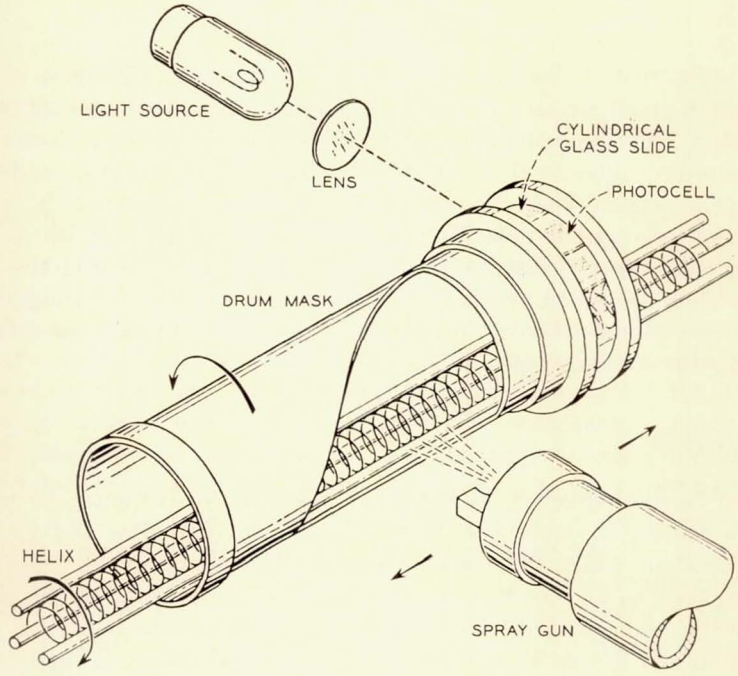


Fig. 9 — Schematic diagram of machine used for spraying aquadag loss section on helix.

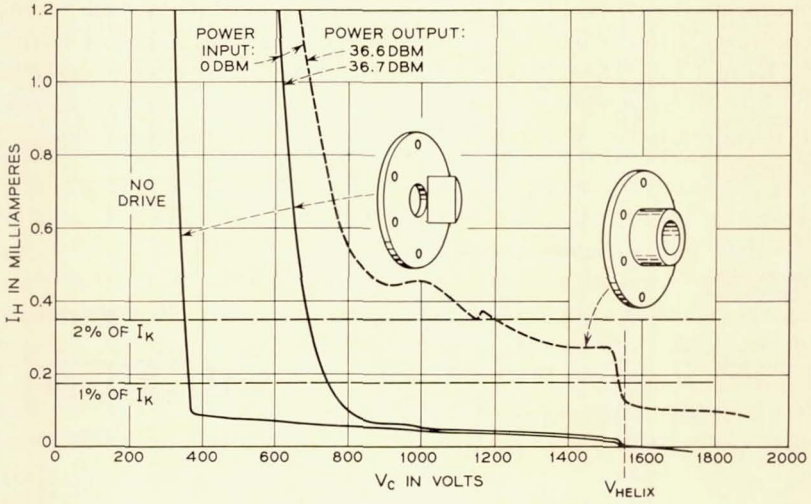


Fig. 10 — Depressed collector operation. Helix current vs collector voltage is shown for symmetrical and asymmetrical output pole-pieces. (Note the suppression of secondary and reflected electrons.) $I_k$ = 17.4 ma, $V_{\text{helix}}$ = 1550 v.

lead to internal oscillations is caused by the returning electrons, which provide a small amount of coupling between the output and input of the helix. The secondary and reflected electrons leave the collector on trajectories similar to those of the primaries, but in the reverse direction. The original collector pole-piece was shaped symmetrically, with a spreading magnetic field. To prevent back-streaming from the inside of the collector, a transverse field was produced in the area of the collector chamber by an asymmetry of the pole-piece. The returning electrons now follow different trajectories and are thereby prevented from leaving the collector again.

### 4.4 *Envelope*

The vacuum envelope in Fig. 11 is made in two sections: the bulb, which consists of concentric details of Corning 7056 glass and Kovar; and the stem, made of the same materials. The stem provides leads and connections to all elements and a tubulation for evacuating the tube, while the bulb provides the surfaces which support the helix and gun assemblies in precise alignment. There are two accurately located reference surfaces. One is the bore of the glass tubing which will enclose the helix; it is held to a diameter tolerance of $\pm 0.2$ mil and a straightness of 3 mils maximum camber. The other surface, which later locates the gun, is machined to the inside of the large Kovar detail and is held with respect to the bore of the glass tubing to a total indicator reading (TIR) of 1 mil. The external reference surfaces, used later to assemble the tube to the circuit, are machined on the outside of the Kovar detail to a concentricity of 1 mil TIR with respect to the inner reference surfaces.

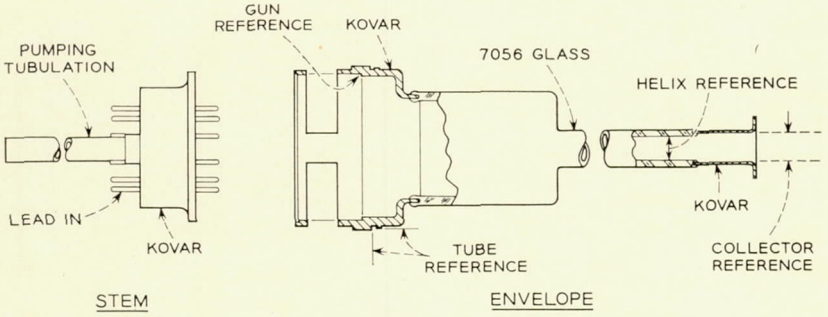


Fig. 11 — Envelope assembly with reference surfaces.

### 4.5 *The Focusing Circuit*

In a satellite system, weight is the controlling factor. The choice of the magnetic focusing circuit is intimately coupled to the problem of over-all system weight. In this connection, the solar plant with its supporting frame, the storage batteries, the regulator and the tube power supply contribute the majority of the weight. The average duty cycle of the tube is low, but because of long operating periods, the supply must be designed close to CW capacity. The solar plant, shielded for protection from particle radiation, and its support frame also add a considerable weight which is almost proportional to the power required by the TWT. To find the lightest over-all system, it was necessary to consider not only the weight of the tube package, but also the tube power requirements, or the tube efficiency. In the present satellite, several pounds must be allowed per watt of power supplied to the TWT.

The lightest focusing package would be a periodic permanent magnet circuit (PPM) which requires approximately one-half pound of magnetic material. The drawback is that it is relatively more difficult to focus the beam, which tends to scallop to a higher degree than in other magnetic circuits. This leads to higher beam interception and to a slightly higher collector voltage. It was estimated that this type of circuit might require 10 to 15 per cent more dc power than a straight field magnet.

From the viewpoint of life and efficiency, a straight field magnet (PM) would be the most desirable circuit since, with it, significant changes in cathode activity can be tolerated without degradation of the focusing. Its magnet weight of about 25 pounds is, however, prohibitive. A compromise is the single-reversal, permanent magnetic circuit (SRPM). It provides the excellence of focusing and high efficiency inherent in the PM design at a considerably lower weight. In common with the PM design, it has the disadvantage of some external magnetic leakage flux. The use of this design results in a magnet weight of 4 pounds, 3.5 pounds greater than the PPM circuit. On the other hand, the SRPM gives a power saving of about 1.5 watts over the PPM circuit. (See Table IV.)

TABLE IV — COMPARISON OF FOCUSING CIRCUITS

| Focusing Circuit, Type | Magnet Weight, Pounds | Focus | Efficiency |
|---|---|---|---|
| PM | 25 | excellent; large leakage flux. | high |
| SRPM | 4 | excellent; some leakage flux. | high |
| PPM | 0.5 | more difficult; not for ultra-long life; no leakage flux. | lower |

From these considerations, the SRPM was chosen for the Telstar satellite. It is comparatively new and has had little coverage in the literature.[5] In the form fully developed for this application, several objectionable qualities have been eliminated, and its operation is much better understood. A detailed description of this circuit and the improvements follows.

The weight of a magnet increases approximately with the third power of the length over which the field must be maintained if the length-to-diameter ratio is notably larger than one. By dividing the magnet in the middle and magnetizing the two halves so that their fields oppose each other, a weight saving of a factor of four can be realized. This is the result of a volume reduction of the leakage flux. The focusing of a traveling-wave tube in such a field should be a straightforward operation, provided the magnetic field can be reversed instantly. In practice, this is difficult to do unless a tapered reversal pole-piece is used between the two magnets, with a hole diameter only a small fraction of the scallop wavelength of the beam. In the present tube, the maximum diameter of the pencil type envelope is 0.319 inch and the measured scallop wavelength, 0.6 inch. The axial magnetic field of such a circuit is shown in Fig. 12. The reversal pole-piece used has a hole diameter of 0.35 inch; we can see that the reversal requires more than 0.6 inch. This means that a serious degradation of the beam focus will take place — the beam starts to scallop with a considerable increase in over-all diameter. Under these conditions, about 20 per cent of the beam current was intercepted by the helix in the reversal region.

A solution had to be found, since an interception of 20 per cent is intolerable. Before describing the solution, it is necessary to describe the behavior of a laminar beam in a uniform magnetic field which includes a small perturbation, as is shown in Fig. 13(a). The perturbation disturbs the laminar flow and forces the beam into a scallop mode. This is, however, reversible; and again observing Fig. 13(a), going from right to left, we can state: a scalloping beam in a uniform magnetic field can be forced back into laminar flow by a field perturbation of the right magnitude and the right phase with respect to the scallop. In Fig. 13(b), two perturbations of the same magnitude are placed a half-scallop wavelength apart. The beam begins to scallop at the first perturbation and is forced back into laminar flow at the second perturbation. Similarly, the second perturbation could be placed $(n + \frac{1}{2})\lambda_{sc}$ away. (If $n$ is even, the perturbation has the same sign; if $n$ is odd, the opposite sign.)* From now on, we will consider the field reversal as nothing but

* An analog can be found in a transmission line with discontinuities or mismatches, where the beam diameter would correspond to the VSWR and the per-

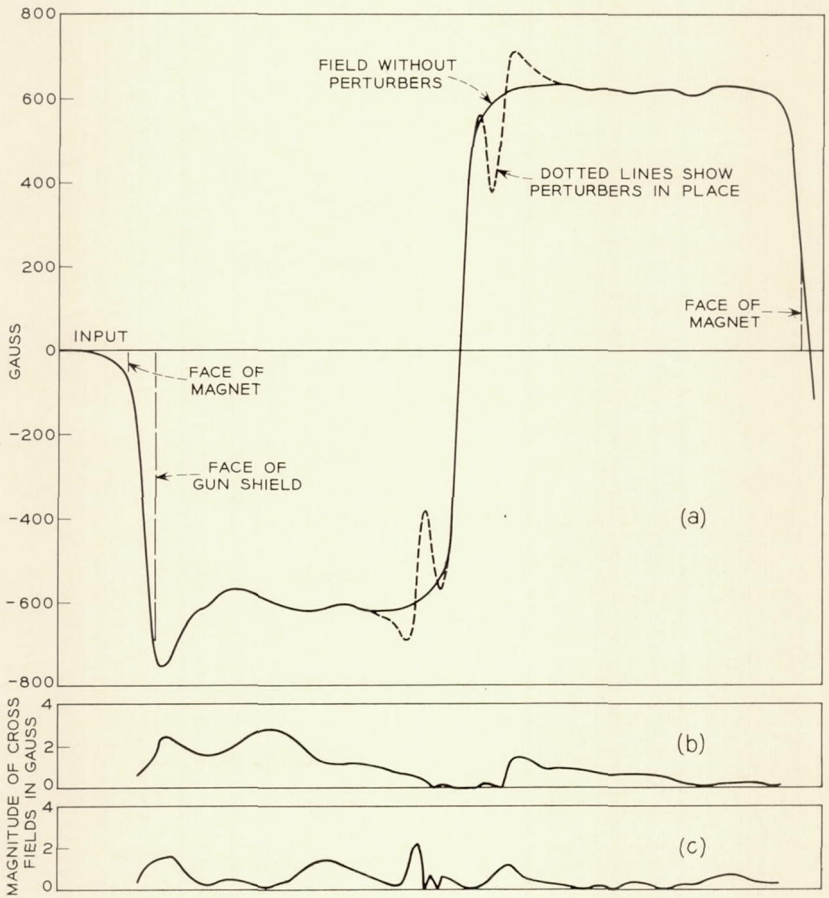


Fig. 12 — Magnetic fields in the single-reversal circuit: (a) axial magnetic field shown without perturbers, and modified field with magnetic perturbers in place; (b) horizontal cross fields; (c) vertical cross fields.

a large perturbation. Earlier SRPM circuits did not use perturbers to counteract the effect of the reversal plane. By mismatching the beam entrance from the gun to the uniform field, one can obtain a scalloping beam, which is shown in Fig. 13(c). If the phasing of the scallop is correct, it can counteract a further beam expansion at the reversal plane. This phasing or phase angle depends on the product of the distance between gun and reversal and the reciprocal of the beam velocity. The

turbations would represent the mismatches. The standing wave produced by one discontinuity can be canceled out by placing a second discontinuity of identical magnitude one-half wavelength away.

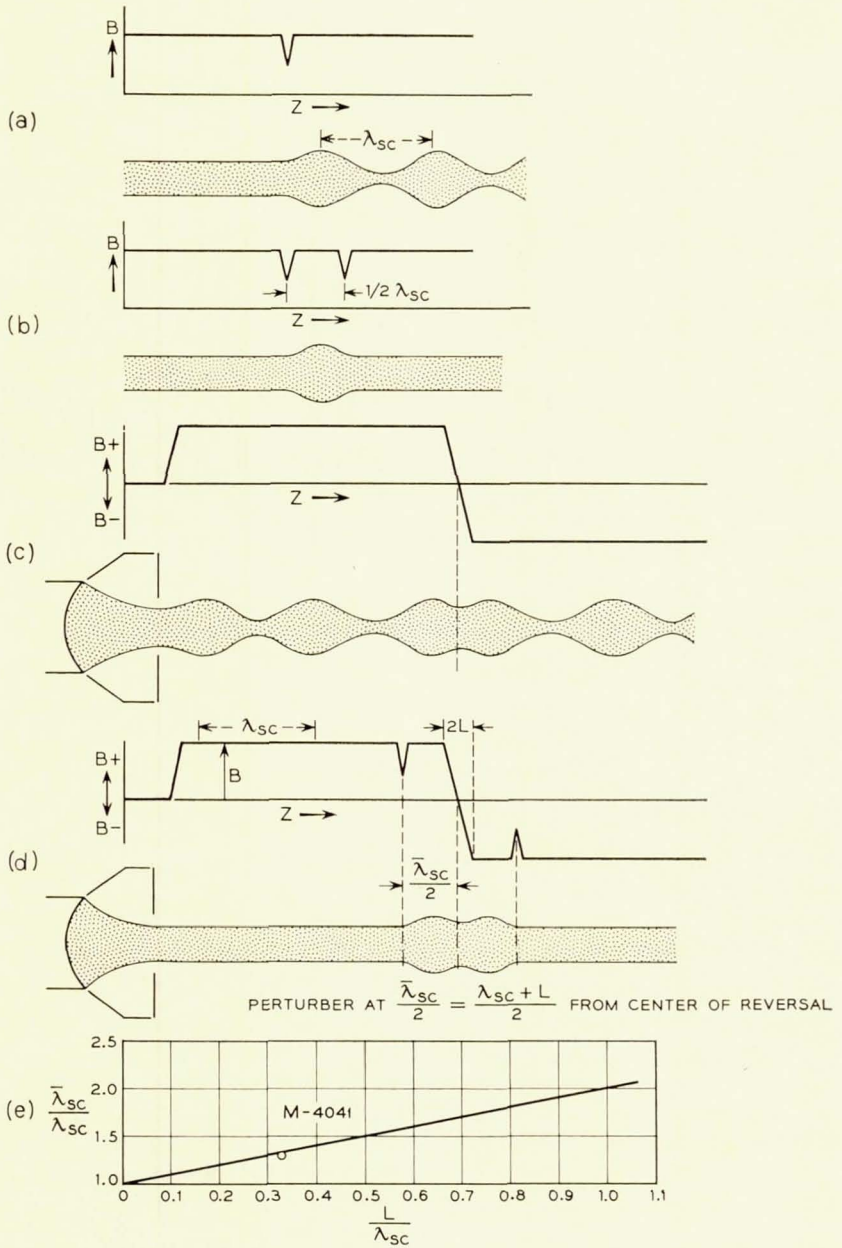


Fig. 13 — Focusing of beam with single-reversal circuit. (a) Laminar beam in uniform magnetic field with single perturbation. (b) Laminar beam in uniform magnetic field with two identical perturbations spaced by a half-scallop wavelength. (c) Focusing of beam through the reversal by pre-scalloping beam at start of magnetic field. (d) Focusing of beam through the reversal, using two magnetic perturbations, each spaced $\bar{\lambda}_{sc}/2$ from center plane. (e) Position of the perturbation computed for a linear field change in the reversal: normalized distance to the reversal plane is plotted vs the normalized length of the reversal. The measured value of the M4041 circuit is indicated and shows excellent agreement.

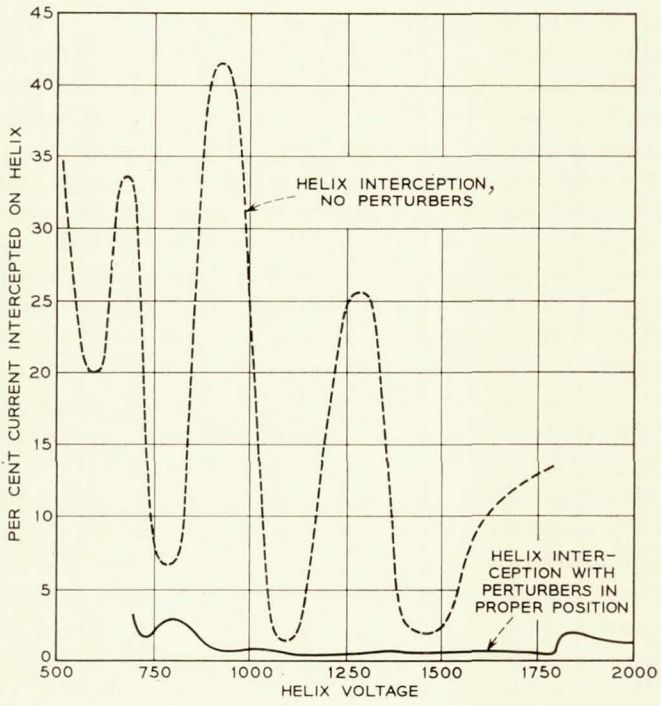


Fig. 14 — Single-reversal circuit, helix interception vs helix voltage.

helix interception measured on such a system is shown in Fig. 14 by the dotted line. The periodicity of the phasing between scallops and reversal is quite pronounced. The voltage passband is only 150 volts. To make the SRPM circuit usable, it is necessary to reduce the voltage dependence. This can be done by reducing the distance between the reversal plane and the point where the beam starts to scallop. For minimum scalloping, proper phasing is achieved with a distance of $(n + \frac{1}{2})\lambda_{cs}$ between perturbation and reversal. It is minimized for $n = -1$, which means that excess field would have to be placed at the reversal plane; this is inconsistent with the basic problem. For $n = 0$ and $n = -2$, we find two possible solutions. To obtain the smallest beam diameter at the reversal and least dependent on voltage, one should place one-half the perturbation, $\frac{1}{2}\lambda_{sc}$, before the reversal and one-half the perturbation, $\frac{1}{2}\lambda_{sc}$, after the reversal. This is shown diagrammatically in Fig. 13(d). In the reversal region, $\lambda_{sc}$ is no longer constant; it depends on the magnetic field, which changes rapidly. The half-scallop wavelength measured from the center

of the reversal and expressed as $\bar{\lambda}_{sc}/2$ can be calculated by integration. For the special case of a reversal with linear dependence of the magnetic field, $\bar{\lambda}_{sc}/2$ has been computed and the values are plotted versus the normalized length of the reversal in Fig. 13(e). The actual improvement in beam transmission and independence of beam voltage is shown in Fig. 14 with the solid line. If the interpretation is correct that the beam now enters and leaves the extended reversal in a laminar mode, one should be able to stack several of these reversals in succession. This has been demonstrated recently in a three-reversal circuit, where only a small degradation in the beam voltage passband had to be accepted. (The weight of the Alnico V magnets was further reduced from the 4 pounds for the SRPM to less than 1.5 pounds for the three-reversal circuit.)

The physical design of a focusing package depends to a large degree on how the RF connections to the tube are made. Since waveguide outputs were required by the system, RF connections were the first feature considered. Direct coupling of waveguide to helix would have required a penetration of the magnets by the waveguides, making for a bulkier and heavier package, and was therefore rejected. Coupled helix matches were considered, but also rejected, because the additional loss in the outputs would have reduced the over-all efficiency, though it would have been very easy to physically combine the SRPM with coupled helix input and output.

The solution finally adopted consisted of nonresonant coaxial couplers at both input and output. A sketch is shown in Fig. 15. The coaxial coupler has two coaxial lines connected symmetrically to the reentrance: one is a feed; the other is a line with a movable short circuit, the position of which determines the impedance of the coupler. These coaxial couplers have been made small enough in diameter to be inserted into a series of uniformly spaced field straightener rings which are needed to reduce the magnetic cross fields on the axis of the tube. These field straightener disks are made of permalloy 45 and are used throughout the length of the magnetic field. Geometrically, it is important that they be held square to the axis of the beam. The resulting crossfields are shown at the bottom of Fig. 12. Because waveguide inputs and outputs were required, a further transducer had to be provided. It consists of a standard coaxial antenna transducer with a specially shaped dielectric cylinder to support the center conductor and give the necessary impedance transform. The over-all cold match from waveguide to helix was quite good over a 10 per cent band, with a VSWR of less than 1.2.

The focusing circuit described is not magnetically shielded. The field has a rotational symmetry about the axis of the circuit. Some knowledge

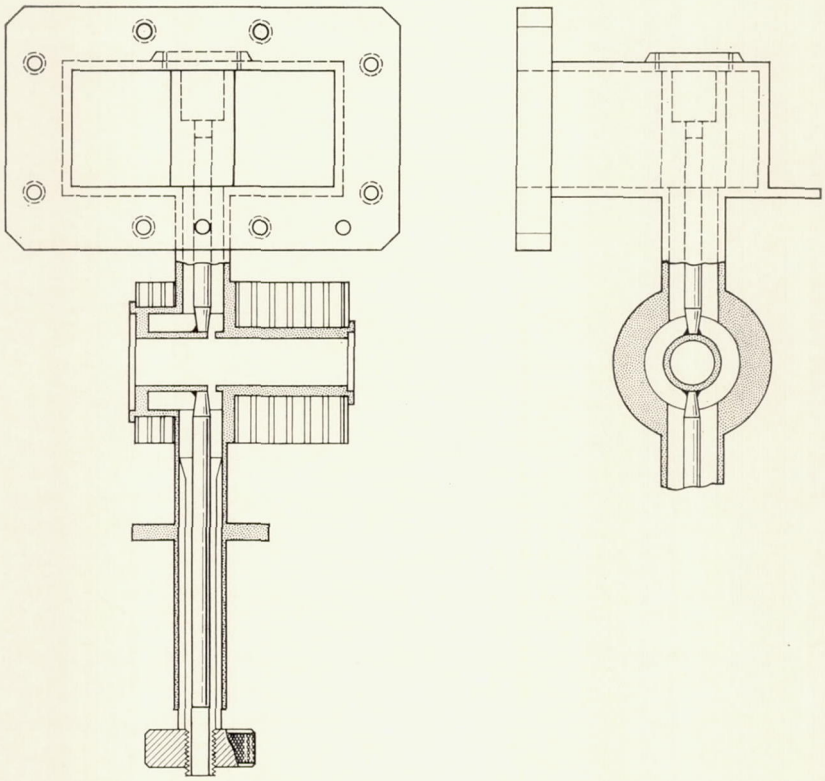

Fig. 15 — Nonresonant coaxial helix coupler with matching stub and transition to waveguide.

of the leakage flux was needed in order to evaluate its effects on other components in the tightly packaged satellite. The external fields are shown in a plane through this axis in Fig. 16. Little interference was experienced, except in the case of the telemetry package, which had to be shielded with permalloy 45.

## V. PACKAGED DESIGN

The packaged traveling-wave tube consists of a tube with its magnetic circuit and RF couplers joined together to form a compact unit. This arrangement has many advantages to recommend it for satellite use. One of these is the optimization of tube characteristics by fine-grained adjustment, at the factory, of the relationship of the magnetic

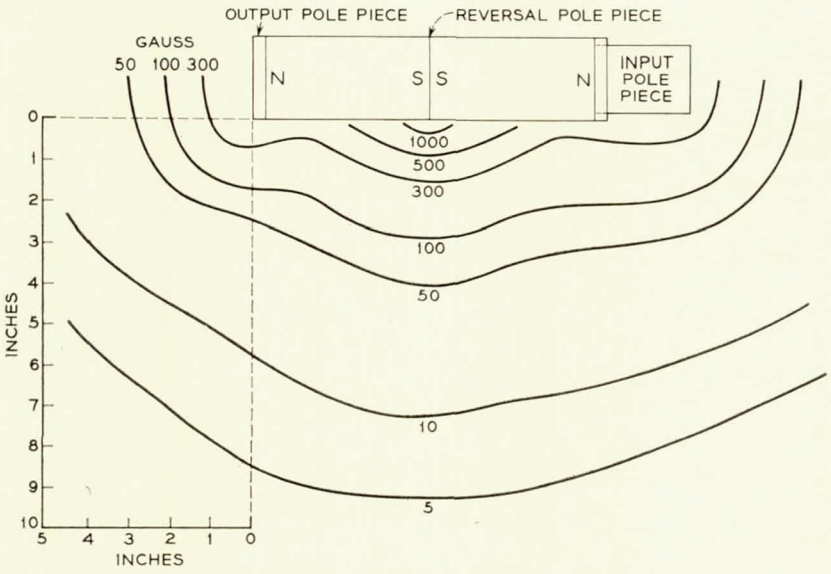


Fig. 16 — External magnetic leakage field of the single-reversal circuit.

field and RF matching sections to the tube. Another is the greater latitude permissible in designing the package to (a) ensure the stability of this relationship for the full life of the unit, (b) provide the ruggedness and support needed to protect the unit against shock and vibration, (c) provide an enclosure as protection against handling and environmental conditions, and finally, (d) provide the most elementary and rugged connections for securing the unit in the repeater.

Fig. 17 shows a graphical cross section of the package. All elements are enclosed by, or mounted on, an aluminum tubular housing which forms the "backbone" of the structure. The tube is a pencil-like figure through the center of the unit. Between it and the inner wall of the housing are two Alnico V magnets and an array of field straighteners. The magnetic circuit is completed by a pole-piece at each end of the magnets and a Permendur septum with its perturber bushings separating the magnets. Mechanical support is given to the tube by means of the pole-pieces at each end, and by contact with two sets of four pins each which cradle the tube at points substantially equidistant between the end supports. Electrical connections are made to the elements by silicone rubber encapsulated leads at the gun end and a single lead at the collector end. Waveguide-to-coaxial transitions are shown at the respective input and output coupling points on the helix. An RF filter

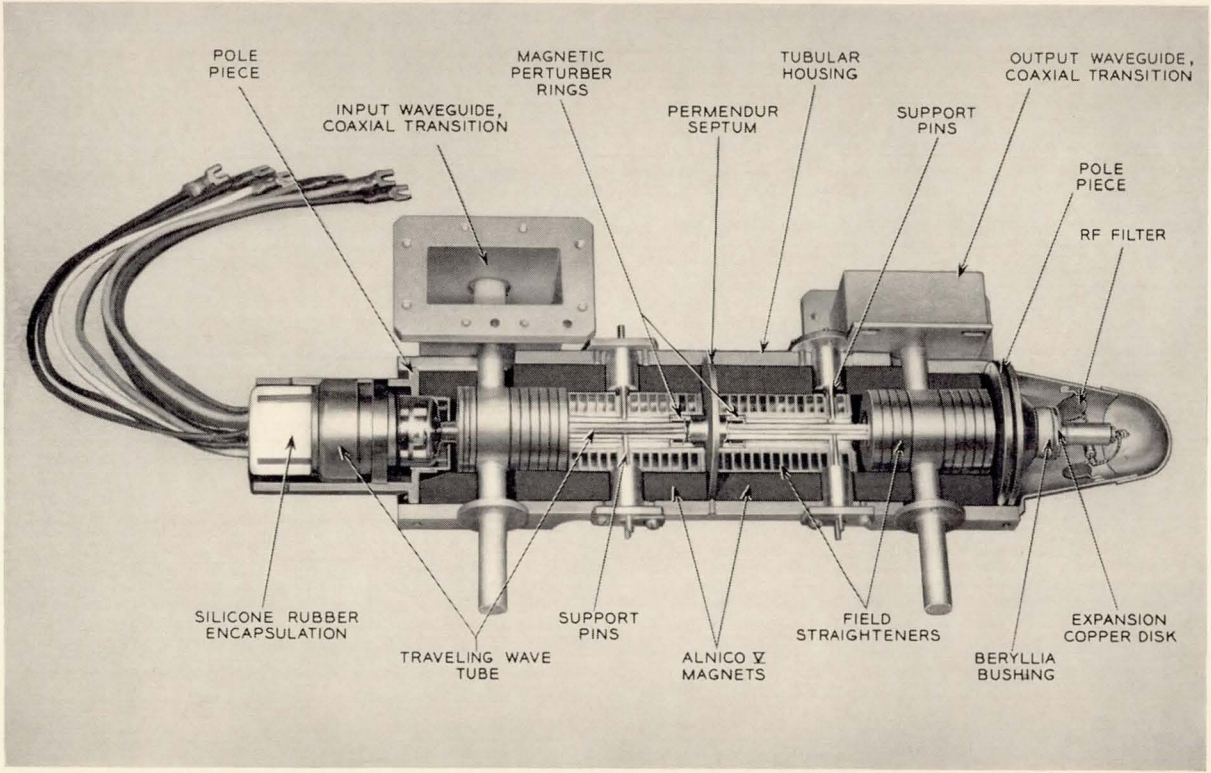


Fig. 17 — Cross-section view of completed amplifier package.

is connected to the collector and supported by the protective aluminum cone that encloses the collector.

The completed amplifier is a package wherein each part is kept in place by a weld or by a screw, and also with cement; the unit cannot be disassembled except by destruction. The package, in effect, floats the tube so that the tube is free to move with changes in temperature without any detectable change in its electrical characteristics. This is achieved by welding the tube to the package at the gun end and soldering to a copper disk at the collector end. The disk, which is 0.005 inch thick, flexes with changes in length brought about by changes in temperature. Furthermore, the disk, which is a part of a subassembly—the other parts of which are a beryllia bushing and a copper cone — also forms part of a thermal path through which some ten watts of collector power is transmitted to the body of the package and dissipated.

Two other constraints are put on the traveling-wave tube to give it the support necessary to resist the vibrations inherent in this application. These are two sets of four aluminum pins, previously identified, located about equidistant between the two end supports. Each set of pins cradles the 0.290-inch diameter glass tubing of the tube in such a way that each pin is deflected laterally approximately 0.002 inch at its point of contact with the glass, to ensure support over a wide temperature range. The result is that the resonant frequency of the tube is increased from an unacceptable value of approximately 700 cps to one of over 3000 cps, well above the specification requirement of 2000 cps.

In installing the package in the repeater, the RF connections are made by connecting the amplifier flanges to the waveguides in the canister giving support to the package. This support is supplemented when the repeater canister is filled with polyurethane foam. Electrical connections are established by flexible insulated leads attached to the tube.

## VI. ELECTRICAL PERFORMANCE

The M4041 TWT was tested under a wide variety of operating conditions, but here we shall restrict the discussion to the Telstar satellite application. The data presented are taken from average tubes, some of them from model number KP24, the tube actually installed in the Telstar spacecraft repeater. The best values attained are quoted only if so indicated.

### 6.1 *The Tube Gain*

The tube gain for KP24 is plotted in Fig. 18 versus helix voltage. The low-level gain is 47 db and occurs at 1380 volts. Here, the maximum

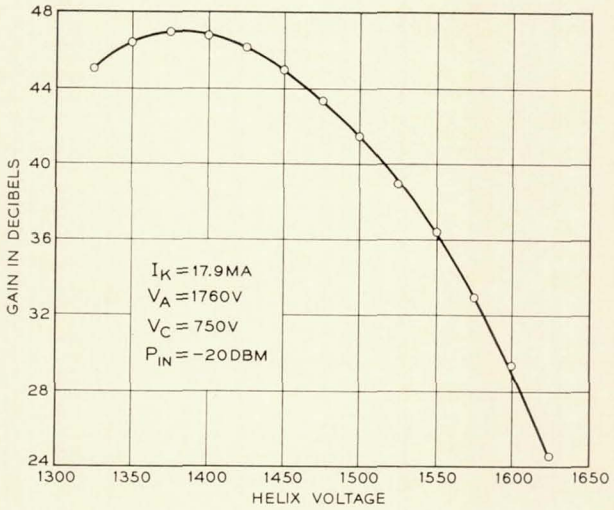


Fig. 18 — Small-signal gain vs helix voltage for KP24 installed in its final circuit.

power output and efficiency are low; to improve both, the tube is run at overvoltage. For the satellite repeater the operating point was chosen at 1520 volts. This point is indicated in the figure and shows a low level gain of 39 db. In Fig. 19 the power output and gain for this same tube are shown for a range of helix overvoltages. The tube was originally designed for an input drive of 0 dbm. Late in the development, a compromise had to be made to permit satisfactory two-signal operation, and to allow for a possible $\pm 3$ per cent voltage drift on all dc voltages. The gain versus frequency is shown in Fig. 20 for three different operating conditions. At the voltage for maximum low-level gain, the peak occurs at about 4.1 gc. Raising the voltage to the overvoltage condition lowers the frequency at which the maximum gain occurs, and thereby increases the gain slope; however, when the tube is driven into saturation, the gain drops off but the slope is greatly reduced. With an input level of $-3$ dbm, the gain slope is 0.5 db over the 4.0–4.2-gc band.

The TWT is not terminated by a well-matched load. The filters and antenna present somewhat of a mismatch. Gain measurements were performed with the tube operating into an attenuator followed by a sliding short circuit. For each attenuator setting, there were periodic positions of the short circuit for which the gain could be enhanced or reduced. In Fig. 21 the maximum and minimum values of the gain are plotted versus twice the attenuator setting, which is equal to the return loss of this load. The gain is not only periodic with the position of the

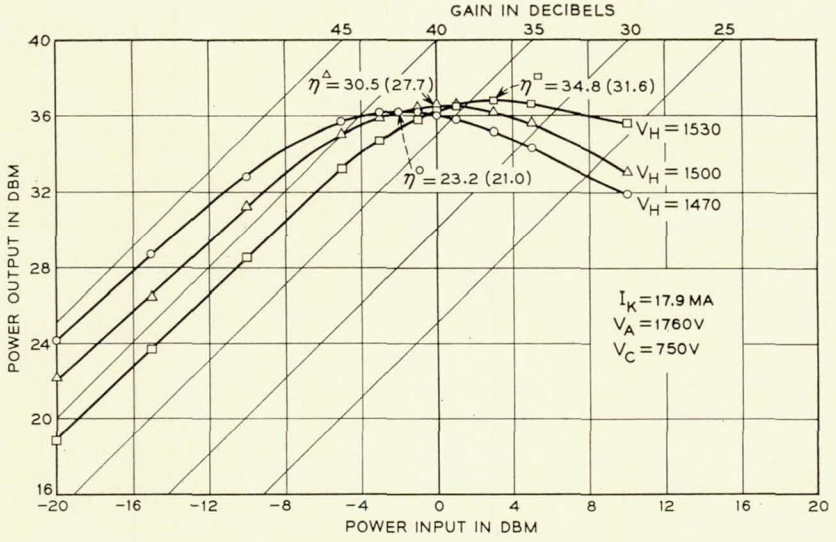


Fig. 19 — Output power vs input power with helix voltage as parameter for KP24. Depressed collector efficiencies are shown at maximum power points; overall efficiencies in brackets include heater power.

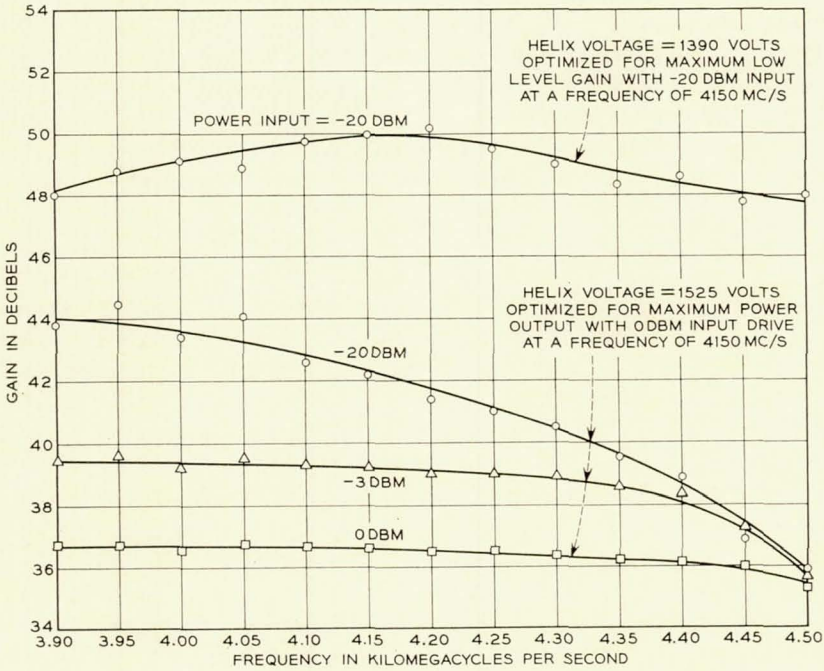


Fig. 20 — Amplifier gain vs frequency for different input power levels.

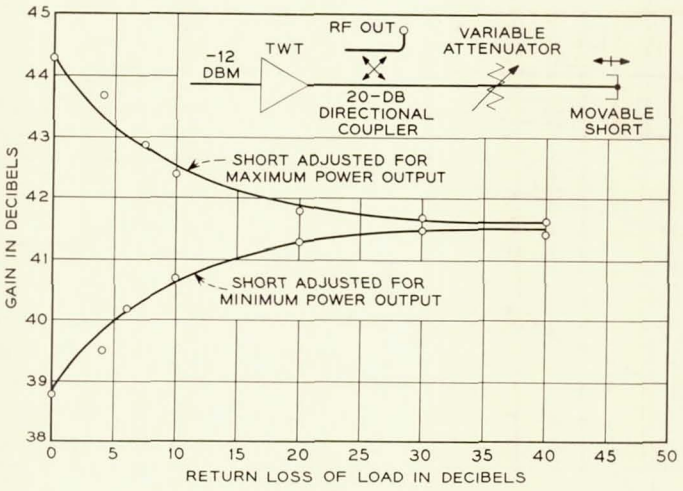


Fig. 21 — Effect of load mismatch on low level amplifier gain.

short circuit, but also with frequency, impressing a ripple on the gain curve. The frequency band between two maxima depends upon the electrical distance between the load and the TWT attenuator. In the region of saturation, these gain variations are considerably reduced.

### 6.2 *Power Output and Efficiency*

The power output and efficiency at 4.17 gc were studied as a function of the input drive and beam currents. The results are shown in Fig. 22. At each point the helix voltage was optimized and the collector depressed until the highest efficiency was obtained. It is interesting to note that the same TWT can maintain efficiencies of over 30 per cent for output powers from 0.3 to 10 watts. It must be remembered that the efficiency falls off much more rapidly when the helix and collector voltage have been set and only the input drive is varied. A curve of this type is shown for 17 ma as a dotted line in Fig. 22.

The highest efficiency measured with this tube type was 43 per cent at the output power level of 5.4 watts, giving an over-all efficiency of 38.5 per cent. Several other models reached 40 per cent, but most of the tubes gave approximately 38 per cent. These efficiencies look attractive; however, they are not realistic for actual satellite conditions, since they can be achieved only with high helix and accelerator interception not permissible in a long-life tube. From our life tests, we know that throughout the life of TWT's, the helix and accelerator interceptions

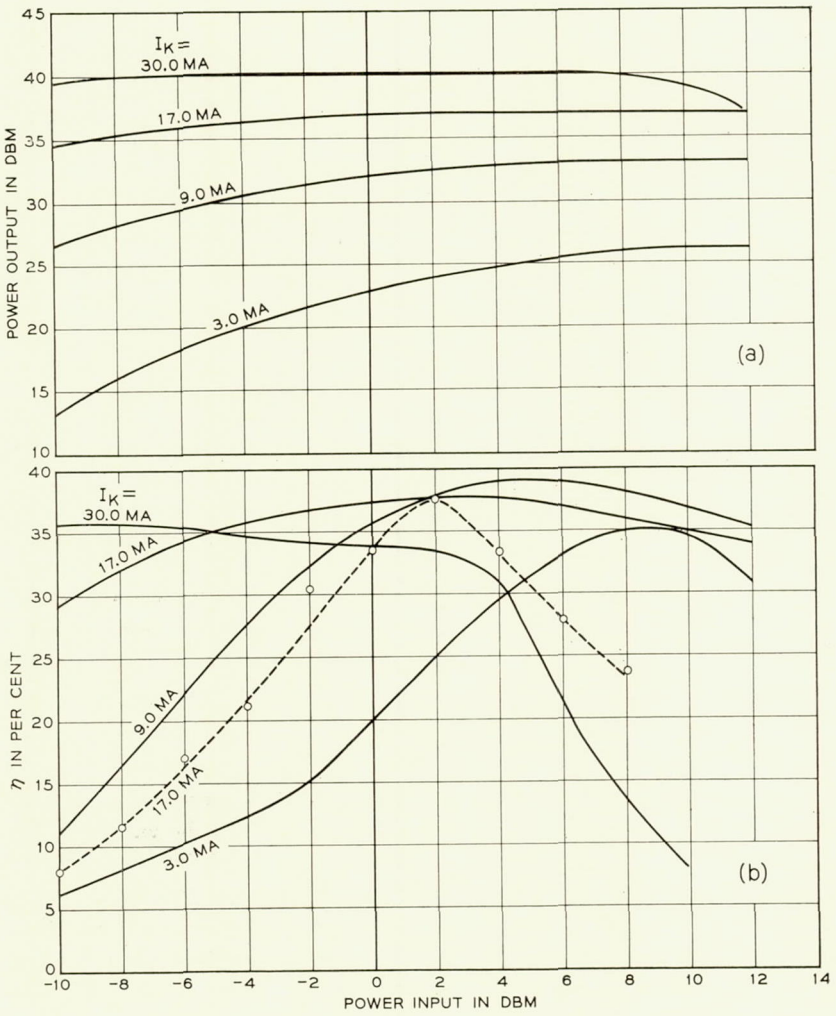


Fig. 22 — (a) Maximum saturated power vs input drive with cathode current as parameter. At each point, the helix voltage is optimized to obtain the maximum power output. (b) For each of the points in (a), the collector voltage is also optimized to achieve the maximum depressed collector efficiency. This efficiency is then plotted vs input drive. Operation with fixed helix and collector voltage is shown for comparison at 17 ma with a dashed line (helix and collector were optimized for highest efficiency with an input drive of +2 dbm).

increase and might eventually be the ultimate cause for tube failure; for this reason, they should be kept as low as possible when the tube is finally installed.

Fig. 23(a) shows both accelerator and helix interception at the oper-

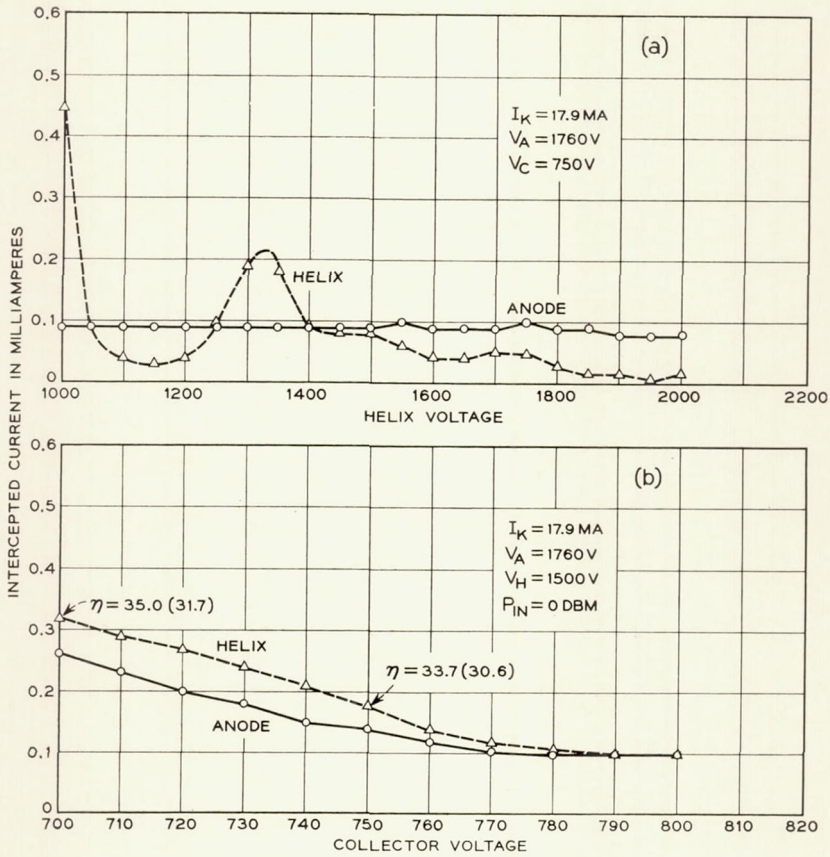


Fig. 23 — Beam current intercepted on helix and anode for KP24 in final package: (a) interception vs helix voltage without RF drive, (b) interception vs collector voltage with RF drive at saturation. Efficiencies, depressed collector and over-all (in brackets), are also shown at two points.

ating point without RF drive as a function of the helix voltage. These data stem from KP24 shortly before delivery for incorporation in the satellite with about 2800 hours of life. The accelerator interception was originally less, but has already climbed from its original value. This has been observed previously with many M1789 tubes on life tests. The hump in the helix interception at 1300 volts is not standard and is most likely caused by residual cross-fields. In Fig. 23(b), helix and accelerator interception is plotted versus collector voltage at full RF drive. Decreasing the collector voltage improves the efficiency, but the interception current exceeds the limit set for long life performance.

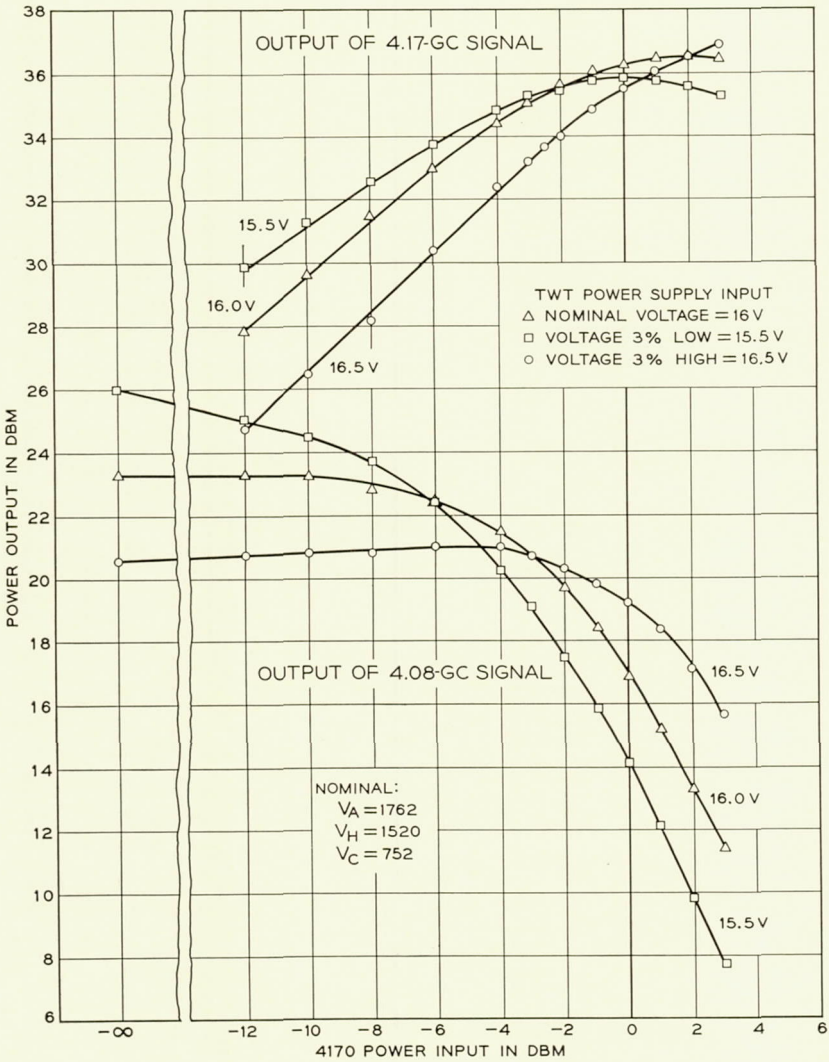


Fig. 24 — Two-signal operation of KP24 in final package. The 4.08-gc beacon input is held constant at −12 dbm as the 4.17-gc signal is varied. Power output is shown for both frequencies with the input voltage to the TWT power supply as a parameter.

### 6.3 *Two-Signal Operation*

After each tube had been tested and approved for flight, a two-signal test was made to determine the actual operating point ($V_{\text{helix}}$). In the

satellite, the tube simultaneously amplifies the beacon and the communication signal. The beacon input is constant at 4.08 gc and −12 dbm. The signal at 4.17 gc has a variable level from −12 to 0 dbm. As the signal level increases, the output of the beacon drops off because the tube is driven into saturation. The beacon and signal outputs are shown in Fig. 24 as a function of the signal level. System limitations were imposed on the operating point to prevent envelope oscillation within the feedback loop of the converter. The limit imposed was that the beacon could not drop off more than 1 db if the signal level were raised by 1 db; this represents a 45° slope on the beacon output. At the nominal input voltage to the dc-to-dc converter, this occurs at −2.5 dbm. This, then, is the operating point chosen for the TWT. The efficiencies, depressed collector and over-all, have been computed for the −2.5- and 0-dbm input levels for the three cases of undervoltage, nominal and overvoltage. These figures are shown in Table V. To satisfy this late system requirement, a noticeable degradation in efficiency had to be accepted to guarantee a stable two-signal operation.

### 6.4 *AM-to-PM Conversion*

Instead of measuring the AM-to-PM conversion directly, a method described by Mr. H. L. MacDowell[6] has been used. Two signals of much different amplitude and frequency are amplified in the TWT. The intermodulation products are measured and the AM-to-PM conversion computed. These values are all plotted in Fig. 25 together with the output power against the input drive. The curves are from measurements made with different input voltages to the satellite dc-to-dc converter, for the nominal voltage of 16 volts, and for 16 volts ± 3 per cent. These are estimated limits of regulation throughout the life of the satellite. The maximum of 4°/db measured with 3 per cent overvoltage is less than the value encountered with the TH relay tube under similar drive conditions.

TABLE V — COMPUTED EFFICIENCIES FOR KP24 WITH TWO-SIGNAL OPERATION

| Input $\eta$ | −2.5 dbm | | 0 dbm | |
|---|---|---|---|---|
| | Depressed | Over-All | Depressed | Over-All |
| −3% | 28.0 | 25.2 | 29.0 | 26.2 |
| Nominal | 27.0 | 24.4 | 32.0 | 29.0 |
| +3% | 17.3 | 15.7 | 24.2 | 22.0 |

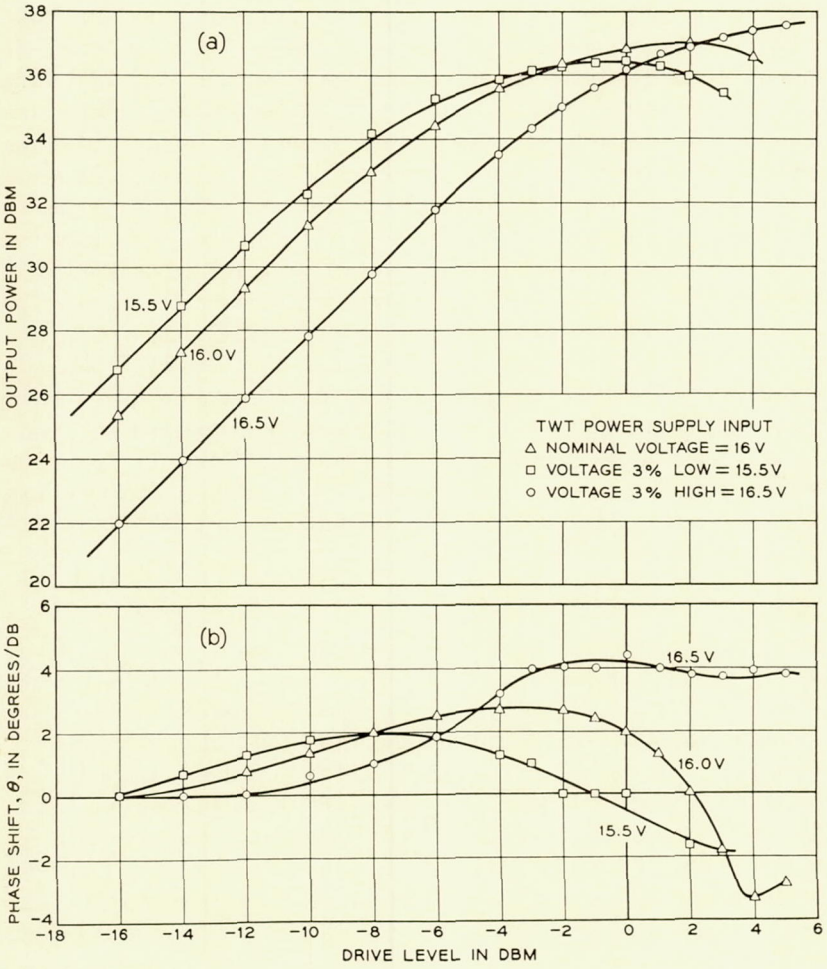


Fig. 25 — AM to PM conversion: (a) power output vs input drive, (b) phase shift vs input drive at 4.1 gc.

## VII. MECHANICAL CAPABILITY

Mechanical capability, in the sense used here, is limited to the conditions the amplifier, or its components, have been shown to withstand by actual tests, and not the ultimate that it can withstand. In all cases, tests were defined to impose conditions more severe than were likely to be encountered in preparation for or in actual satellite flight.

Before a unit is passed for satellite use, it is subjected to the following

vibration tests: 15-50-15 cps at 0.3 inch displacement (3.5-38-3.5 g), 50-100-50 cps at 20 g, 100-2000-1000 cps at 10 g.

During development, typical packages were subjected to mechanical and thermal tests as follows:

(1) Thermal cycle, three packages, heater off: −30°F to +105°F to −30°F.

(2) Thermal cycle, one package, heater operated on and off: +15°F to 90°F to 15°F.

(3) Thermal cycle, six guns after 28,000 to 38,000 on-off cycles of heater: −30°F to 150°F to −30°F.

(4) Vibration tested four guns after 11,000 on-off cycles of heater: 15–2000 cps from 4–20 g.

(5) Shock tested four guns after 11,000 on-off cycles of heater: three to 400 g without harm; one to destruction at 1600 g.

(6) Vibration check of five heater-cathode structures: 100-3000 cps at 40 g.

(7) Cycled 31 heaters in guns made exactly as in tube from 4000 to 44,000 on-off cycles with no losses. Fourteen were opened, carefully dissected and examined for deterioration at cathode and heater coatings. None was found. Seventeen still on cycling life.

(8) Two heaters same as item (7) put on continuous life. Satisfactory after 6100 hours and still on.

(9) Vibration (to remove foreign particles) applied to all guns and helices during fabrication: 50-2000-50 cps at 20 g.

## VIII. BUILDING THE FINAL TUBES FOR SATELLITE USE

### 8.1 *General Cleaning and Processing Procedure*

To ensure an end product free of contamination and mechanical defects, procedures and processes are spelled out in great detail. All operations are inspected upon completion, and these inspections are supplemented by inspection of subassemblies. Assembly is done under pressurized hoods in areas where the atmosphere is controlled and personnel traffic is minimized. A general listing of these activities is:

(1) All piece parts and subassemblies are inspected for defects as received and again at several points in the assembly procedure.

(2) All subassemblies are inspected for particles, either airborne or by-products of fabrication, and particles are removed by hand or vacuum.

(3) All parts and subassemblies must pass an atomizer test, which is a very sensitive indicator of surface cleanliness, just prior to assembly.

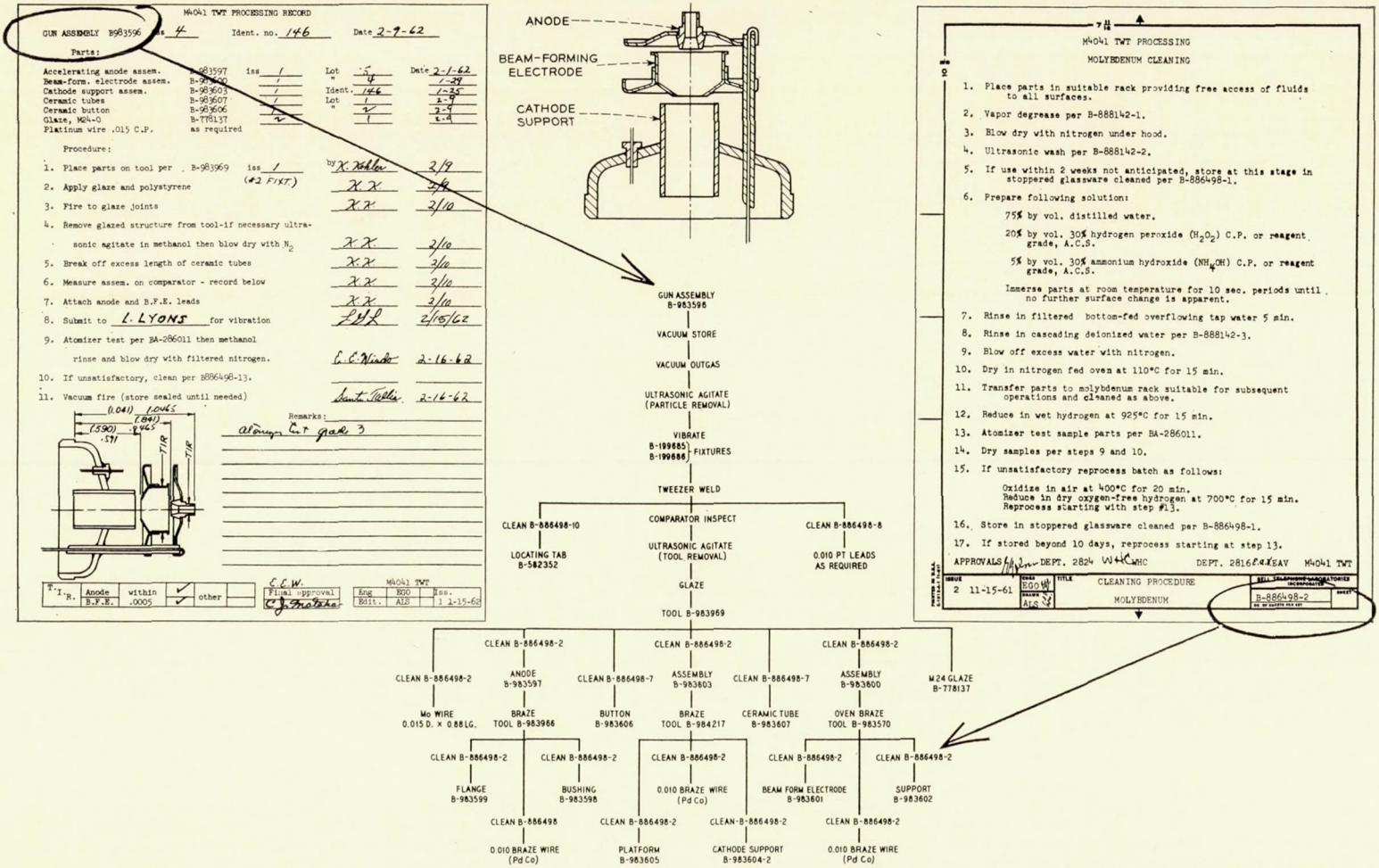


Fig. 26 — Typical flow chart of a subassembly procedure, with detailed specifications for a cleaning operation and the check sheet used to insure careful observation of each step required.

(4) Cleaning operations:
  (a) trichloroethylene wash — liquid or a vapor (all metal parts)
  (b) hydrogen reduction (all metal parts)
  (c) air firing (all ceramics)
  (d) ultrasonic agitation in detergent or solvents (all parts and subassemblies)
  (e) cascade rinsing in deionized water — rinse used after operation (d)
  (f) chemically reactive immersion (some metal parts: i.e., cathode surface, gun parts)
  (g) oxidation-reduction (gun parts)
  (h) liquid honing (glass stem leads, cathode surface)
  (i) vacuum outgassing (all subassemblies)

(5) Storage

All cleaned parts are stored in containers which have passed an atomizer test. The limit of storage is ten days, after which they are automatically recleaned. The coated cathode is the only assembly that departs from this procedure; if held ten days, it is rejected.

(6) All fixtures and tools used in assembly are cleaned to the same standards as the parts.

(7) All vacuum outgassing containers are equipped with filters to entrap airborne particles when the container is open to air.

(8) Extraordinary "clean room" procedures are followed, in that assembly is done under a protective pressure hood in a dust-free temperature- and humidity-controlled room located within a similarly controlled area. The movement of personnel in the inner room is restricted to essentials.

The meticulous cleaning and assembly procedure is guided by a flow chart for the tube as a whole and subordinately for each subassembly. Each cleaning process is separately listed. This system is illustrated in Fig. 26 with a flow chart for the gun subassembly and the cleaning procedure for molybdenum. To prevent omission of any step, check lists are used for each individual component, small or large.

### 8.2 *Processing on the Pump Station*

To check for subsequent changes, the tube undergoes an additional inspection before it is sealed on the pump station. A similarly designed station was used for the M1789 TWT. This system uses a roughing pump, followed by an oil diffusion pump and two liquid $N_2$ cold traps. After a vacuum of $1 \times 10^{-5}$ mm Hg is obtained, the tube is baked at slightly less than 450°C for a minimum of 16 hours. Subsequently, the helix is outgassed at 650°C by passing current through it, and the col-

lector is baked in a small oven to higher temperatures to make sure all surfaces which are directly exposed to the beam have been freed from occluded gases. After the tube is thoroughly outgassed, the Ni-Zr cathode is broken down at a temperature of 1000°C for 4 minutes. Then a maximum of 500 volts is applied and a beam of about 2.3 ma drawn to helix and accelerator. The cathode temperature is gradually lowered, provided space-charge-limited emission can be maintained. The TTW is then sealed off.

### 8.3 *Preaging*

The TWT is now inserted into a focusing circuit and preaged. The cathode nickel is fairly inactive, and it takes the tube about one-half to one hour until full emission (20 ma) can be drawn with the nominal accelerator voltage, at a temperature of 900°C. For the next few hours the tube is permitted to age in before full RF drive is applied. Most of the tubes remain for about 100 hours on preaging. The tube is now removed from the aging circuit; the leads are attached and based in a silastic rubber cap. Thorough mechanical inspection follows, to eliminate further processing of a defective tube.

### 8.4 *RF Testing*

The tube is now ready to be checked for its RF performance. Thorough tests are made on all parameters to determine whether the tube passes the limits set for satellite use. At this point a considerable number of tubes are already marked "nonfly." The highest number of rejections are caused by a poor hot output match and an associated tendency to oscillate when the tube is short-circuit terminated. Some of these tubes, however, continue through this testing and are used for life studies.

### 8.5 *Aging and Life Tests*

All of the care in designing and building this tube is of little value if confidence in its life capability is not established. The aging-in phase is the only period in which the tube can be observed. Various observed characteristics can be used as indications of the later behavior and give confidence in the long-life abilities and reliability by eliminating poor or questionable tubes. An extremely sensitive method, the dip test,[7] was selected to measure relative changes in the average cathode work function, more commonly known as the "activity level." This test is initiated by a precisely timed interruption of the heater power to the tube under study while observing changes in cathode current, particularly the maximum drop which occurs shortly after the heater power is re-

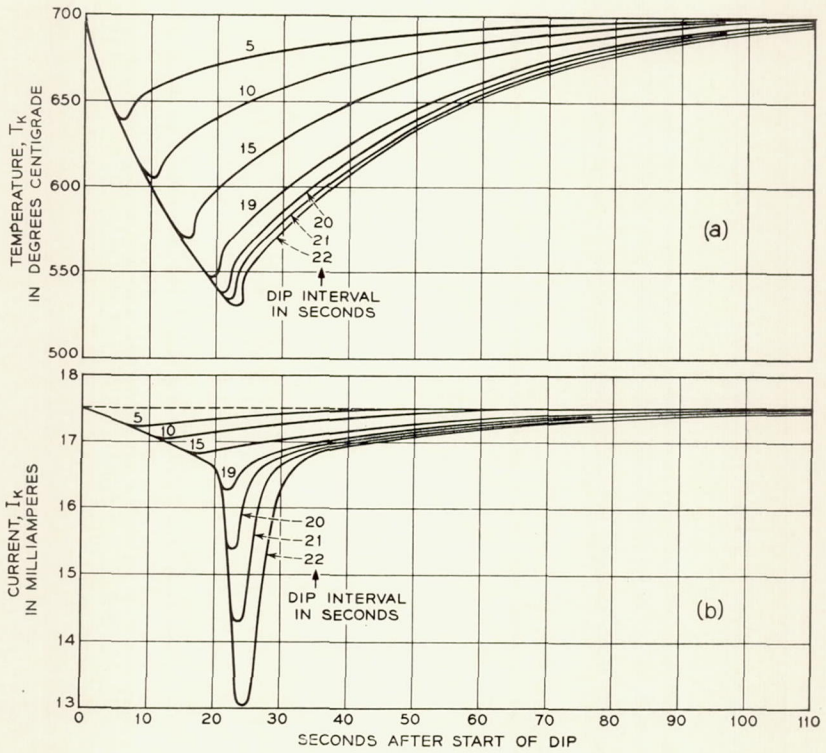


Fig. 27 — Dip test of typical M4041: (a) cathode temperature measured with built-in thermocouple during dip test, with dip interval as parameter; (b) corresponding cathode current.

stored to the tube. Fig. 27 shows composite plots of cathode currents and temperature, as measured with a built-in thermocouple, versus time. The sensitivity of the test can be increased by lengthening the timed dip interval and is shown for several values. This test basically gives a measure of how far below the set operating point the emission of the cathode changes from space charge to temperature limitation. The temperature at which the emission becomes temperature-limited changes downward in early life, reaches a minimum after several thousand hours, and eventually starts to climb again, until at the end of life it reaches the operating temperature of the cathode.

The shape of the dip curve reveals a further quality of the cathode, the uniformity of work function over the surface. A dip which breaks sharply indicates uniformity; one which is well rounded, a geometrical spread of different work function. These two dip curve types are shown in Fig. 28.

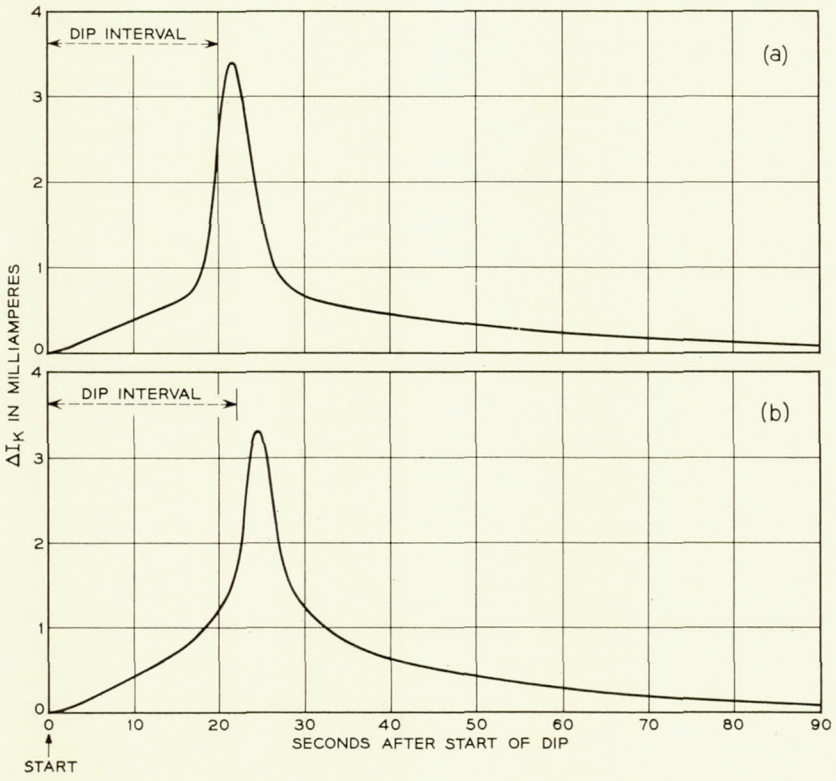


Fig. 28 — Shapes for cathode current dip curves: (a) uniform emission — uniform work function, (b) nonuniform emission caused by work function which is irregular throughout the cathode surface.

The tubes which have gone through the RF testing are now ready for the aging phase. They are installed in an aging rack. Each tube is driven by an individual high-reliability power supply, which has a large number of safety controls to prevent damage to the tube in case of certain failures. The RF drive power to each tube is also individually controlled. The cathode temperature is set at about 750°C and the tubes adjusted for 4 watts output. The tubes are tested daily and their temperature and cathode current dips recorded on a strip chart. When the activity has improved and the 20-second dip no longer exceeds 2 ma, the cathode temperature is lowered. After 1000 hours of aging, the best tubes are selected for possible fly candidates. At this point, the tubes are removed from life test and taken out of their packages to be given the most thorough mechanical inspection. The good tubes are then in-

stalled in selected focusing circuits. A series of electrical tests follows to assure tube performance. The repackaged tubes, with their own circuits, are installed once more in the life area. Activity and stability of interception currents were especially observed. Even at this point it is found that the helix and accelerator interception change slightly with improving activity levels. This phase of the aging period extends over several hundred hours.

So far the tube was approved only for continuous operation. The next phase consisted of a switched life test. The voltages were switched on and off to simulate the actual satellite conditions: 3 minutes heater warmup, 15 minutes operation, and 12 minutes cool-off. At this point, an interesting phenomenon was observed. The cathode current climbed continuously at a very small rate as switching cycles were accumulated. This was first attributed to changes in mechanical tolerances due to the heat cycling, but precise measurements of the gun dimensions discredited this theory. The change had to be attributed to changes of the cathode itself. At the same time, it was discovered that test diodes in an entirely different vehicle displayed a similar behavior. Changes of 2 per cent were observed in cathode current and gun perveance over a period of 1000 switching cycles. For this reason, all fly tubes were cycled for an excess of 1000 cycles, when the time schedule permitted.

### 8.6 *Final Sealup of Tube and Circuit*

At the point where a tube and its focusing circuit had proven themselves by performance, the two were mated together, a process which is irreversible, since neither tube nor circuit can be recovered. The final steps in this operation are outlined below. First, the tube is rotated and input, as well as output, pole-pieces are slightly readjusted to obtain best focus at an input level of 0 dbm. The waveguide and coaxial transitions are moved longitudinally, and the coaxial plungers trimmed to obtain a match at input and output optimized for satellite performance. The unit is now ready for final packaging. It is positioned so that the central line of the tube is vertical and the gun end is up. The tube is gently lifted off its seat about 0.02 inch and allowed to fall back into position, after which it is lifted and held 1 mil off its seat, at which point it is locked in place by soldering the collector carefully to its collector support. The one-mil gap precludes the possibility of a bend in the tube as a result of pole-piece displacement during adjustment, or by the nonsquareness of the reference surface, either on the tube or on the circuit. A bend would serve to bind the tube in its supports so that it would resist "falling" into place. As a result, the tube is fastened and supported

in a free and unstressed state. All adjustments are pinned or locked. An epoxy resin is used as an additional bond so that all individual parts (housing, magnets, pole-pieces, waveguide tube, etc.) are locked together into an inseparable integrated unit. The resin is cured and the completed package subjected to the final vibration test.

Once more the tube is installed in the life rack to be observed for a few more days. The operating voltages are set accurately to the values which are expected at the beginning of life in the satellite. Interception and activity should now have stabilized. At this point, all the records of the tube are reviewed to make sure no detail or trend in its life history has been missed. The tube is now cleared for satellite use and remains on life until called for.

The final step consists of the marriage between the TWT and its power supply. For optimum performance, the TWT voltages are adjusted individually. For reasons of efficiency of the dc-to-dc converter, this is accomplished by selecting the best taps on the primary side of the transformers. The tube, converter and the assigned microwave network are assembled for tests. Subsequently, the helix voltage is chosen and the dc-to-dc converter completed. Once the taps are set, the converter is embedded in foam: no further changes are possible.

## IX. CHOICE OF CATHODE TEMPERATURE

A word is advisable on the choice of the cathode temperature. It was pointed out earlier that the life of the tube is highly dependent on the cathode temperature. To be able to compare this cathode with those of other tubes, we have tried to find a parameter which would be independent of operating temperature and the dip interval chosen for the test. It is possible from the dip curves to obtain for each tube the actual point where the tube goes into temperature-limited operation by correlating the knee of the cathode current curve with the corresponding cathode temperature. On some tubes, estimates had to be made, since they were not dipped all the way into temperature-limited emission. For comparison, a point was chosen in life as a standard time for comparison: specifically, 1000 hours. In Fig. 29, the transition temperature from space charge limited emission to temperature-limited emission is plotted for each tube in chronological order. These values are not steady-state values, since they are taken on a transitional basis; however, they suffice for comparison with other dip tests. We see that these transition temperatures lie at 550° to 600°C. Where was the operating point now chosen? Similar points of the M1789 lie about 50° higher, namely 600° to 650°C. This difference can be attributed to the lower cathode current

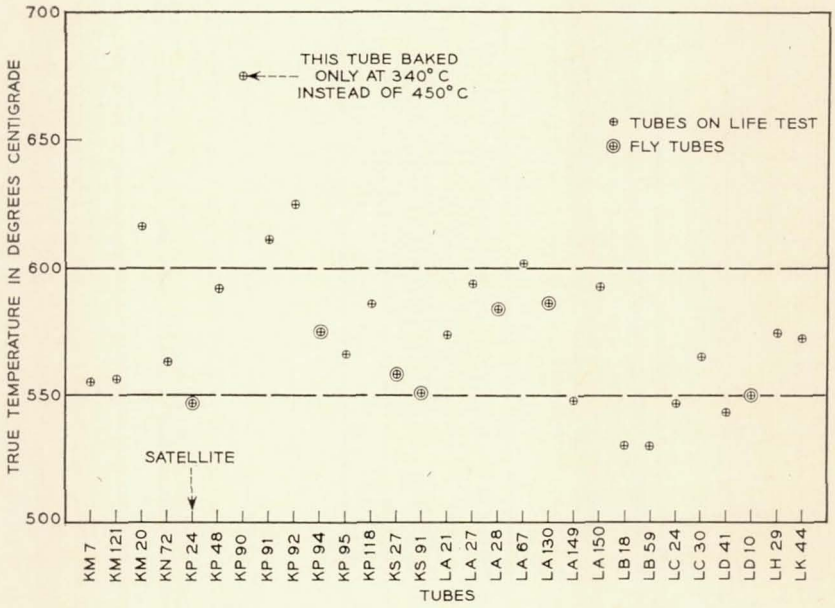


Fig. 29 — Transition temperature of cathodes for the 29 tubes put on life test (space-charge–temperature-limited emission).

loading and to the improvements in tube techniques and cleanliness. The point chosen for the M1789 was 775°, about 150° higher than the transition temperatures. It was found desirable to maintain about the same margin in the satellite tube. A lower cathode temperature would have extended the life but reduced the safety margin towards cathode deactivation; the choice was therefore made to favor reliability.

The data plotted in Fig. 29 are uniform to a high degree with the exception of tube KP90. This tube was accidentally baked at a lower temperature of 340°. This single deviation in processing resulted in an increase of the transition temperature by 100° from the average. No other tube shows such a large deviation. This test illustrates the true uniformity of all the tubes made, since no tubes were eliminated for activity reasons prior to the 1000-hour test. However, in most of the tubes the transition temperature continues to decrease with further aging; usually a minimum value is reached between 3000–10,000 hours.

## X. KP24 DATA SINCE ITS INJECTION INTO ORBIT

The telemetry system in the Telstar satellite transmits once every minute the following data concerning the tube: heater voltage, helix

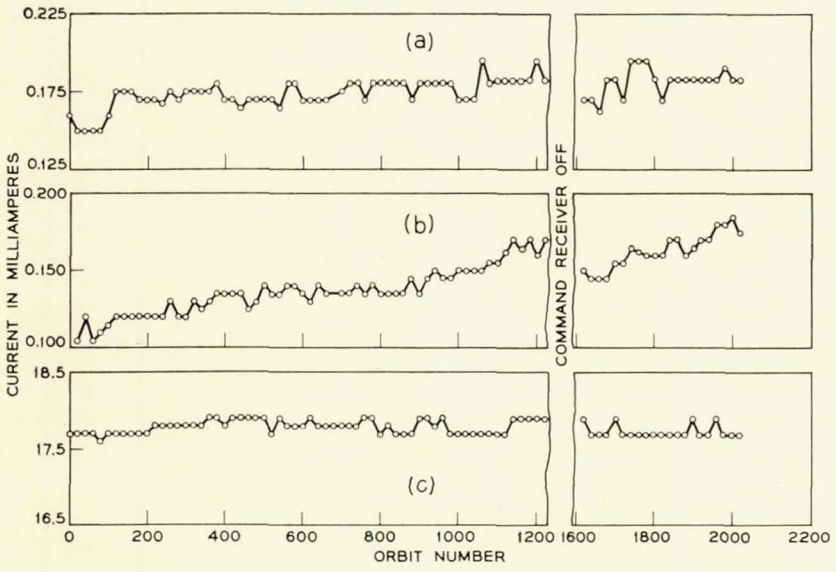


Fig. 30 — Telemetry data for KP24 after injection into orbit: (a) helix current, (b) anode current, (c) collector current.

current, accelerator current, collector current, and finally the temperature of the tube package as measured at the output waveguide flange. The values are transmitted in digital form and are therefore quantized. The smallest increments are: helix, 10 microamperes; accelerator, 5 microamperes; and collector, 200 microamperes.

In Fig. 30, the points represent data selected from active passes during which the TWT was operating under reasonably similar drive conditions. The intercepted currents on helix and accelerator vary to a certain degree; this is caused partly by the telemetry and partly by the varying experiments being performed with the satellite. Nevertheless, some trends can be observed. While the helix current remains steady, the accelerator current shows a slow but gradual increase, similar to that observed in the M1789. The collector or the cathode current (the sum of all three) shows a slight but noticeable increase, such as had been previously discussed under switched life tests. At the moment of writing (January, 1963) the tube has been turned on in excess of 400 times and has accumulated at least 100 hours of operation in orbit. There is no indication that the tube performs differently than if it had remained on the life rack.

## XI. CONCLUSIONS

A high-reliability, long-life TWT has been designed, built, tested, and injected into orbit. The basic design philosophy of the conservative approach, based wherever possible on thoroughly proven experience, has paid off. There were only four new concepts used; these, however, had been thoroughly proof tested before incorporation. They are: (a) new cathode nickel (b) on-off operation (c) cathode heater structure (d) SRPM circuit. None has shown any undesirable side effects.

## XII. ACKNOWLEDGMENTS

Many members of the Laboratories contributed to the successful development of the satellite traveling-wave tube amplifier. The authors wish to call attention to the excellent performance of all the highly skilled personnel involved in fabrication and assembly of the tube. Mr. C. J. Mataka was responsible for close supervision of the tube assembly line and resolution of the many problems arising from fabrication and assembly of the device. Mr. A. L. Stevens assisted in overseeing the many inspection points incident to ensuring the quality of fabrication. He also conducted tests to evaluate certain mechanical properties of the gun structure.

Mr. J. F. Milkosky undertook the mechanical development of the magnetic circuit and parts related to packaging the tube. In this work he was assisted by Mr. B. Smith. Mr. D. O. Melroy handled the interface problems which were encountered in associating the TWT with the microwave components and power supply in the satellite.

Messrs. A. J. Chick and A. C. Fodor took charge of conducting the life testing experiments. Messrs. H. J. Oudheusden, L. M. Reveron, and D. L. Van Haren were responsible for processing the completed tube on the pump station and for the complex electrical testing which immediately followed. Mr. D. L. Van Haren undertook the final development of the single-reversal magnetic circuit.

## REFERENCES

1. Pierce, J. R., *Traveling-Wave Tubes*, D. Van Nostrand, New York, 1950.
2. Olsen, K. M., High Purity Nickel, Metal Progress, **72**, 1957.
3. Kern, H. E., earlier data in Proc. of 6th Nat'l. Conf. on Tube Techniques, Sept. 1962. Test diodes described in *Handbook of Physics*, **XXI**, McGraw-Hill, New York, 1958, pp. 145–146.
4. Olsen, E. G., The Use of Powdered Glass as a Binding Medium in TWT Construction, Third Nat'l. Conf. on Electron Tubes, 1956.

5. Murphy, B. T., and Kelly, J., Reversed Field Focusing, Proc. of Internat'l. Congress on Microwave Tubes, Munich, 1960; see also Winwood, J. M., Permanent Magnet Focusing of Low-Noise TWT's, Proc. of Internat'l. Congress on Microwave Tubes, Munich, 1962.
6. Laico, J. P., McDowell, H. L., and Moster, C. R., Medium Power Traveling-Wave Tube for 6000-mc Radio Relay, B.S.T.J., **35,** November, 1956, p. 1336.
7. Bodmer, M. G., Dip Testing, a New Method for Measuring Cathode Activity, I.R.E. Trans. PGED, **ED-5,** January, 1958, p. 43.

# The Design and Construction of the Electronics Package

By R. H. SHENNUM and E. J. REID

(Manuscript received April 1, 1963)

*The electronics system of the Telstar satellite is described from the point of view of philosophy of design and construction rather than that of circuit details. The reliability is emphasized, and steps taken to preserve the inherent reliability of the components are discussed. The physical construction of modules, subsystems, and finally the entire system is described, including the foam encapsulation and the eventual hermetic sealing of the canister.*

## I. INTRODUCTION

The reliability program of the Telstar satellite is based upon three factors: component reliability, conservative circuit design with few innovations, and rugged equipment design with quality construction insured by specially trained craftsmen and extensive inspection. Wherever possible, past experience with proven reliable systems provided a guide when applying these factors. In contrast to the approach used in many other satellite programs, the Telstar spacecraft contains a minimum of redundancy. It is also unusual in that the mechanical design encloses most of the electronic circuitry in a hermetically sealed canister filled with polyurethane foam. This prevents readjustment and unit replacement; however, it provides a very rugged unit which is safe from tampering. To further enhance reliability, "white room" conditions were observed during all construction stages.

## II. COMPONENTS[1]

Component reliability, together with redundancy, sets an upper limit on the reliability of the system, for the circuit designer can at best preserve the inherent level of reliability built into the components furnished to him. The selection of semiconductor types was based upon proven reliability in previous systems. A large number of units of a single type

were tested, and those used in the spacecraft were obtained by choosing the best — about 33 per cent of the total number tested. These tests consisted of operating each unit at a controlled power dissipation or exposing each unit to a controlled amount of radiation while observing the degradation against time of such properties as gain, voltage breakdowns and leakage currents. To further improve reliability, deratings of approximately ten to one were typically used with respect to power rating, voltage breakdowns and leakage current.

The types of passive components used were also chosen for their proven reliability in previous systems. In addition, each component was individually tested before use. The passive components used were not a selection of the best of a large group, as with the semiconductor devices, but those components which passed the tests. This provided, in most cases, a better than 90 per cent yield from those tested. Derating factors of at least two to one were used with respect to power ratings and voltage breakdowns to improve reliability. All other special components were carefully examined and tested to insure good over-all component reliability.

The careful screening of components means that the construction program of circuit modules, subassemblies, and entire canisters need not be based on having large numbers from which to select the best units. This results in the electronic circuit tests being utilized chiefly to find design errors and interface incompatibilities.

## III. CIRCUIT DESIGN

Reliable circuit operation is obtained by minimizing the need for new inventions; by basing the circuit design on well established methods; and by including in the design as much margin as power consumption, size, and weight will permit. In the case of microwave design, the Bell System has a great fund of knowledge which has been built up over the years with the two transcontinental microwave systems, the TD-2 and TH systems, operating at 4 and 6 gc respectively. Since both of these frequencies are used in the Telstar project, it was possible to follow earlier designs of such equipment as filters and frequency converters. Similarly, years of Bell System experience in designing circuits for operation from dc to very-high-frequency form a basis for development in these areas.

During the circuit development stages, the circuits were temperature cycled between $-20°C$ and $+60°C$. Circuits with components which would be severely affected by these temperature extremes were given as wide a temperature test as their components would allow. The mini-

mum design temperature range is 0°C to +40°C. To be acceptable, a circuit was required to operate completely satisfactorily within the design temperature limits and to operate with little loss in performance between the −20°C to +60°C temperature limits. Groups of circuits were also exposed to these temperature tests to investigate circuit interface problems.

As early as possible the circuit was wired into its first equipment layout form and foamed to assure proper operation in its final environment. It was then given vibration tests with vibration magnitudes equal to or greater than those specified in the satellite qualification test specification.[2] These requirements were more stringent than the conditions expected during handling and launching. Those circuits which would normally operate during the launch were electrically tested during the vibration test. Circuits not expected to be operational during the launch phase, such as the microwave circuits, were electrically tested for survival only.

Following the design of a circuit, a computer analysis was used, time permitting, to investigate the effects of variations in active and passive components which would result from temperature effects, aging, and initial tolerances. A variational study permitted the investigation of "worst-worst" conditions.

## IV. EQUIPMENT DESIGN, CONSTRUCTION, AND TEST

The equipment design used in the Telstar satellite is conservative and is based when possible on past experience. No microminiaturization is utilized, but rather the usual methods associated with microwave and lower-frequency circuits have been used. To aid in explaining the equipment design approach, an example of the construction and evaluation process in the form of a regulator will be described in some detail.

The initial step in the production of a unit such as the regulator is the compiling of the necessary components. As described in a companion paper,[1] each component is serialized before being delivered to the assembly area. Clerical personnel assemble all the necessary components for a particular circuit into a kit and record the serial number of each component, together with the location of that component in the circuit. This careful record keeping on devices can be of considerable value in diagnosing failures. A case in point is the command circuit malfunction in the satellite.[3] In this case, once the transistor which caused the malfunction was determined, it was possible to review that transistor's original characteristics.

Certified wiremen with special training then assemble the circuit.

Special precautions were observed when the more delicate components were handled. Operators handling point-contact semiconductor devices wore grounded bracelets, and those handling units with critical finishes wore white nylon gloves. Fig. 1 shows the completed wiring of one of the boards making up the regulator. The miniature magnetic latching relays used for controlling the traveling-wave tube are shown together with a number of passive components. Much thought was put into the type of mechanical structure and the type of electrical connections employed in such boards to assure the necessary mechanical and electrical reliability.[4] Upon completion of wiring, the board shown in Fig. 1 is sent to the inspectors.

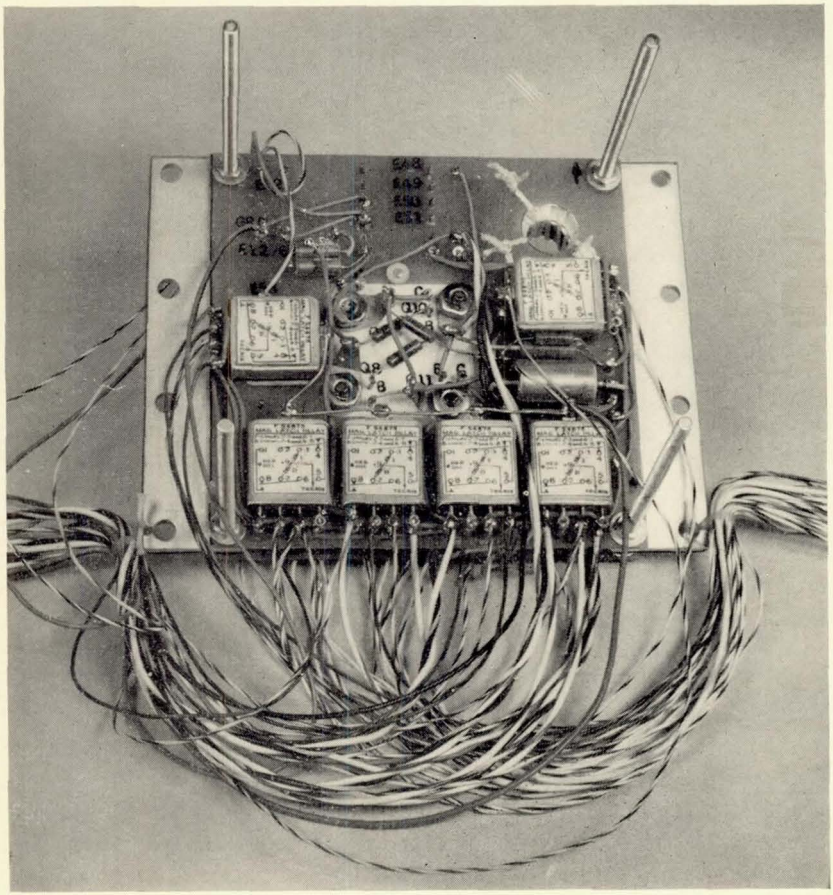

Fig. 1 — First circuit board of regulator.

Visual inspection plays an important part in assuring mechanical reliability. The Bell System's experience in the development of the submarine cable repeaters, where an equal or greater degree of mechanical reliability was necessary, had indicated the need for inspection and developed suitable methods to be used. This function was felt to be important enough to have the inspection group placed under the supervision of the engineering division. The circuits are inspected for correct wiring and every solder joint is examined under a microscope. Each component is examined for correct polarity and value; it is also examined to determine that no harm has been done to it during installation. The trained inspector also observes the over-all circuit to catch any potential trouble conditions. In all cases, a sufficient number of wiring and inspection steps is included to assure that no component is buried beneath another card or component before it has been checked. Fig. 2 shows the result of a number of such steps. The completely wired regulator in this figure is ready for extensive electrical tests.

The initial electrical tests are performed at room temperature and

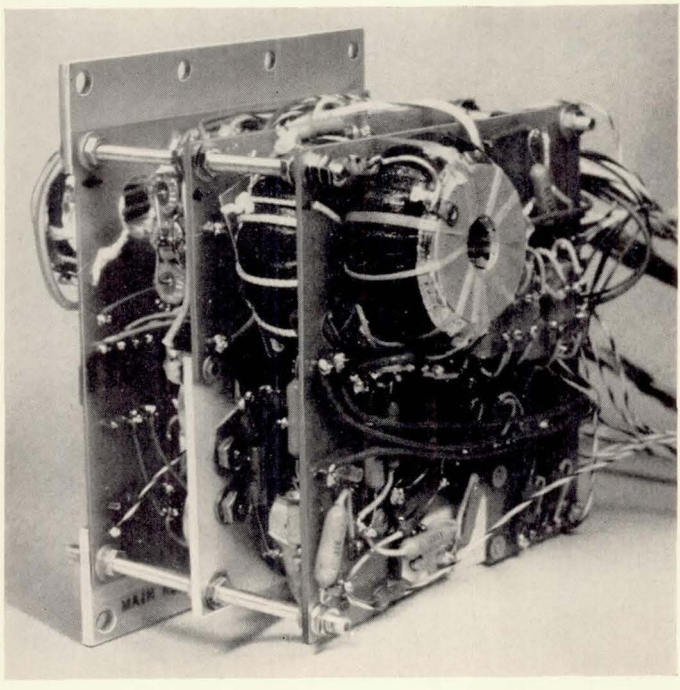

Fig. 2 — Completely wired regulator.

include any adjustments and component selection called for in the normal testing program for proper operation of the circuit. The selected components are then wired in place and inspected as indicated before. At this point, the circuit is rechecked for proper operation while it is exposed to changes in temperature, power supply voltage, and other variable quantities peculiar to that circuit. In the case of the regulator used as the example in this discussion, it is also exposed to the magnetic field of the traveling-wave tube and to a change in input voltage and output load. No vibration tests are included at this time because the unit has not yet been foamed. The foam, which encases every component, provides the necessary strength for the rather light circuit board structure.

Fig. 3 shows the regulator placed in an aluminum mold ready for foam encapsulation, and Fig. 4 shows the same unit upon completion of the encapsulating process. Special attention was given to the selection

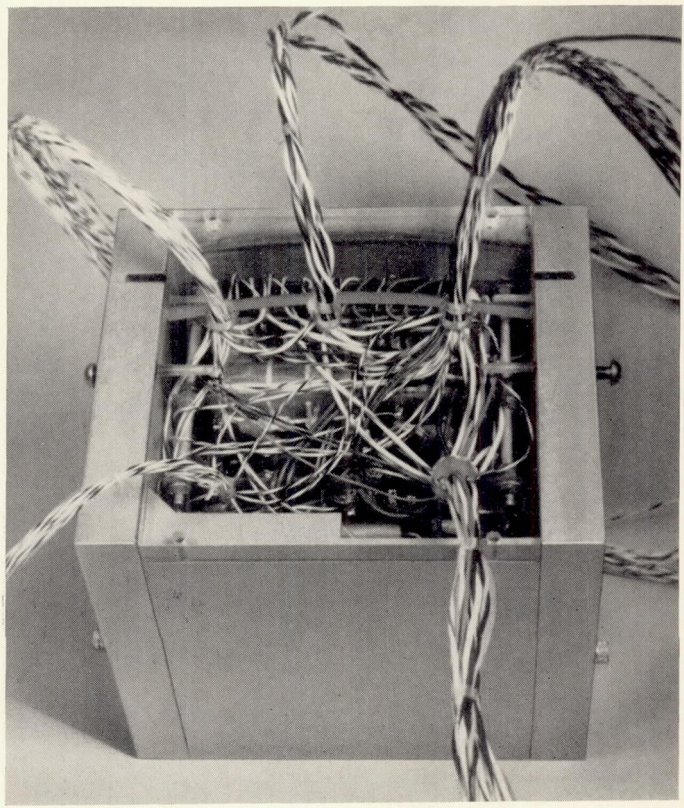

Fig. 3 — Regulator in mold ready for foam encapsulating.

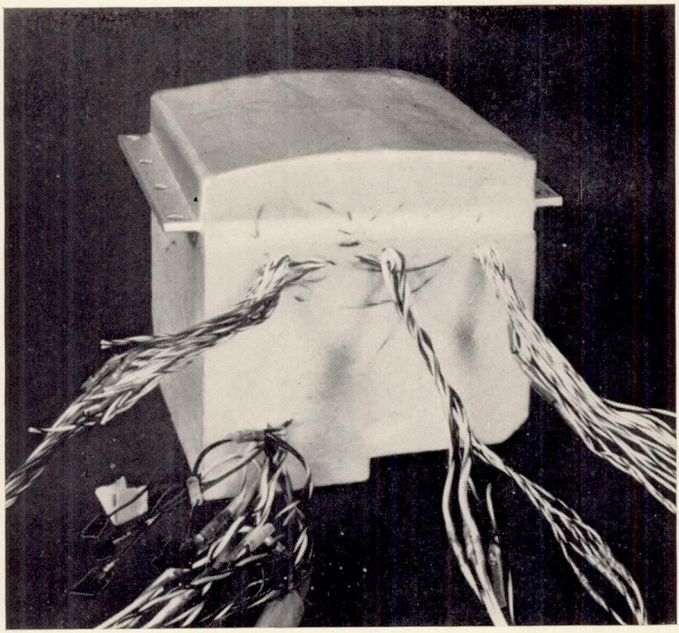

Fig. 4 — Encapsulated regulator.

of foam material and its density, to assure a reasonable compromise between supporting strength and weight.[4] Bell System experience with foam encapsulation in a missile control X-band guidance system had indicated that considerably improved mechanical reliability could be obtained by encapsulating the circuits with foam.

After foaming, the circuit is put through all the electrical tests performed prior to foaming and vibration tests with vibration magnitudes equal to those specified in the satellite acceptance test specification.[2] Because the regulator would normally operate during the launch, it was electrically tested during the vibration test. At this time, the construc tion and evaluation process of the unit is complete.

It can be seen that careful control of the assembly process plays an important part in establishing the high level of reliability which we believe to be incorporated in the Telstar satellite. Fig. 5 is a copy of the first of several control sheets describing the steps through which the regulator progressed on its way to completion. Most circuits have as many as 50 to 60 steps, which have all been recorded on such sheets. In each case, the person involved in a particular step signs his initials and the date, signifying the proper completion of his task. This careful record keeping assures no steps are bypassed, gives a permanent record

ROUTE SHEET POWER SUPPLY REGULATOR
B-890049 Iss. 3 (Schem)

| | Date Recv'd. | Date Compl. | Sign. |
|---|---|---|---|
| B-133491 Iss. 2 (Assem) Board 1 of 3 | | | |
| 1. Assemble board as per above drawings. Serial No. FS-8515 | 2-8-62 | 2-9-62 | Jaw |
| 2. Record transistor and diode serial numbers | 2-8-62 | 2-9-62 | Jaw |
| 3. Inspect Step 1 | 2-10-62 | 2-10-62 | Ejm |
| 4. Inspect Step 2 | 2-10-62 | 2-10-62 | Ejm |
| 5. Electrical Test and Adjust | 2-14-62 | 2-14-62 | AET |
| 6. Inspect Step 5 | 2-15-62 | 2-15-62 | Ejm |
| B-133489 Iss. 4 (Assem) Board 2 of 3 | | | |
| 1. Assemble board as per above drawings. Serial No. FS-8519 | 2-10-62 | 2-10-62 | DTN |
| 2. Record transistor and diode serial numbers | 2-10-62 | 2-10-62 | DTN |
| 3. Inspect Step 1 | 2-12-62 | 2-12-62 | JaF |
| 4. Inspect Step 2 | 2-12-62 | 2-12-62 | JaF |
| 5. Electrical Test and Adjust | 2-16-62 | 2-16-62 | AET |
| 6. Inspect Step 5 | 2-18-62 | 2-18-62 | JaF |
| B-133490 Iss. 7 (Assem) Board 3 of 3 | | | |
| 1. Assemble board as per above drawings. Serial No. FS-8523 | 2-14-62 | 2-14-62 | Jaw |
| 2. Record transistor and diode serial numbers | 2-14-62 | 2-14-62 | Jaw |
| 3. Inspect Step 1 | 2-16-62 | 2-16-62 | Ejm |
| 4. Inspect Step 2 | 2-16-62 | 2-16-62 | Ejm |
| 5. Electrical Test and Adjustment | 2-19-62 | 2-19-62 | AET |
| 6. Inspect Step 5 | 2-21-62 | 2-21-62 | Ejm |

ATTACHED PAPERS: Transistor and diode serial numbers

Fig. 5 — Copy of one of the regulator route sheets.

of who handled the unit, and keeps everyone constantly aware of the need for care and caution. If trouble should develop, the sheets provide a history from which the trouble can be traced and evaluated.

## V. CANISTER AND ITS ASSEMBLY INTO THE SPACECRAFT

After every individual unit such as the regulator is completed, the process of mounting in the canister is started. Fig. 6 shows the canister in an early stage of assembly, together with the electronic equipment it will contain when completed. The traveling-wave tube is shown directly below the canister on the rotary table of the stand. Clearly visible are several pieces of silver-plated magnesium waveguide, and near the extreme left is the regulator which has been described in some detail in the previous section. Fig. 7 shows the same canister almost fully as-

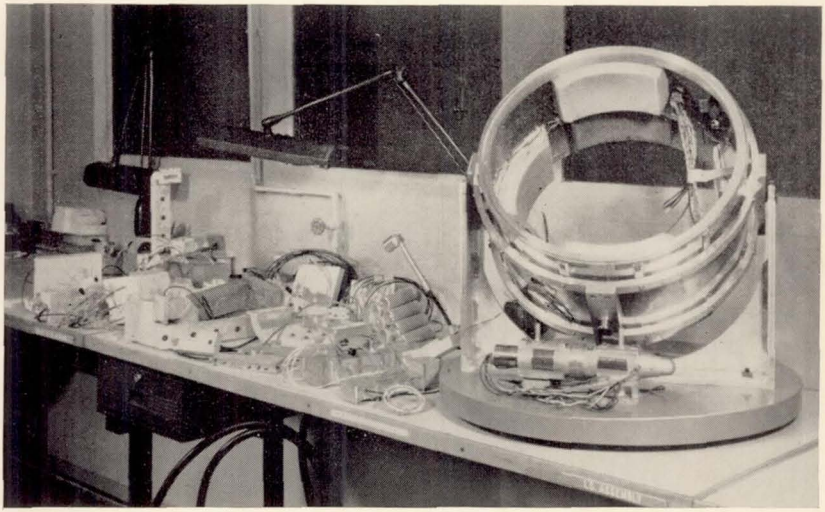

Fig. 6 — Partially assembled canister with subassemblies.

sembled, with the traveling-wave tube mounted in the center and the waveguide surrounding it in a roughly circular arrangement. The digital, low-frequency, and VHF circuits fill in the remaining available space. The units are interconnected in nearly all cases by crimped connections. The use of connectors is kept to a minimum, because of the difficulty in determining whether a good connection has been made by the cable into each of the mating parts and whether the mating parts have been properly seated into each other. The connectors used in the canister are all tested for shorts during various mechanical manipulations of the cable and connector, and most are X-rayed. The X-ray analysis is only partially successful, however, because the inner connection is masked by the massive body of the connector.

Prior to the foaming operation, the completed canister is given an all-feature inclusive electrical test at room temperature. The only parameter changed during this test, other than the radio frequency signals, is the supply voltage. The goal of this test, as well as future tests, is not to establish a level of reliability but rather to uncover design oversights and errors made in the design process. Upon successful completion of this test, the canister is subjected to a +25°F temperature electrical test, and a +95°F* temperature electrical test. These electrical tests are not as inclusive as the initial program; however, they give a complete check of the satellite's operation.

* This value was used rather than the 40°C design value to protect the Ni-Cd cells, as explained in Ref. 5.

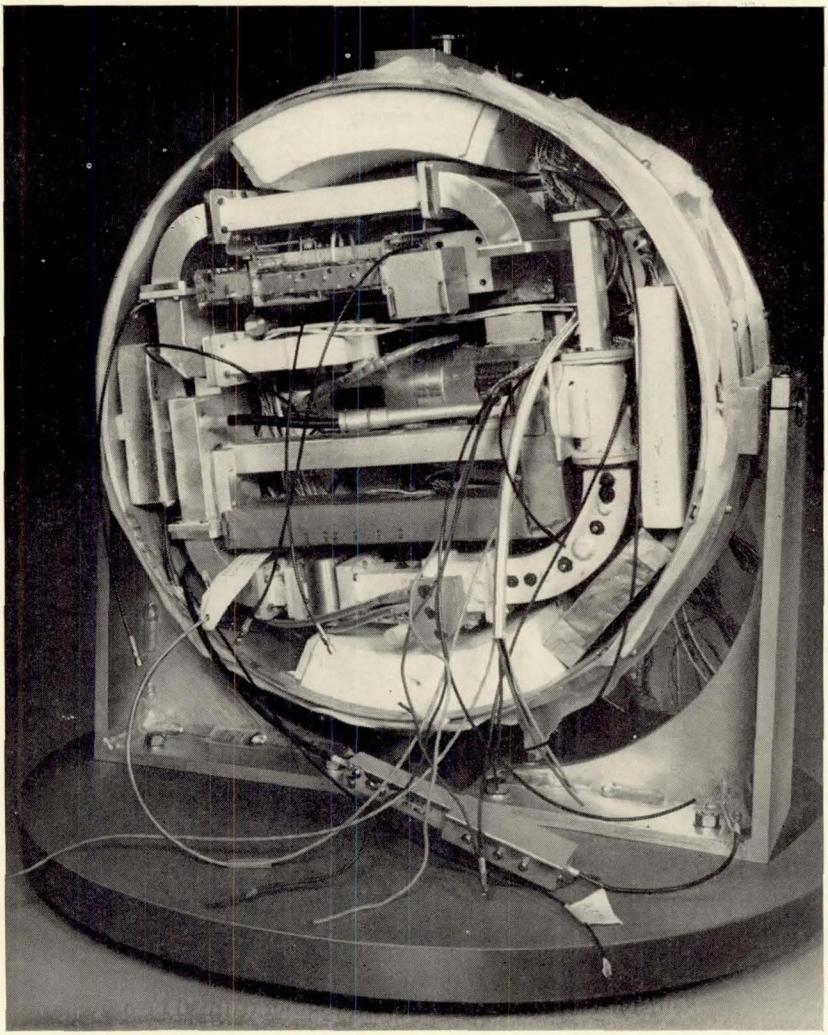

Fig. 7 — The electronics canister.

The next step is the foam encapsulation of the canister. Fig. 8 shows the canister in the last stages of the foaming process. A detailed explanation of the process is given by Shennum and Haury.[4] The properties of foam in a hermetically sealed canister in a radiation environment have been investigated; tests indicate the foam to be a stable material. During the foaming process the chief gaseous material generated is carbon

dioxide with only the slightest traces of potentially corrosive materials. Careful chemical analysis has indicated that these materials are of such small quantity that they represent no threat to the enclosed components for periods of at least several years.

Upon completion of the foaming process, the canister is subjected to a +125°F temperature soak for six hours, a 0°F temperature soak for six hours, a +25°F temperature electrical test, and a +95°F temperature electrical test. These tests are the same as the last complete tests performed on the canister prior to foaming.

Fig. 9 shows the completed canister with the domes welded in place. Before it is installed in the frame, the hermetically sealed canister is

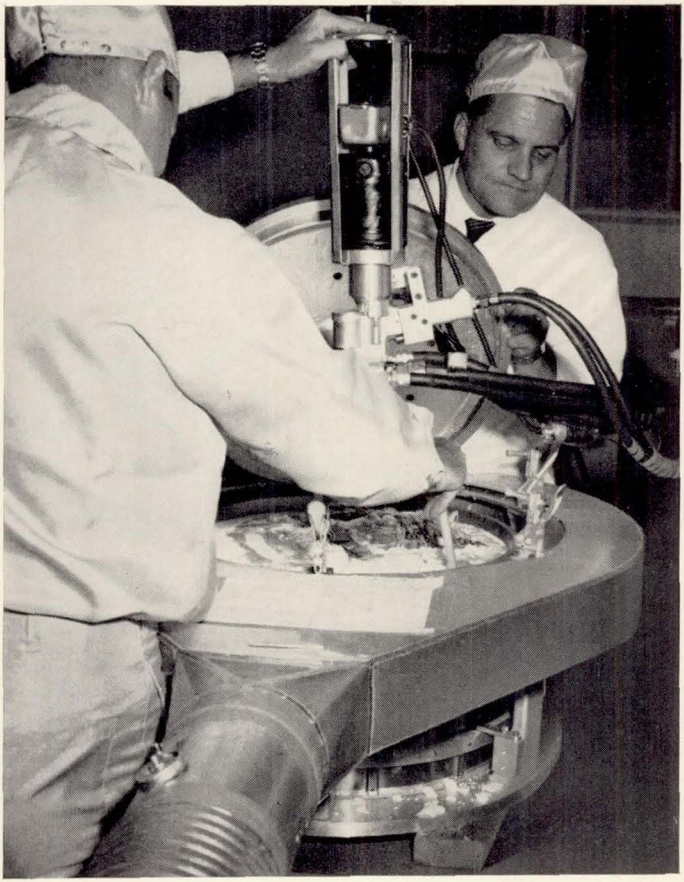

Fig. 8 — Foam encapsulation of the canister.

Fig. 9 — Mounting of electronics canister into the frame.

checked for leaks.[4] There are a number of headers which provide electrical access to the circuitry inside the canister for such things as solar power, antenna feeds, and the radiation experiment. It is important that these headers as well as the canister dome welds be leakproof, for a complete loss of pressure in the canister when in orbit might cause permanent damage to the circuits within. Upon successful completion of the leak test, the canister is wrapped with insulating material and the thermal shutter is attached.[4] A final electrical test at room temperature assures that the canister has not been harmed during performance of the operations described.

The canister is then lowered into the frame and attached to the mounting rings, which are suspended from the frame by nylon lacing.[6] The required electrical connections are made between the external framework and the canister, the top half of the frame is attached, and the aluminum panels which support the 3600 solar cells are electrically connected and screwed into place. This completes the construction of the satellite. Prior to the detailed environmental tests which the complete satellite must undergo, an all-feature electrical test is conducted to assure that the above assembly process was complete and correct.

The detailed environmental tests include vibration on the thrust axis and on the lateral axis, and a thermal-vacuum test.[2] After every stage of the above tests, complete electrical tests are made. Each electrical test is designed to indicate that no harm was done during the environmental test. Upon completion of these tests, a successful leak test and a successful all-feature inclusive electrical test indicate that the spacecraft is of launch quality.

Fig. 9 also illustrates the working conditions which were enforced during the entire construction process. The construction area was air-conditioned; air-conditioning provided triple filtering to remove foreign particles, a 75°F* temperature, and a 35 per cent† relative humidity. In addition to the special mechanical and electrostatic air filtering, stringent controls were imposed to minimize the introduction of contaminants. These included:

1. Providing special lint-free uniforms and caps for all white area operating personnel.
2. Providing lint-free smocks and caps for all occasional personnel and visitors. Visitor entry was minimized.
3. Requiring that all personnel wash their hands and clean their shoes on each entry.
4. Cleaning all equipment to be brought into the white areas with alcohol and lint-free cloths.
5. Using paper, writing implements, and cloths that would not produce lint or dust. For example, ball point pens were used in place of pencils and dust-free crayon boards were used in place of chalk boards.
6. Mopping and dusting all white areas daily.

To monitor the effectiveness of this program, a dust count was made twice weekly and posted on local bulletin boards. The Bell System's experience in the construction of the submarine cable repeaters had

* Temperature was maintained at nominal 75°F, but was always in the range 73 to 77°F.

† Relative humidity was maintained at nominal 35 per cent, but was always in the range 30 to 40 per cent.

established the value of this sort of environment and discipline in the construction of high-reliability equipment.

## VI. SUMMARY

The care exercised in assuring a spacecraft of maximum reliability has proven valuable. An unexpected level of radiation inside the canister of two orders of magnitude above the anticipated value caused command decoder circuit operation to become intermittent after four and one-half months in space with over 1100 orbits around the earth. This unexpected radiation caused one command link to become intermittent after one month of operation. The command link is completely redundant, however, so normal operation of the satellite continued. It was not until four and one-half months had passed that the other command link became intermittent and hence operation of the satellite curtailed.

It was after the second command link had failed that it was possible to make meaningful experiments on the satellite in space to determine the source of trouble. Telemetry continued to operate giving indications that the command receiver was operating normally. Exercising the command decoders with a modified command code finally operated the satellite via the command link which had failed first. This isolated the failure in that decoder to a single transistor stage.[7] The cause of the second command link failure has not been so narrowed as yet. Following the removal of power from the decoders for several passes, normal commands operated the satellite via both command links. This recovery characteristic, plus other observations at the original time of failure, indicated that the trouble was associated with a surface ionization effect on the active surfaces of transistors caused by radiation.

The telemetry unit, which has continued to operate satisfactorily, supplies information concerning the health of other parts of the system, including the communications repeater, the battery and the solar plant, and indicates that all units in the satellite are operating normally. By the use of normal commands, the Telstar repeater is again carrying communications information on an operational basis. These tests, carried on from Andover to Andover and from Andover to both England and France, indicated that the communications repeater was operating with no measurable degradation. A second period of loss at command began in late February, 1963.

## VII. ACKNOWLEDGMENTS

As in any corporate effort, many people contributed to the work described in this paper. The leadership and advice of Mr. E. F. O'Neill is particularly worthy of acknowledgment.

REFERENCES

1. Peck, D. S., and Wooley, M. C., Component Design, Construction and Evaluation for Satellites, B.S.T.J., this issue, p. 1665.
2. Delchamps, T. B., Jonasson, G. C., and Swift, R. A., The Spacecraft Test and Evaluation Program, B.S.T.J., this issue, p. 1007.
3. Mayo, J. S., Mann, H., Witt, F. J., Peck, D. S., Gummel, H. K., and Brown, W. L., The Command System Malfunction of the *Telstar* Satellite, B.S.T.J., this issue, p. 1631.
4. Shennum, R. H., and Haury, P. T., A General Description of the *Telstar* Spacecraft, B.S.T.J., this issue, p. 801.
5. Moose, L.. F, and Bomberger, D. C., Nickel-Cadmium Cells for the Spacecraft Battery, B.S.T.J., this issue, p. 1687.
6. Hrycak, P., Koontz, D. E., Maggs, C., Stafford, J. W., Unger, B. A., and Wittenberg, A. M., The Spacecraft Structure and Thermal Design Considerations, B.S.T.J., this issue, p. 973.
7. Peck, D. S., Blair, R. R., Brown, W. L., and Smits, F. M., Surface Effects of Radiation on Transistors, B.S.T.J., **42**, January, 1963, p. 95.

# The Solar Cells and Their Mounting

By K. D. SMITH, H. K. GUMMEL, J. D. BODE, D. B. CUTTRISS, R. J. NIELSEN and W. ROSENZWEIG

(Manuscript received March 28, 1963)

*Objectives in development of the solar plant for the Telstar spacecraft were to provide a power source which would withstand launching stresses and the expected space environment, with optimum end-of-life performance. Radiation damage to the silicon solar cells is the primary factor limiting their useful life; the effect of energetic protons or electrons is the generation of recombination centers in the silicon which reduce the minority-carrier diffusion length and therefore the long-wave response of the cell.*

*The spacecraft solar cells use the n-on-p structure, in preference to conventional p-on-n structure, to obtain a factor of 3 to 10 increased life expectancy. Response to light in the 0.4 to 0.7 micron range is enhanced by using a thin n-layer (about 0.5 micron) and an antireflection coating with minimum reflectance at 0.55 micron wavelength. Early estimates of electron and proton fluxes in the satellite orbit showed that even the best cells would not give sufficient life without radiation shielding. Therefore the cells are protected against electrons of energy up to 1 Mev by 0.3 gm/cm² sapphire cover plates. The cell mountings are designed to withstand peak vibration stresses of 200 g and repeated temperature cycles from +65°C to −100°C.*

*The 3600-cell solar power plant is composed of 300 twelve-cell groups of 1 cm × 2 cm cells, yielding a nominal initial power of 14 watts at 28 volts for any spin-axis orientation relative to the sun. Telemetry information on performance of the solar plant indicates degradation of the shielded solar cells equal to that measured in the laboratory on unshielded cells with a 1-Mev normal incidence flux of 6 × 10¹² electrons/(cm² day). From this comparison it is estimated that the plant will degrade to 68 per cent of its initial output after two years in orbit.*

## I. INTRODUCTION AND BACKGROUND

### 1.1 *Introduction*

General objectives in design of the solar plant for the Telstar spacecraft were to provide cells and mounting arrangements suitable for

prolonged operation in a radiation environment and, consistent with the state of technology and the program schedules, to optimize the output per cell after some years in orbit. Preliminary estimates clearly indicated that deterioration of cell output through energetic particle radiation damage would be the most serious effect, and that, unless this damage could be held within reasonable bounds, we would be forced to over-design the initial power considerably, perhaps by a factor greater than two, as compared to end-of-life requirements. Answers to the following questions were urgently needed:

(1) What power must be supplied by the solar plant?

(2) What orbit will be used?

(3) What radiation will be encountered?

(4) What will be the effect of this radiation on the solar cells?

(5) What design choices may be made and how do they interact to affect life?

(6) What other factors are of importance besides radiation effects?

(7) What temperatures and temperature gradients must be designed for?

(8) Can manufacturing feasibility be shown for structures of optimum or near-optimum design?

This report will consider: the radiation effects study; design, fabrication and evaluation of the solar cells; design and engineering of the mounting of solar cells into groups; mounting and arrangement of cell module groups on the satellite; performance estimates and measurements leading to the choice of total number and connection of cells; and measurements of performance. It begins with consideration of the historical background of the solar cell and ends with evaluation of the flight performance.

### 1.2 *Background*

Silicon photovoltaic converter cells of moderate-to-high solar conversion efficiency were first prepared in 1954.[1] In the following two years, a few cells with 11 per cent conversion efficiency were made, and in the laboratory it became possible to fabricate cells in the 8 per cent to 10 per cent range with good yield.[2] The process was at this time given to Bell System licensees, some of whom continued development through the next several years.

In the early development, cells of both p-on-n and n-on-p structure were made. However, during the greater part of the development program n-type silicon of appropriate resistivity was more readily available

than p-type; also, the p-on-n cells made at that time gave somewhat higher conversion efficiency than n-on-p cells — perhaps because of the low reflectance of the degenerate surface layer characteristically resulting from the boron trichloride diffusion process. The result was that the standard or conventional solar cells made in the U. S. have been of the p-on-n structure. Russian development engineers, and possibly others in Europe, appear to have concentrated on n-on-p cells, perhaps because of material availability or the state of their diffusion technology, or both.

### 3.1 *Principles of Operation*

A brief discussion of the operation of the solar cell is in order as an introduction to more detailed consideration of the merits of different cell structures and effects of radiation and other environmental factors. The silicon photoelectric energy converter or solar cell, shown schematically in Fig. 1, is representative of a class of devices in which radiant energy is absorbed within a material, thereby upsetting an equilibrium condition and permitting electrical power to be delivered to an external circuit. In the solar cell, the absorbed photons create electron-hole pairs in the silicon. In the frequency range of interest, one pair is produced for each photon.

Referring to Fig. 2, it can be seen that events subsequent to the arrival of photons at the cell surface may be:

(1) Photons are reflected and thus no energy is available.

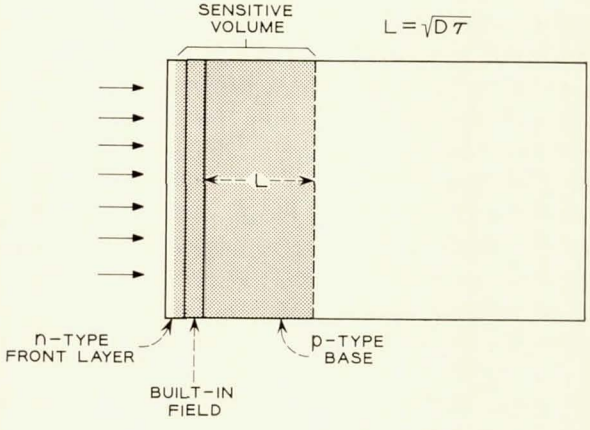


Fig. 1 — Schematic of n-on-p solar cell.

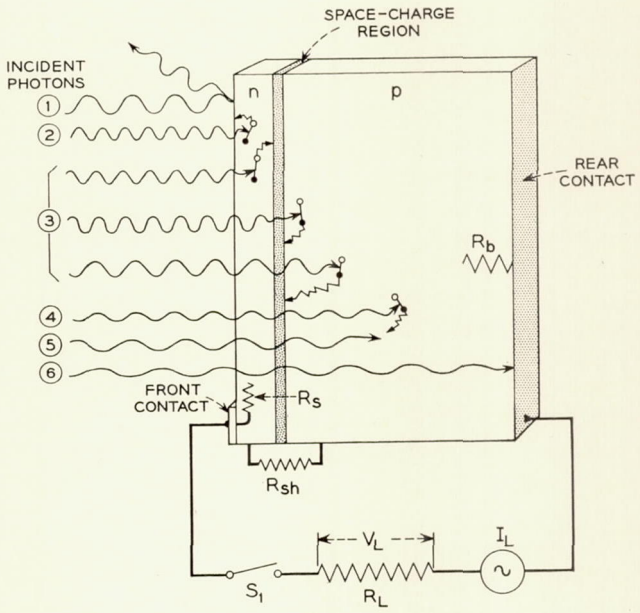


Fig. 2 — Photon and resistive losses.

(2) Photons are absorbed near the cell surface, creating hole-electron pairs, but the holes recombine with electrons without reaching the field region at the p-n junction. No electric energy is available from this reaction; however, thermal energy appears.

(3) Hole-electron pairs are created near enough to the junction for the minority carrier to reach the field region and cross the junction, contributing to the useful output current. Some heat is also generated.

(4) Pairs are created, but too far from the junction to be useful.

(5) Photons are absorbed, but have insufficient energy to create hole-electron pairs. Only heat is generated.

(6) Low-energy photons may not be absorbed in the semiconductor.

Since only the photons of (3) are effective in contributing to the electrical output of the cell, every effort will be made to optimize conditions so as to make use of as many photons as possible.

The external power which can be generated by the charge carriers which reach the junction is affected by the following considerations:

(a) The terminal voltage of the device cannot exceed that value which will drive across the junction a forward current equal to the photon-generated current. If we consider the situation with switch $S_1$ of

Fig. 2 open, we see that the forward bias current will just equal the generated current; the efficiency will then be zero.

(b) The generated current must flow to the external circuit through the series resistance $R_S$ of the diffused layer and the series resistance of the semiconductor body, $R_b$. Generally, the body resistance can be made much lower than the surface layer resistance.

(c) There will be some shunt resistance, $R_{sh}$, effectively in parallel with the p-n junction. Generally this may be neglected in power circuits.

From the above discussion, it becomes evident that performance optimization will require consideration of:

(1) the spectral distribution of solar radiation
(2) the environment
(3) the properties of the semiconductor
(4) reflection losses
(5) recombination losses
(6) parasitic resistive losses
(7) load impedance and
(8) the useful life desired — if the environment is destructive.

### 1.4 *Significance of Van Allen Belt*

Before 1957, estimates of expected life of satellite solar power plants did not generally include deterioration of performance resulting from energetic particle radiation, since no continued high-intensity source was known and the integrated effects from cosmic rays and solar flares were not expected to be serious. The discovery of the Van Allen belts[3] changed this situation completely. For satellites at altitudes in the 1000–10,000-mile range, particle radiation is the principal cause of solar cell performance loss. Therefore, it became of immediate importance to evaluate the radiation effects and, if possible, design solar cells and solar power plants to be radiation resistant. A development program initiated at U. S. Army Signal Research and Development Laboratories (USASRDL), with the objective of obtaining solar cells of improved conversion efficiency, had resulted in a feasibility demonstration of n-on-p cells comparable in conversion efficiency to the p-on-n cells commercially available in 1960. Also, these cells had a thin n layer, so they were more sensitive in the short-wave end of the visible spectrum and better matched to space sunlight than conventional cells.

In the course of radiation evaluation experiments[4] on USASRDL cells conducted by Radio Corporation of America under NASA contract, these n-on-p cells were found to be significantly more resistant to both

electron and proton radiation than p-on-n cells of equivalent initial performance. On December 8, 1960, USASRDL presented their results, together with a complete description of their laboratory scale fabrication operations for the n-on-p cell, to representatives of the major industrial laboratories.

Bell Telephone Laboratories development effort on the radiation-resistant n-on-p cell was initiated in October, 1960, as a result of the early radiation reports[5,6] and informal discussion with Signal Corps personnel. Some of the Laboratories staff assigned to this development had also engaged in the p-on-n cell feasibility development (1955–56), and so had considerable experience in solar cell technology. Laboratory fabrication of n-on-p cells was undertaken about the end of October, 1960, and the first cells exhibiting satisfactory performance were made about a month later.

### 1.5 *Solar Cell Requirements for the Telstar Spacecraft*

During the early part of the n-on-p solar cell development, and even into the initial Western Electric Co. fabrication, the satellite power requirements were not firm and the number of cells to be used on each vehicle was not known. The objectives were to achieve the highest end-of-life performance consistent with manufacturing feasibility. Having established this performance level, the total number of cells required for a particular end-of-life power requirement could be determined to the accuracy with which the environmental conditions could be predicted. Coordinated work on evaluation of radiation effects, technology of cell fabrication, environmental studies, and satellite power drain was therefore required. This work is considered in the following sections.

## II. RADIATION DAMAGE STUDIES

### 2.1 *Background*

Proton and electron particle radiation, such as is found in the Van Allen radiation belts, produces permanent damage in silicon by reduction of the minority-carrier lifetime. This degrades the solar cell performance by decreasing the collection efficiency for carriers generated by penetrating light and by increasing the saturation current of the junction. The degradation of lifetime with particle bombardments of the type and energy expected in the Van Allen belts is thus of primary interest, as is the correlation between the performance of a given type of solar cell and its bulk minority-carrier lifetime.

The type of information on radiation damage in semiconductors available at the beginning of the project is quite well summarized in Ref. 7. Work on damage rates for protons had been almost nonexistent (the nature of the defect was considered too complex to allow simple analysis), and the electron damage studies had emphasized the search for the location of energy levels in the forbidden gap. All evaluations of the defect introduction rates had indicated that the results were dependent on the presence of impurities, both controlled and uncontrolled. Electron spin resonance experiments carried out since that time have indicated that the important defects, at least in n-type silicon, arise from complexes of vacancies in association with impurity atoms.

In light of this situation the radiation damage problem was approached with the following objectives:

(1) the evaluation of the outer space solar cell performance on a good statistical sample of cells bombarded by a convenient source of radiation (1-Mev electrons) and the correlation of this performance with the minority-carrier lifetime;

(2) the determination of lifetime degradation rates for protons of various energies and for electrons of various energies and under various shielding thicknesses; and

(3) the synthesis of the above information for the best available Van Allen belt spectrum with the assumption of "equal performance for equal lifetime" for a specific type of cell.

### 2.2 *Measurement Techniques*

The most important parameter characterizing the outer space performance of the solar cell is its outer space short-circuit current. Once this quantity has been accurately determined, the output characteristics can be measured under any convenient light source whose intensity has been adjusted to produce the predetermined outer space short-circuit current.

Determination of outer space short-circuit current was carried out by measuring the response of the cells at various discrete wavelengths and using this information to synthesize the outer space cell response.[8] The synthesis is achieved by multiplying the response at a given wavelength by an appropriate weighting factor, so that the summation of these products over all wavelengths yields the integral which represents the outer space short-circuit current. This procedure also allows one to assess the contributions to the total current of the various wavelength components, and thus to optimize the design in regard to spectral response.

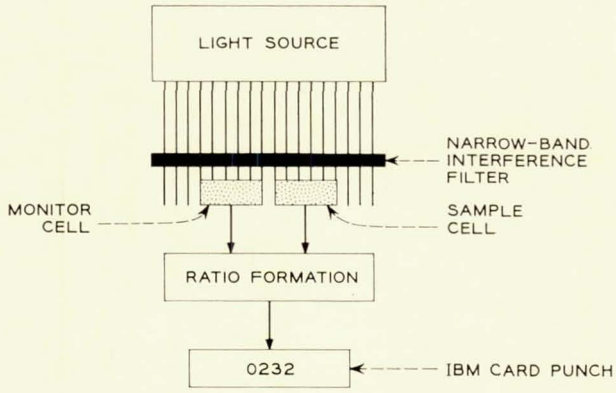


Fig. 3 — Schematic representation of spectral response ratio measuring apparatus.

An automatic test set was developed[9] which carries out spectral response measurements at eight wavelengths, in addition to making five other tests which serve to evaluate the cell junction characteristics. Fig. 3 shows schematically the method used for measuring the spectral response. Electronic ratio formation of the response of the sample relative to the monitor cell is used to eliminate the influence of fluctuations and aging in the light source. All measurements appear in digital form and are punched on IBM cards to permit further processing.

The minority-carrier lifetime was determined by measuring a related parameter, the minority-carrier diffusion length. Diffusion length measurements were carried out by a technique which utilizes the ionizing properties of penetrating radiations such as high-energy electrons, protons, and gamma rays.[10]

### 2.3 *1-Mev Electron Statistical Experiment*[11]

A statistical evaluation of solar cell performance was carried out with a 1-Mev electron Van de Graaff generator. Groups of 16 or more solar cells of the following types were used:

(1) Blue-sensitive n-on-p cells produced by Western Electric Co.: these cells were randomly selected from a lot of 10,000 cells, from which only those cells having an efficiency less than 7.5 per cent under outer space light had been removed.

(2) Normal p-on-n cells secured from a commercial source and rated as 14 per cent efficient under tungsten light.

(3) Blue-sensitive p-on-n cells secured from a commercial source and rated as 12 per cent efficient under outer space light.

To achieve uniform exposure for all cells, the solar cells were mounted near the perimeter of an aluminum disk, which was continuously rotated during the irradiations in such a way that the cells passed through the center of the beam.

The cells were irradiated in five steps to integrated fluxes of $1.8 \times 10^{13}$, $9.0 \times 10^{13}$, $5.4 \times 10^{14}$, $2.7 \times 10^{15}$ and $1.8 \times 10^{16}$ electrons/cm$^2$. Before the first and after each successive bombardment the cells were subjected to optical and electrical measurements and to measurements of the minority-carrier diffusion length. The results of the experiment are shown in Figs. 4, 5, and 6. Fig. 4 is a plot of the outer space short-

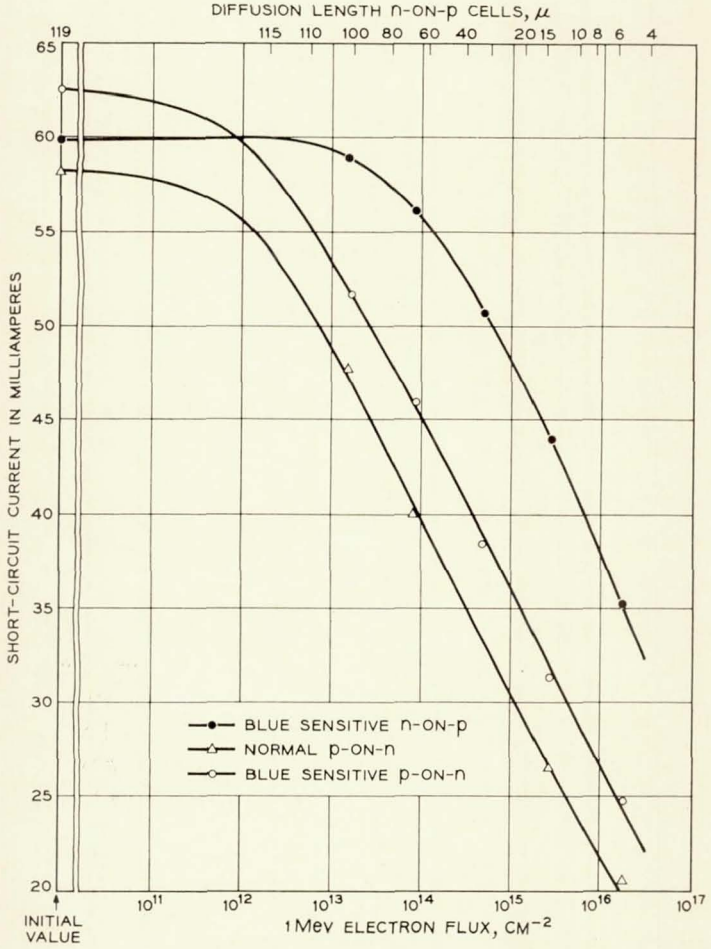


Fig. 4 — Outer space short-circuit current as a function of 1-Mev electron flux.

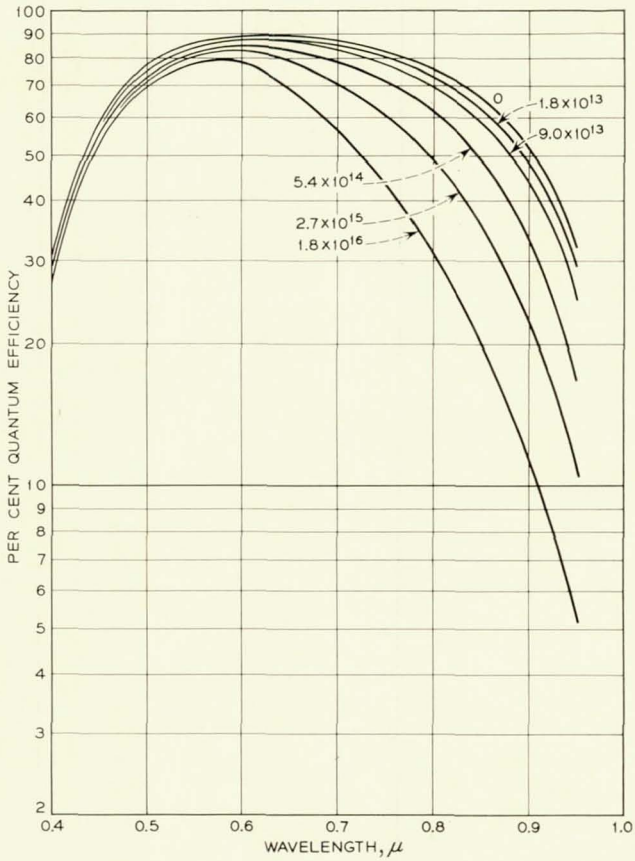


Fig. 5 — Per cent quantum efficiency as a function of wavelength for n-on-p cells, with 1-Mev electron flux as parameter.

circuit current as a function of bombardment flux. A detailed analysis[11] shows that the short-circuit current degradation is consistent with the diffusion length degradation and its effect on the quantum efficiency. Fig. 5 is a plot of the per cent quantum efficiency, defined as the number of carriers collected per 100 incident photons of a given wavelength, as a function of wavelength for various levels of bombardment of the n-on-p cells.

The predicted maximum power for outer space sunlight as a function of flux is given in Fig. 6. The decrease in maximum power with bombardment is caused not only by the decrease in short-circuit current but also by the degradation of the junction characteristics.

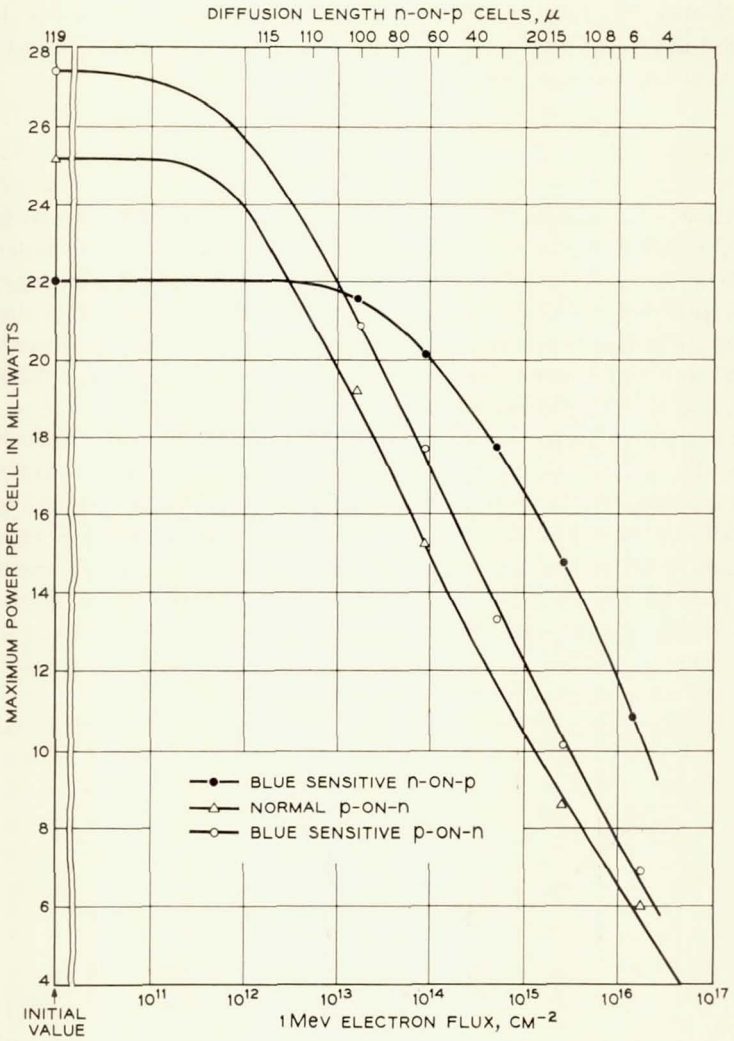


Fig. 6 — Outer space maximum power as a function of 1-Mev electron flux.

### 2.4 *Proton Bombardments*[12]

The proton bombardment damage study of solar cells required the use of four accelerators for coverage of the energy range of interest. At the higher-energy accelerators, the solar cells were stacked with aluminum absorbers to allow a simultaneous exposure at energies ranging from the initial beam energy down to about 20 per cent of this value.

The ionizing property of the proton beams was used to monitor the radiation-induced diffusion length changes. This change was found to follow quite closely the formula

$$\frac{1}{L^2} = \frac{1}{L_0^2} + K\Phi \tag{1}$$

in which $\Phi$ is the bombardment flux in $cm^{-2}$, $L$ is the diffusion length in cm for that flux, and $L_0$ is the initial diffusion length. The damage coefficient, $K$, can thus be determined as a function of proton energy in these experiments. The damage coefficient, $K$, is a measure of the damage rate for a given type of radiation on the cell. The relative fluxes of two different radiations to produce the same damage may be obtained by forming the inverse ratio of their damage coefficients.

The results are summarized in Fig. 7, which is a plot of $K$ vs proton energy. The $K$ values appearing in the figure are those which are observed after two weeks of room temperature annealing, which results in a recovery of about 15 to 20 per cent in diffusion length. Relative $K$ values were also obtained for one set of 1 ohm-cm p-on-n cells in the energy range 16.8 Mev to 130 Mev, and were found to be greater by a factor of $6.2 \pm 2$ independent of energy.

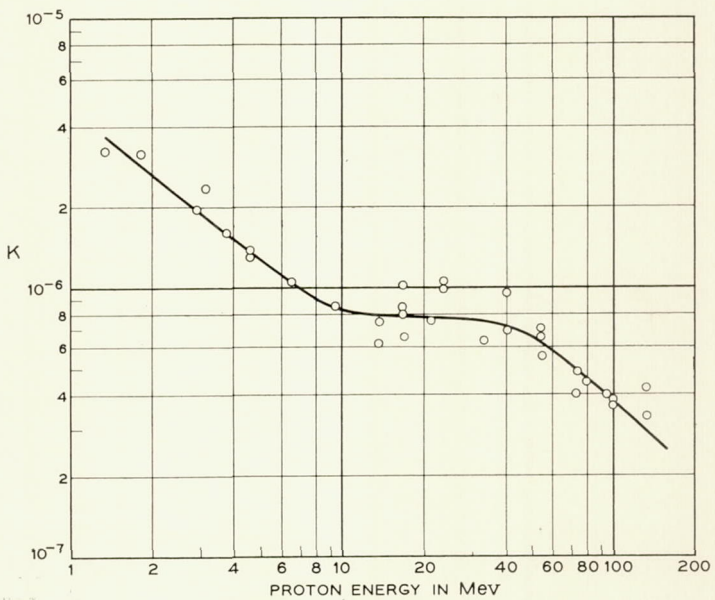


Fig. 7 — Damage rate as a function of proton energy.

2.5 *Original Estimates of Solar Plant Radiation Damage*

During the design phase, the data available for estimating the Van Allen belt radiation fluxes were quite limited. An integral omnidirectional proton spectrum was estimated by constructing a composite curve which above 40 Mev had a slope as determined by Freden and White,[6] and at lower energies as determined by Naugel and Fichtel.[13] Such a curve was made to pass through Van Allen's[3] point, $2 \times 10^4$ cm$^{-2}$ sec$^{-1}$ at 40 Mev for the heart of the belt. The resulting omnidirectional integral spectrum is shown in Fig. 8. For protons, the effect of shielding can be taken into account readily by making use of the range-energy relationship to calculate the energy attenuation. The result of shielding calculations is given as the upper curve in Fig. 9. The calculation is based on the proton spectrum of Fig. 8 and expressed in terms of an equivalent 1-Mev electron flux that would cause equal damage when normally incident on unprotected cells. This curve shows that the damage is reduced by a factor of about 10 when the shielding thickness is increased from 0.1 to 0.3 gm/cm$^2$. The relatively smaller advantage with larger shielding thickness is mainly due to the hardening of the proton spectrum for energies above 40 Mev. The shielding thickness used on the Telstar spacecraft is about 0.3 gm/cm$^2$, in the form of 30 mils of sapphire.

The electron component was estimated from Van Allen's[3] measurements, which indicated for the heart of the inner belt omnidirectional

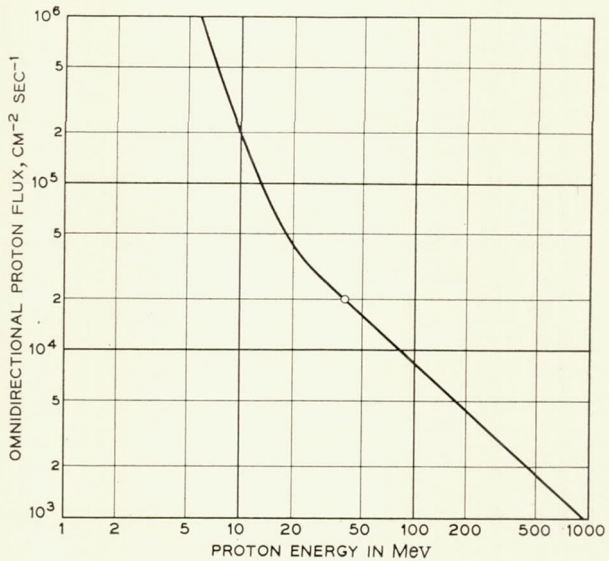


Fig. 8 — Omnidirectional integral proton flux as a function of energy.

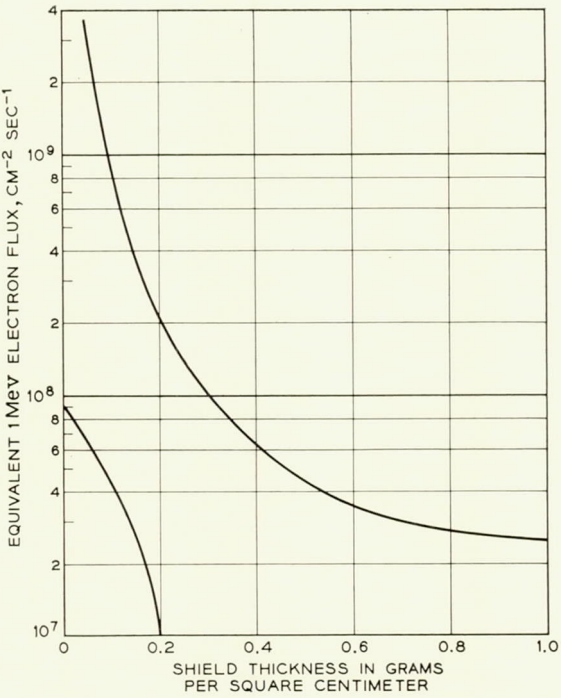


Fig. 9 — Equivalent 1-Mev electron flux as a function of shielding thickness.

intensities of $2.5 \times 10^{10}$ cm$^{-2}$ sec$^{-1}$ for energies greater than 20 Kev, and $1 \times 10^{8}$ cm$^{-2}$ sec$^{-1}$ for energies greater than 600 Kev. Cells covered with various thicknesses of sapphire were subjected to electron bombardments at a set of energies (0.4, 0.6, 0.8 and 1.0 Mev) with intensities designed to simulate the above spectrum. The resultant equivalent 1-Mev flux as a function of shielding thickness is also shown in Fig. 9. According to these data, the electron damage is small compared to the proton damage. However, in view of data taken after the July 9, 1962, high-altitude nuclear test explosion, the equivalent fluxes of Fig. 9 are not applicable to the satellite which was launched on July 10, 1962. In Section 5.6, the flight performance of the solar plant will be discussed in the light of our present understanding of the radiation belts.

## III. CELL DESIGN AND FABRICATION

### 3.1 *Considerations Leading to Decision to Develop N-on-P Cells*

During the fourth quarter of 1960, the superiority of n-on-p over p-on-n silicon cells in high-level radiation environments was firmly

established. Cells of the n-on-p type are more resistant than p-on-n cells to 1-Mev electron irradiation by a factor of as much as ten. They are also from 3 to 8 times less sensitive to protons than p-on-n cells in current use.

At that time, there were no n-on-p silicon cells in production in commercial quantities. However, experimental n-on-p cells were obtained from several suppliers, and information was made available by the Signal Corps on methods of fabrication of n-on-p cells. This information, combined with our own development studies, led to the conclusion that the n-on-p cells would not be essentially more difficult to manufacture than p-on-n cells of comparable initial performance in space, except that (a) an antireflection coating would be required, which was not necessary as a separate operation on the p-on-n cell, and (b) development effort would be required to obtain a highly manufacturable electrical contact of good integrity and low electrical resistance. We concluded that these problems could be solved and that a suitable cell could be nearly as economical in quantity fabrication as p-on-n cells of comparable initial performance in space. The decision to initiate the n-on-p cell program was based on the two prime considerations: (1) the cells would give longer life in a radiation environment, and (2) they appeared feasible for manufacture.

### 3.2 *N-on-P Solar Cell Design*

#### 3.2.1 *Material*

Silicon material characteristics usually considered important in semiconductor work are (1) the impurity concentration or doping level, (2) the minority-carrier lifetime, (3) the crystal structure perfection, and (4) the crystallographic orientation. For solar cell fabrication, the size of the crystal may also be a consideration, particularly if cells are to be carried through several fabrication steps as multiple elements.

For n-on-p cells for satellite service, the effects of changes or variations in these characteristics required evaluation. Silicon was obtained from several sources over a range of resistivity for comparative process evaluation. Since the prime effect of the radiation environment on the cell is a reduction in carrier lifetime, there appeared to be no advantage in requiring high initial lifetime in the starting material, or extreme perfection of structure. Therefore, during the period of manufacture, the silicon material used by Western Electric Co. for this project was not held to a stringent lifetime requirement, nor were the imperfections controlled by monitoring the etch pit count. The crystals were sliced parallel to the

[111] crystal plane, and twinned material was rejected for mechanical reasons. It was found feasible to grow crystals of sufficient diameter that one-inch square slices could be cut. These were used as the starting material for cell fabrication. One hundred or more such slices were usually cut from a single crystal.

The impurity concentration in the cell body, which determines the specific resistivity, can affect the cell voltage, the sensitivity to radiation damage, and the effective series resistance of the cell. This last effect is small in the range of resistivity usually used: it would reach 0.1 ohm with a body resistivity of 5 ohm-cm. The envelope of open-circuit voltage measurements vs material resistivity obtained with experimental cells is shown in Fig. 10. As expected from theoretical considerations, better radiation resistance would be obtained with high-resistivity silicon used as starting material. However, the loss in open-circuit voltage obtained with experimental cells of high resistivity silicon led to a decision to use nominal 1 ohm-cm p-type silicon for the initial production, and this was continued through the program.

### 3.2.2 *Cell Structure*

Early in our development program, a decision was made to keep the physical dimensions of the cells compatible with commercially available p-on-n cells, if this could be done without serious sacrifice in performance. Fig. 11 shows the cell dimensions and front contact arrangement. The cell was made about 5 mils thinner than the conventional product; this resulted in a minor weight saving without serious loss in strength.

An etch-polished front surface was adopted to reduce surface recombination losses and permit application of a smooth antireflection

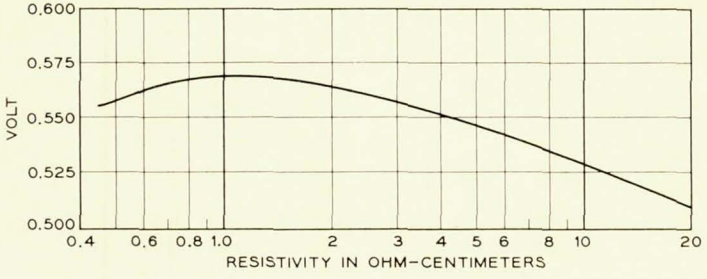


Fig. 10 — Solar cell open-circuit voltage vs resistivity.

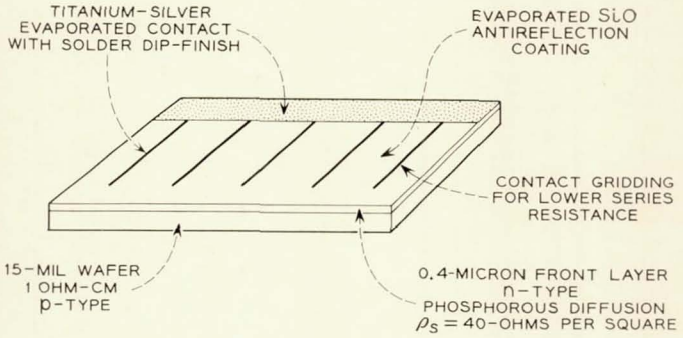


Fig. 11 — Cell structure.

layer of uniform thickness. Good adhesion and integrity of this antireflection coating required coordinated effort on the diffusion process, postdiffusion cleaning, and the contact application process, which is discussed in more detail in Section 3.3.

The diffusion process was selected after a series of diffusion experiments, combined with contact studies and model fabrication. Control of the diffusion operation was used as the principal method of adjusting the spectral response of the cell. The control was exercised by requirements placed on the diffusion environment and temperature, leading to a specified n-layer sheet resistance and desired n-layer thickness.

The cells were designed to be sensitive in the blue-green region of the solar spectrum. No particular efforts were made to obtain good long-wave response since, as discussed in Section II, the long-wave or infrared response is degraded rapidly in a radiation environment. The photon sensitivity peak was chosen to be near the wavelength for maximum incident photon flux from the sun. Fig. 12 shows calculated short-circuit current response, initial quantum efficiency, and relative response for equal energy input vs wavelength for a typical n-on-p cell after antireflection coating.

At the start of the development program, it was realized that improved cell contacts would be required. Intensive work was initiated, leading to the titanium-silver evaporated contact used on all Western Electric Co. n-on-p cells. This in turn required special attention to the solder used for cell tinning and assembly. Many experiments were made to determine optimum methods for assembling the cells in series groups, as will be considered in Section IV.

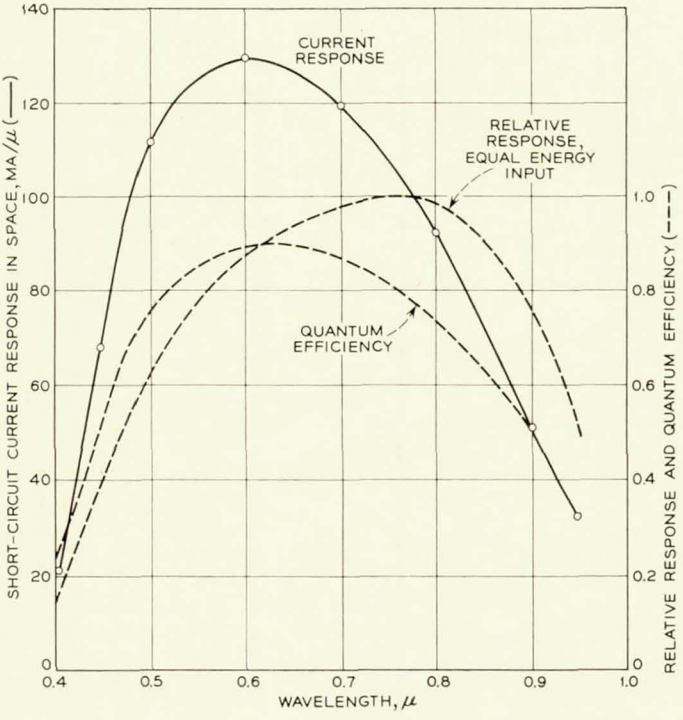


Fig. 12 — Spectral response, n-on-p solar cell.

### 3.3 *Fabrication Technology for N-on-P Cells*

#### 3.3.1 *General*

This section describes some development experiments and the fabrication methods for making radiation resistant solar cells. During the period October 1960–June 1961, a moderate scale model fabrication operation was conducted in the laboratory. This model line was used for design experiments and to provide cells of specified characteristics for radiation damage study. The "going rate" was a fabrication of about 100 cells per week, and a total of some 2000 experimental cells was made in this period in the laboratory.

The first cells were delivered to the Laboratories by Western Electric Co. on January 28, 1961, and the desired program was completed about March 30, 1962. A total of approximately 100,000 n-on-p cells was made by Western Electric Co. for the program; however, not all of these re-

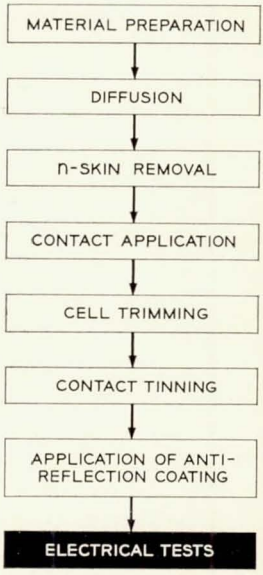


Fig. 13 — Fabrication sequence for n-on-p solar cells.

ceived antireflection coatings, and not all of those coated were considered acceptable for satellite use.

Fig. 13 indicates the principal steps in our fabrication of n-on-p solar cells. These steps are considered in sequence, and some of the development experiments and analyses leading to the final cell are mentioned. Since no n-on-p cells were in quantity manufacture (in the U. S. A.), considerable development engineering was required. Also, the time schedule for manufacture required that equipment and facility orders be placed on the basis of advance engineering judgment, without the benefit of a "proved in" process. Fortunately, it was not necessary to scrap any major equipment as the fabrication methods became shaken down.

### 3.3.2 *Silicon Material and Preparation*

3.3.2.1 *Material.* The material specified for the Telstar cells was p-type single-crystal silicon, sliced parallel to the [111] crystal plane with resistivity $1.0 \pm 0.50$ ohm-cm and minority-carrier lifetime greater than 5 $\mu$sec. No requirement was placed on etch pit density. The silicon slices were cut from the parent crystal with a multiple gang saw to a thickness of 20 mils, minimum. The slice was made 1.0 inch square (nominal),

in order that two cells could be prepared on one slice of the starting material. The crystals were pulled approximately one and one-half inches in diameter and from four to five inches long.

In laboratory experiments, material of resistivity in the range 0.05–20 ohm-cm was used. Several experimental fabrications were made, with material of different resistivity processed through the same operations at the same time to reduce the number of independent variables and establish the effects of material resistivity on cell performance. As previously indicated, optimum initial performance was obtained with silicon near 1 ohm-cm, and this was specified.

Silicon material was usually pulled into single-crystal form by Western Electric Co.; however, some single-crystal stock was obtained from other material suppliers and used for comparative fabrication. Little difference in cell performance was found attributable to the source of the single-crystal starting material, and for most of the operation no restrictions were placed on the source of the material used.

Experiments were also made in which solar cells were fabricated from twinned material, both with a single grain boundary and with many grain boundaries indicated on a cell. No significant deterioration in electrical performance was found until the number of grain boundaries became very large (of the order of 100), so that the material would more properly be called "multicrystalline, with large grain size" than "single-crystal, twinned." However, silicon slices showing grain boundaries were rejected for satellite use because of their inferior mechanical strength.

3.3.2.2 *Slice Preparation.* After the crystal was sawed into slices, the slices were lapped on both sides, and then one side was etch-polished; about three mils of material were removed by the etch. The slices were demounted from the etching racks, cleaned, and inspected for stains, scratches, and mechanical dimensions. The purpose of the etch-polishing step was to provide the best possible surface for the diffusion operation, to avoid crystal imperfections in the finished cell which would cause high surface recombination, and to facilitate application of an effective antireflection coating. A "modified CP4" type etch was usually used. To obtain consistent results, both the bath temperature and the agitation were carefully controlled.

### 3.3.3 *Diffusion, N-Skin Removal*

The diffusion process used for preparation of the thin n-layer is shown schematically in Fig. 14. This was chosen only after extensive development experiments using different methods of application, time-tem-

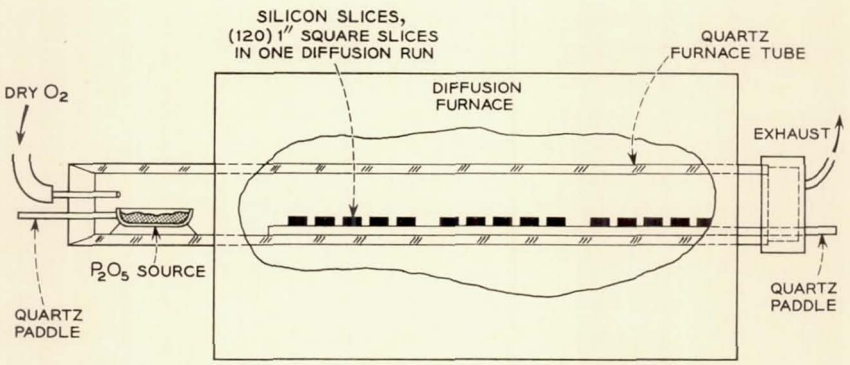


Fig. 14 — Schematic of phosphorus diffusion system.

perature programs, and sequences of operations. Significant factors in control of the diffusion process were found to be: cleanliness of silicon samples, temperature and quantity of the $P_2O_5$ source, method of introducing source and carrier gas, velocity of carrier gas flow, cleanliness of quartz trays and, of course, the time and temperature of the diffusion.

Fig. 15 shows the response of experimental (pre-antireflection-coated)

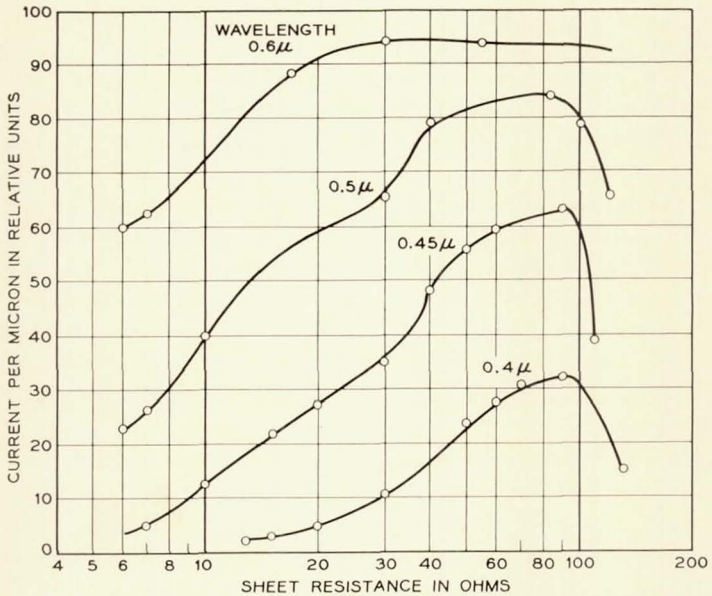


Fig. 15 — Spectral response vs sheet resistance.

cells vs the measured sheet resistance of the diffused layer at four wavelengths in the visible range. For these cells, it would at first appear that the optimum diffused layer sheet resistance would be about 90 ohms/square; however, attempts to fabricate cells in quantity with such thin diffused layers showed that further development would be required to obtain reasonable yields. A principal difficulty was local shorting of the cell in later process steps, particularly in contact application. As a compromise, the sheet resistance of production cells was specified to be greater than 30 and less than 60 ohms/square. The diffusion time and temperature were programmed to produce a diffusion depth in the order of 0.4–0.5 micron, with sheet resistance of perhaps 37 $\pm$ 5 ohms/square. As the diffusion depth was not subject to accurate measurement in the slightly irregular surface provided by the etch-polishing operation, this was not held as a requirement.

After diffusion and postdiffusion inspection, the n-skin was removed from the lapped side of the slice by a light abrasive blast, or by etching. Considerable care is required at this step, as the thin n-p junction on the polished face is quite sensitive to local damage if roughly handled in the presence of abrasive particles. It was found expedient to mask the face of the slice during the blasting or etching operation, as by cementing or waxing to a glass cover slide.

### 3.3.4 *Contact Application*

Adherent, low-resistance contacts to the n and p regions of the n-on-p solar cell presented a major problem. Electroless nickel plating followed by sintering would make a satisfactory mechanical connection, but was unacceptable for the n-layer, as the very thin diffused region would be penetrated during the sintering, and the n-p junction would be seriously degraded, if not shorted entirely. A new approach was needed. After some study, effort was concentrated on development of a new semiconductor contact, in which a reactive metal, titanium, is applied to the silicon surface in vacuum, and the titanium is covered with silver before removal from the vacuum chamber. The silver serves to protect the titanium from oxidation and permits ready tinning at a later point in the fabrication.

Silicon is normally covered with a thin $SiO_2$ layer, which is one cause of difficulty in forming good electrical contacts to it. In the titanium-silver contact process, the titanium is applied to this thin oxide layer. After removal from the vacuum station, the silicon slices are baked for a few minutes in an inert atmosphere at a temperature near 600°C.

During this heat treatment, the titanium reacts sufficiently with the $SiO_2$ surface layer to penetrate it and make electrical contact to the underlying silicon. This forms an adherent, low-resistance contact, without forming any liquid alloy and without damage to the n-p junction. If the surface is clean and if the vacuum deposition is properly carried out, the metal-silicon bond is very good. For example, if a heavy wire lead is soldered along the back of the cell and the combination is immersed in liquid nitrogen, thermal contraction differentials will rip the wire from the silicon body. However, the parting line is usually not at the metal-silicon interface, but rather inside the silicon. Because of the good electrical and mechanical properties of the Ti-Ag contact, it was used for both front and back contacts on all Telstar spacecraft cells.

Accessory contact "grid lines" or "fingers" are necessary on high-efficiency solar cells to reduce ohmic losses in the thin surface layer. This becomes more important as the diffused layer is made even thinner to optimize short-wave spectral response, as required for use in a radiation environment. However, the number of fingers should not be made too large, as the light which they intercept does not contribute to useful output. A compromise must be made. The "best" choice of finger array will depend on the width of the fingers, the cell geometry, and particularly on the diffused layer sheet resistance. For the Telstar spacecraft cell, five fingers were used. Experimental cells, fabricated alike up to the point of contact application, but made with both five fingers and seven fingers (each 0.006 inch wide) showed little difference in performance. If the sheet resistance of the diffused layer were increased, say to 60–80 ohms/square, then seven-finger cells would be preferred.

3.3.4.1 *Relief of Back Contact Margin.* The cells made early in the program had the rear contact applied over the entire rear surface of the slice. After assembly of several modules and thermal shock tests, it was found that small cracks would sometimes become evident at or near the edge of the cell beneath the top contact. This was attributed to strains set up by the solder and the metal mounting strip, these being attached directly to the bottom of the cell at the edge. Several means for avoiding this strain concentration were examined. The method adopted was to mask a narrow region along the edge of the cell, so that during evaporation of the rear contact this region would not be metallized and therefore, would not "take" solder. This operation required registration of front and back contact evaporation masks, however.

3.3.4.2 *Contact Adherence Tests.* After contact evaporation and heat treatment, the contacted slices were subjected to a "Scotch Tape" adherence test in which a strip of pressure-sensitive tape was applied to

each slice and stripped away. Defective contact adherence was shown by portions of the silver or silver and titanium adhering to the tape. Such slices were rejected at this point without further process effort.

### 3.3.5 *Cell Trimming and Tinning*

To this point in the process, two 1-cm × 2-cm cells have been prepared on a single silicon slice. These cells are now cut apart with a ganged diamond saw, which also trims the other edges of the cell to final dimension. Fig. 16 shows top and bottom views of the contacted slice with the trimming cuts. It will be evident that the width of the saw kerf in the cut which separates the cells must be allowed for in dimensioning the contact evaporation masks.

By trimming the cells on their entire perimeter after the contact application, any metallization across the exposed n-p junction is avoided. Also, some simplification of operations results from handling the cells as multiples of two through part of the fabrication. The cells, after trimming, are demounted from the cutting block, cleaned, and solder-tinned. This operation is done by dipping each cell in a bath of molten solder in an inert atmosphere. The solder contains about 3 per cent silver to prevent dissolving the silver already present on the cell. Some control of the amount and location of the solder on the rear face of the cell is available by adjustment of solder temperature, time of immersion, and method of removal of the cell from the solder bath. After tinning, the

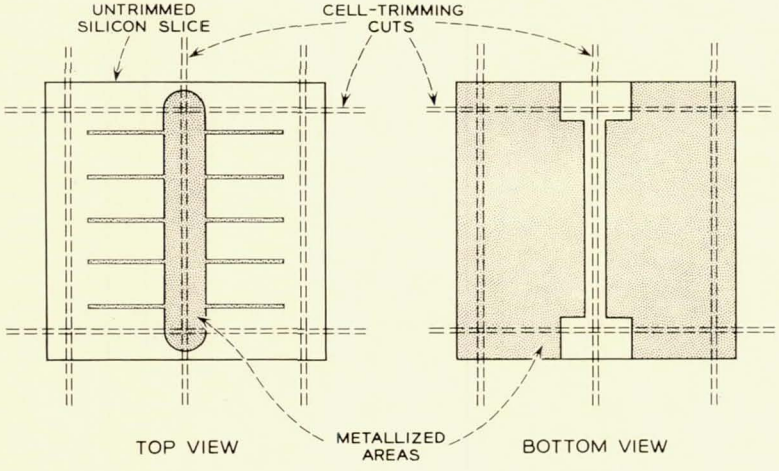


Fig. 16. — Contact configuration and cell trimming.

cells are cleaned with acetone and are delivered for preliminary electrical tests.

In our program, the edges of the cell were not given any etching or smoothing treatment after the diamond saw trimming operation. It was originally planned to provide some form of etch treatment to remove material damage introduced in sawing; however, experiments indicated that little improvement was obtained. The thin n-p junction is highly susceptible to mechanical damage on the face of the n-layer but is rather tolerant of damage at the exposed perimeter (6 cm) of the cell. The relative importance of etching the junction perimeter appears to diminish as the diffused layer is made very thin.

### 3.3.6 *Preliminary Electrical Tests*

Before application of the antireflection coating, the cells were subjected to electrical tests. All cells were tested for open-circuit voltage, short-circuit current, current into 0.45-volt load, reverse leakage current, and ac resistance at 50 ma dc. These tests were intended to serve as process checks and to weed out defective units before the coating process.

In addition to the above, 100 cells from each week's production were obtained, given identification numbers, and subjected to detailed spectral response tests; these cells were then antireflection coated and retested in detail. This permitted continued evaluation of the spectral behavior of the uncoated production cells, and of the improvement obtained by the coating process.

The test equipment for production line electrical tests used a slightly modified 35-mm slide projector as a light source. The heat absorbing glass filter in this projector cut off rather sharply in the near infrared; the resultant light was therefore "bluer" than sunlight at ground level. This test set was maintained by secondary standard cells which were calibrated in the laboratory spectral response set. As routine in-plant color tests were not made, the control of spectral response of the production cells was maintained indirectly — that is, by control of the diffused layer of the etched surface and of the antireflection layer later applied.

### 3.3.7 *Cell Antireflection Coating*

A single-layer interference antireflection film of SiO is vacuum evaporated onto the surface of the solar cell as the final step in its fabrication. SiO is generated by heating a mixture of pure Si and quartz (1:2 weight ratio, between 100 and 200 mesh) in a vertical tantalum tube

(0.157 inch ID, 2 inches long) pinched shut at the bottom and resistance heated. The solar cells are held by spring-loaded clips in a stainless steel dome of 13-inch radius, mounted 20 inches above the SiO source.

The film deposition is monitored by measuring the reduction in light reflection from a square of polished Si held in the center of the dome. A light source and blue-sensitive phototube pickup are mounted inside the vacuum chamber. A film about 800 Å thick is deposited in seven to ten minutes with a source heated to 1300°C and the vacuum at $5 \times 10^{-6}$ torr or better. Deposition is stopped when the reflectance is a minimum for light between 0.50-$\mu$ and 0.55-$\mu$ wavelength.

The quality of the film is checked by suspending the coated cells for 30 minutes in steam over boiling water, and then visually inspecting them under diffuse light. Adherence of the film is tested by the simple Scotch Tape test. An acceptable coating shows no discoloration after steaming and none of it is stripped off by the Scotch Tape. Final electrical tests are relied upon to confirm the optical quality of the film.

### 3.4 *Initial Performance of Completed Cells*

Typical performance of production cells after antireflection coating is shown in Figs. 17 through 21, which summarize measurements on statistical samples from a group of more than 10,000 cells made in Sept., 1961. Fig. 17 shows the open-circuit voltage at 28°C. Although this is slightly lower than can be obtained with conventional p-on-n cells having a thicker diffused layer, the distribution of voltage values is consistent with a controlled process.

Fig. 18 shows the distribution of short-circuit currents and of cur-

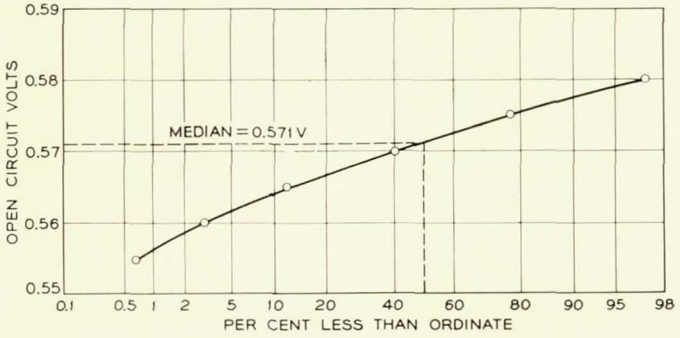


Fig. 17 — Open-circuit voltage distribution.

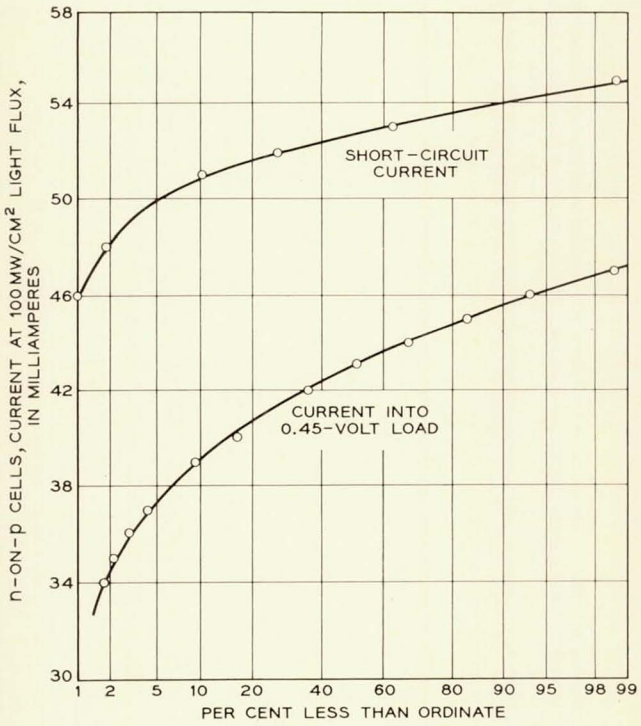


Fig. 18 — Short-circuit current and current into 0.45-v load.

rents into an output load of 0.45 volt, made at an equivalent light flux of 100 mw/cm² sunlight. Fig. 19 shows the electrical conversion efficiency at a load voltage of 0.45 volts for 100 mw/cm² illumination with the light source described in Section 3.3.6. Fig. 20 shows a typical *V-I* curve and conversion efficiency versus load voltage. Fig. 21 shows typical improvement in current output, resulting from the SiO coating operation, versus incident wavelength.

### 3.5 *Selection of Cells for Module Assembly*

The range in cell current output into a 0.45-volt load (see Fig. 18) was from less than 36 ma to 47 ma. Advantages in performance would result if all cells of like current were grouped together or, more generally, if knowledge of the voltage, current, and temperature characteristics of the cells were used to optimize the performance of the solar cell modules and strings. As a practical operation, such optimization could

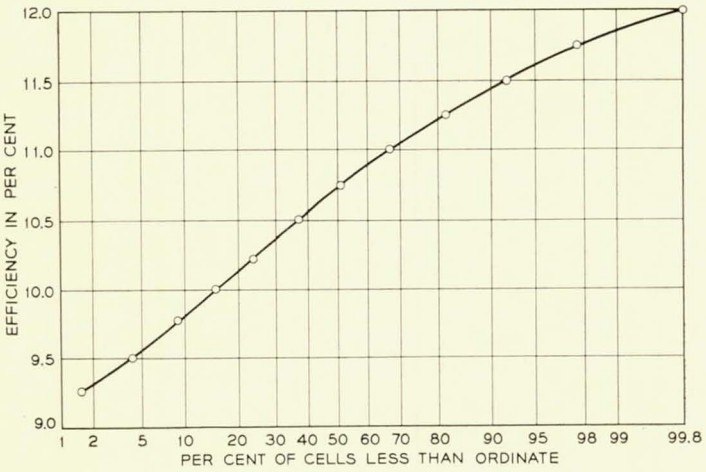


Fig. 19 — Conversion efficiency at 0.45 v.

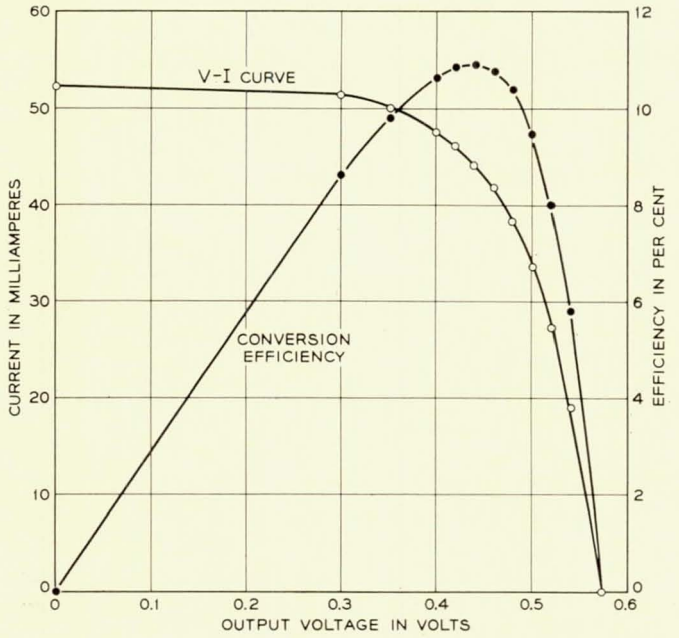


Fig. 20 — Solar cell *V-I* and conversion efficiency vs load voltage.

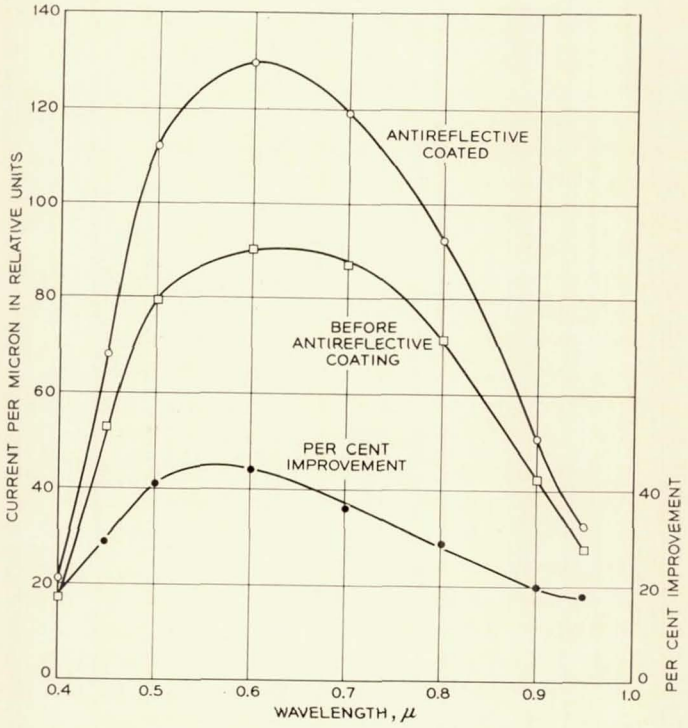


Fig. 21 — Improvement in current response after application of antireflection coating.

only be approximated. To this end, the cells were sorted into groups; the current range for all cells in one group was held to 1 ma. For a particular 12-cell module, only cells from a particular group were used. Records were kept in such form that the performance of the completed module could be compared to that expected from the cells with which it was made. This information could be used to find modules in which serious changes or deterioration of cell performance resulted from the assembly operation. In most cases, however, there appeared to be little change in the cell performance when assembled into modules.

## IV. MODULE DESIGN AND CONSTRUCTION

### 4.1 *Solar Cell Module Requirements*

The module must withstand two widely different environments: the launching environment, where it is subjected to extreme mechanical

vibration stresses; and the orbital environment, where it is subjected to radiation and cyclic thermal stresses. The following list of items is given as the primary design requirements for the module:

(1) provide radiation protection
(2) withstand thermal cycling stresses
(3) withstand vibration during launch and
(4) minimize temperature of cells.

The need for radiation protection has been discussed earlier in this paper. The protection should be provided on all sides of the cells. The protective material over the active surface of the cell must be transparent and not be affected by the radiation bombardment.

As the satellite assumes various attitudes with respect to the sun, surface temperatures vary from $+69°C$ to $-100°C$. These extremes might occur once or twice during the life of the satellite should the spin axis point toward the sun. The normal temperature range is $+10°C$ to $-50°C$ for full sunlight and maximum eclipse with the spin axis nearly perpendicular to the sun. The differential expansion of the materials induces stresses in the component parts of the module, when cycled over the stated temperature range. Continuous thermal cycling will eventually result in fatigue failures if the stress is not limited.

The modules are mounted on the external surfaces of the satellite and measurements show that, at resonances in the structure, accelerations in excess of 200 g's are present.

As the temperature increases, the conversion efficiency of the cells decreases, making it desirable to minimize the temperature of the cell. Considerations of temperature effects in the design of the solar plant are given in Section V.

### 4.2 *Design Objectives*

The design of the module can be divided into four main sections: the electrical design, the mechanical design, the thermal design and the radiation protection. These, of course, are all closely interwoven: for example, the mechanical design might dictate the expansivity of a material being chosen for a particular application, the thermal requirements limit the choice to a single material, and the radiation protection dictates the thickness of the material for minimum weight.

Electrically, the design must provide a series connection between the cells, insulate them from the satellite structure and provide terminals for interconnecting the modules.

The major mechanical objective is that the module withstand the vibration during launch. Fortunately, the mass of the module is small

so that even with accelerations of 200 g's the forces are small. Damping has been provided in the spring tabs that are used to fasten the modules to the panels.

It is important to minimize the temperature of the solar cells. The incident power not converted into electrical power must be removed from the cells and eventually reradiated into space. Direct reradiation through the sapphire covers is not possible, because a "greenhouse" situation exists: i.e., at the wavelength of the black-body radiation of the cell, the cover is opaque. Thus a thermally conducting path to the cover is required, and this should be of low thermal impedance. As the modules must withstand a wide range of temperature, coexpansive materials must be used.

Radiation protection is provided by enclosing the cells in a box structure consisting of the ceramic mounting plate, the transparent covers and a metal frame to join these two. The thickness of the material is obtained by dividing the required protection of 0.3 gm/cm$^2$ by the density of the material. Using this relationship, the thickness of the cover plates and ceramic is 30 mils and the thickness of the platinum frame is 8 mils.

### 4.3 *Module Design*

The solar cell module, shown in Fig. 22, is $4\frac{5}{8}$ inches long, $\frac{7}{8}$ inch wide, and $\frac{1}{8}$ inch thick, and weighs 0.8 ounce. It is made of two assemblies: the cover assembly, which consists of sapphire cover plates brazed into the platinum frame; and the solar cell assembly, which consists of the solar cells, shingled to provide a series connection, mounted on the ceramic plate. The two assemblies are joined by soldering the cover assembly to the cell assembly along the edges of the ceramic plate.

Several materials were considered for the transparent cover over the solar cells. Measurements of the transmission before and after exposure to radiation showed the suitability of certain glasses, quartz and sapphire. In weighing the other characteristics of the materials, sapphire was chosen for its higher thermal conductivity and the availability of processes for joining it to metals.

Table I shows some of the properties of the materials used in the module. As can be seen, the thermal conductivity of sapphire is 20 to 30 times greater than that of glass or quartz. Alumina ceramic, which is a polycrystalline form of sapphire, has approximately the same expansivity as sapphire. Platinum was chosen to join these together because it provides the closest expansion match and is nonmagnetic.

The selection of coexpansive materials limits the stress where these

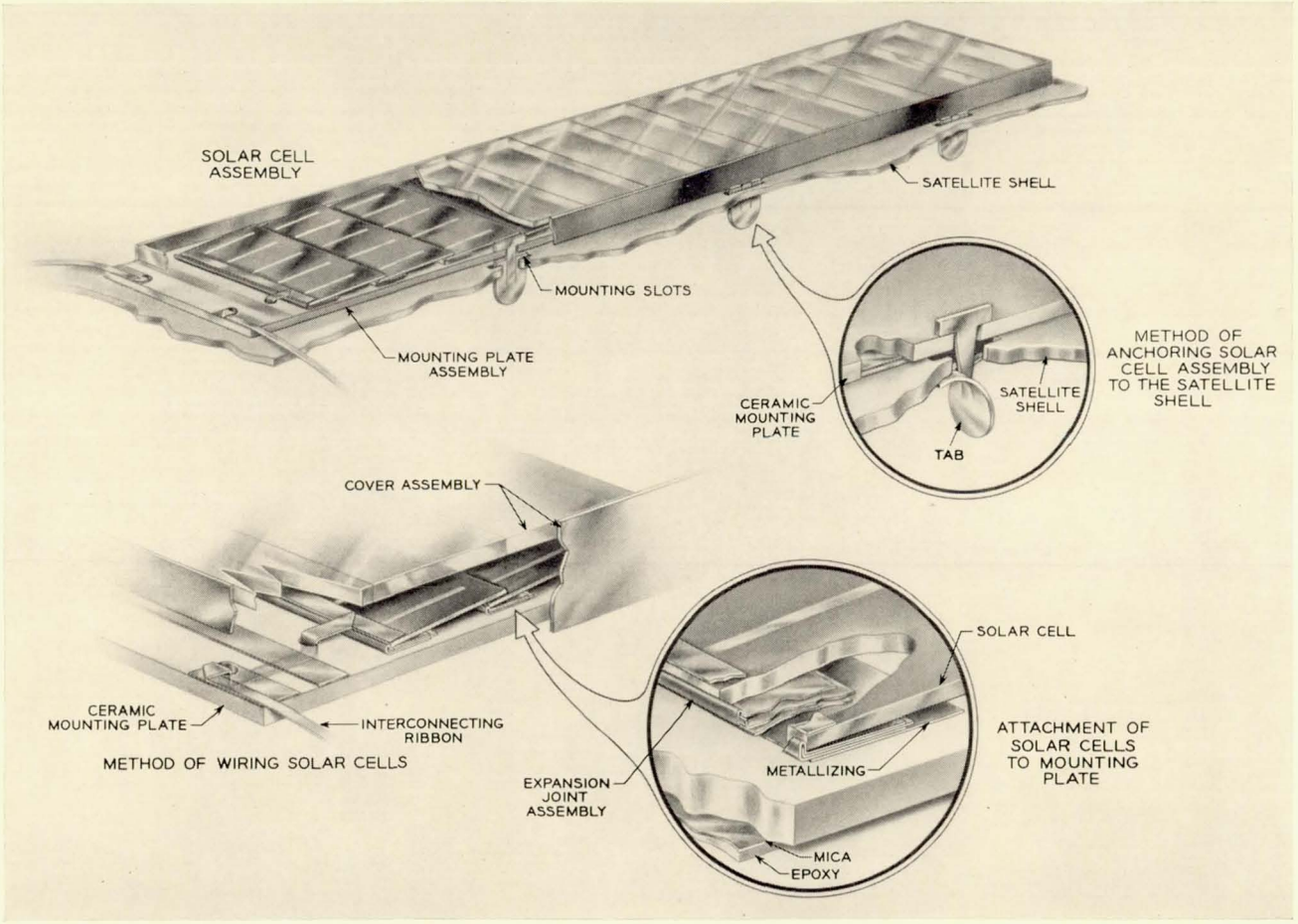


Fig. 22 — Solar cell assembly for communications satellite.

TABLE I — MATERIALS CONSIDERED FOR MODULE

| Material | Expansivity, $10^{-6}$ in/in/°C | Thermal Conductivity, cgs Units |
|---|---|---|
| Silicon | 2.4( 20° C)<br>−0.3(−173° C) | 0.20 |
| Sapphire | 7.0 | 0.06 |
| Fused quartz | 0.5 | 0.003 |
| Glass | 10.0 | 0.002 |
| Alumina ceramic | 6.8 | 0.06 |
| Platinum | 8.0 | 0.16 |
| Silver | 19.0 | 1.06 |
| Invar | 0.5 | 0.03 |

materials are joined. The joints must have a low thermal impedance, since they are in the heat conduction path. A zirconium-silver active metal seal was developed for the joint between the sapphire and platinum.

Also shown in Table I is the expansivity of silicon. It should be noted that the expansivity decreases with temperature, reversing at a temperature of −180°C. Since no insulating material could be found which was coexpansive with the silicon, flexibility was provided by incorporating hinges or expansive joints between the cells and the ceramic. Silver is used for the expansion joints because of its ductility and good thermal conductivity. The conductance of the 1.5-mil silver expansion joint is the same as that of the 30-mil ceramic, since the coefficient of thermal conduction of silver is 20 times greater than that of the ceramic.

To compensate for the mismatch between the silver and the silicon, inserts of 0.001-inch thick Nilvar are used. When soldered between the silver and the silicon, the Nilvar retards the expansion of the silver and produces a joint capable of withstanding the thermal cycling.

### 4.4 *Module Fabrication*

#### 4.4.1 *Cover Assembly*

The cover assembly is made by brazing 13 sapphire plates into a platinum frame with zirconium-silver. To minimize the gap between the covers, it is important that the long edges be parallel to and the short edges be perpendicular to them. Intimate contact for brazing was obtained by procuring the covers in sets matched within one mil in length.

The sapphire covers are brazed to the platinum frame in a fixture which maintains a planar surface for all covers and provides sufficient clamping pressure to insure intimate contact between the covers. The fixtures are placed in a retort which contains a purified nitrogen atmosphere and brazed at 975°C ± 10°C for 3 minutes. The temperature cycle during brazing is carefully controlled to minimize thermal shock.

4.4.2. *Antireflection Coating of Sapphire*

The polished sapphire covers placed over the solar cells to protect them from radiation damage transmit only 85 per cent to 87 per cent of the incident light. This loss, caused by surface reflection, reduces the solar cell output more than can be tolerated. An antireflection coating, therefore, is deposited on both sides of the sapphire cover assembly. The coating consists of a single-layer interference film of $MgF_2$ about 1000 Å thick. It increases the transmission to 90 per cent or more in the wavelength range from 0.4 $\mu$ to 1.0 $\mu$, with a maximum transmission greater than 98 per cent between 0.5 $\mu$ and 0.6 $\mu$. With this higher transmission, the covers reduce the solar cell module output by less than 5 per cent.

Micrometeorites will reduce the sapphire cover transmission by abrading the exposed surface. If this abrasion removes a 200 Å layer per year, as postulated by Jaffe and Rittenhouse,[14] the outer antireflection coating will be removed in three to four years, leading to a loss in initial cell output of about 6 per cent. Laboratory tests showed a 3 per cent loss in output for a mild abrasion of the antireflection-coated sapphire cover, and an 18 per cent loss for frosting of the sapphire. However, since the number and distribution of micrometeorites in space is not accurately known, a quantitative calculation of their effect on solar cell output cannot be made.

The antireflection coating is applied by evaporating $MgF_2$ from a hot, open tantalum boat in a vacuum of $9 \times 10^{-5}$ torr or better. The boat is heated until the $MgF_2$ just melts, and the film is deposited in less than 3 minutes. The sapphire covers are held 20 inches above the boat on a stainless steel dome of 13-inch radius. Specially designed heaters are mounted on the dome so the sapphire covers can be kept at 300°C during the evaporation to assure a hard, adherent film. The film deposition is monitored by measuring the light reflected from one of the covers, using a blue-sensitive phototube as the pickup.

The quality of the antireflection film is checked by subjecting sample covers to 30 minutes in steam above boiling water in a covered vessel, then visually inspecting them. Transmission of the steamed covers is also measured at 0.4, 0.6, 0.8, and 1.0 $\mu$.

4.4.3 *Mounting Plate Assembly*

The solar cell mounting plate consists of the solar cells, the expansion joints, the ceramic mounting plate and the electrical leads from the cells to the terminals.

The solar cells are delivered in matched sets as previously described. The expansion joint, which consists of a folded silver sheet with two narrow strips of Nilvar soldered to one edge and a mica sheet inserted in the fold, is soldered to the back edge of each cell. The mica insert prevents the solder from joining the flaps of the fold, which would spoil the flexibility of the expansion joint.

The cells are assembled in a fixture with the ceramic mounting plate for the soldering operation. The ceramic plates have metallized areas which are located to join the free end of the cell expansion joint. Prior to assembly in the fixture, the metallized areas are silver plated and coated with solder. Other metallized areas are provided on the ceramic that serve as the terminals and joining surfaces for the cover assembly. Individual weights on the cells force the expansion joints into contact with the ceramic. The fixtures are placed in a retort with a nitrogen atmosphere and heated to flow the solder. The nitrogen atmosphere is used in all soldering operations in lieu of organic fluxes. After removal from the fixture, the leads are connected to the terminals and the assembly is tested for continuity.

#### 4.4.4 *Module Assembly and Test*

The two assemblies are soldered together at the joint between the platinum frame and the edge of the ceramic. This is done in a fixture in which pneumatic cylinders press electrically heated pads against the platinum frame and force it into contact with the ceramic plate. The temperature of the pads is controlled by thermocouples, and the soldering cycle is controlled by a timer.

The completed modules are evaluated mechanically, electrically and thermally. The mechanical test consists of a microscopic inspection which eliminates any obvious mechanical flaws such as cracked cells, incomplete solder joints or poor alignment of cells on their mounting plates. Because of the fragility of the cells and the inaccessibility of some solder joints for microscopic inspection, two stressing tests are used. The first of these tests is a vibration test during which the module is vibrated for 30 seconds at 20 g's at 600 cps. The second test is a thermal cycling test, in which the modules are cycled from $+65°C$ to $-100°C$ for a total of 6 cycles. The stresses induced by these tests eliminate the manufacturing freaks. The electrical tests are measurements of the electrical output of the module under a controlled illumination. The results of these tests are used for grouping the modules into different classes, and will be discussed in detail later.

### 4.5 *Module Mounting*

Each module is equipped with six beryllium-copper twist tabs for mounting. These tabs are inserted in slots in the reinforced aluminum panels. A molybdenum strip, with matching slots, is placed in back of the panel with the tabs projecting through the slots. The tabs are twisted a quarter turn, which causes slit ends to emerge from the slots and to form spring fingers which hold the module in contact with the panel.

Six modules are connected in series to form a string which provides the required 28 volts. Omega loops made of braided copper wire are soldered to adjacent terminals to connect the modules in series. The end terminals in the string are connected to glass seal terminals mounted in the panel. Two additional terminals are provided for each string of cells and are positioned approximately $\frac{3}{4}$ inch above the string terminals. A blocking diode is connected between the string terminal and the adjacent added terminal. A connection is provided between the upper terminals, so that the output of a string appears at one side of the panel. This arrangement has the advantage that all current paths are brought back upon themselves, so that no retarding torques due to current loops in the solar cell wiring are applied to the satellite. The same precautions are taken in the internal wiring harness that connects the solar cell plant to the electronics chassis.

### 4.6 *Solar Cell Module Testing*

Fig. 23 shows the expected temperature ranges on the surface of the satellite with the sun perpendicular (pos. 1) and parallel (pos. 2) to the spin axis. Thermal test ranges and test results are also given.

The slow cycling tests were conducted in an oven-refrigerator combination in which the maximum rate of change of temperature was 3°C/min. The temperature was varied from +65°C to −100°C. This rate of change was faster than the expected 2°C/minute in space, and the temperature excursion was greater than the 40° range expected for any module under orbital conditions. The results are indicated on the graph. After 800 cycles, 3 modules had failed, with the failures occurring at 300, 675 and 800 cycles. The failures were at solder joints.

For the thermal-vacuum tests, modules were sealed in evacuated glass vials. These were mounted on a sun-seeking servo system which maintained the surface of the module perpendicular to the sun. Maximum and minimum temperatures of +60°C and −10°C were observed. Twelve modules have been on test over a year with electrical checks at

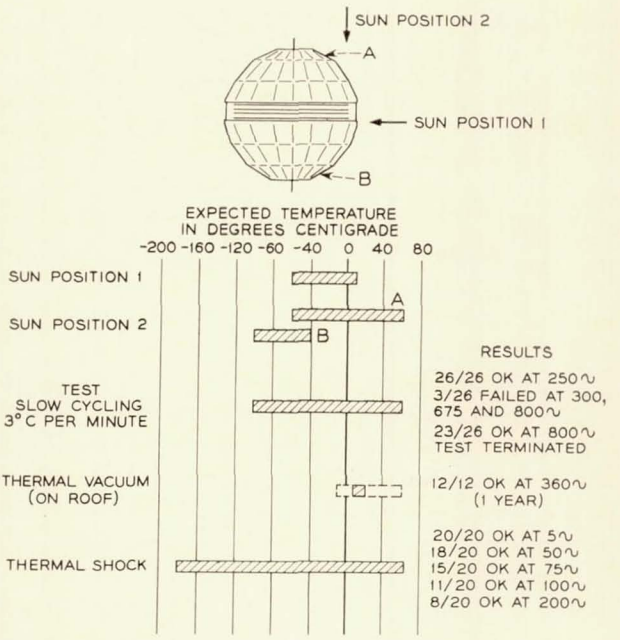


Fig. 23 — Expected satellite skin temperature for two conditions of illumination.

3-month intervals. There have been no significant changes in the modules on test.

For thermal shock tests, modules were sealed in polyethylene containers to prevent condensation. They were then heated and stabilized at 65°C in an oven. They were removed and immediately plunged into liquid nitrogen and held there until the temperature stabilized. The procedure was then repeated. After 200 cycles, 8 of the 20 modules were still operable. In all cases the failures occurred at the soft solder joints to the solar cells.

During early development, vibration tests were made on individual modules, using levels of 100 g's. These tests were all successful. However, it was not until a frame and panels were available that the transmissibility of the structure was known. A complete complement of 300 modules was mounted on the mechanical model satellite. Table II shows the tests to which the cells mounted on the satellite were subjected. Peak accelerations of 200 g's were measured. The failures that occurred at the fifth-resonance dwell test were all at solder joints. These

TABLE II — VIBRATION TESTS ON 300 MODULES MOUNTED ON MECHANICAL MODEL SATELLITE

| Test | Number of Tests | Module Condition |
|---|---|---|
| Qualification level in thrust direction | 5 | ok |
| Resonance dwell | 4 | ok |
| Resonance dwell | fifth test | 6/300 modules failed at soft solder joints |

failures were due to fatigue of the solder, which had been subjected to 750,000 cycles at the time of failure.

The foregoing tests were in essence qualification tests of the module. During production of the module it was necessary to detect any modules that would not withstand the thermal or vibration environment. All modules were therefore subjected to two environmental tests: a thermal cycling test and a moderate-level vibration test. The purpose of these tests was to subject the module to cyclic stresses that would cause weak joints to fail.

The thermal test consisted of cycling the modules from +65°C to −100°C at a maximum rate of change of 3°C/min for a total of 6 cycles. The modules were evaluated by a microscopic inspection and electrical tests. Ninety-five per cent of the modules subjected to this test were later found acceptable.

All modules were vibrated at 600 cps for 30 seconds at an acceleration of 20 g's. Again, 95 per cent of the modules were acceptable, based on microscopic inspection and electrical tests.

## V. SOLAR PLANT DESIGN AND PERFORMANCE

### 5.1 *General Design Considerations*

The integration of individual solar cells or of modules into a solar plant depends on several variables with strong interactions and possible trade-offs between them. The key variables are satellite shape and available surface area, operating temperature, satellite orientation in space, and required average output if chemical batteries are used, or required minimum output otherwise.

The Telstar spacecraft is a spherical, spin-stabilized satellite with solar cells attached to its surface. For such a solar plant the most favorable orientation is one where the spin axis and the sun-satellite line form an angle of 90°, i.e., equatorial illumination of the satellite. Such an

orientation of a spinning satellite will result in the lowest solar plant operating temperature. In the absence of perturbations, the satellite orientation will remain constant. However, interactions of the earth's magnetic field with any residual magnetic moment of the satellite cause precessions of the spin axis. Although ground commandable torquing coils are provided on the spacecraft for controlling such spin-axis precession, it was required for reasons of over-all reliability that the solar plant give usable power for any orientation. The design problem was thus to find the best distribution of the cells on the surface that would do this. Since the output current of series-connected cells is governed by the cell having the lowest output, all cells in a series string should have matched characteristics and should be mounted in one plane so as to receive the sunlight under the same angle of incidence. Thus, while electrically such a group of cells represents a string, in their geometrical layout they form a block or a patch.

If the temperature of the skin were uniform under all conditions, then the design objective would be achieved by distributing solar patches uniformly over the surface. However, since thermal conduction along the skin of the satellite is negligible, temperatures are established predominantly by radiative energy exchanges; therefore, the region facing the sun gets hottest. Under equatorial illumination, a given region near the satellite's equator receives sunlight at near normal incidence only a fraction of the time. Half of the time it is in the shade facing away from the sun. Thus, the average temperature on the equatorial band is low (1°C) and that of the poles is even lower (−3°C). Since the satellite's period of revolution is small compared to the thermal time constants, the instantaneous temperatures deviate little from the average temperature. Under polar illumination, however, one polar region faces the sun all the time and gets hot (+69°C) while the other gets very cold (−100°C). As the solar cell output in the voltage range of interest decreases with increasing temperature, the output under polar illumination would be lowest and that under equatorial illumination highest if solar patches of equal output characteristics were distributed evenly over the sphere. Some equalization is needed; it can be achieved by selective placement of high-output patches, and by increasing the patch density in the polar regions.

The output of the solar plant is connected directly across the batteries and the input regulator. The battery voltage, and thus the voltage into which the solar plant delivers its current, varies under normal operation between 25 and 28 volts, depending on the power demand schedule. One is thus interested, not in the solar plant current at a fixed voltage

only, but rather in the current-voltage output characteristic of the solar plant. Knowing the current-voltage characteristic of the individual cells as functions of temperature and angle of sunlight incidence, and knowing the temperatures of the solar patches for a given geometrical patch distribution and a given solar aspect (i.e., angle between sun-satellite direction and spin axis), the solar plant output characteristic can be calculated. While simple in principle, such calculations are quite lengthy and are most conveniently done on an electronic computer. The details of these calculations are presented in Section 5.5, and computed output curves representing the final design are shown in Figs. 28 and 29 of that section.

Finally, since the Telstar satellite operates with chemical storage batteries, it is the average output power which must satisfy the minimum output requirement, and not the instantaneous output power. Thus, the distribution of the solar cells need not be uniform over the entire surface — only the distribution averaged over one satellite rotation need be considered.

### 5.2 *Solar Plant Size and Configuration*

Since it is known that the output of the solar plant will decrease with time because of radiation damage, the most efficient use of this reduced output will be obtained if the solar plant delivers its maximum end-of-life power at the terminal voltage of the power plant when the batteries are being charged. Radiation damage studies have shown that a solar cell of the type used delivers its maximum power at approximately 0.4 volt after damage corresponding to about two years in orbit.[15] Since the terminal voltage of the power plant is roughly 28 volts when the batteries are being charged, strings of 72 series-connected solar cells were chosen to be the basic building blocks for the solar plant.

Considerations for the distribution of the patches were given above. One variable, however, has not been discussed yet, and that is the ratio of solar cell area to total satellite surface area. At places where there are no solar cells, the skin is covered with a material (aluminum oxide) which is highly reflective to or has a low absorptivity for sunlight in the 0.4-$\mu$ to 1.5-$\mu$ wavelength range containing most of the sunlight's power, but which is highly emissive at long wavelengths corresponding to the black body radiation at the temperature of the satellite. The ratio $\alpha/\epsilon$ of the absorptivity at short wavelengths to the emissivity at long wavelengths is $\approx 0.22$ for aluminum oxide and 1.7 for the solar cell

patches. Thus the larger the coverage with solar cells is, the higher will temperatures be. Since the canister is in radiative temperature equilibrium with the skin, its temperature is governed by the average skin temperature. For reliability reasons, a canister temperature near room temperature is highly desirable. Thus the canister temperature provided a strong constraint in decisions concerning the solar cell coverage. Another constraint was the weight per unit power. With higher coverage, a larger power output can be obtained on a sphere of given diameter. However, since the cells are then hotter, they work with lower efficiency, and the solar cell weight per watt goes up.

In the final design 50 parallel strings are used, incorporating a total of 3600 cells. This provides an initial power of about 14 watts and allows for an average of about 3.5 hours of transmission time per day — a reasonable figure, since the time of mutual visibility between Andover and Europe is about four hours when apogee is in its most favorable position. The distribution of cells on the surface is shown in Fig. 24.

### 5.3 *Selection and Placement of Modules*

The assembled modules were tested under a light source which provided uniform illumination over the 12-cell area of an intensity equivalent to 100 mw/cm$^2$ of solar illumination. The short-circuit current and the current at 5.4 volts (an average voltage of 450 mv per cell) were measured and recorded, and those modules having lower output than 38 ma at 5.4 volts were rejected for satellite use. The accepted modules were grouped into six-module strings by selection of modules which had matched short-circuit currents and currents at 5.4 volts under the test conditions. If there were insufficient modules having matched output currents to form a string, modules having higher current output under either or both test conditions were used to complete the string.

The six-module strings having the highest output currents were located on the bands nearest the poles of the satellite. This was done to provide the maximum output possible under the most unfavorable condition of illumination, namely, that of the spin axis of the satellite pointing toward the sun. The strings having the least output (of those selected for solar plant use) were located on the bands nearest the equator of the satellite, since cells on these bands operate at the lowest temperature.

Fig. 25 shows the distribution of currents at 5.4 volts obtained for 345 assembled modules at an equivalent light intensity of 100 mw/cm$^2$.

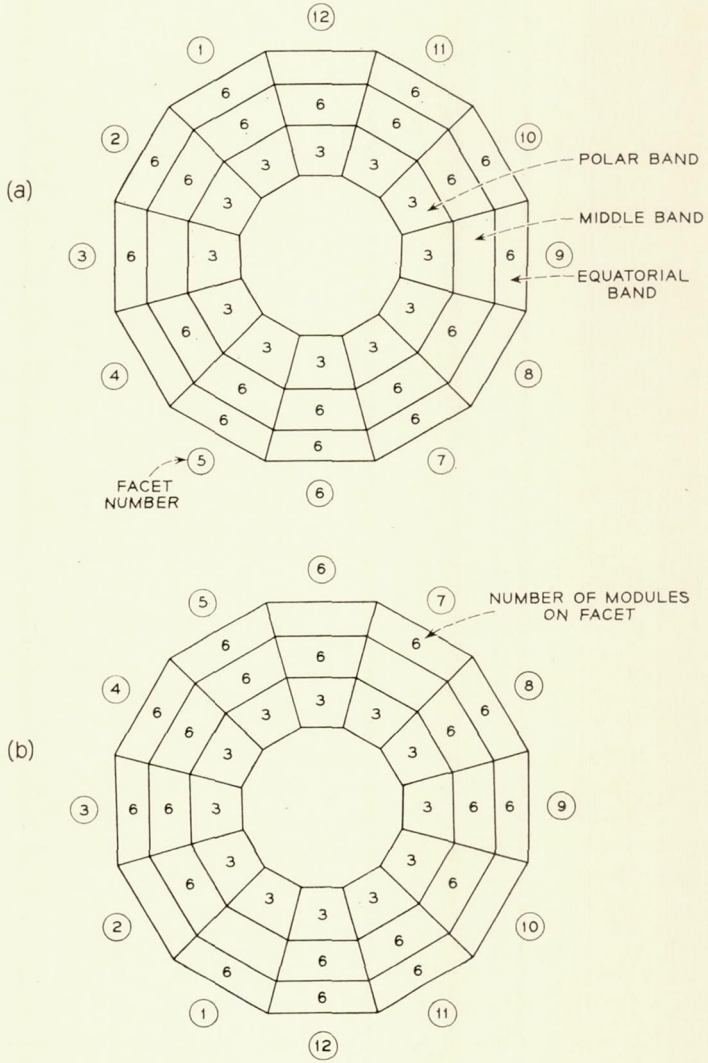


Fig. 24 — Distribution of solar cell modules on surface of Telstar spacecraft.

### 5.4 *Blocking Diodes*

The solar cell strings cannot be connected in parallel directly, since the dark cells would constitute a current drain. Instead, the positive terminals of all the strings are connected to the output bus by rectifier diodes. These diodes present a low impedance to the output current of

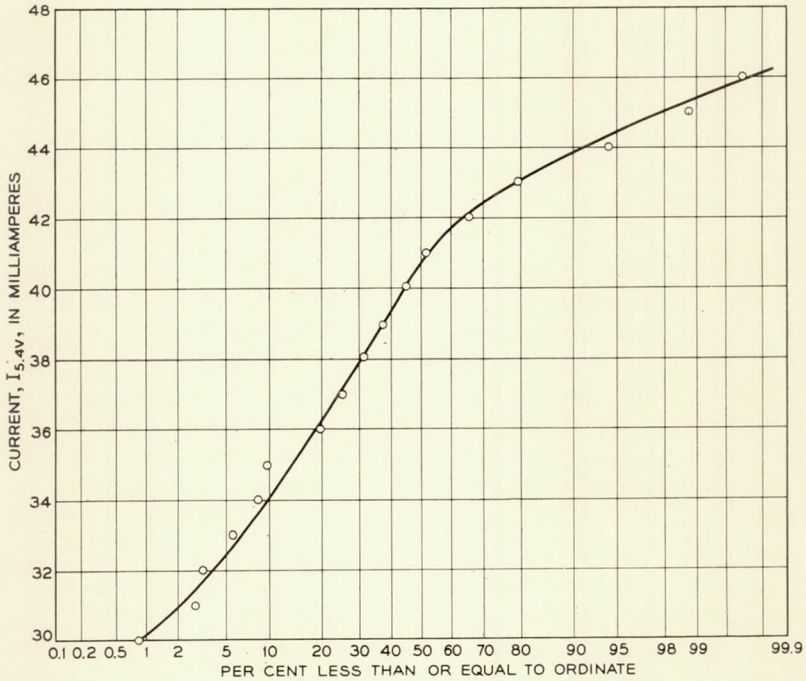


Fig. 25 — Module output current at 5.4 v.

illuminated strings, while their high reverse impedance prevents current leakage through dark cells. The rectifier diodes also prevent discharge of the batteries if a short from any portion of a string to the frame should develop, as might be the case under micrometeorite impact.

### 5.5 *Solar Plant Output Characteristic*

In the Telstar program, inspections and performance checks after each assembly step were undertaken whenever possible. The testing of the individual solar cells and of the modules was described above. However, adequate tests under simulated space environment of the completed solar plant on the satellite shell were not feasible. While thermal tests were made when the satellite was in a space-simulation chamber, the uniformity and collimation of the light source (3 carbon arc lamps) were insufficient to allow precision measurements of the expected outer space performance, and calculations had to be relied on. Such calculations were also important during the design phase, when the various trade-offs

were explored. These calculations were initially done by hand, but were later programmed for an IBM 7090 computer. We shall sketch below how the input information was obtained and present the important results of the calculations.

For convenience, all strings on a given band were considered to consist of 72 identical series-connected cells having characteristics representative of the cells used on the band. The output characteristic of a cell on the satellite shell depends on the angle of incidence and on temperature. In measuring cell characteristics, it was convenient to introduce the short-circuit current as an intermediate variable. One thus needed the output characteristic as a function of short-circuit current and temperature, and the short-circuit current as a function of angle. Simple geometrical reasoning would lead one to expect a cosine-law dependence for the latter; actually, however, between the incident light and the solar cell there is the antireflection coating of the solar cell and the sapphire cover with antireflection coatings on either side. Thus, a more complicated angular dependence results.

To determine the combined effect of these factors, as well as the effect of any shading or reflections caused by the module structure at near glancing angles of incidence, measurements were made of the short-circuit current output of sapphire-covered solar cells as a function of the angle of illumination using terrestrial sunlight. For these measurements, a baffle tube having a 0.1-radian acceptance angle was used to eliminate sky radiation, and the cells were mounted on a temperature-controlled base which could be rotated. Measurements were made at temperatures ranging from $-70°C$ to $+65°C$ on unbombarded cells and on cells bombarded with $2 \times 10^{16}$ 1-Mev electrons/cm$^2$. The relative variation of short-circuit output current with the angle of illumination was found to be independent of both temperature and bombardment level. A normalized plot of this variation is shown in Fig. 26.

A typical output characteristic for short-circuit currents of 25 and 50 ma and temperatures of $-20°$ and $+40°C$ is shown in Fig. 27. To the first order, a change in short-circuit current corresponds to a shift of the characteristic parallel to the current axis. Second-order changes result from the front layer sheet resistance and contact resistance. To obtain the characteristic as a function of short-circuit current and temperature, precision measurements were made of the characteristic of a median cell at a set of 13 short-circuit currents and 6 temperatures. These are stored in the computer program, so that by interpolating between them reliable characteristics can be obtained for any short-circuit current and temperature required in the calculations.

Using the input data just described, the initial current and power out-

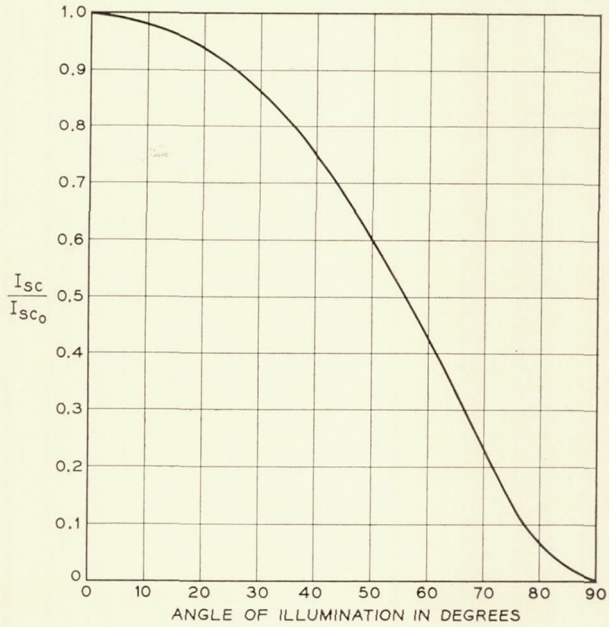


Fig. 26 — Normalized short-circuit current vs angle of illumination.

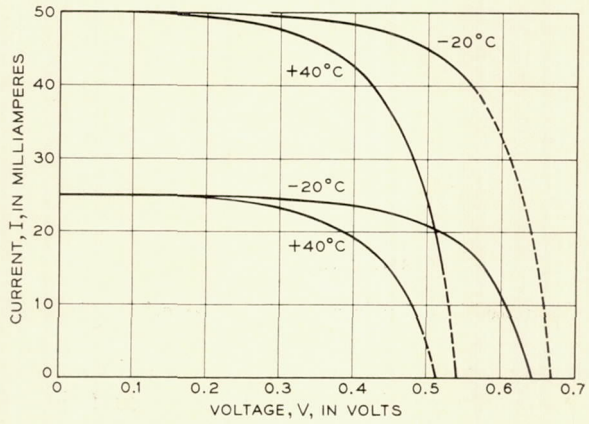


Fig. 27 — Typical solar cell output characteristic.

put characteristics of the spacecraft solar plant for four conditions of illumination were calculated and are shown in Figs. 28 and 29. The angles which identify each curve in these figures define the aspect angle between the spin axis of the satellite and the satellite-sun line. The time-

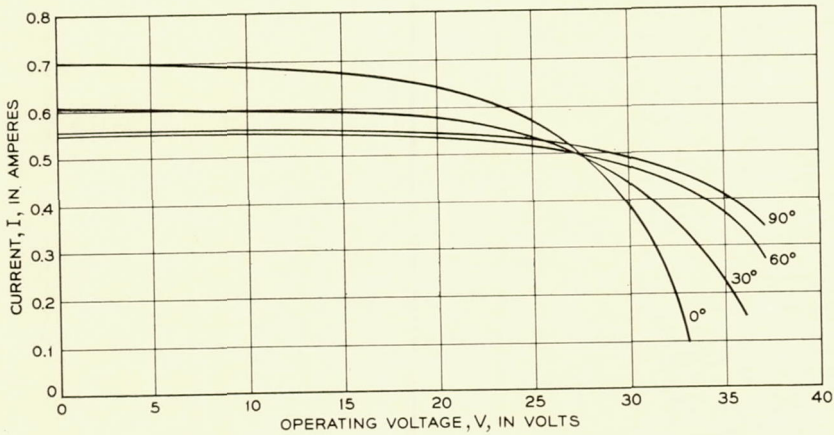


Fig. 28 — Calculated initial current output characteristic of the spacecraft solar plant.

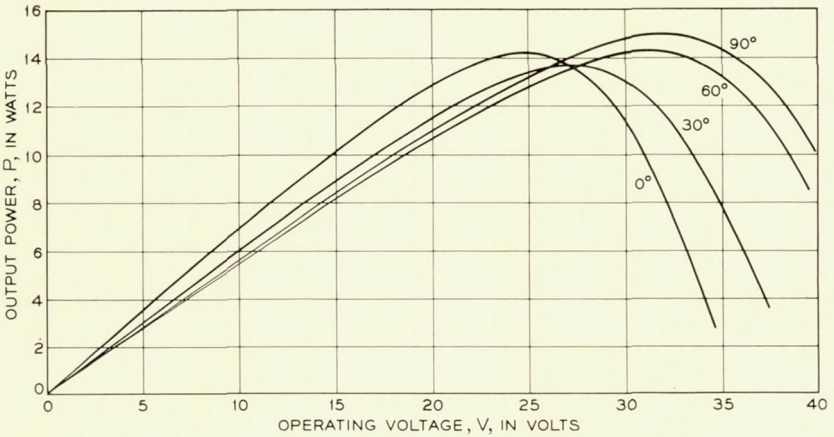


Fig. 29 — Calculated initial power output characteristic of the solar plant.

averaged output current contributed by each band was computed as a function of the operating voltage, taking into account the aspect angle, the calculated operating temperature of the cells on the band, the angle between the normal to the band and the spin axis, the efficiency of the strings and the number of strings on the band. The average solar plant output current is then the sum of the individual band outputs. The variation in the output characteristic with aspect angle is due primarily to the increased operating temperature of the solar cells as the aspect

TABLE III—CALCULATED BAND TEMPERATURES AS A FUNCTION OF ASPECT ANGLE

| Band | Aspect Angle | | | |
|---|---|---|---|---|
| | 0° | 30° | 60° | 90° |
| 1 | 69°C | 49°C | 15°C | −3°C |
| 2 | 63°C | 44°C | 25°C | 8°C |
| 3 | 13°C | 8°C | 8°C | 1°C |
| 4 | | −70°C | −34°C | 1°C |
| 5 | | | −41°C | 8°C |
| 6 | | | −69°C | −3°C |

angle changes from 90° to 0° as shown in Table III.[16] The increased short-circuit current at an aspect angle of 0° is the result of locating modules of a greater short-circuit current output near the poles of the satellite, as described earlier. The more rapid decrease of output current with increasing voltage at this aspect angle is entirely due to the high operating temperature of the modules. The solar plant was designed so that these two effects tend to compensate, and thus the initial output current at the battery charging voltage of about 28 volts is nearly constant, regardless of the orientation of the satellite in space.

### 5.6 *Flight Performance of the Solar Plant*

The first average current output from the Telstar solar plant after launch was obtained from telemetry data taken during pass 6. The average current during this pass was 492 ma at an average solar plant operating voltage of 24.8 volts. At the time of launch, the solar intensity was approximately 3.3 per cent less than mean solar intensity. Therefore, at mean solar intensity the output current would have been 509 ma for the same operating voltage. This is to be compared with the computed initial output current of 530 ma at 24.8 volts as shown in Fig. 28.

Immediately prior to launch it was discovered that one solar cell module in each of two strings had developed an open circuit due to thermally induced stresses during preflight testing. Since time did not permit replacement of these defective modules, they were electrically bypassed. Thus, two of the 50 strings of solar cells on the Telstar satellite are operating with only 60 series cells. Since near the operating point the output current varies only slowly with voltage, this defect has resulted in a loss of only about 0.2 per cent in average output current.

The average solar plant current for the first 160 days of operation is plotted as circles in Fig. 30. A number of corrections were applied in

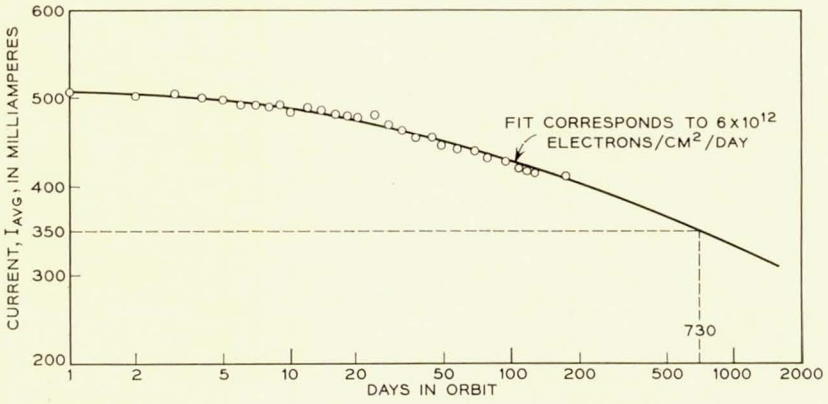


Fig. 30 — Average solar plant output current vs time in orbit.

Fig. 30 in order to suppress variations in output current that are not caused by radiation damage. The output current shows a peak-to-peak ripple of approximately 15 per cent. This ripple profile is scanned at a varying strobe rate as the spin rate changes. Care was taken to obtain a representative sample of the profile when extracting an average current. The variation due to solar distance changes was eliminated by normalizing to mean solar distance. The effect of changing load voltage was minimized by using only the measurements taken when the battery was near 25 volts. Corrections for temperature variations and variations in solar aspect were not applied. Thus the data in Fig. 30 must be considered preliminary; it is expected that the influence of the neglected corrections is small, but that their application may reduce the scatter in the points.

If the Telstar satellite had been exposed to a time-invariant radiation environment, then it should be possible to fit the observed output current points of Fig. 30 to a degradation curve under 1-Mev electrons similar to Fig. 4 by using a proper scale factor to convert time into 1-Mev electron flux. Fig. 4 shows the degradation of the short-circuit current of an average single cell; what is needed here is a corresponding curve for the output current of the solar plant at standard conditions (voltage, temperatures, solar aspect). Such a curve was computed, using the 1-Mev electron bombardment results of Section II, and is shown as the solid curve in Fig. 30. The ordinate scale was adjusted so that the initial value coincides with the measured one. The conversion factor for the abscissa which gives the best fit is $6 \times 10^{12}$ electrons/cm$^2$ per day. Thus, the average radiation environment at the surface of the solar cell (i.e.,

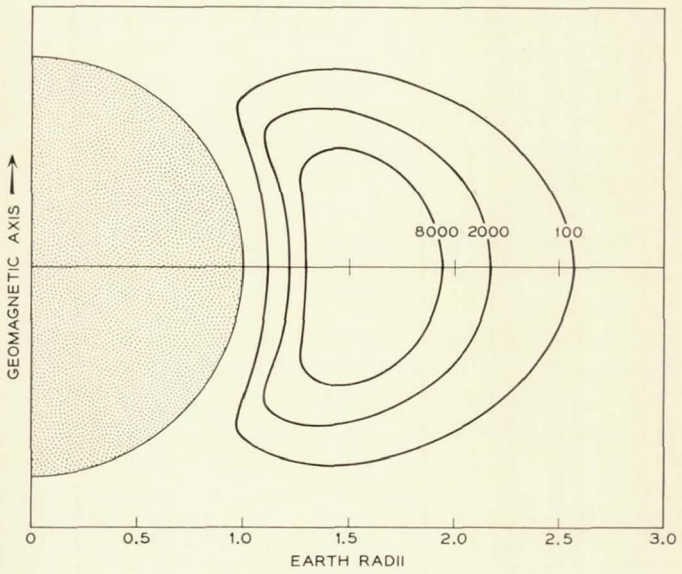


Fig. 31 — Isointensity contours of omnidirectional 24–36 Mev flux in protons/cm² per second.

behind the sapphire) can be characterized as being equivalent to a normal-incidence 1-Mev flux of $6 \times 10^{12}$ electrons/cm² per day. We shall now compare this number with recently measured particle fluxes.

The satellite carries three proton counters, which cover the energy range of 3.5 to 80 Mev in three noncontiguous channels. Analysis of the counter data is only preliminary, and absolute flux values are of limited accuracy because of uncertainties in counter calibrations. The data of the counter whose sensitivity is in the 24 to 36 Mev range yield isointensity contours of omnidirectional flux as shown in Fig. 31 in equivalent dipole coordinates. Satellite perigee and apogee are at 1.15 and 1.9 earth radii, respectively, in geocentric coordinates, and are variable by about $\pm 0.1$ earth radius in dipole coordinates because of the magnetic irregularity of the earth. Measurements within the highest contour are not sufficiently extensive to allow the plotting of another contour, but they do indicate the existence of flux values three times as high as shown. Fluxes of this magnitude are not sufficient to account for the radiation damage observed in Telstar. More recent proton measurements on Explorer XV indicate fluxes of three orders of magnitude greater than the above for the energy range 4 to 12 Mev.[17] It thus appears reasonable that protons of energies greater than 14 Mev, which includes those protons able to penetrate the 30 mils of sapphire shielding, occur in

sufficiently high fluxes to produce an appreciable portion of the observed damage to the solar plant.

The electron counter on the satellite was designed to measure efficiently electrons of energy below 1 Mev.[18] The pulses are sorted into four channels, covering an energy-event range of 180 Kev to 990 Kev. The depletion layer width of the counter is such that electrons of energies between 200 Kev and 600 Kev are counted with relatively good efficiency as compared to those of higher energies. Thus, if the counter is operated in a radiation environment containing relatively high intensities of multi-Mev electrons, it is possible to get flux values only by making assumptions concerning their energy distribution. In arriving at the average electron flux to which the Telstar solar plant has been exposed, it has been assumed that in the high-intensity regions of the radiation belt the energy distribution is that of a uranium fission electron spectrum.[19] Under this assumption, the average intensity for the four-month interval from July to October, 1962, of the omnidirectional flux is found to be about $10^8$ cm$^{-2}$ sec$^{-1}$, for electrons of all energies.*

Time variation of the electron intensity arises from two causes: (1) a decay in intensity at a fixed position in space, the decay rate factor varying with position, and (2) a variation due to the precession of perigee. Both of these factors were estimated from the variation of counting rate in the third highest energy channel and were used in evaluating the July through October time average flux.

Preliminary experiments on the damage rates for multi-Mev electrons as a function of energy and absorber thickness indicate that a fission spectrum flux of omnidirectional intensity of $10^8$ cm$^{-2}$ sec$^{-1}$ corresponds to an equivalent 1-Mev electron flux (normal incidence on an unshielded cell) of about $3 \times 10^{12}$ cm$^{-2}$ day$^{-1}$.

On the basis of the calculated equivalent electron flux of $3 \times 10^{12}$ cm$^{-2}$ day$^{-1}$ for the radiation belt electron contribution to the solar plant degradation as compared to the observed $6 \times 10^{12}$ cm$^{-2}$ day$^{-1}$ equivalent flux, it now appears that multi-Mev electrons are responsible for about half the observed damage, and protons are responsible for the remainder. A detailed comparison of the equivalent 1-Mev flux damage with the measured proton and electron fluxes is given in Ref. 20.

## VI. SUMMARY AND CONCLUSIONS

Analysis of environmental effects on the performance of medium-altitude communication satellites showed that a severe radiation dam-

* Recent electron counter measurements on Explorer XV indicate that the average multi-Mev electron intensity may have been overestimated by about a factor of two.[17]

age problem exists. However, a useful power plant life on the order of years can be obtained by use of solar cells designed for high radiation resistance and by shielding of the solar cells.

Radiation resistance of silicon solar cells in space is achieved by designing them to be highly responsive to short-wave photons near the solar peak, by using the n-on-p structure, and by minimizing all losses which are not radiation-damage dependent. These include reflection losses, series and shunt resistive losses, and surface recombination losses. Special attention was given to development of a low-resistance electrical contact with good adherence to polished silicon surfaces.

The cells are mounted in 12-cell modules designed to be resistant to thermal shock and cycling, to provide a minimum of 0.3 gm/cm$^2$ protective shielding, and to withstand acceleration and vibration stresses encountered in launching. Inorganic materials are used in the module assembly to avoid deterioration in the space environment. Fifty strings of six modules each are connected in parallel to provide a nominal 28-volt output of 14 watts. The strings are mounted on the satellite skin in a configuration which provides substantially constant output for any orientation of the spin axis relative to the sun-satellite line.

The Telstar spacecraft solar plant output, as obtained from telemetry data, decreases with time as a result of particle irradiation. The time dependence agrees with that of an unbombarded solar cell that is exposed in the laboratory to a 1-Mev electron flux of $6 \times 10^{12}$ electrons/(cm$^2$ day). From this comparison it is estimated that the plant will degrade to 68 per cent of its initial value after two years in orbit. Without other failures, occasional operation of the video channel should be possible even after 20 years in orbit, when the charging current will be in the order of one-half the initial value.

In future communication satellites, where switching is not used, the extension of solar power plant life to many years will be feasible by increasing the number of cells over that required initially. The penalty is not particularly severe, however, because of the logarithmic dependence of output on integrated radiation flux. For example, to extend the life of a particular power plant from two years to 20 years would require only about 20 per cent more cells on the satellite.

## VII. ACKNOWLEDGMENT

The authors wish to express their appreciation for important contributions from many associates in Bell Telephone Laboratories and the Western Electric Co.; without their aid this work would not have been possible.

REFERENCES


1. Chapin, D. M., Fuller, C. S., and Pearson, G. L., A New Silicon p-n Junction Photocell for Converting Solar Radiation into Electrical Power, J. Appl. Phys., **25**, Jan., 1954, p. 676.
2. Smith, D. H., A 1-Watt Solar Power Plant, Communications and Electronics, No. 54, November, 1959.
3. Van Allen, J. A., Geomagnetically-Trapped Corpuscular Radiation, J. Geophys. Res., **64**, Nov., 1959, pp. 1683–1689.
4. Loferski, J. J., Rappaport, P., and Scott-Monck, J., Radiation Damage to Silicon Solar Energy Converters, R.C.A. Labs Quarterly Report No. 1, NASA Contract NAS5-47, October 15, 1960.
   Mandelkorn, J., Kesperis, J., McAfee, R., and Pharo, W., A New Radiation Resistant High Efficiency Solar Cell, NASA meeting on Radiation Damage to Semiconductors by High Energy Protons, Washington, D. C., October 20, 1960.
5. Naugle, J. E., and Kniffen, D. A., Flux and Energy Spectra of Protons in the Inner Van Allen Belt, Phys. Rev. L., **7**, July, 1961, pp. 3–6.
6. Freden, S. C., and White, R. S., Particle Fluxes in the Inner Radiation Belt, J. Geophys. Res., **65**, May, 1960, pp. 1377–1383.
7. Conference on Radiation Effects in Semiconductors, J. Appl. Phys., **30**, May, 1959.
8. Gummel, H. K., Smits. F. M., and Froiland, A. R., Method for Terrestrial Determination of Solar Cell Short Circuit Current under Outer Space Solar Illumination, I. R. E. WESCON Proc., July, 1961.
9. Gummel, H. K., and Smits, F. M., to be published.
10. Rosenzweig, W., Diffusion Length Measurement by Means of Ionizing Radiation, B.S.T.J., **41**, Sept., 1962, pp. 1573–1588.
11. Rosenzweig, W., Gummel, H. K., and Smits, F. M., Solar Cell Degradation under 1-Mev Electron Bombardment, B.S.T.J., **42**, Mar., 1963, pp. 399–414.
12. Rosenzweig, W., Smits, F. M., and Brown, W. L., Nuclear Electronic Effects Program, Tenth Triannual Note, July 15, 1962.
13. Naugle, J. E., and Fichtel, C. E., Flux and Energy Spectra of Protons in the Inner Van Allen Belt, Am. Phys. Soc. Bulletin II, **6**, Feb., 1961, p. 53.
14. Jaffe, L. D., and Rittenhouse, J. B., Behavior of Materials in Space Environment, Am. Roc. Soc., Meeting, Oct. 9–15, 1961.
15. Smits, F. M., Smith, K. D., and Brown, W. L., Solar Cells for Communication Satellites in the Van Allen Belt, J. Brit. Inst. Radio Eng., **22**, Aug., 1961, pp. 161–169.
16. Hrycak, P., Koontz, D. E., Maggs, C., Stafford, J. W., Unger, B. A., and Wittenberg, A. M., The Spacecraft Structure and Thermal Design Considerations, B.S.T.J., this issue, p. 973.
17. Brown, W. L., private communication.
18. Brown, W. L., and Gabbe, J. D., Electron Distribution in the Earth's Radiation Belts during July, 1962, as Measured by Telstar, J. Geophys. Res., **68**, Feb. 1, 1963, p. 607.
19. Carter, R. E., Reines, F., Wagner, J. J., and Wyman, M. E., Expected Cross Section from Measurements of Fusion Fragment Electron Spectrum, Phys. Rev., **113**, Jan., 1959, pp. 280–286.
20. Brown, W. L., Gabbe, J., and Rosenzweig, W., Results of the *Telstar* Radiation Experiments, B.S.T.J., this issue, p. 1505.

# The Satellite Ferrimagnetic Power Limiter

By L. J. VARNERIN, R. L. COMSTOCK, W. A. DEAN, and R. W. KORDOS

(Manuscript received February 11, 1963)

*To limit the 4080-mc local oscillator signal power input to the beat oscillator modulator of the Telstar satellite communications repeater, a subsidiary absorption limiter was used which consisted of an optically polished sphere of single-crystal yttrium iron garnet (YIG), placed in a resonant transmission cavity between the amplified 4080-mc output of the traveling-wave tube and the BO modulator input. The limiter holds the output power nearly constant above a given input threshold; below this threshold the YIG is linear and introduces only a small loss. The threshold is determined, for a given sample at a given frequency, by the external magnetic bias field. Temperature compensation over the desired range was obtained by orienting the crystal with the dc magnetic field along a [100] or "hard" axis. The total weight of the limiter package, including the bias magnet and cavity, is 13 ounces.*

## I. INTRODUCTION

The traveling-wave tube[1] in the Telstar communications repeater[2] serves to amplify both the 4170-mc output signal and the low-level (−12 dbm) 4080-mc local oscillator-beacon signal. The TWT gain for the 4080-mc signal is strongly dependent upon the 4170-mc signal level. If the signal to the satellite is lost, no 4170-mc signal is generated and the gain for the 4080-mc signal increases significantly. Additionally, temperature variations can cause undesired level changes. As can be seen from Fig. 1 of Ref. 2, the 4080-mc signal is the local oscillator for the beat oscillator modulator, which generates the 6300-mc local oscillator signal for the input down converter. This increased 4080-mc level can cause the modulator to oscillate.

To eliminate these effects a microwave ferrimagnetic power limiter was designed and incorporated to limit the 4080-mc level. Because this type of limiter incorporates a resonant cavity, it serves a required filter func-



In its Telstar I, Vol. 3 Jun. 1963
p 1817-1827 Refer (See N64-11079 02-01)

tion of rejecting undesired signals which might cause instability. The limiter cavity loaded $Q$ was designed to fulfill this need.

### 1.1 *Properties of Limiters*

Microwave power limiters are passive two-port devices which limit output power to a nearly constant value beyond some input threshold power level. Below this threshold limiters are linear and ideally introduce negligible loss. At a single frequency the power output ($P_o$) vs available power input ($P_a$) response of a limiter is shown in Fig. 1. The two thresholds, $P_{o\ \mathrm{crit}}$ and $P_{a\ \mathrm{crit}}$, are indicated as well as the shape of the limiting characteristic below and above the threshold. In the Telstar satellite application the limiter electrical and mechanical requirements are given in Table I and the mechanical requirements will be discussed in Section III. The temperature behavior of the device will be considered in detail in Section II.

Degenerate parametric oscillators make possible excellent power limiting devices, in which case the signal to be limited is used as the "pump" signal. Above the oscillation threshold the losses in the pump circuit increase since energy is required to sustain the oscillation, resulting in power limiting. For microwave ferrimagnets the pump circuit is the uniform precession motion of the magnetization coupled to a microwave circuit, and the parametrically excited systems are the "spin waves" which are bounded by the sample and not coupled to the external circuitry. A ferrimagnetic limiter employing single-crystal yttrium iron garnet (YIG) was chosen for the satellite requirements.

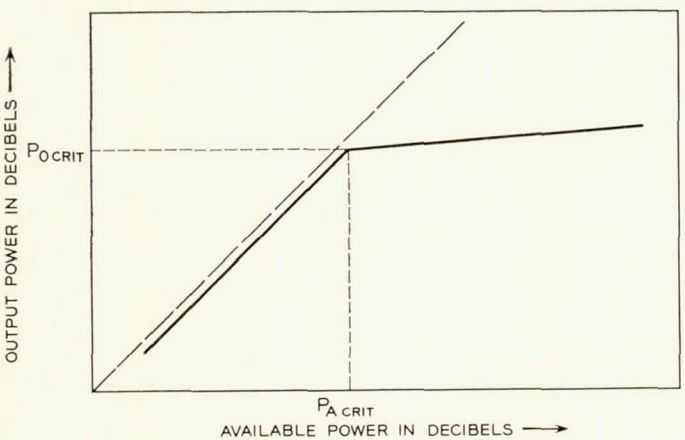


Fig. 1 — Output power ($P_o$) vs available power ($P_a$) for a power limiter.

TABLE I — POWER LIMITER REQUIREMENTS

Frequency of operation: 4080 mc
Bandwidth: to have a loaded $Q$ of about 200
Quiescent point of operation: +14.5 dbm output power at +18.0 dbm input power
Output power at +26.0 dbm input power: < +17 dbm
Insertion loss below limiting level: <1.0 db
Temperature range of operation: +35°F to +120°F
Waveguide: silver-plated magnesium.

### 1.2 *The Subsidiary Absorption*

The degenerate parametric coupling of half-frequency spin waves in a ferrimagnet by the uniform precession has been discussed by Suhl.[3] Suhl's theory gives the threshold RF magnetic field at the sample ($h_{crit}$) as a function of the dc bias magnetic field, as shown in Fig. 2 for spherical samples. The ordinate is the ratio of $h_{crit}$ to $\Delta H_k$, the "spin wave" linewidth, while the abcissa is the ratio of the precession frequency, $\omega_o = \gamma H_e$ to the operating frequency $\omega$, where $\gamma$ is the gyromagnetic ratio. $H_e$ is an effective bias field, the sum of the bias magnetic field $H_{dc}$ and $H_a$ the anisotropy field appropriate to the crystallographic axis with which $H_{dc}$ coincides (see Section II). $\omega_m$ is $\gamma 4\pi M_s$, where $4\pi M_s$ (1750 oersteds for

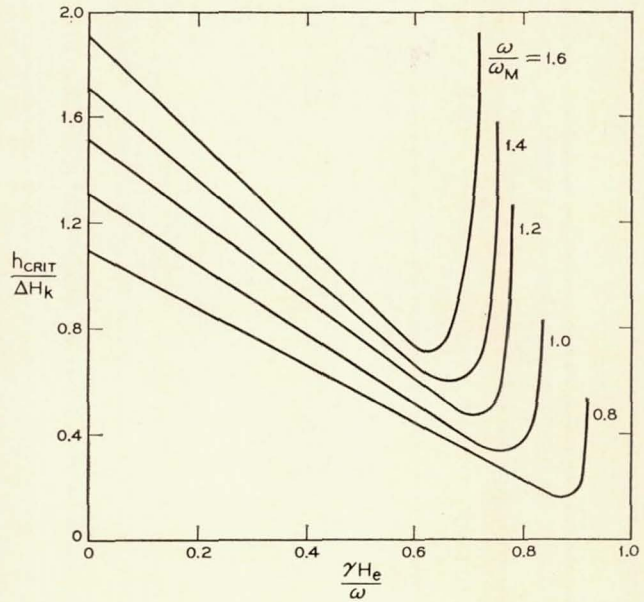


Fig. 2 — The subsidiary absorption threshold ($h_{crit}$) vs $\gamma H_e/\omega$ with $\omega/\omega_M$ as a parameter (from Ref. 3).

YIG) is the ferrimagnetic saturation magnetization. The subsidiary absorption described by this curve always occurs at field values less than the resonance value, $(\omega_o/\omega) = 1$. For 4-kmc operation with YIG, $\omega/\omega_M$ is 0.816. It is apparent from these curves that the threshold for the subsidiary absorption can be varied at a given frequency by varying the magnetic bias field. Above the threshold for the subsidiary absorption the losses in the ferrite sample increase, resulting in power limiting.

### 1.3 *The Ferrimagnetic Limiter*

A photograph of the completed limiter with the biasing magnet in position is shown as Fig. 3. A single-crystal spherical sample of YIG was mounted in the transmission resonant cavity and biased to the subsidiary absorption, with the external dc magnetic field perpendicular to the RF magnetic fields of the cavity mode. Single-crystal YIG was used since in this material the spin wave linewidth $\Delta H_k$ is extremely low

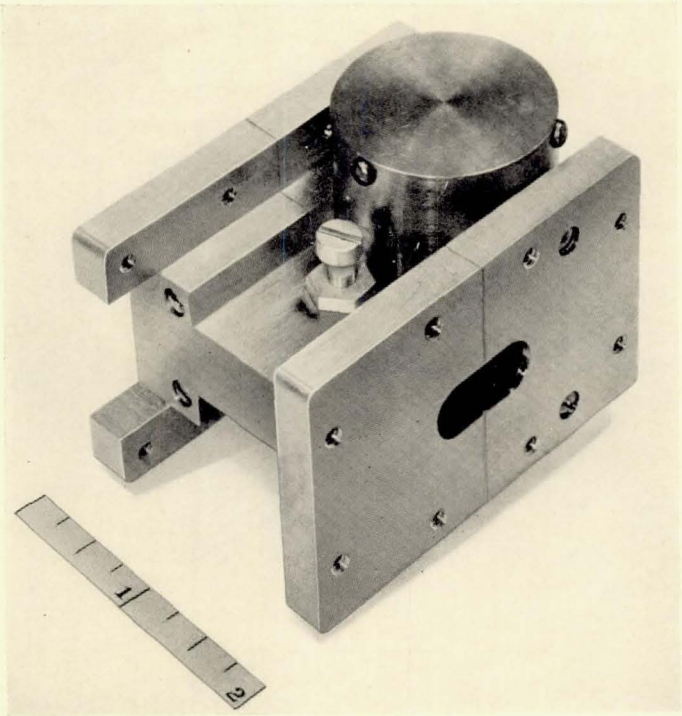

Fig. 3 — Ferrimagnetic limiter, showing the microwave cavity and external biasing magnet.

($\approx$0.3 oersteds) resulting in low thresholds (Fig. 2). Spherical geometry was chosen to minimize temperature effects since the ferromagnetic resonant frequency does not depend on the saturation magnetization, which varies with temperature.

## II. ELECTRICAL DESIGN CONSIDERATIONS

### 2.1 *Insertion Loss and Limiting Threshold*

The transmission microwave cavity was made of reduced-height waveguide coupled to the external transmission lines with inductive irises. The cavity was excited in the $TE_{101}$ mode as shown in Fig. 4. The YIG sphere was placed near the sidewall of the cavity and biased as shown. It is necessary to have a large ratio of sample to cavity volume so that the losses in the sample will represent a large change in the total cavity losses above the threshold (see Section 2.2). In this model it was found necessary to use spheres nominally 0.250 inch in diameter with cavities only slightly greater in height. Because of this large volume the sample contributes significant loss and reactance to the cavity mode below the threshold. The reactance contributed by a ferrimagnetic sample biased below the uniform precession resonance raises the cavity resonant frequency and thus can be compensated in part by a tuning screw placed in the maximum of the electric field, which will lower the cavity resonance by adding shunt capacitance. The transmission coefficient of the cavity at resonance is given by

$$T = \frac{1}{\left[1 + \frac{Q_e}{2Q_o}\right]^2} \tag{1}$$

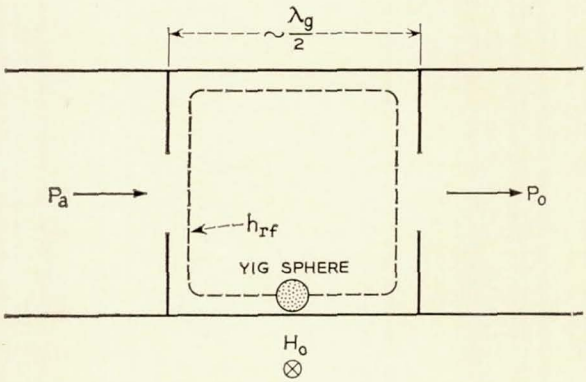


Fig. 4 — Schematic of the Telstar limiter.

where the loaded cavity $Q(Q_L)$ is given in terms of the external and unloaded $Q$'s ($Q_e$ and $Q_o$) by

$$\frac{1}{Q_L} = \frac{1}{Q_o} + \frac{2}{Q_e}.$$

In order to keep the low-level loss as low as possible, all precautions were taken to insure the largest value possible for $Q_o$. This included silver plating the cavity walls. (See Section III.) Thus the only electrical parameter available to maintain a low insertion loss is $Q_e$. However, the limiting threshold power also depends on $Q_e$ as given by

$$P_{o\,\mathrm{crit}} = \frac{\omega}{Q_e} \frac{\mu_o h_{\mathrm{crit}}}{2} \int_{V_c} h^2 dV$$

where $V_c$ is the cavity volume, with the sample placed where the RF magnetic field is maximum. Since the range of values of $h_{\mathrm{crit}}$, at a given frequency, is bounded (Fig. 2) the specification of insertion loss and $P_{o\,\mathrm{crit}}$ are not independent. However, it was found possible to achieve a satisfactory insertion loss and still meet the threshold requirement given in Table I as well as the required $Q$ (200) to serve the required filter function. The dc magnetic field required for this threshold was 1200 oersteds, resulting in $(\omega_o/\omega) = 0.840$ (neglecting the effect of crystalline anisotropy, as will be discussed presently). This operating point was chosen to lie somewhat on the low-field side of the minimum of the $h_{\mathrm{crit}}$ curve. The similar high-field point was found to have unsatisfactory temperature characteristics as well as a poorly defined break at threshold.

### 2.2 *Limiting Slope*

The behavior of the limiter in the nonlinear region of its operation depends critically on the ratio of sample to cavity volume. With the same cavity, reducing the sample size from 0.250 inch to 0.180 inch resulted in severe degradation of the limiting action. It was found that the limiting curve above the threshold was nearly a straight line over at least a 28-db dynamic range with a slope which decreased rapidly with sample volume. The sharpness of the discontinuity in the limiting curve from the linear to the nonlinear region was found to depend critically on the degree of sample polish. This result is unexplained on the basis of Suhl's theory. Experimental limiting curves are discussed in Section IV.

### 2.3 *Temperature Compensation*

Two limiter properties were found to vary to a significant degree over the temperature range given in Table I. These are the limiting threshold

and a thermal detuning resulting in increased low-level insertion loss. The variation in limiting threshold is due primarily to changes in $h_{crit}$ caused by the temperature variation of the saturation magnetization ($4\pi M_s$), spin wave linewidth ($\Delta H_k$), and anisotropy field ($H_a$). In the present case the crystal has cubic symmetry with the "easy" and "hard" magnetic axes long [111] and [100] directions, respectively. The temperature variations of $4\pi M_s$ and $\Delta H_k$ are such as to partially compensate the change in $h_{crit}$ with respect to temperature, with the largest contribution being that due to variations in $4\pi M_s$ ; the net result is that $h_{crit}$ increases with temperature. The anisotropy field can be used to compensate the residual temperature sensitivity, as can be shown using the curve in Fig. 5. This curve shows the variation in the effective bias magnetic field, including anisotropy, with respect to an angle $\theta$ measured from [100] as the sample is rotated about a [110] axis. In the two extreme cases $\theta = 0°$, 54° 44′, i.e., when the sample is oriented so that a "hard" and an "easy" axis are lined up along $H_o$ , the effective field is given by

$$H_e\Big|_{[100]} = H_o - 2\frac{|K_1|}{M_s}$$
$$H_e\Big|_{[111]} = H_o + \frac{4}{3}\frac{|K_1|}{M_s} \qquad (2)$$

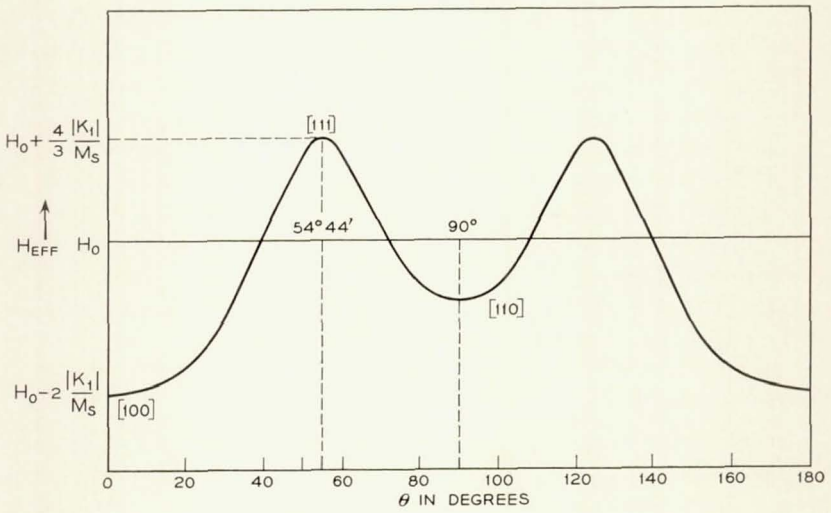


Fig. 5 — Effective static magnetic field, including anisotropy, for a cubic ferrimagnet for rotation about the [110] axis with $\theta = 0°$, corresponding to [100].

where $K_1$, the first-order anisotropy constant, is negative for YIG and decreases with temperature. The temperature variation of $h_{crit}$ due to the temperature variation of $H_e$ is given by

$$\frac{1}{h_{crit}}\frac{dh_{crit}}{dT} = \frac{1}{h_{crit}}\frac{\partial h_{crit}}{\partial H_e}\frac{dH_e}{dT}$$

where we see from Fig. 2 that $(\partial h_{crit}/\partial H_e) < 0$. Since it is necessary to compensate a positive value of $(1/h_c)(\partial h_c/\partial T)$ arising from changes in $\Delta H_k$ and $4\pi M_s$, it is seen that a positive value for $dH_e/dT$ is needed, which can be obtained by orienting the sample with the dc magnetic field along [100]. Experimental results were obtained with orientation along both [100] and [111] which gave striking confirmation of the temperature compensation obtainable with this technique. The experimental results of Section IV show the effect of proper temperature compensation.

## II. MECHANICAL DESIGN CONSIDERATIONS

### 13.1 *Cavity*

The limiter is constructed in a reduced-height, silver-plated magnesium cavity. The cavity is composed of two waveguide half-sections joined along the broad dimension, as shown in Fig. 3. Each half-section is of unit construction; the iris half-plates and the waveguide flanges at each end are an integral part of the machined piece to eliminate lowered $Q$'s resulting from soldered iris plates. The over-all length of the cavity is 1.976 inches. The iris plates are 0.062 inch thick with centrally placed coupling irises (0.375 × 0.800 inch). Internal cross-section dimensions of the cavity are 0.400 inch high by 1.872 inches wide. The YIG sphere is placed 0.062 inch from the side wall of the cavity in a region of maximum RF magnetic field. The reduced-height cavity serves not only to give a large filling factor but to reduce appreciably the size and weight of the magnet required to bias the YIG sphere across the narrow waveguide dimension.

A silver-plated brass tuning screw is inserted in the broad dimension of the cavity and centrally placed along the length.

### 3.2 *Permanent Magnet*

An efficient permanent magnet capable of producing a field of approximately 1200 gauss across a 0.400-inch air gap was required in order to realize a practical limiter design. The magnet, designed for this application by M. S. Glass, contains two truncated cones of Alnico VI material of the proper length-to-diameter ratio to eliminate irreversible losses over the temperature range of interest. In addition it provides a very nearly

temperature-independent bias field. Two soft iron pole-pieces are used to concentrate the magnetic flux, and an outer case of heat treated tubing is used both as a return path and as an effective magnetic shield. The weight of the magnet assembly is approximately 9 ounces; the total weight of the limiter is 13 ounces.

### 3.3 *The YIG Sphere*

The diameters of the single-crystal YIG spheres used in the flight and test models of the satellite limiter ranged from 0.2470 inch to 0.2988 inch. Each sphere exhibited a highly polished surface which reduced the low-level insertion loss, made the slope transition more abrupt at the threshold and decreased the limiting slope.

The single-crystal YIG sphere was positioned in the cavity so that one of its three hard axes of magnetization was aligned along the direction of the static magnetic field. The hard magnetic axes of the YIG sphere were determined by first finding the four easy axes by allowing the sample to rotate freely in a uniform dc magnetic field so as to align itself along each of the [111] axes. Then a [100] or hard axis is uniquely defined and can be located and marked. This procedure eliminates the need for X-ray orientation and is sufficiently accurate for the required temperature compensation as shown in Section IV. The YIG sphere was supported 0.062 inch away from the cavity sidewall by encasing it in a Tellon package which was held firmly to the waveguide wall by a screw.

## IV. PERFORMANCE

### 4.1 *Temperature Testing*

Fig. 6 shows the electrical characteristics of the 4080-mc limiter as a function of temperature. As noted, the compensated temperature performance of the device over the range from 35°F to 120°F was due to the alignment of a hard axis of magnetization of the YIG sphere with the direction of the applied dc magnetic field. All of the properties of the limiter fell within the specifications given in Table I over this temperature range.

### 4.2 *Mechanical Tests*

The limiter was subjected to the standard shock and vibration test with the following maximum test parameters:

| | |
|---|---|
| Force | 33 g |
| Frequency | 40–2000 cps |
| Period | 4.75 minutes |

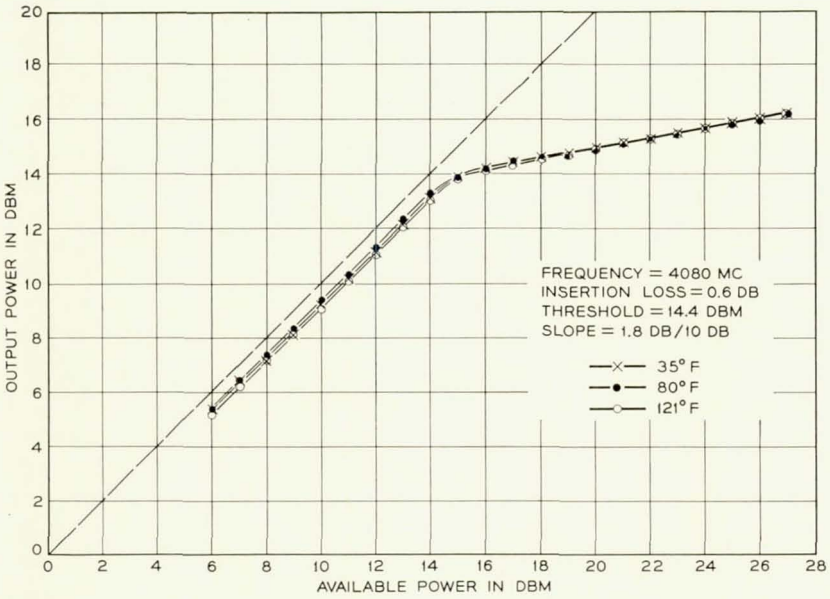


Fig. 6 — Experimental limiting curves for three operating temperatures. The YIG sample is oriented with a hard magnetic axis along the bias direction.

No degradation in the electrical performance of the limiter was observed following these tests. A centrifuge test was also performed with a maximum force of 30 g for three minutes and again no change in limiter performance was observed.

### 4.3 *Radiation Testing*

The ionizing radiation in the lower Van Allen belt consists of protons, electrons and gamma rays. The electrons have a moderate energy level (1 Kev to 100 Kev) and nearly all of them are stopped in the outer shell of the Telstar satellite. Nevertheless, electron radiation testing was conducted on the limiter, which is part of the electronic package within the satellite. Proton radiation testing was also performed on the limiter, since the protons of the lower Van Allen belt have relatively high energy (0.1 Mev to 1 Mev) and penetrate the entire satellite.

The irradiation test program on the limiter consisted of subjecting the single-crystal sphere of YIG and the Tellon package to the various types of radiation. Electrical tests were performed on a test limiter before and after radiation exposure, and it was found that the electron bombardment experiments had the largest effect. However, the electron energy

(1 Mev) corresponded to *unshielded* exposure in the lower Van Allen belt, and thus the effects under shielded conditions are expected to be much less than observed in this experiment. This effect probably is completely ascribable to electron radiation-induced dissipation in the Tellon holder. In the case of proton radiation with 10-Mev energy, slight degradation in the limiting slope characteristic was noted. It is conceivable that this also is attributable to the Tellon package; however, the highly polished YIG surface was observed to be slightly clouded. It is known that surface polish may have similar effects, and thus it is possible that there was an effect on the YIG sample primarily through surface damage. The gamma radiation test consisted of exposing the operating limiter to a low-intensity cobalt 60 source (1.3 curie) simulating conditions in the lower Van Allen belt. No effects on limiter characteristics were observed during the test.

## V. CONCLUSIONS

As with many contributions to the Telstar project, the limiter development required considerable extension of existing device capabilities. Although the principle of ferrimagnetic limiting had been known for some time, there existed no well developed device technology or detailed design theory. The temperature stability requirements presented a particularly challenging problem. The basic understanding of ferromagnetic resonance and spin wave instability, particularly in single crystals, provided the basis for the rapid development of a design theory and limiter realization. The temperature dependence of the magnetocrystalline anisotropy (anisotropy field) provided the key which made possible the limiter design described in this paper.

## VI. ACKNOWLEDGMENTS

The authors wish to acknowledge the many stimulating discussions with and contributions of R. C. LeCraw, E. G. Spencer, F. C. Rossol, V. Czarniewski, T. W. Mohr and J. Degan.

## REFERENCES

1. Bodmer, M. G., Laico, J. P., Olsen, E. G., and Ross, A. T., The Satellite Traveling-Wave Tube, B.S.T.J., this issue, p. 1703.
2. Davis, C. G., Hutchinson, P. T., Witt, F. J., and Maunsell, H. I., The Spacecraft Communications Repeater, B.S.T.J., this issue, p. 831.
3. Suhl, H., Theory of Ferromagnetic Resonance at High Signal Powers J. Phys., and Chem. of Solids, **1**, April, 1957, pp. 209–227.

# The Ground Station High-Power Traveling-Wave Tube

By R. J. COLLIER, G. D. HELM, J. P. LAICO, and K. M. STRINY

(Manuscript received February 27, 1963)

*The M4040 is a 2-kw CW traveling-wave tube developed specifically for communications applications. It was used as the power amplifier in the Project Telstar ground transmitter. Analytic methods employed in the design of the electron gun, the beam collector, the RF circuit and the output match are presented. Typical performance characteristics and drawings of the tube subassemblies serve to describe the electrical and physical features of the M4040 traveling-wave tube. Methods used to inhibit oscillation and the effects of ion drainage and collector depression on tube performance are also discussed.*

## I. INTRODUCTION

This paper describes the design of the M4040 2-kw CW traveling-wave tube amplifier which was developed specifically for communications applications. It was used as the final power amplifier in the Telstar transmitters at Andover, Maine, and Pleumeur-Bodou, France. It was necessary for the Telstar amplifier to meet the requirements shown in Table I.

The M4040 was designed to have sufficient instantaneous bandwidth to operate anywhere in the communications band from 5.925 to 6.425 gc. The design approach was a conservative one aimed primarily at delivering an operable tube in time for the Telstar experiment. The development time was approximately 18 months. In describing the M4040, we shall discuss only briefly its mechanical aspects. The prime intent is to present electrical design and operating information which may be applicable to future high-power traveling-wave tube development. Topics concerned with the electrical design of the electron gun, the beam collector, and the slow-wave structure will be discussed. Finally, some performance characteristics will be presented, accompanied by comments on the tube operation.

TABLE I — REQUIREMENTS

| | |
|---|---|
| Output power (maximum) | 2 kw CW |
| Small-signal gain | 30 db |
| Large-signal gain | 27 db |
| Bandwidth | 25 mc |
| Center operating frequency | 6.39 gc |
| Output amplitude ripple (small signal) | ±0.5 db |
| Input signal amplitude range | 30 db |

## II. GENERAL DESCRIPTION OF THE M4040

The M4040 is an all metal and ceramic electron tube 4 feet in length, 17 inches in diameter, and 230 pounds in weight. These dimensions include an aluminum foil solenoid which produces an axial beam-focusing field of 730 gauss along the 13 inches of slow-wave circuit. The electron gun is magnetically shielded, as is the solenoid and collector. The gun is a Pierce convergent type. The slow-wave circuit is a coupled-cavity structure with coupling slots rotated by 180° in each successive cavity. A single sever is employed. The sever attenuators are located in short waveguides matched to the circuit but are still in the vacuum. Microwave power is fed into and coupled out of the tube through ceramic windows, step transformers, narrow-height guide and matching cavities which form part of the slow-wave structure. The beam diverges into the beam collector under the action of space-charge forces alone. The slow-wave structure, solenoid and beam collector are separately water-cooled. Fig. 1 is a photograph of the M4040 located in the solenoid. The appendage ion pumps shown in the figure continuously pump the tube at the gun, as well as at the collector end. In the picture, the collector is at the top and the gun is at the bottom.

Fig. 2 is a cutaway section. Axial alignment of the tube in the magnetic field is preplumbed, and no adjustments are necessary to optimize their relationship. Figs. 3 to 7 are sketches showing more detail of the tube construction: respectively, the gun, RF circuit, collector, sever, and coupling assemblies. The construction materials are typical of those used in electron devices in that they have low vapor pressures and can withstand vigorous cleaning and the heating associated with outgassing. The residual gas pressure in a sealed-off M4040 is less than $1 \times 10^{-8}$ torr. The tube is outgassed by heating, not only when the tube is finally processed, but also in the subassembly stages indicated in substance by Figs. 3 to 7, inclusive.

The gun shown in Fig. 3 is made of molybdenum, tungsten, and ceramic parts welded, brazed or glazed together. The spacing of the beam-forming electrode to the cathode is held to ±0.0003 inch, and the

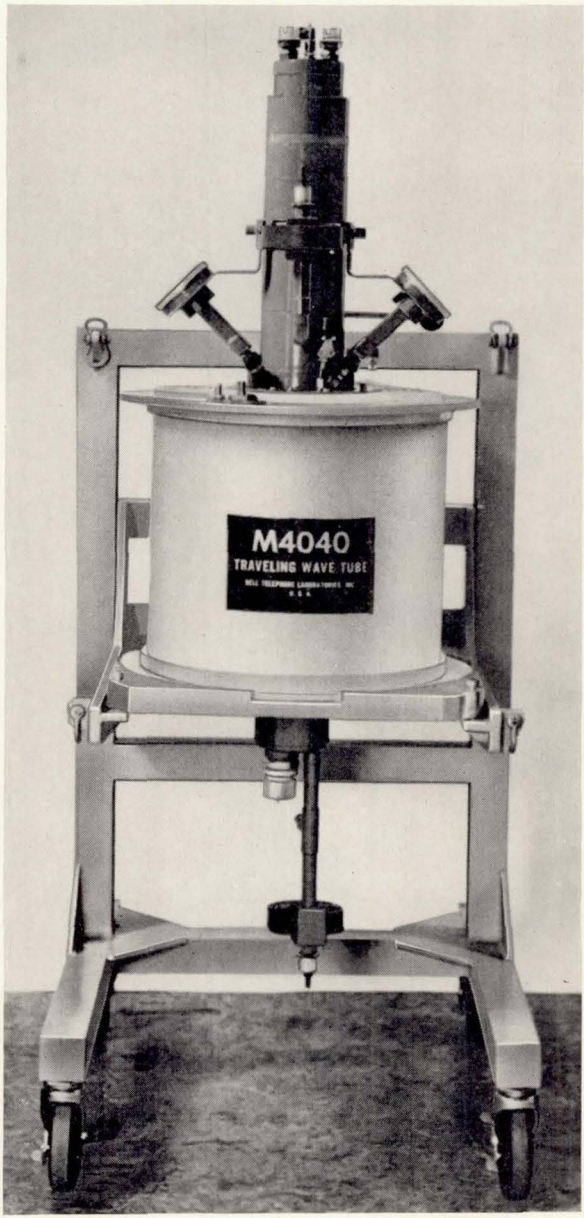


Fig. 1 — The M4040 traveling-wave tube.

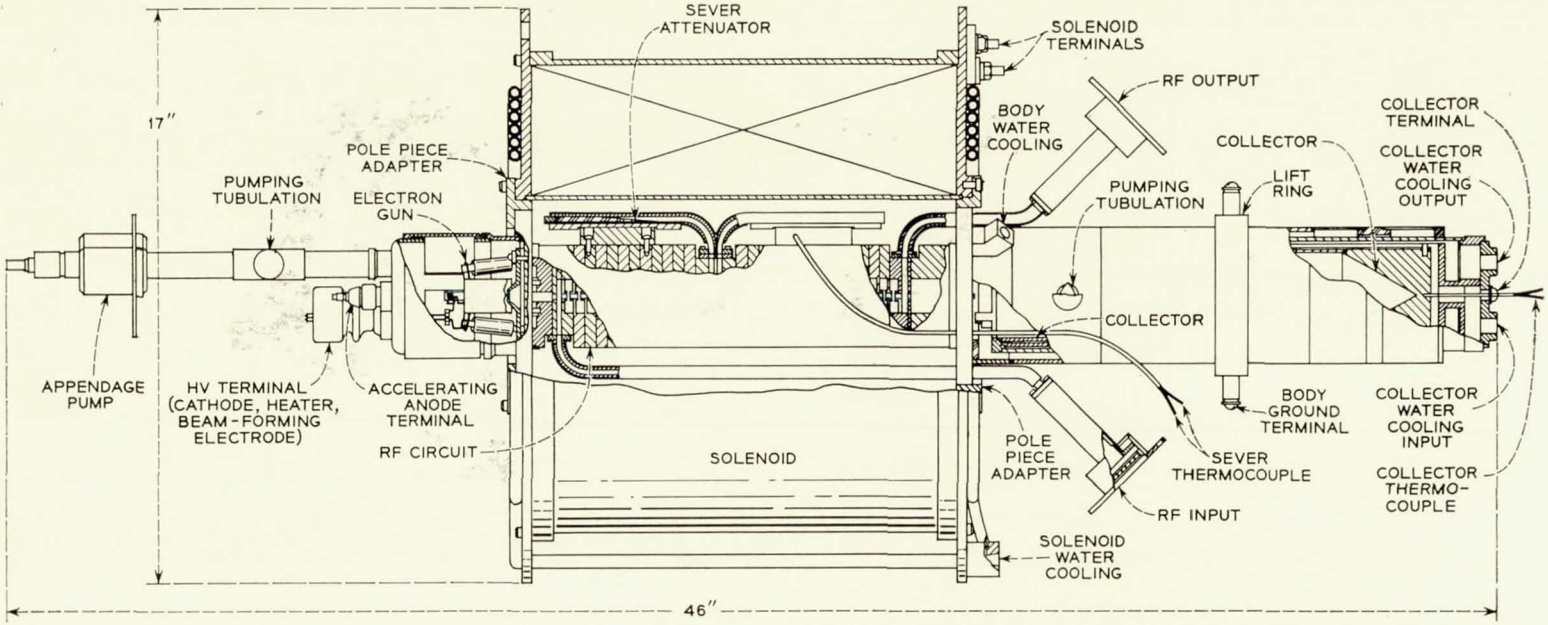


Fig. 2 — Internal structure of the M4040 tube.

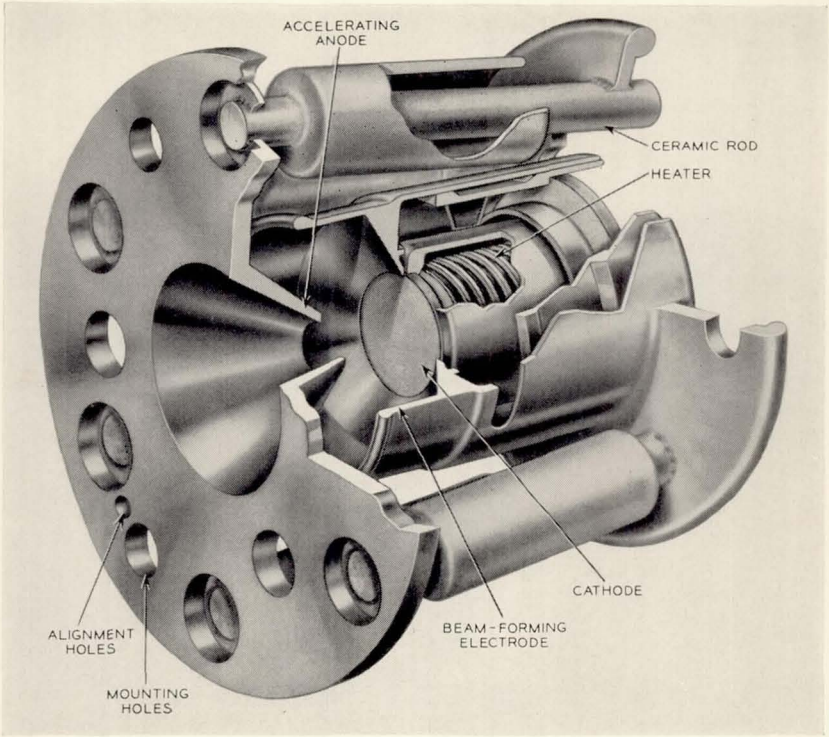


Fig. 3 — M4040 electron gun.

concentricity of these with respect to each other and to the accelerating anode is held to $\pm 0.001$ inch. Six Alsimag 475 insulators support and electrically isolate the accelerating anode from the cathode and the beam-forming electrode so as to safely withstand 18,000 volts. Re-entrant skirts are an integral part of these insulators and insure against electrical leakage arising from the deposition of metallic vapors emanating principally from the cathode; the latter is a Phillips Metallonics type B tungsten matrix cathode.

The RF structure identified in Fig. 4 consists of a stack of 29 copper cavities capped at each end by a steel pole-piece and machined at its center to provide for the addition of the sever sections. Adjacent to each steel pole-piece is the input or output waveguide, respectively. In each cavity and pole-piece, holes or channels are machined so that when the parts are finally brazed together, they not only form the RF circuit but also provide the path for circulating cooling water. The brazed assembly

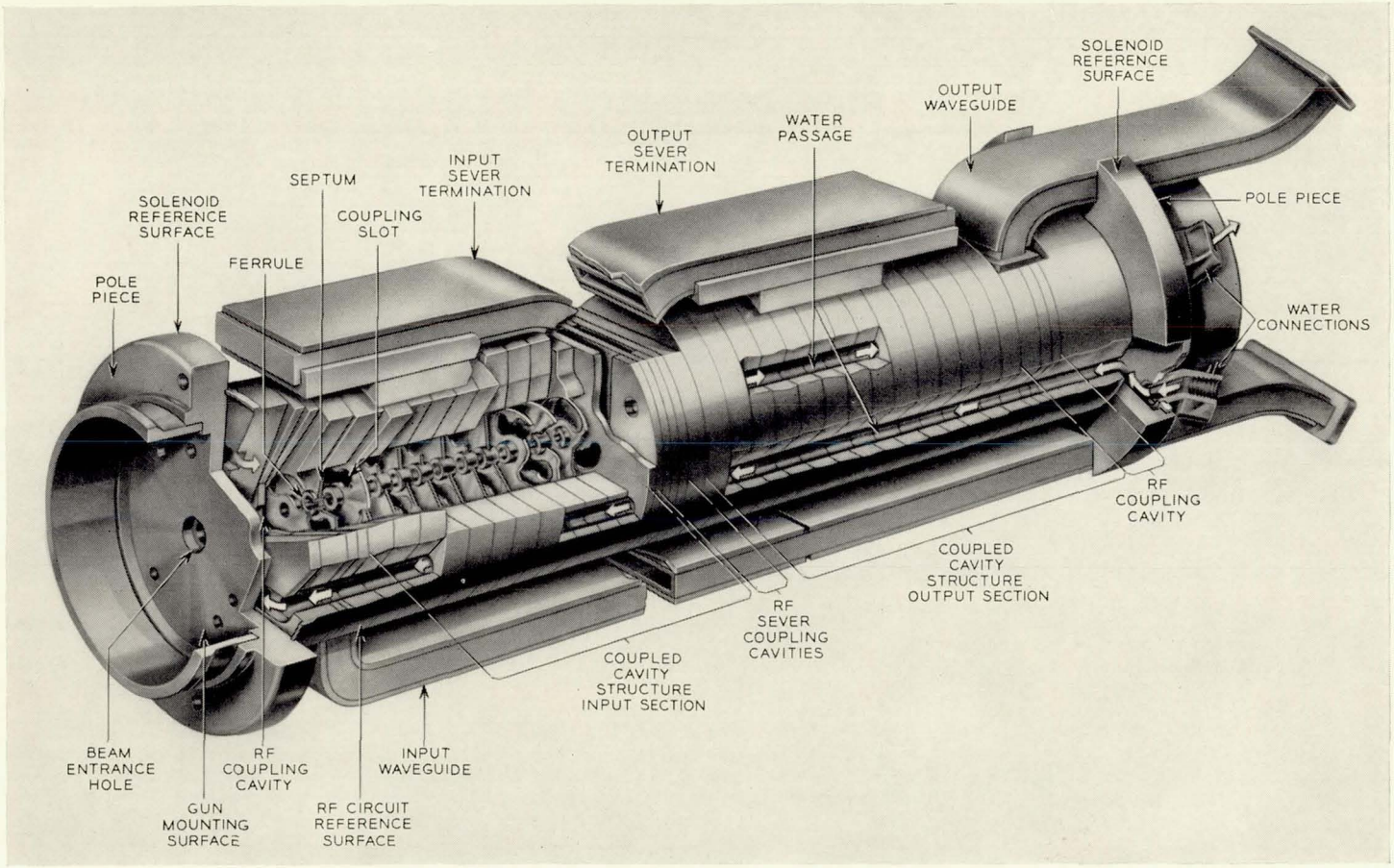


Fig. 4 — M4040 RF circuit.

meets the concentricity requirement of 0.004 inch on all central holes with respect to each other and to the outside diameter of the pole-pieces. After auxiliary subassemblies such as the sever sections and waveguides are assembled, the unit is outgassed by heating to about 500°C until a pressure of $5 \times 10^{-6}$ torr is achieved.

In Fig. 5 the collector subassembly is shown. This is a set of concentric tubes of copper and steel to provide, in addition to the beam collector cavity, an annular channel for the passage of cooling water at the rate of 18 gpm. The collector is electrically isolated from the body of the tube by a ceramic insulator, allowing any beam current intercepted by the slow-wave structure to be monitored.

A sever section subassembly is shown in Fig. 6. A significant feature of this unit is the carbonized ceramic attenuator, which is a wedge of porous alumina $0.156 \times 1.372$ inches at one end and tapering to a point at the other end. To aid in dissipating some 300 watts of unwanted power, it is brazed to a molybdenum base plate. One surface of the ceramic is metallized with standard molybdenum manganese powder mixture in the empirically determined pattern shown in Fig. 6. Carbonizing is accomplished by soaking the unit in sugar solution and then converting the sugar to carbon by heating to 900°C in a purified dry hydrogen atmosphere.

The RF coupling assembly shown in Fig. 7 is the same for the input and output. It contains a step transformer section and an RF window which also forms part of the vacuum wall. The metal member of this vacuum seal is especially designed to provide sufficient elasticity to compensate for the mismatch in expansion between it and the ceramic and to better withstand thermal shocks.

An electrical description of the M4040 is furnished by Tables II, III and IV.

## III. VOLTAGE SCALING OF AN ELECTRON GUN

To minimize development time, it was decided to scale in voltage a gun whose properties were previously measured at 1000 volts. We were able to predict the beam minimum radius and perveance quite successfully, enabling work on the slow-wave circuit to progress in parallel with the gun measurements program. The measurements of the beam cylindrical symmetry and the beam profile as a function of voltage and of distance from a reference surface on the beam-forming electrode were performed using the "pin-hole collector" technique.

Figs. 8(a) and 8(b) present measurements of the beam minimum radius and its location as a function of voltage. The radius is taken as

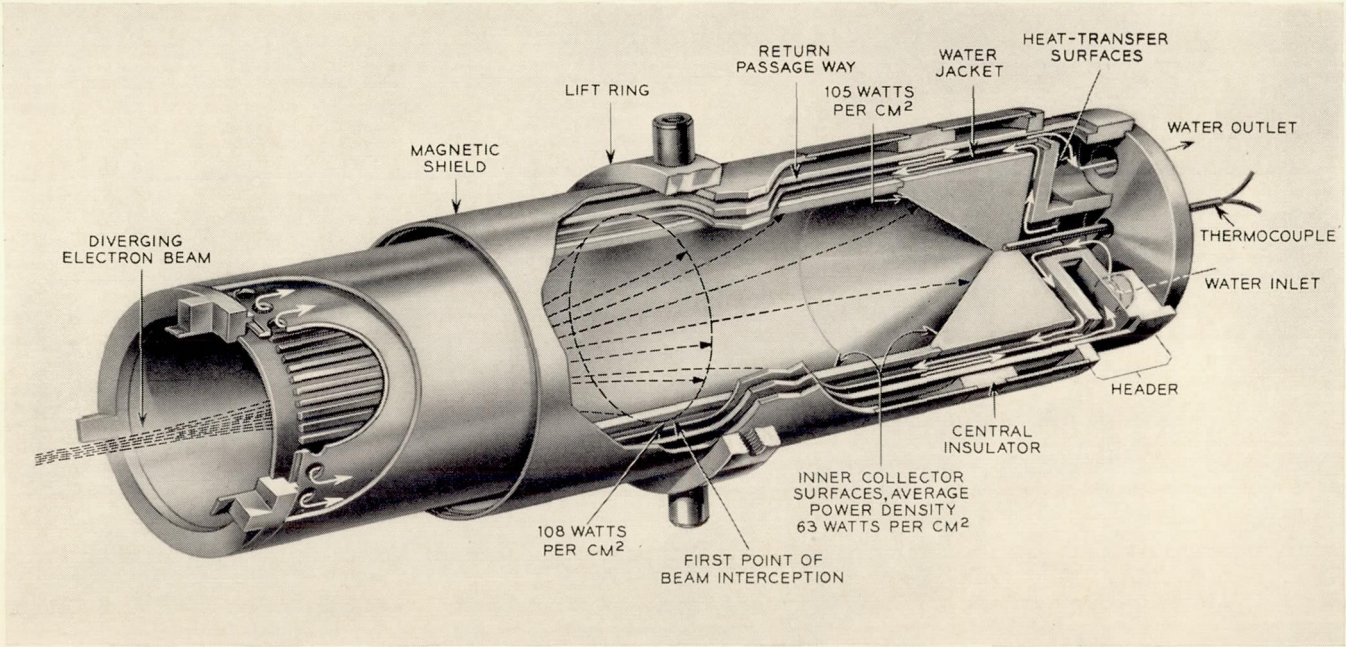


Fig. 5 — M4040 collector.

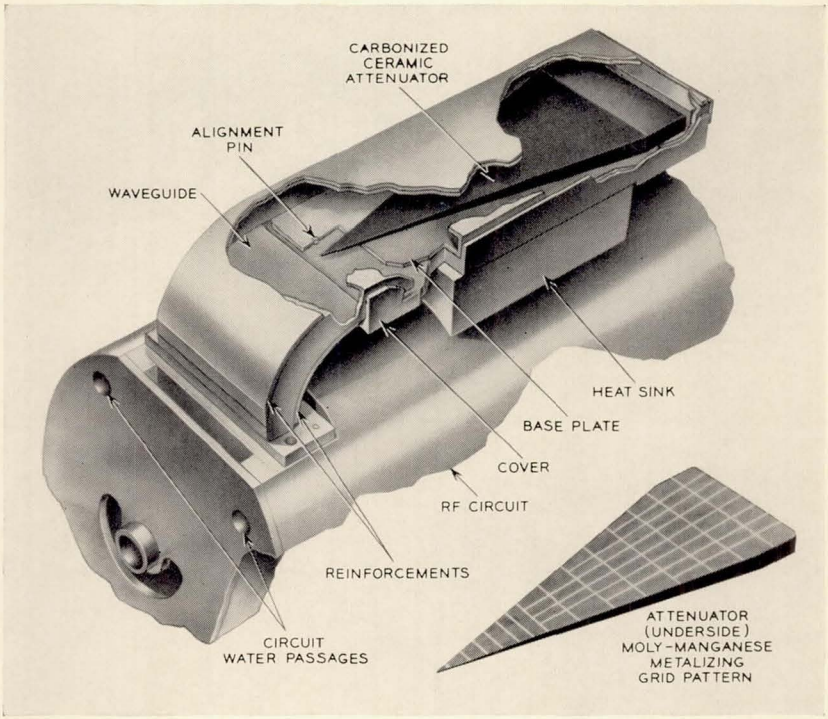


Fig. 6 — M4040 sever termination.

that which encloses 95 per cent of the total current. If the thermal motion of the electrons is neglected, these quantities are theoretically constant and are given by the curves labeled "universal beam spread." The latter were calculated by the methods described in Pierce[1] but with an additional correction for the focal length of the anode-aperture lens given by $\Gamma = 1.1$, where $\Gamma$ is defined as in Danielson, Rosenfeld and Saloom.[2] On the other hand, transverse thermal velocities of the electrons cause the beam minimum radius to be smaller and closer to the cathode than predicted by the universal beam spread curve.

Danielson, Rosenfeld and Saloom have devised a theory which predicts the size and location of the beam minimum radius as a function of voltage and cathode temperature for several values of perveance. Their results were generalized by Herrmann[3] who presented curves having a wider applicability. The results predicted by Herrmann are shown in Figs. 8(a) and 8(b) for comparison with the experimental data and the universal beam spread values.

Fig. 8(a) suggests that a useful rule to apply when predicting the

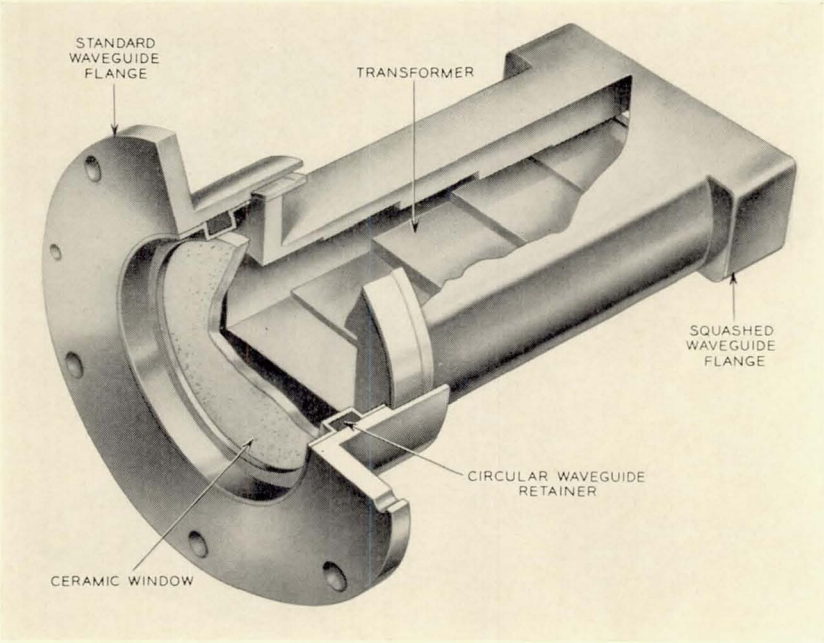


Fig. 7 — M4040 RF window assembly.

beam properties of an electron gun at a scaled voltage is that the theoretical behavior is given by the Herrmann curves up to the voltage at which they intersect the universal beam spread values and by the latter quantities at higher voltages. In comparing theory and experiment, we note that the experimental beam minimum radius is larger by 10 to 20 per cent, and its location falls within 10 per cent of the expected distance from the cathode.

TABLE II — ELECTRICAL DESIGN PARAMETERS AT MIDBAND

| | |
|---|---|
| Midband frequency | 6.15 gc |
| Gun perveance | $0.47 \times 10^{-6}$ amp/(volts)$^{\frac{3}{2}}$ |
| Gain parameter, C | 0.062 |
| Space charge parameter, QC | 0.3 |
| (Radial phase constant) × (beam radius), $\gamma r_b$ | 0.65 |
| Growing wave parameter, X | 0.65 |
| Velocity parameter, $b$ | 1.0 |
| No. of beam wavelengths, N | 20 |
| No. of active cavities | 29 |
| Beam radius ($r_{95}$), $r_b$ | 0.049 inch |
| Tunnel radius, $a$ | 0.082 inch |
| Cathode radius, $r_c$ | 0.205 inch |

TABLE III — TYPICAL CHARACTERISTICS FOR M4040 OPERATED IN THE *Telstar* GROUND STATION

| (a) Input | |
|---|---|
| Cathode potential | −17,000 v |
| Accelerator potential | +600 v |
| Circuit potential | 0 v |
| Collector potential | 0 v |
| Heater current | 6.2 amps |
| Heater voltage | 7.25 v |
| Solenoid current | 23 amps |
| Solenoid voltage | 15.3 v |
| Total cathode emission current | 1030 ma |
| Collector water flow rate | 18 gal/min |
| Circuit water flow rate | 3.5 gal/min |
| Solenoid water flow rate | 0.5 gal/min |
| Maximum signal power | 3 watts |
| **(b) Output** | |
| Rated frequency range | 6.35-6.45 gc |
| Rated maximum output power | 2000 watts |
| Small-signal gain | 31.8-30.8 db |
| Output amplitude ripple | ±0.2 db |
| Gain at 2000-watt level | 28 db |
| Magnetic field | 730 oersted |
| Circuit interception current (no drive) | 4 ma |
| Circuit interception current (with drive) | 35 ma |
| Accelerator interception current | 0.1 ma |

TABLE IV — TYPICAL M4040 CHARACTERISTICS FOR BROADBAND HIGH-POWER OPERATION

| (a) Input | |
|---|---|
| Cathode potential | −17,400 v |
| Total cathode emission current | 1040 ma |
| Signal power | ≈4 watts |
| (Other values are the same as in Table IIIa) | |
| **(b) Output** | |
| Center frequency, $f_0$ | ≈6.15 gc |
| Output power at center frequency | 2500 watts |
| Gain at $f_0$ and at 2500-watt level | 28 db |
| 1-db instantaneous bandwidth (i.e., band edge power = 2 kw) | 12.7% = 780 mc |
| Efficiency at $f_0$ | 13.8% |

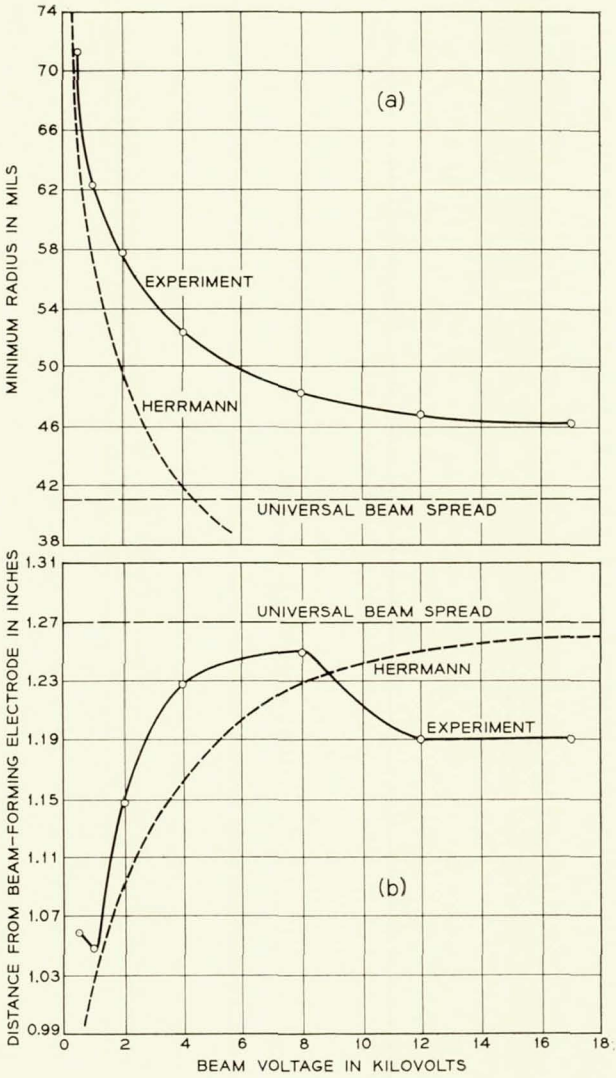


Fig. 8 — (a) Minimum beam radius (95 per cent of total current) vs beam voltage; (b) position of beam minimum vs voltage.

## IV. DISTRIBUTION OF BEAM POWER IN THE COLLECTOR

If size and weight are of little consequence, the beam collector of a traveling-wave tube should be designed to minimize temperature inside the vacuum. Let us consider the spread of a monovelocity, homogeneous beam into an ideal hard-vacuum, field-free region. The universal beam

spread curve referred to in the previous section has been derived by several authors.[1,4] The relation between the axial distance the beam has drifted and the beam radius can be written as

$$z = \frac{r_0 Z}{\sqrt{K}} \tag{1}$$

where $r_0$ is the beam radius on entering the field-free region and

$$K = \frac{I}{V^{3/2}} \cdot \left(\frac{m}{e}\right)^{1/2} \cdot \frac{1}{2\sqrt{2}\pi\epsilon_0}. \tag{2}$$

The beam radius $r_b$ appears in the expression for $Z$, viz.

$$Z = \int^{t} 2e^{t^2}\, dt \tag{3}$$

where $t = \sqrt{ln\ R}$, in the form of a normalized radius $R = r_b/r_0$. The half-value of the integral in (3) is tabulated by Jahnke and Emde[5] for various values of $t$. One can plot the normalized radius $R$ against the normalized axial distance $Z$ to obtain the "universal beam spread curve." Applying the specific values of the normalizing constants associated with the M4040, we plot in Fig. 9 $r_b$ versus $z$. Also plotted in

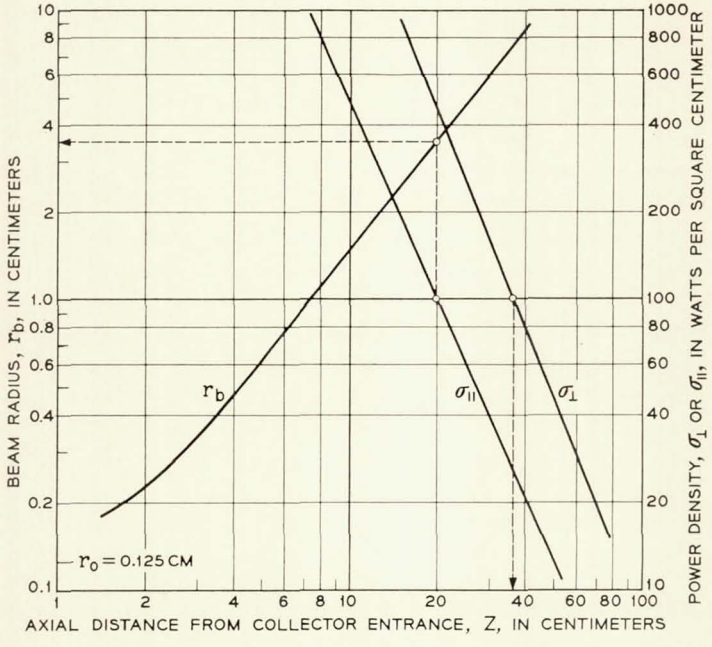


Fig. 9 — M4040 collector design chart.

Fig. 9 is the power density incident on a surface normal to the beam axis, $\sigma_\perp$, whose value is obtained for any value of $z$ by dividing the total beam power by the area of a circle whose radius is read from the $r_b$ versus $z$ plot. The M4040 has been designed with a total beam power of about 17.7 kw so that the power density at the minimum radius of the beam ($r_0 \approx 0.125$ cm) is $\sigma_\perp \approx 360$ kw/cm$^2$.

If it is assumed that the collector is cylindrical in shape, the power density incident on a surface parallel to the beam axis, $\sigma_\parallel$, will be of interest. Consider the beam to be spreading such that the edge electrons make an angle $\varphi$ with the initial beam axis. Then the power illuminating a small area, $A_\perp$, which is located at the beam edge and is perpendicular to the initial beam axis, is given by $\sigma_\perp A_\perp$. When $A_\perp$ is projected by the beam illumination onto the surface parallel to the initial beam axis, it takes the value $A_\parallel$ such that

$$\frac{A_\perp}{A_\parallel} = \tan \varphi = \frac{dr_b}{dz} = r_b'. \tag{4}$$

Equating the power incident on $A_\perp$ to that on $A_\parallel$

$$\sigma_\perp A_\perp = \sigma_\parallel A_\parallel \tag{5}$$

where $\sigma_\parallel$ is the power in the beam edge incident on a square unit area parallel to the initial beam axis. Upon the substitution of (4) into (5), we find that

$$\sigma_\parallel = \sigma_\perp r_b' = \sigma_\perp \sqrt{K}\, \sqrt{ln\, r_b/r_0}\,. \tag{6}$$

The expression for $r_b'$ is obtained in deriving (1). $\sigma_\parallel$ is plotted as a function of $z$ in Fig. 9. Note that the interception of the beam edge on the cylindrical walls of the collector corresponds to the highest power density incident on those walls, since tan $\varphi$ becomes smaller for all other conditions. Therefore, the collector may be designed such that the cylinder length determines when $\sigma_\perp$ equals the maximum desired and the cylinder radius determines the same value for $\sigma_\parallel$. The length and radius corresponding to a power density of 100 watts/cm$^2$ are indicated on Fig. 9 for the M4040. This chart indicates the hottest spots. The power density on the side wall will average to the order of half $\sigma_\parallel$.

## V. ANALYTICAL METHODS FOR DESIGNING AND MATCHING THE SLOW-WAVE CIRCUIT

Fig. 4, the sketch of the RF circuit, indicates that a relatively rugged, easily fabricated slow-wave structure can be formed from an induc-

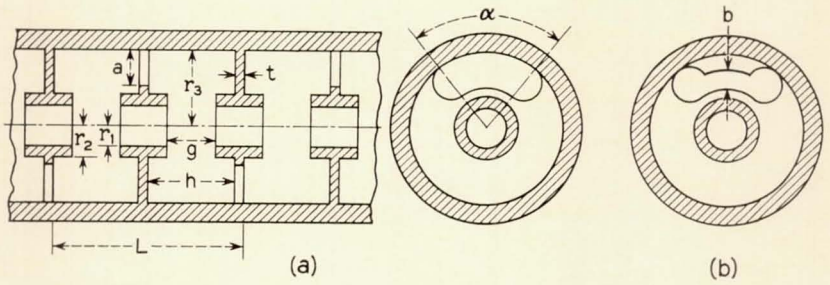


| SUMMARY OF M4040 CIRCUIT DIMENSIONS | | | |
|---|---|---|---|
| a | 0.325″ | $r_1$ | 0.082″ |
| b | 0.1625″ | $r_2$ | 0.122″ |
| g | 0.116″ | $r_3$ | 0.5235″ |
| h | 0.294″ | L | 0.668″ |
| t | 0.040″ | $\alpha$ | 75° |

Fig. 10 — (a) Slow-wave circuit dimensions showing unloaded coupling iris; (b) septum with a loaded coupling iris.

tively coupled chain of cylindrical cavities. Excellent heat dissipation properties are combined with a good impedance-bandwidth product. The important dimensional parameters are designated in Fig. 10; the parameter labels are those used in the analysis below.

$\omega$-$\beta$ diagrams for the four lowest modes are shown in Fig. 11. The M4040 is designed to operate on the first forward wave space harmonic of the $TM_{01}$ cavity mode. Where the resonant frequency, $\omega_s$, of the coupling slot is appreciably higher than the upper cutoff frequency, $\omega_2$, of the cavity, the dispersion curve of the $TM_{01}$ cavity mode may be approximated by the equation

$$\cos\left(\frac{\beta L}{2}\right) = 1 - 2\frac{\left[\frac{1}{\omega^2} - \frac{1}{\omega_2^2}\right]}{\left[\frac{1}{\omega_1^2} - \frac{1}{\omega_2^2}\right]}. \tag{7}$$

Here $\omega_1$ is the lower cutoff frequency of the mode and $L$ is the periodic length of the circuit.

The choice of the electron gun design establishes the electron beam radius, $r_b$, and the beam velocity, $u_0$. These in turn determine the cavity beam hole radius $r_1 \approx 1.67\ r_b$ and the periodic length $L \approx 3\pi u_0/\omega_0$,

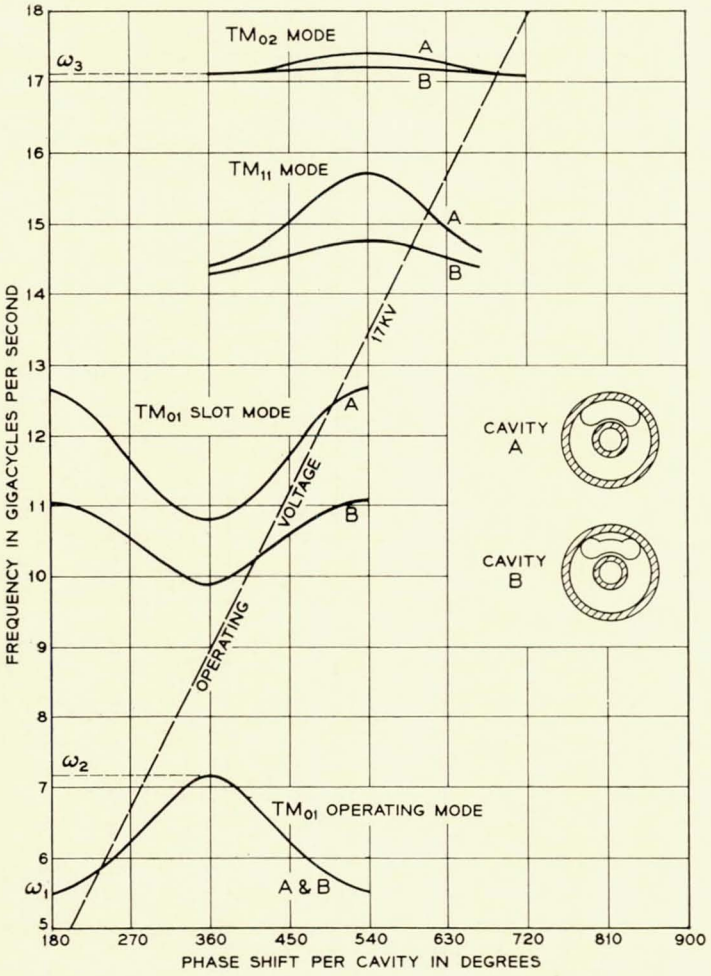


Fig. 11 — $\omega$-$\beta$ diagrams.

where $\omega_0$ is the synchronous frequency. The gap, $g$, between the ferrules capacitively loading the cylindrical cavities, is used to optimize the interaction impedance of the forward wave space harmonic. To this effect the gap-to-period ratio $g/L$ is selected to lie between 0.1 and 0.2. The outer radius of the ferrule, $r_2$, and the septum thickness, $t$, are designed to be as small as possible consistent with the heat energy to be dissipated.

Following Ramo and Whinnery,[6] the cavity may be analyzed as a

foreshortened radial line resonator. The major cavity radius, $r_3$, which sets the upper cutoff frequency, $\omega_2$, may be calculated from the expression

$$\theta_3 = \tan^{-1}\left[\frac{\sin\theta_2 + (2\pi r_2/\omega_2 C_0 Z_{02} h)\cos\psi_2}{\cos\theta_2 - (2\pi r_2/\omega_2 C_0 Z_{02} h)\sin\psi_1}\right] \tag{8}$$

where

$$\theta_i = \tan^{-1}\left[\frac{N_0(kr_i)}{J_0(kr_i)}\right]$$

$$\psi_i = \tan^{-1}\left[-\frac{J_1(kr_i)}{N_1(kr_i)}\right]$$

$$Z_{0i} = 377\left[\frac{J_0^2(kr_i) + N_0^2(kr_i)}{J_1^2(kr_i) + N_1^2(kr_i)}\right]^{1/2}$$

and $k = \omega/c$, the wave number. $J_0$, $J_1$, $N_0$, $N_1$ are Bessel functions of the first and second kinds and $C_0$ is the loading capacitance. The latter is estimated as the sum of four parallel connected capacitances

$$C_0 = C_g + C_h + C_{d1} + C_{d2}. \tag{9}$$

The gap capacitance, $C_g$, is the equivalent parallel plate capacitance for an area equal to that on a ferrule edge, $\pi(r_2^2 - r_1^2)$, and a separation, $g$. Thus

$$C_g = \epsilon_0\pi(r_2^2 - r_1^2)/g. \tag{10}$$

The "hole" capacitance, $C_h$, is an artifice made by assuming a parallel plate capacitor with area equal to the beam hole area and a separation $L/2$. Then

$$C_h = 2\epsilon_0\pi r_1^2/L. \tag{11}$$

The capacitances $C_{d1}$ and $C_{d2}$ are the discontinuity capacitances located at $r_1$ and $r_2$, i.e., where the cavity height changes. For a symmetric step

$$C_{di} = \pi r_i C_d' \tag{12}$$

where the value of $C_d'$ as a function of gap ratio is obtained from a curve in Ramo and Whinnery.[7] The gap ratio at $r_1$ is considered to be $2g/L$. (Note that once $r_3$ is calculated, it may be inserted back into (8) to obtain the higher order cavity mode resonant frequency, $\omega_3$, corresponding to the $TM_{02}$ mode.) The ratio of upper to lower cutoff

frequency of the operating mode is related to the coupling iris angle $\alpha$ in the following manner.

$$\frac{\omega_2}{\omega_1} = \sqrt{\frac{180}{180 - \alpha}} \tag{13}$$

for $\alpha$ in degrees. The final dimensions of the M4040 cavities are summarized in Fig. 10.

Some insight into the manner in which the slow-wave structure may be matched to rectangular waveguide can be obtained by considering a lumped-element equivalent circuit. One such circuit, suggested by Pierce,[8] appears in Fig. 12(a). Using the Tee equivalence in Fig. 12(b),

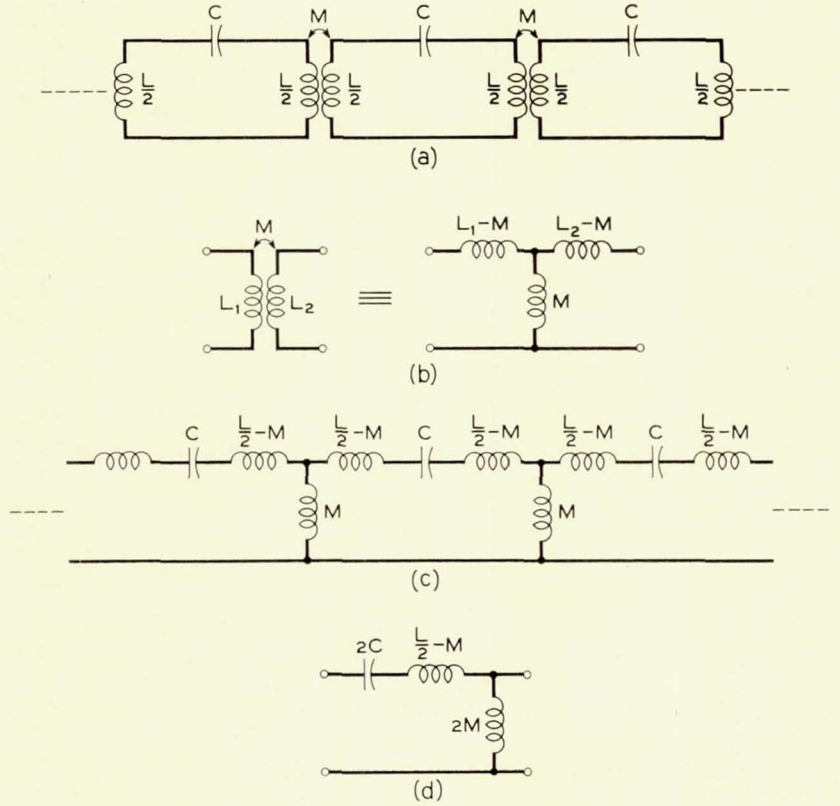


Fig. 12 — (a) Equivalent circuit for a chain of coupled cavities; (b) equivalent Tee circuit for a transformer; (c) transposition of circuit 12(a); (d) half section of circuit 12(c).

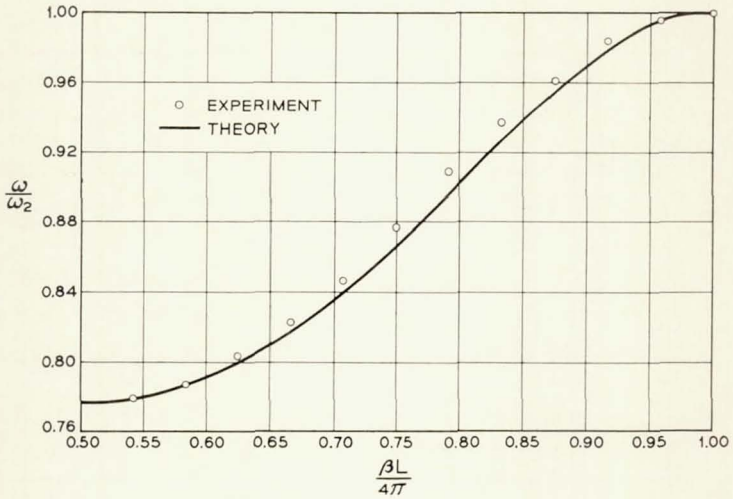


Fig. 13 — Comparison of an experimental $\omega$-$\beta$ curve with the theoretical dispersion curve of the assumed equivalent circuit.

the circuit of Fig. 12(a) may be transposed to that of 12(c), which in turn has the characteristic half-section of Fig. 12(d). The dispersion curve of this circuit (when the alternation of fields by $\pi$ radians for adjacent cavities is properly accounted for) is precisely that of (7). Fig. 13 offers a comparison between a typical measured $\omega$-$\beta$ curve and the theoretical curve from the lumped-circuit approximation. The upper and lower cutoff frequencies are related to the circuit values as shown below.

$$\omega_2 = [C(L - 2M)]^{-\frac{1}{2}} \quad \text{upper cutoff} \tag{14}$$

$$\omega_1 = [C(L + 2M)]^{-\frac{1}{2}} \quad \text{lower cutoff} \tag{15}$$

whence

$$\frac{\omega_2}{\omega_1} = \left[\frac{(L - 2M) + 4M}{(L - 2M)}\right]^{1/2} \tag{16}$$

and

$$\frac{L}{M} = \frac{2(\omega_2^2 + \omega_1^2)}{\omega_2^2 - \omega_1^2} . \tag{17}$$

The equivalent circuit for the last two cavities and the terminating waveguide is represented in Fig. 14(a). The values $L$, $C$, and $M$ define

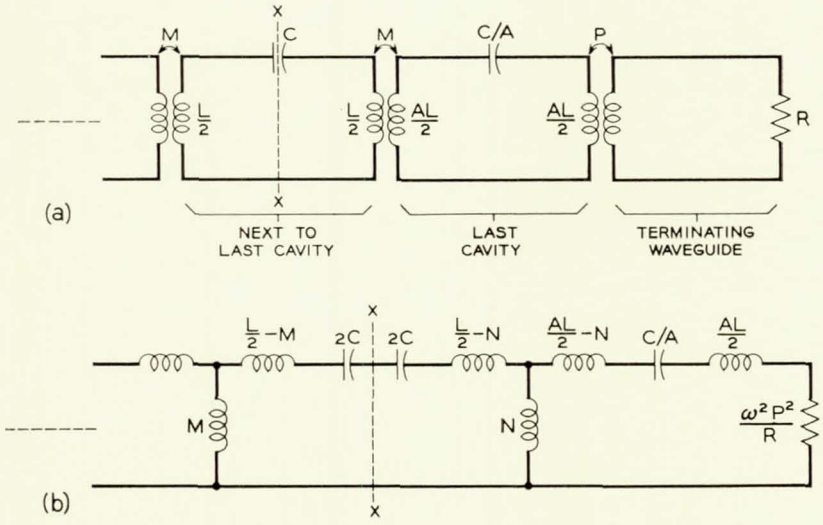


Fig. 14 — (a) Equivalent circuit of terminating cavities and waveguide; (b) transposition of circuit 14(a).

the general cavity circuit and the mutual coupling as before; the coupling between the last two cavities and between the last cavity and the waveguide, however, has been allowed to change to $N$ and $P$, respectively. The inductance and capacitance of the last cavity have been modified by the factors $A$ and $1/A$, which is roughly equivalent to changing the axial dimensions of the cavity by the factor $A$. We will assume the inductance of the waveguide termination is negligible. Again applying the circuit equivalence of Fig. 12(b), we arrive at the circuit of Fig. 14(b). Referring to the reference plane x-x, the impedance looking back to the left into the semi-infinite cavity chain is just the Tee impedance of the half-section circuit of Fig. 12(d)

$$Z_T = \sqrt{\omega^2 M^2 - \frac{K^2}{4}} \tag{18}$$

where

$$K = \omega L - \frac{1}{\omega C} = \frac{\omega^2 LC - 1}{\omega C} .$$

The impedance looking to the right of the reference plane can be written

$$Z_R = \frac{R(\omega^2 NP)^2}{(\omega P)^4 + (RAK)^2} + j2K\left[\frac{(\omega P)^4 + (RAK)^2 - 2A(\omega NR)^2}{(\omega P)^4 + (RAK)^2}\right]. \tag{19}$$

$Z_R$ will be real if

$$(\omega P)^4 + (RAK)^2 = 2A(\omega NR)^2 \tag{20}$$

so that

$$R = \frac{(\omega P)^2}{2A\sqrt{\frac{(\omega N)^2}{2A} - \frac{K^2}{4}}}. \tag{21}$$

Substituting (20) and (21) back into (19) and equating $Z_R$ to $Z_T$, we get

$$\sqrt{\omega^2 M^2 - \frac{K^2}{4}} = \sqrt{\frac{\omega^2 N^2}{2A} - \frac{K^2}{4}} \tag{22}$$

or

$$N = \sqrt{2A}\, M\,. \tag{23}$$

Let us assume that we may choose

$$P = \sqrt{B}\, M \tag{24}$$

where $\sqrt{B}$ is a constant. Then we have

$$R = \frac{B}{A}\left[2\sqrt{\frac{(\omega M)^2}{\omega^2 M^2 - \frac{K^2}{4}}}\right] \equiv \frac{B}{A} R_0. \tag{25}$$

For convenience the height of the last cavities in the M4040 was left unchanged. This implies that $A = 1$ and that $(L - 2M)$ in (16) is a constant quantity. Combining (13) and (16) with the above constraints yields a prediction for the coupling iris angle for $N$ of

$$\alpha_N = 180^\circ\left[\frac{5.656}{L/M + 3.656}\right]. \tag{26}$$

Using $L/M = 8.09$ for the M4040, a figure evaluated from (17), we predicted a value of $\alpha_N = 86.7^\circ$, whereas the empirically determined angle turned out to be 92°.

An inherent difficulty arises when attempting to calculate $R_0$, since

(14) and (15) define three circuit values, $L$, $C$, and $M$, in terms of only two known parameters, $\omega_1$ and $\omega_2$. It remains then to select a suitable reference surface in the cavity in order to estimate one of the lumped-circuit values at that surface. The appropriate surface would seem to be a cylinder, concentric with the cavity, whose radius bisects the coupling iris since the waveguide impedance is presented to the final cavity in this region. The capacitance at this surface may be estimated by making an impedance transformation of the capacitance $C_0$, calculated in (9) through (12), over the radial waveguide from radius $r_2$ to $(r_3 - a/2)$. The calculation of $R_0$ may be simplified if the midband frequency is chosen as the mean of the cutoff frequencies ($\omega_M = \sqrt{\omega_1\omega_2}$). Combining (14), (15) and (25), one obtains

$$R_0 = \frac{(\omega_2 - \omega_1)(\omega_2 + \omega_1)^2}{16C(\omega_1\omega_2)^2}. \tag{27}$$

The resultant value for $R_0$ is 3.01 ohms. Since the midband impedance (on a voltage-current basis) of the reduced-height waveguide is 93.5 ohms, $P$ is required to be

$$P = \sqrt{B}\,M = \sqrt{\frac{93.5}{3.01}}\,M.$$

Using the same procedure as when calculating $\alpha_N$, we arrive at a predicted value of $\alpha_P = 141.7°$. The experimentally determined value is 132°.

Experimentally it was also found necessary to increase the ferrule separation in the last two cavities in direct proportion to the sum of the coupling iris angles on the two end walls of the cavity. Identical transition sections are used for input, output and sever waveguides. A typical curve of reflection coefficient versus frequency is shown in Fig. 15.

Considering the devious nature of the above calculations, plus all the usual inadequacies of a lumped-circuit approximation, the predicted and experimental values of iris angles show reasonable agreement. The equivalent circuit approach is valuable, however, even when it discloses only the qualitative aspects of the matching technique.

## VI. METHODS USED TO INHIBIT OSCILLATION

The $\omega$-$\beta$ diagram, Fig. 11, shows the higher-order modes associated with the coupled cavity slow-wave structure. At the cutoff frequencies for these, as well as the fundamental mode, there is a substantial prob-

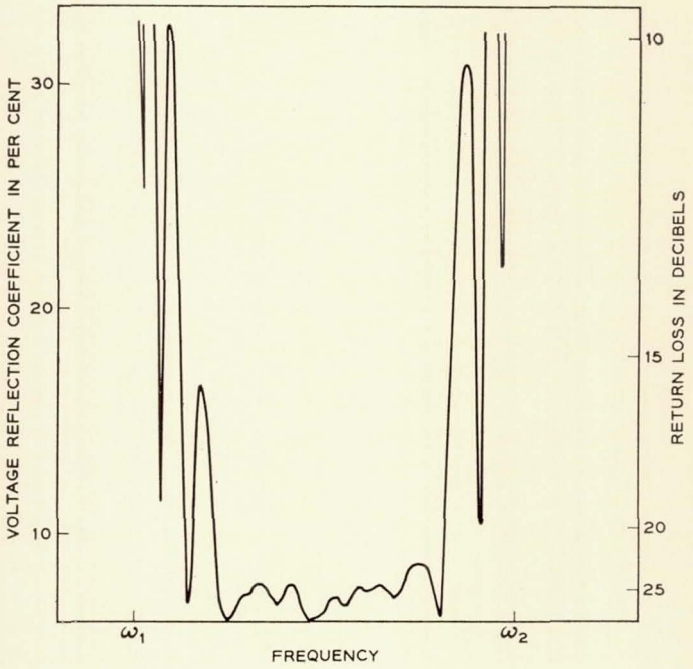


Fig. 15 — Reflection coefficient vs frequency looking into a single section of the slow-wave circuit.

ability that the tube will oscillate if the corresponding wave phase velocities lie close to the electron beam velocity. The intersection of the line, in Fig. 11, labeled "operating voltage" with any of the $\omega$-$\beta$ plots indicates a synchronism of the wave velocity, for the corresponding mode, with the beam velocity. The slope of the "operating voltage" line is proportional to the electron velocity. Thus, it may be seen that as the beam voltage is raised from 0 to the operating value, synchronism at a cutoff frequency can occur for many modes. The magnitude of the interaction impedance for these modes will determine whether oscillation can occur, and at the cutoff frequency this magnitude may be very large. Oscillations have definitely been identified at 7.1 gc, 12.7 gc and 17.1 gc and at voltages as low as 4 kv and as high as 18 kv. Several techniques have been used to inhibit and avoid the oscillations.

For normal operation, the beam is intended to interact with the first forward wave harmonic of the lowest-order mode. As the beam voltage is raised toward the operating value, the tube will break into a very

strong oscillation at the upper cutoff frequency of 7.1 gc. If one attempts to raise the voltage through the oscillation range with full beam power available, the tube will gas up; arcing will occur; and the beam supply will shut off. Since the Philips cathode can be run at full voltage under temperature-limited conditions, the following turn-up method was used. The cathode temperature is lowered until it is capable of emitting only 15 per cent of full current. The strength of the oscillation under these conditions will be greatly reduced. The beam voltage may now be turned up through the oscillating range to the operating point. Finally, the cathode temperature is returned to its normal value, resulting in full beam power at the operating point. After the tube is sufficiently aged in, the full beam power of 17.7 kilowatts can be applied abruptly by means of a vacuum relay connecting the tube to the power supply.

The original version of the slow-wave circuit had a kidney-shaped cavity coupling slot (cavity A in Fig. 11). The operating voltage line cut the phase-frequency curve for the first higher-order mode (slot-mode) at a high impedance point near the upper cutoff. Oscillation occurred at 12.7 gc. Fig. 11 shows that by capacity-loading the slot to produce the dumbbell shape (cavity B), the mode is lowered in frequency without affecting the operating mode. The impedance of the slot-mode decreases toward the low-frequency end of its passband. Therefore, the elimination of the slot-mode oscillation was accomplished by lowering its frequency until the operating voltage line intersected the phase-frequency curve for the slot-mode at a low impedance point.

A better understanding of the nature of the slot-mode can be obtained from the following analysis. It is assumed that the effects of the ferrule are merely to lower the various passband frequencies since it is placed in a region of large electric fields. This should not affect the slot-mode too greatly. A further assumption is that there is no reaction between slots, which will be nearly true if there is a 180-degree rotation from slot to slot. One may consider the coupled-cavity circuit as a $TM_{01}$ circular waveguide of characteristic impedance $Z_{01}$ and propagation constant $\beta_{01}$ shunted by a normalized reactance $jx$ corresponding to the circular end walls which form the cavities. If we treat a section, $l$, of this guide as a TEM transmission line, the eigenvalue equation is given by[9]

$$\cos \theta = \cos \beta_{01} l + \frac{1}{2x} \sin \beta_{01} l \tag{28}$$

where $\theta$ is the phase shift per section. The band edge frequencies may be solved for by setting $\theta = 0$ and $\theta = \pi$. For $\theta = 0$

$$\cot \frac{\beta_{01} l}{2} = 2x \quad \text{or} \quad \sin \frac{\beta_{01} l}{2} = 0, \qquad \text{i.e.,} \quad \beta_{01} l = 0, 2\pi, 4\pi, \cdots.$$

For $\theta = \pi$

$$\tan \frac{\beta_{01} l}{2} = -2x \quad \text{or} \quad \cos \frac{\beta_{01} l}{2} = 0, \qquad \text{i.e.,} \quad \beta_{01} l = \pi, 3\pi, \cdots.$$

If the periodic spacing, $l$, is small compared to a wavelength at the $TM_{01}$ frequency, $\beta_{01} l = \pi, 2\pi \cdots n\pi$ will occur only at much higher frequencies. Thus, at $\theta = 0$

$$\cot \frac{\beta_{01} l}{2} = 2x \quad \text{or} \quad \beta_{01} l = 0; \tag{29}$$

at $\theta = \pi$

$$-\tan \frac{\beta_{01} l}{2} = 2x \tag{30}$$

where

$$(\beta_{01})^2 = \left(\frac{\omega}{c}\right)^2 - \left(\frac{\omega_2}{c}\right)^2 \tag{31}$$

and $\omega_2$ is the cutoff frequency for the $TM_{01}$ mode.

If the form of the reactance $x$ can be determined, we can solve (29) to (31) for the band edge frequencies. For the $TM_{01}$ mode in circular guide, an inductor would appear as a circular disc with a sector removed, while a capacitor would appear as a circular disc with an annular slot. The large slots generally used might be represented by a parallel $LC$ circuit such that

$$x = \frac{\omega L}{1 - \left(\frac{\omega}{\omega_s}\right)^2} \tag{32}$$

where $\omega_s^2 = 1/LC$ the slot resonant frequency.

It is necessary to make an estimate of $L$ and $C$ and then solve (29) to (31) graphically. In the case of the M4040, the change to the dumbbell-shaped slot increased the slot capacity without changing the inductance. Thus, the main mode would not be much affected because its bandwidth is mainly determined by the slot inductance. However, $\omega_s/\omega_2$ is diminished, lowering the slot-mode passband center frequency and decreasing the ratio of upper to lower cutoff frequency in the slot-mode.

From the above discussion, one concludes that (*i*) the slot-mode is a perturbed $TM_{01}$ mode; (*ii*) because of this, rotation of the slots (avoiding slot-to-slot coupling) would not be expected to change the slot-mode passband; and (*iii*) neither the upper nor the lower cutoff frequency corresponds to the slot resonant frequency.

The operating mode, high-frequency cutoff oscillation at 7.1 gc may also be "drive-induced." That is, when the input signal power (the drive level) is sufficiently high, the electron velocity can be reduced, by conversion of kinetic to microwave energy, to the point where it is again synchronous with the phase velocity corresponding to the 7.1-gc cutoff. Since this occurs at full beam power and the oscillation is very strong, it is necessary to limit the signal input level to prevent possible tube damage.

## VII. ASPECTS OF TUBE PERFORMANCE

Figs. 16 to 22 are plots of power, gain and interception currents as functions of frequency, magnetic field, etc., for various parameter values. They were taken from the performance data of a tube presently located at the Andover station and are believed to be typical of the M4040. Although the graphs are self-explanatory, there are several points worth noting:

(*i*) The variation of small-signal gain with frequency is similar to that calculated, using the theory of Birdsall and Brewer,[10] except that

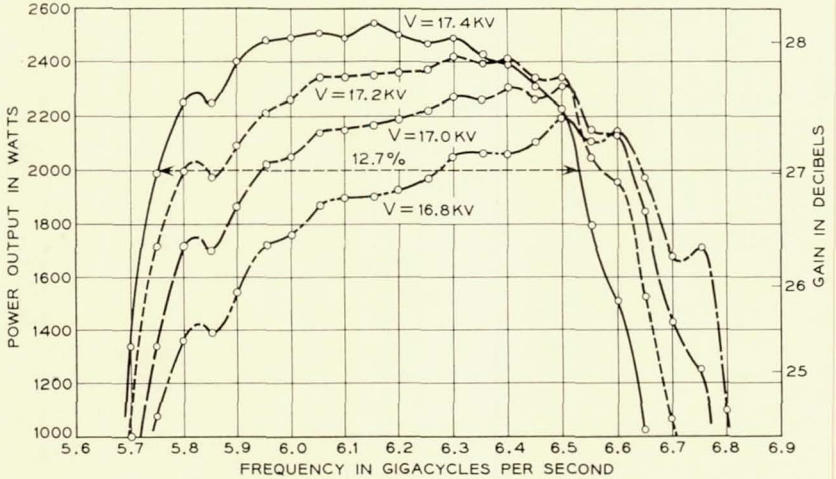


Fig. 16 — High-level output vs frequency [H = 1.2 H (Brillouin); power in = 4.2 watts; parameter is beam voltage].

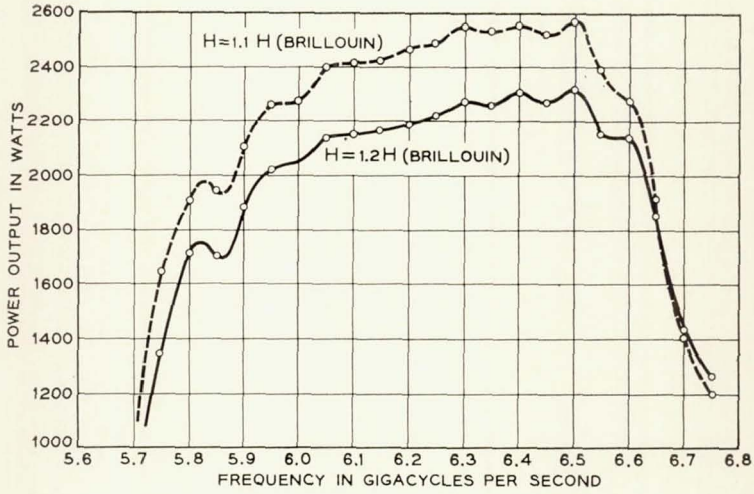


Fig. 17 — High-level output vs frequency [V = 17.0 kv; power in = 4.2 watts; parameter is magnetic field].

the tube requires slightly higher voltages than those calculated. The tube must operate at a voltage of 17.4 kv to achieve a gain-frequency curve similar to that calculated for 16.8 kv. (This latter voltage includes the relativistic correction.) The high-level output observed matches that calculated near the center frequency but is in disagreement at the low-

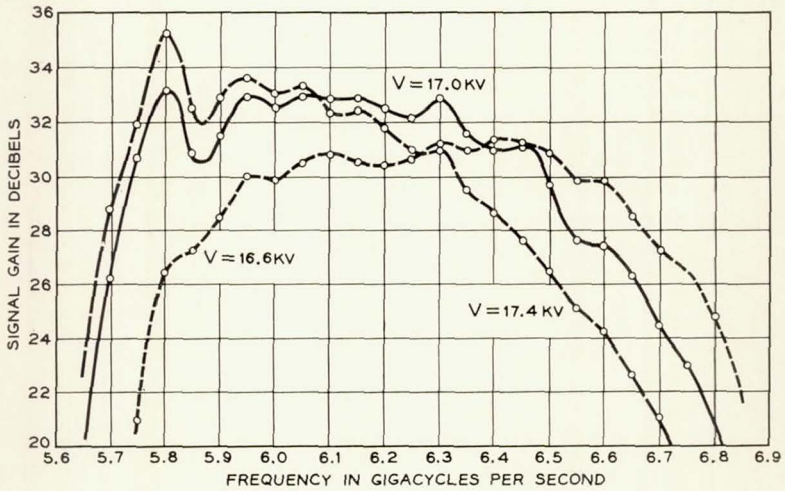


Fig. 18 — Small-signal gain vs frequency [H = 1.2 H (Brillouin); parameter is beam voltage].

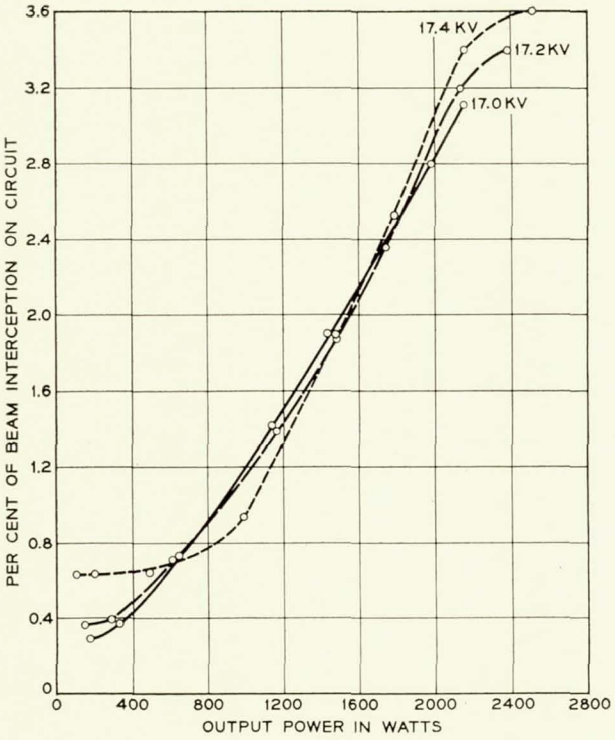


Fig. 19 — Beam interception vs output power [H = 1.2 H (Brillouin); parameter is beam voltage].

frequency end of the band. It is likely that a combination of higher applied voltage and higher input signal power might reproduce the curve shape of sharply rising power with decreasing frequency calculated for 16.8 kv. Here, the experimental data of C. C. Cutler[11] were combined with the small-signal calculations of Birdsall and Brewer to predict output power as a function of frequency.

(*ii*) The M4040 is operated with a focus field value fairly close to the Brillouin magnetic field value. To correlate the several parameters used as a measure of magnetic field, we note that

$$H \text{ (Brillouin)} \approx 600 \text{ oersted}$$

$$H = 1.1\,H \text{ (Brillouin)} \approx 660 \text{ oersted} \approx I_{\text{mag}} = 21 \text{ amps}$$

$$H = 1.2\,H \text{ (Brillouin)} \approx 720 \text{ oersted} \approx I_{\text{mag}} = 23 \text{ amps.}$$

(*iii*) The gross "wiggles" in the small-signal gain and high-level out-

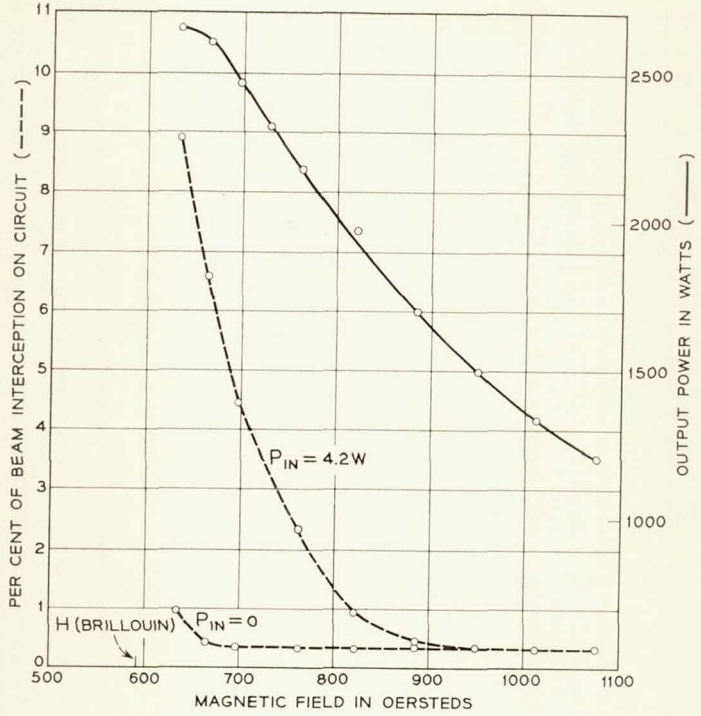


Fig. 20 — Output power and beam interception as a function of magnetic field [V = 17.0 kv; f = 6.4 gc].

put power versus frequency plots can be correlated with variations in the cold input and output matches.

(*iv*) The best explanation, at present, for the increase in gain with collector depression is that the resulting ion drainage from the beam allows the latter to expand. The increase in gain is about 1 db for a 300-volt depression. Not much is gained by going to higher potentials. Three hundred volts is about the magnitude of the potential of the beam center relative to the enclosing walls.

Particularly in the tubes produced early in the development period, positive ion effects were noticed. They can neutralize the beam and therefore change its diameter and, with it, the gain. Relaxation effects, much as described by Sutherland,[12] with frequencies dependent on nearly every adjustable parameter were observed. Improved vacuum processing has brought the magnitude of the effects to the point where they are of no concern. Ion effects were observed at an early stage in the electron gun region. It was necessary to maintain the accelerating

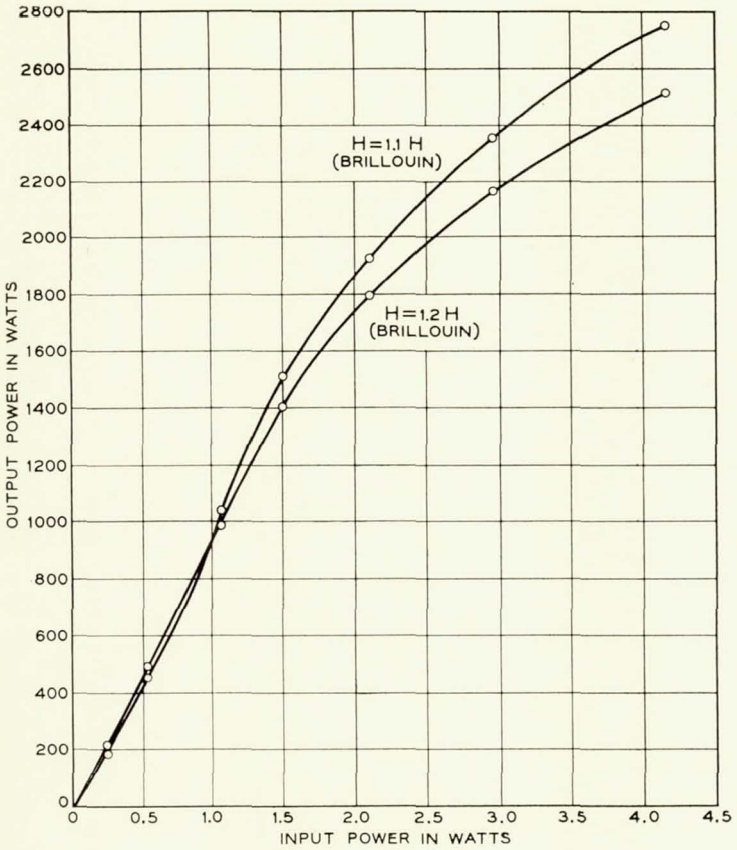


Fig. 21 — Output power vs input power for two values of magnetic field [$V_k$ = 17.4 kv; f = 6.4 gc; parameter is magnetic field].

electrode positive relative to the slow-wave circuit by about 600 volts. If this voltage is allowed to drop below +450 volts, a poisoning of the cathode takes place, presumably due to ion bombardment.

To convince ourselves that the M4040 would indeed serve as a communications device and do its job in the Telstar system, we set up closed-circuit television apparatus to observe and compare a TV picture first transmitted through a straight waveguide and then transmitted through the M4040 substituted for the waveguide. No observable deterioration of the transmitted picture occurred with the M4040 included. The M4040 was operated over a 30-db range of signal power in these experiments. We also measured the second harmonic output power as

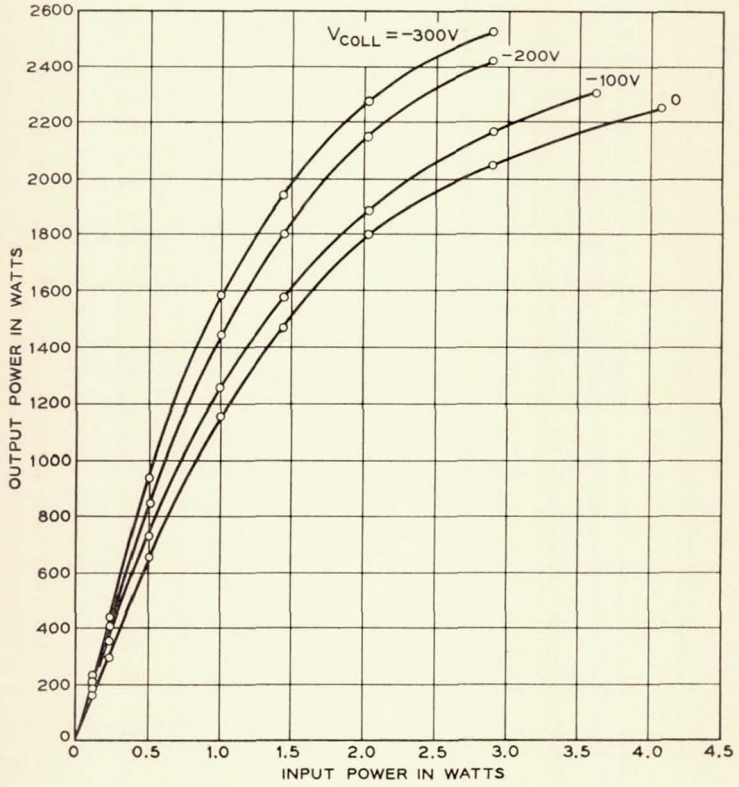


Fig. 22 — Output power vs input power [$V_k$ = 17.0 kv; H = 1.2 H (Brillouin); f = 6.4 gc; parameter is collector depression].

30 db below the output signal level at full output level. With zero applied signal, the noise output is 2 milliwatts as detected through a low-pass filter cutting off at 7.2 gc. Over the narrow, 30-mc bandwidth of the Telstar system, this noise output is 0.4 milliwatt.

## VIII. CONCLUDING REMARKS

The M4040 CW traveling-wave tube is capable of operation over a 12.7 per cent bandwidth centered at 6.15 gc with output power exceeding 2000 watts and a gain exceeding 27 db. In the Telstar experiment, the tube has performed satisfactorily as a television transmitter over a 30-db range of input signal power. At the time of writing, both the ground station at Andover, Maine, and the one at Pleumeur Bodou, France, are still using as the power amplifier the original M4040 tubes employed

during the first Telstar broadcasts. The tube at Andover has been operated for approximately 1500 high-power hours.

Recently, several experiments have indicated that much improved performance can be expected from the M4040. Two more cavities have been added to the output section of the tube, increasing the gain. At the midband frequency of 6.15 gc, the small-signal gain becomes 35 db and the gain, at the maximum output power of 2700 watts, is 30 db. Further experiments demonstrated that the water cooling rate could be drastically reduced and that ion drainage could be achieved by applying a negative voltage to a pair of electrodes concentric with the beam. The M4040 has been operated without the aid of appendage pumps after an age-in period of some 50 hours. Finally, and perhaps most significantly, the collector potential has been depressed 9 kv below the potential of the slow-wave circuit.[13] The resulting over-all tube efficiency becomes greater than 30 per cent, and a relatively unregulated power supply can be used to provide the beam power. The latter benefit is obtained because of the insensitivity of tube performance to collector voltages depressed beyond 400 volts. If one depresses the collector potential below 9 kv, undesirable effects of electrons returning to the gun region from the collector can be observed.

## IX. ACKNOWLEDGMENTS

The development of the M4040 is the result of the cooperative efforts of a great many people in the engineering, assembly, and fabrication areas. The authors thank Messrs. J. W. Gewartowski, H. N. Carlson, and F. R. Ashley for allowing the inclusion of information developed during the course of their work on the M4040 traveling-wave tube.

## REFERENCES

1. Pierce, J. R., *Theory and Design of Electron Beams*, Van Nostrand, New York, 1954, Chap. 10.
2. Danielson, W. E., Rosenfeld, J. L., and Saloom, J. A., Analysis of Beam Formation with Electron Guns of the Pierce Type, B.S.T.J., **35**, March, 1956, pp. 375–420.
3. Herrmann, G., Transverse Scaling of Electron Beams, J. Appl. Phys., **28**, April, 1957, pp. 474–478.
4. Spangenberg, K. R., Field, L. M., and Helm, R., *Production and Control of Electron Beams*, Federal Telephone and Radio Corp., New York, 1942.
5. Jahnke, E., and Emde, F., *Tables of Functions*, Dover Publications, New York, 1945, p. 32.
6. Ramo, S., and Whinnery, J. R., *Fields and Waves in Modern Radio*, John Wiley and Sons, First Edition, New York, 1944, pp. 406–408.
7. Ibid., p. 376.
8. Pierce, J. R., *Traveling-Wave Tubes*, D. Van Nostrand, New York, 1950, p. 68.

9. Collin, R. E., *Field Theory of Guided Waves*, McGraw-Hill Book Co., New York, 1960, p. 385.
10. Birdsall, C. K., and Brewer, G. R., Hughes Technical Memo, No. 396, June, 1955.
11. Cutler, C. C., The nature of Power Saturation in Traveling-Wave Tubes, B.S.T.J., **35**, July, 1956, pp. 841–876.
12. Sutherland, A. D., Relaxation Instabilities in High Perveance Electron Beams, I.R.E. Trans. on Electron Devices, ED-7, October, 1960, p. 268–273.
13. Melroy, D. O., private communication.

# Masers for the *Telstar* Satellite Communications Experiment

By W. J. TABOR and J. T. SIBILIA

(Manuscript received January 28, 1963)

*This paper discusses the design and characteristics of ruby traveling-wave masers operating at 4 gc. These masers, characterized by an average gain of ≈35 db over a bandwidth of 25 mc, are equipped with waveguide input transmission lines, rather than the previously employed coaxial cables. This change results in an over-all noise temperature of 3.5°K for these devices, rather than the 10°K exhibited by earlier masers. The maser noise temperature now closely approximates sky temperatures, which set the ultimate limit on earthbound receiver sensitivity. The improvements to be had by further reduction in amplifier noise are therefore almost negligible. A less well known maser property, i.e., its freedom from distortion, even when driven well into gain saturation, is discussed.*

## I. INTRODUCTION

In an active satellite communication system, the ultimate in ground station receiver performance is highly desirable, if not absolutely necessary. This follows directly from the limitations imposed by present rocketry on the payload, and thereby on the transmitter power, which can be placed in orbit. A major improvement in over-all system signal-to-noise ratio can be achieved much more easily and economically on the ground than in the satellite. Recognition of this fact led to the adoption of a giant horn-reflector antenna, and the selection of a ruby traveling-wave maser as a preamplifier in order to fully exploit this antenna's remarkable low-noise performance. The design considerations and performance of this maser are the subjects of this paper.

## II. DESIGN OBJECTIVES AND THEIR SIGNIFICANCE

At the outset of the maser development program the following objectives and constraints were established:

(a) a minimum stable gain of 25 db

(b) an instantaneous bandwidth of 25 mc centered at 4170 mc

(c) lowest possible noise temperature

(d) an input impedance match better than or equal to 1.5:1 VSWR, and

(e) bath temperature of 4.2°K.

A minimum gain of 25 db is needed to render negligible the noise contribution of subsequent receiver stages. In the early receiver concept, the maser was to be followed by a low-noise traveling-wave tube. A typical value for the noise temperature of such a tube is 600°K. A maser with 25 db of gain would reduce the TWT noise contribution to the over-all system noise temperature to 1.9°K, a value which is small when compared to the initially projected total receiver noise temperature of approximately 50°K. Additional gain would reduce this even further, a point which will be pursued in a later paragraph.

The 25-mc instantaneous bandwidth requirement follows directly from consideration of the information transmission rate and wide index FM mode of transmission.

The demand for the lowest possible maser noise temperature is self-evident.

A good input impedance match is necessary in order to minimize delay distortion: i.e., the generation of weak reflected signals delayed in time with respect to the original. This could cause "ghosts" in TV transmission. In the Telstar system such distortion could arise through the following mechanism. A mismatch in the antenna-maser complex would reflect part of the incident signal, which would then be re-radiated. The radome, not being perfectly transparent, would in turn reflect a portion of this energy back to the receiver. Consideration of the path lengths and reflection coefficients in the entire system, together with the tolerable limits on delay distortion, led to the stipulation of maser input matching to a VSWR better than 1.5:1.

Operation at 4.2°K, rather than at some lower temperature where the gain and bandwidth requirements could be more easily satisfied, was dictated by the fact that this maser was intended to operate continuously over periods of several months. At 4.2°K, liquid helium is in equilibrium with its vapor at atmospheric pressure. If lower temperatures were required, the dewar would have to be maintained under a partial vacuum. This would mean periodic interruptions of service, since the dewar is opened to the atmosphere during each liquid helium transfer. Approximately two hours are needed to re-evacuate the dewar, thus lowering the temperature and restoring gain. For this reason, operation at 4.2°K was selected, and the attainment of the required gain-bandwidth product sought by means other than reduced temperature.

## III. MASER DESIGN

### 3.1 *General Considerations*

The points of departure in maser design are the gain equation[1]

$$G = 27.3\ (-\chi'')(FfL/v_g) \tag{1}$$

where

$G$ = electronic gain in db
$\chi''$ = imaginary part of the ruby paramagnetic susceptibility
$F$ = filling factor
$f$ = frequency
$L$ = maser physical length
$v_g$ = group velocity of signal

and the gain-bandwidth relationship for the traveling-wave maser

$$B = \sqrt{\frac{3}{G-3}}\, B_m \tag{2}$$

where $B$ is the 3-db bandwidth of the amplifier and $B_m$ is the material linewidth (assuming a Lorentzian shape).

If slowing, $S$, is defined as $S = (c/v_g)$, where $c$ is the free-space velocity of light, (1) can be rewritten in a form more easily interpreted for practical design

$$G = 27.3(-\chi''F)\frac{1}{\lambda_0} SL, \tag{3}$$

where $\lambda_0$ = free-space signal wavelength. In this form, it is evident that increased gain can be achieved equally well by increasing either the slowing or the physical length of the maser. Since the maser requires a highly homogeneous transverse magnetic field, a very large magnet cross section is required. Therefore, a heavy penalty in weight is paid for gain achieved through increased maser length. This consideration led to the choice of a 5-inch maser length. The gain requirement has to be satisfied by maximizing the parameters $\chi''$, $F$, and $S$. $\chi''$ is a property of the active material and $S$ is controlled by slow-wave structure design. $F$ is partially determined by both.

The gain-bandwidth expression (2) in the case of a ruby (linewidth 60 mc) maser immediately leads to the conclusion that even for the minimum gain of 25 db, the obtainable bandwidth will be inadequate [taking an electronic gain of 30 db in order to allow for losses, the bandwidth would from (2) be 20 mc]. For this reason, the need for broad-

banding techniques, to be discussed in later paragraphs, was evident in the earliest stages of design.

### 3.2 *Ruby*

Amplification in a maser is the result of the interaction of a microwave signal with a paramagnetic crystal in which a negative susceptibility, $\chi''$, has been established through the inversion of the spin populations of two energy levels. In ruby at 4 gc, $\chi''$ is maximized when the $C$ axis of the crystal is aligned perpendicular to the applied dc magnetic field ($\theta = 90°$). The signal transition occurs between the lowest two energy levels $(-\frac{3}{2}, -\frac{1}{2})$, and pump power is applied between the outermost levels $(-\frac{3}{2}, +\frac{3}{2})$.[2]

The susceptibility of a ruby crystal in thermal equilibrium can be calculated as outlined in the Appendix. However, what is needed in order to evaluate the gain obtainable with a particular maser design is the "inverted" susceptibility: i.e., the susceptibility when the population distribution of spins between two energy levels has been inverted through the application of microwave pump power. No reliable method exists for calculating this susceptibility. An experiment, together with the calculated equilibrium susceptibility, will provide the required information. One can measure the ratio of the microwave gain obtained from a ruby crystal when pump power is applied to the microwave absorption when the crystal is in thermal equilibrium. This ratio is just that of the magnitudes of the inverted to equilibrium susceptibilities. Therefore, one obtains the inverted susceptibility by simply multiplying the calculated equilibrium value by this empirically determined number.

The magnitude of the inverted $\chi''$ is strongly dependent upon the concentration of chromium in the ruby. At low concentrations, where there is essentially no interaction between neighboring $Cr^{+++}$ ions, the inverted susceptibility is directly proportional to the concentration. As the concentration is increased, the $Cr^{+++}$ ions interact more strongly with one another because of their greater proximity, and this interaction (cross-relaxation) renders pumping less efficient, reducing the inversion ratio and, thereby, the available gain. Typical behavior of the inverted susceptibility as a function of chromium concentration (measured at 5.6 gc and 4.2°K) is presented in Fig. 1. The concentration at which $\chi''$ is a maximum occurs in the range 0.03–0.04 atomic per cent. Operating at a temperature of 4.2°K, the optimum inversion ratio obtainable at 4 gc has been found to be approximately 5.0. The corresponding calculated values for the inverted susceptibilities are

$$\chi_{xx}'' = -0.028,$$

$$\chi_{yy}'' = -0.0054,$$

and

$$\chi_{xy}'' = i\,0.012,$$

where the $Z$ direction is taken parallel to the dc magnetic field and the $X$ axis parallel to the $C$ axis of the ruby.

Since the paramagnetic susceptibility is a tensor, the interaction of a microwave signal with the ruby is highly dependent upon the spatial coincidence of the crystal and RF fields of the proper polarization. This leads to the inclusion of the filling factor $F$ in the gain equation. The term $\chi''F$ when expanded is

$$\chi''F = \frac{\int_m [\chi_{xx}''\,|\,H_x\,|^2 + \chi_{yy}''\,|\,H_y\,|^2 - \chi_{xy}''(H_xH_y^* - H_x^*H_y)]\,dv}{\int_s [|\,H_x\,|^2 + |\,H_y\,|^2]\,dv} \tag{4}$$

where

$$H_x = h_x' + ih_x''$$

$$H_y = h_y' + ih_y''$$

and where $h_{x,y}'$ is the amplitude of the RF magnetic field along the $x,y$ axis of the ruby (see Fig. 2) and $ih_{x,y}''$ is the amplitude of the RF magnetic field that is 90° out of phase with $h_{x,y}'$. The subscript $m$ on the in-

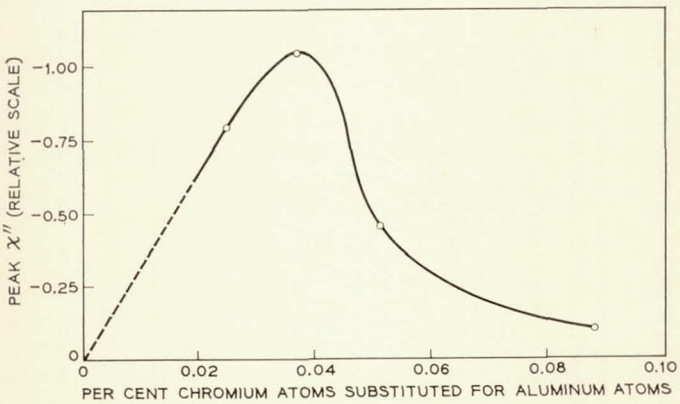


Fig. 1 — Inverted susceptibility vs concentration for ruby at 5.6 gc and 4.2°K.

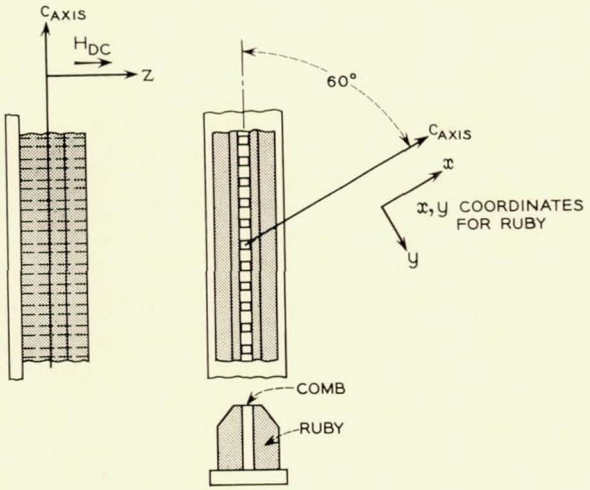


Fig. 2 — Orientation and coordinates for the ruby and comb structure.

tegral in the numerator means that the integral should be taken only over the volume occupied by the maser material, and the subscript $s$ implies that the integral in the denominator should be taken over the entire volume of the structure. The term $|H_z|^2$ does not appear, since the fingers of the comb are resonating in a TEM mode and the $Z$ direction is taken parallel to the fingers.

It is not possible to calculate the term $\chi''F$ with accuracy, since the configuration of the fields in the comb structure is only approximately known. An estimate can be made at the low-frequency edge of the traveling-wave structure passband where the RF magnetic field is approximately linearly polarized and parallel to the comb axis. At this frequency, $H_x = H \cos 60°$ and $H_y = H \sin 60°$ and, therefore, $\chi''F = -0.011$. This value for $\chi''F$, together with the 5-inch maser length, allows the evaluation of slowing required to achieve a given gain at 4 gc. Equation (1), with the insertion of the parameters

$$L = 5 \text{ inches}, \qquad f = 4 \text{ gc}, \qquad \chi''F = -0.011,$$

reduces to

$$G_{db} \approx 0.50\ S \text{ (from theory)}. \tag{5}$$

This calculated result led to the conclusion that it would not be difficult to design a maser with 40 db of net gain, since previous experience indicated that structures with slowings of 100 and losses of the order 10 db could be constructed.

It is possible to evaluate $\chi''F$ experimentally by building a trial structure of known slowing and measuring its electronic gain. This was done and a value of $\chi''F$, obtained from the gain equation (1), found to be $-0.0076$, i.e., 70 per cent of the theoretically derived value. This agreement, in view of the approximate knowledge of the RF fields in the comb structure, is surprisingly good. Equation (5) for a practical design should therefore read

$$G_{db} \approx 0.35\ S \text{ (experimental)}. \tag{6}$$

The ruby used in these masers was purchased from the Linde Company in the form of standard 60° boules; i.e., the angle between the $C$ axis and the rod axis was approximately 60°. The boules were selected for a chromium concentration of $\approx$0.035 atomic per cent by comparing the paramagnetic absorption of small samples cut from each boule with standard samples.

### 3.3 *Structure*

It is evident from (6) that a high slowing is required in order to provide adequate gain. A comb type structure, consisting of sixty-two 0.040-inch square fingers spaced 0.080 inch on centers, loaded on both sides with ruby, was employed (see Fig. 3). The transmission characteristics of such a comb not only are determined by the geometry of the metallic structure, but are strongly dependent upon the dielectric loading pro-

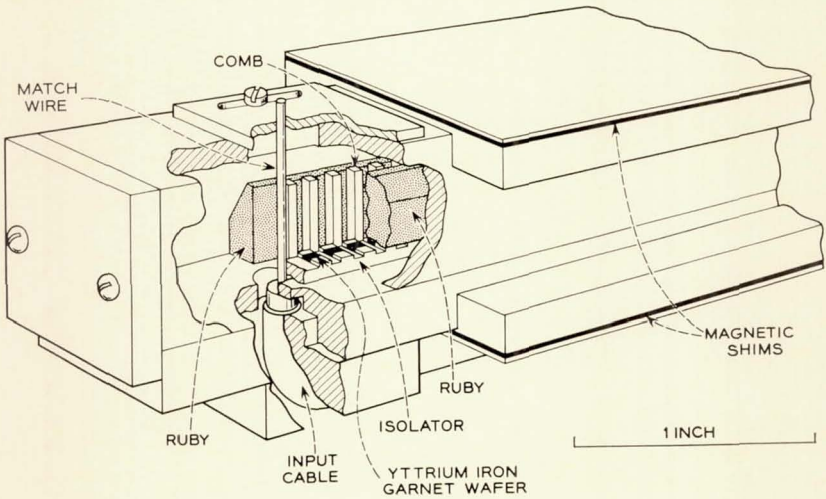


Fig. 3 — Cutaway view of structure.

vided by the ruby. Such a structure can be characterized by an $\omega$-$\beta$ response: i.e., the phase shift introduced per unit length ($\beta$) as a function of frequency ($\omega$). The slowing is given by $c(d\beta/d\omega)$.

It is of advantage to use as much ruby as possible in such a structure, since by heavily loading with dielectric the structure size required for operation at a given frequency is reduced, thereby minimizing magnet weight. Further, the filling factor $F$ is maximized.

When the cross section of the ruby loading is rectangular, the upper and lower cutoff frequencies of the loaded comb can be calculated. A variety of rectangular loadings was studied (see structures 1 and 2 of Fig. 4 and their $\omega$-$\beta$ diagrams), but it was found impossible to obtain sufficient slowing without the onset of "fold-over." "Fold-over" is the term applied to the occurrence of a double-valued $\omega$-$\beta$ diagram (curve 2 of Fig. 4). This phenomenon arises when the effective dielectric loading of the fingers of the comb is not a monotonic function of frequency. Knowledge of the field configuration within the structure is required

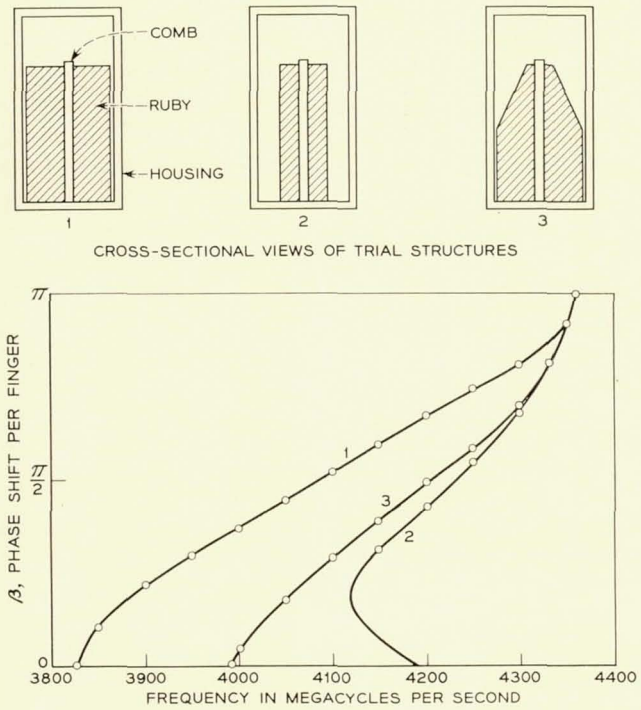


Fig. 4 — Bandpass characteristics for different types of dielectric loading.

for an understanding of this effect. At the lower cutoff frequency, the phase shift per unit length is zero, which implies that the electric field lines extend largely from the fingers to the side walls, as illustrated in Fig. 5. The effective loading is then a highly sensitive function of the gap between the ruby and wall. At the upper cutoff, there is a $\pi$ phase shift per finger and the fields are concentrated in a region very near the fingers. The loading is then nearly independent of the ruby-to-wall gap. This can be summarized by the statement that the ruby-to-wall gap has a decreasing effect on the effective dielectric loading, and therefore the

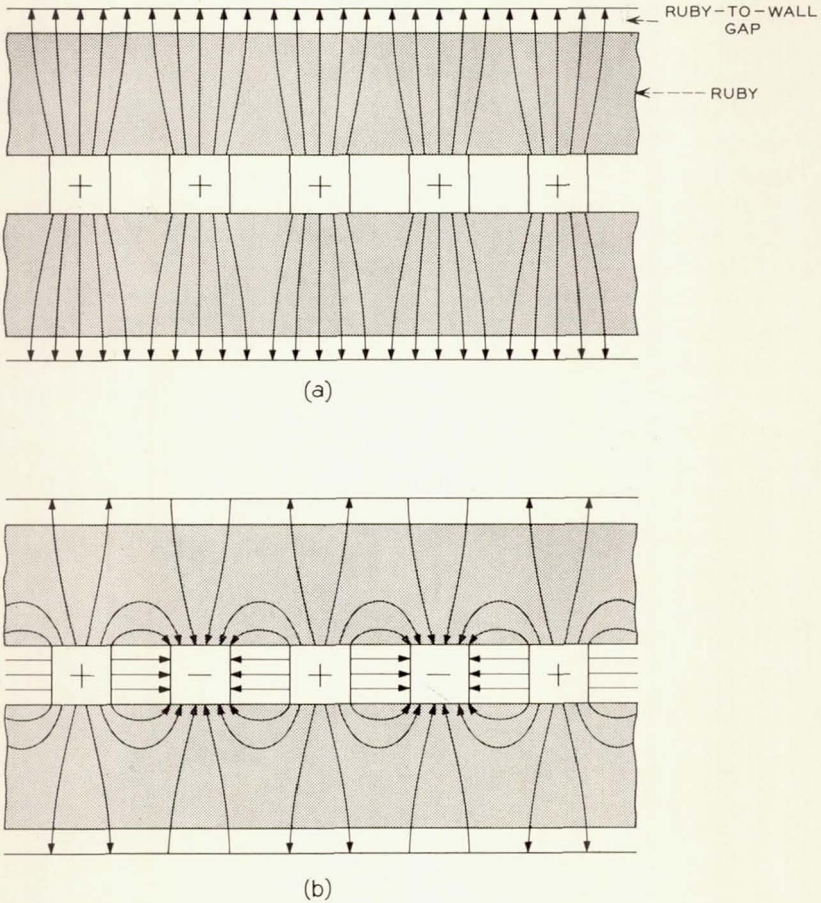


Fig. 5 — Field configuration in the comb structure: (a) zero phase shift condition at lower cutoff frequency; (b) $\pi$ phase shift condition at upper cutoff frequency.

phase shift, as one traverses the passband from lower to upper cutoff. Increased slowing is achieved in a given structure by increasing the ruby-to-wall gap, thereby raising the lower cutoff frequency. If this process is carried too far, it is possible to reduce the effective loading at the lower cutoff to a value less than that present at a higher frequency. This results in the double-valued $\omega$-$\beta$ response. Maser operation under this condition is highly undesirable.[3] A "backward," as well as "forward" wave is supported. The sense of polarization associated with the "backward" wave is the reverse of that of the "forward" wave, and therefore the isolator (to be discussed) is rendered inoperative, leading to regeneration or oscillation. Therefore, other ruby geometries were tried in an attempt to account for the changing field configuration as a function of frequency and thereby obtain an effective loading which is monotonic. The cross section illustrated as structure 3 in Fig. 4 was selected as best. This gave the largest slowing ($S = 130$), with a single-valued $\omega$-$\beta$ characteristic. The slowing as a function of frequency is presented in Fig. 6.

With ruby symmetrically loaded on both sides of the comb as shown in Fig. 4, the maser will exhibit gain in either direction. Therefore, in order to prevent regeneration or oscillation, which would result from reflections due either to structure defects or imperfect input or output matches, an isolator must be incorporated within the structure. The amount of isolation provided should be sufficient for unconditional stability, so that the gain of the maser is not a function of the externally presented terminal impedances. The criterion for unconditional stability of a maser is that the round trip (input to output, back to input) loss must exceed the corresponding gain; i.e.

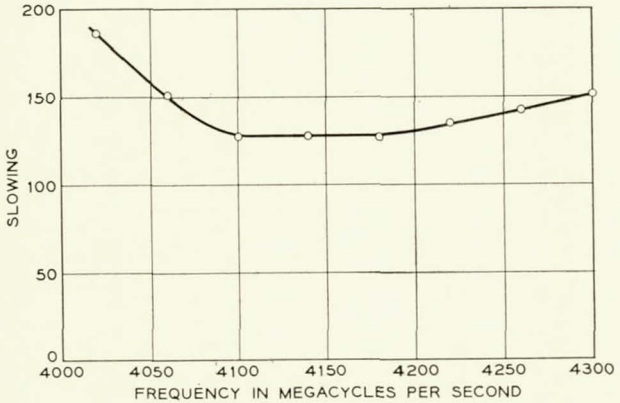


Fig. 6 — Slowing vs frequency for the masers at 4.2°K.

$$2(G_F - A_c) - A_{IF} - A_{IR} < 0 \tag{7}$$

where all quantities are expressed in db and

$G_F$ = forward electronic gain (equal to reverse gain)
$A_c$ = forward copper attenuation
$A_{IF}$ = forward isolator attenuation
$A_{IR}$ = reverse isolator attenuation.

The isolator employed is a linear array of 0.040-inch square polycrystalline yttrium iron garnet (YIG) wafers 0.004 inch thick, bonded, 0.080 inch on centers (see Fig. 3), to an alumina substrate. The aspect ratio of these wafers is so chosen that they are resonant at the signal frequency in the dc magnetic field required by the ruby. This array is placed on one side at the base of the comb and positioned to occupy that region of RF field most nearly circularly polarized (this optimizes the ratio of reverse to forward insertion loss). Typical performance of this iterated isolator is: reverse attenuation > 120 db; forward insertion loss approximately 4 db, at center band. The isolator forward loss rapidly rises on either side, since the slowing increases, thereby strengthening the interaction; and further, the circularity of the RF field polarization deteriorates. This behavior, as well as that of the copper losses, is illustrated in Fig. 7. With a slowing factor of 130, these masers should exhibit electronic gains of the order of 50 db and copper losses of approximately 2–4 db. Substitution of these numbers into (7) shows that the maser short-cir-

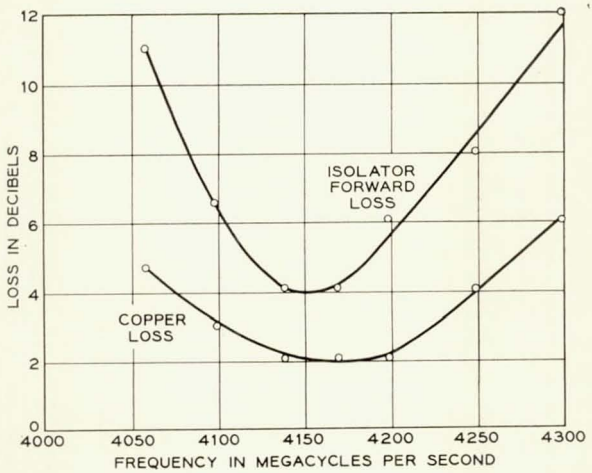


Fig. 7 — Typical losses for the structure at 4.2°K.

cuit stability margin should be greater than 30 db. In practice this is very desirable since it insures a smooth variation of the gain-frequency characteristic even in the presence of structural imperfections.

## IV. MASER CHARACTERISTICS

### 4.1 *General*

In a uniform magnetic field the masers had net gains equal to or in excess of 42 db (corresponding to electronic gains $\geqq$ 47 db) and instantaneous 3-db bandwidths of approximately 16 mc centered at 4170 mc. These measured gains and bandwidths are in close agreement with those predicted by (5) and the bandwidth relationship. Since this was more gain and less bandwidth than required, it was necessary to correct this situation. Two distinct approaches were taken. The first of these was to exchange, within the maser, the excess center frequency gain for increased bandwidth by shaping the magnetic field along the length of the ruby, thereby broadening its effective linewidth. The second approach toward increasing the bandwidth was to consider the entire receiver as a whole, and to introduce equalization in the postamplifier. This latter course, which at first glance appears inefficient, actually leads to a larger effective gain-bandwidth product than broadening the ruby linewidth. This is illustrated in Fig. 8, which shows the ideal trade of center-frequency gain for effective bandwidth obtainable through the application of each technique. Both approaches were carried through experimentally, and will now be presented separately in the two following sections.

### 4.2 *Broad-Banding by Magnetic Field Shaping*

Since the resonant frequency of ruby is dependent upon the intensity of the dc magnetic field in which the crystal is immersed, its effective linewidth can be increased by making the field inhomogeneous over its volume. This was considered by Ostermayer[4] for several different variations of field along the maser length, and his results show that for a 25-mc bandwidth, the optimum exchange of gain for bandwidth is achieved if the magnetic field is made uniform for one-half the ruby length, and also uniform but of a different intensity over the remainder. A maser immersed in such a field is equivalent to two half-length masers in series tuned to different frequencies. It follows that for most effective inversion, two pump frequencies are required.

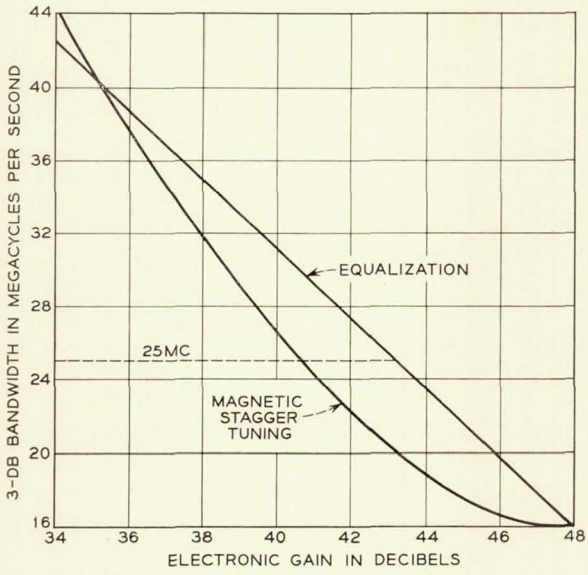


Fig. 8 — Trade of gain for bandwidth for a single-step stagger-tuned maser and for an equalized maser.

In practice it is not possible to achieve an abrupt step in magnetic field; there will be a finite transition region. In order to minimize this, the step in field was produced by inserting magnetic shims as close to the maser as possible, rather than by shaping the magnet pole pieces outside the dewar. The configuration of the shims used is illustrated in Fig. 3.

Using magnetic shims, the bandwidth was increased to 26 mc and the electronic gain reduced to 34 db, corresponding to a net gain of 28 db. Reference to Fig. 8 reveals that this loss in gain is 6 db greater than predicted by theory. There are two possible causes for this: first, a single-frequency pump was used; and second, the lateral homogeneity of the field may have been degraded by the shims, the width of which was severely limited by the dewar dimensions.

Fig. 9 is a plot of the electronic and net gain versus frequency over the tunable range of this maser. The electronic gain is nearly proportional to the slowing of the structure (Fig. 5); the small deviation (within 10 per cent) probably reflects slight changes with frequency of the filling factor. Fig. 10 is an oscillogram of instantaneous gain versus frequency. This maser was successfully employed at Holmdel, New Jersey, during the Telstar experiments.

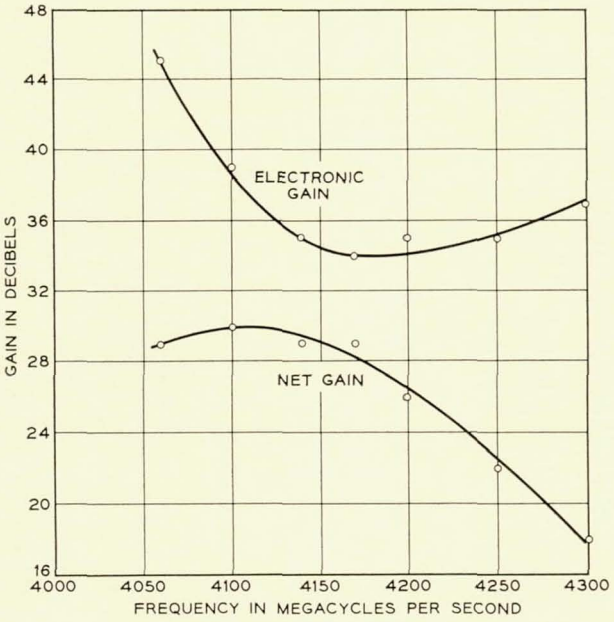


Fig. 9 — Gain of the stagger-tuned maser at 4.2°K.

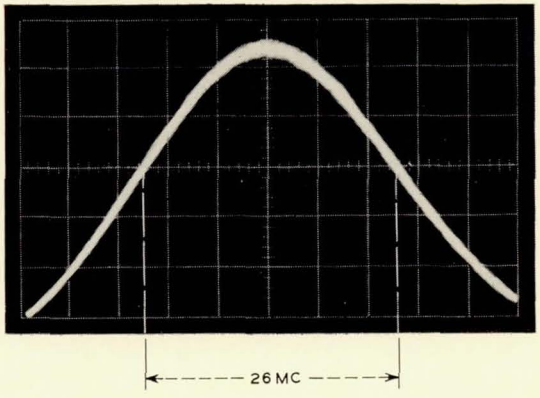


Fig. 10 — Oscillogram of instantaneous gain vs frequency for the stagger-tuned maser; the horizontal center line represents the 3-db point.

4.3 *Broad-Banding by Equalization of Amplifier following Maser*

In this approach, the maser is not modified, but rather the response of subsequent receiver stages is so equalized that the resultant over-all response has the required 25-mc bandwidth.

The gain-bandwidth relationship for equalization is simply generated by taking the electronic (not net) gain versus frequency characteristic of the maser, and finding the gain available at the appropriate deviation from center frequency as shown in Fig. 11. The shaded area then represents the excess gain to be absorbed by an equalizer. From Fig. 8, it is clear that the use of this technique would provide 2.5 db additional gain for a bandwidth of 25 mc beyond that ideally available by magnetic field shaping. Indeed, equalization is the more efficient method of increasing bandwidth up to approximately 40 mc. Magnetic field shaping should be employed for larger bandwidths. (The exact crossover is dependent upon both the detailed ruby line shape and the initial electronic gain.)

The theoretically ideal point for the insertion of an equalizer would be between the antenna and the maser input, for then the maser output would be flat over the band. Such an equalizer would have to be purely

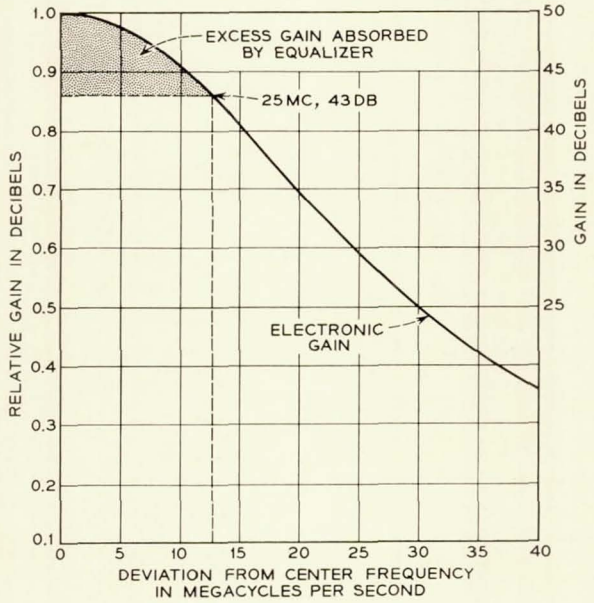


Fig. 11 — Determination of effective gain available with equalization.

reactive in nature in order not to seriously degrade the system noise temperature. The center band signal would have to be attenuated by approximately 7.5 db and this, if done resistively, would result in a noise temperature approaching 1500°K, which is clearly intolerable. A reactance in the input is, however, not acceptable in that it is incompatible with the requirement of a good input VSWR. For this reason, the equalizer was located after the maser in the receiver chain and took the form of a simple lumped RLC circuit at IF.

In going to IF equalization, one possible problem arises: maser gain saturation. The maser shows gain saturation; i.e., a monotonic decrease in gain when the signal level at its output exceeds −40 dbm. Since the center band gain of the unstaggered maser is 43 db, gain saturation will set in well below the level of the strongest signals to be encountered. This was investigated over the range of signal levels expected in the Telstar experiments (−90 to −70 dbm input). The results are presented in Fig. 12. When the input was increased from −90 to −70 dbm the gain of the maser decreased by 5 db, resulting in a signal level increase at the mixer of 15 db. This gain reduction will raise the system noise temperature somewhat, but since the gain reduction is present only when the signal level is high, the slight increase in system noise temperature is of no consequence. In this sense, the maser gain saturation does nothing more than to provide weak limiting action.

A second-order effect noted was a change in the shape of the gain-frequency characteristic arising from the fact that signals at the center frequency drive the amplifier further into saturation than do signals at the band edges. The maximum change was a 3-db reduction in center frequency gain compared to the band edge gain, as illustrated in Fig. 12. These measurements were made on a CW single-frequency basis, and could easily overemphasize, by an order of magnitude, the effect which would be found in an FM system. This effect would cause difficulty in designing a proper equalizer since exact compensation could be accomplished at only one signal level. However, it was decided that if the equalizer were so adjusted as to provide a low signal gain characteristic with a 1.5-db peak at center frequency relative to the band edge, then at high level, the response would at worst show a 1.5-db dip. This behavior would meet the normal 3-db bandwidth specification, and therefore this change in response with signal level was considered acceptable.

An additional factor to be considered when a maser is operated in the gain saturation regime is distortion. In conventional amplifiers, such as the electron tube, gain saturation and distortion are closely related, and formulae exist for the calculation of the distortion products from gain

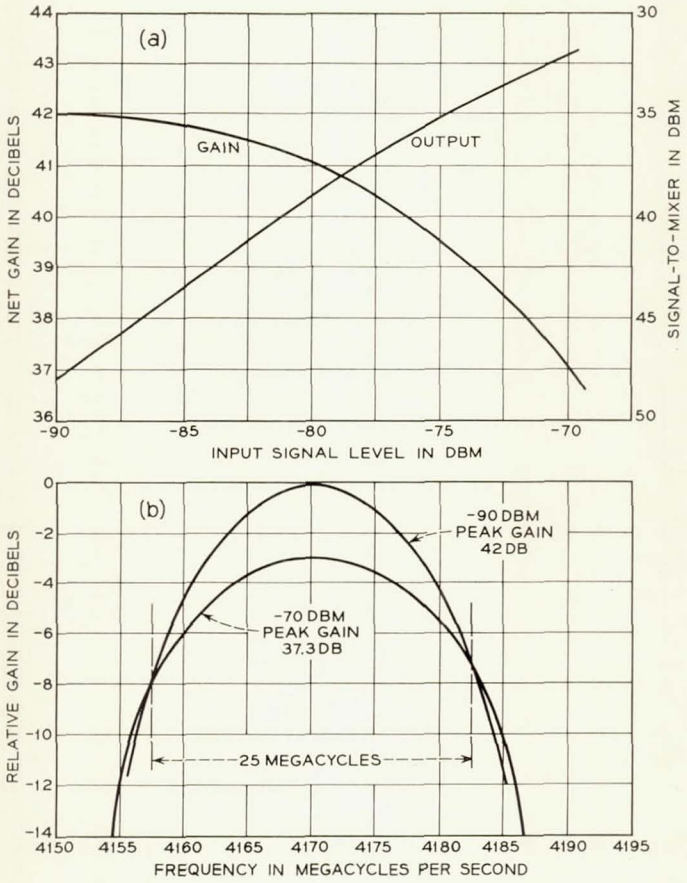


Fig. 12 — Maser signal saturation characteristics: (a) maser gain saturation; (b) maser response as a function of input level.

saturation curves. The behavior of a maser is, however, very different. This can be seen by considering the basic amplification process, stimulated emission.

The probability that photons will be added to the exciting RF field in a maser is given by the expression

$$W_{12} = K \mid \mu \mid^2 (N_2 - N_1) H_{rf}^{\ 2} \tag{8}$$

where

$K$ is a collection of physical constants,

$\mid \mu \mid^2$ is the matrix element of the transition, a measure of the

intrinsic probability of the transition occurring, which to first-order approximation, (i.e., low RF fields), is a constant.

$(N_2 - N_1)$ is the difference in the spin population of the two levels under consideration,

and

$H_{rf}^2$ is a measure of the power level of the stimulating radiation.

The population difference $(N_2 - N_1)$ is a function of the signal power level at which a maser is operated, decreasing monotonically as the level is raised. At any fixed average power level it is a constant, since a time constant which is very long compared to the period of the carrier frequency is associated with it. The value of this time constant is different for each of two cases: a sudden increase in signal level or a sudden decrease in level. A calculation based on the reduction of the energy stored in the inverted spin system shows that for a typical ruby maser the time required for the gain to reach a new equilibrium after the input signal has been raised from zero to $-70$ dbm is approximately 1 second. The time characteristic of gain recovery, when the signal level is reduced, is approximately 0.1 second, as governed by the spin lattice relaxation times. Gain changes are therefore very slow at signal levels consistent with the use of a maser as a low-noise preamplifier. The distortion arising from these gain changes is therefore no more serious than that introduced by an AGC system.

Higher-order solutions for the matrix element $|\mu|^2$ do exhibit a dependence upon $H_{rf}^2$, and therefore a source of distortion exists. A theoretical analysis and experiments[5] both show that, at signal levels normally found in a low-noise maser preamplifier, the power in distortion products lying within the significant frequency range is well below the noise generated by the maser itself. For example, if two signals at frequencies $f_1$ and $f_2$ simultaneously emerge from a maser at a level of $-30$ dbm, the third-order intermodulation products, $2f_1 - f_2$ and $2f_2 - f_1$, will be found at a level of $-185$ dbm,[5] which is approximately 95 db below the output noise of a 4°K, 25-mc maser.

For the reasons presented, the maser is, from the system engineering point of view, a completely distortion-free amplifier.

The use of this combination of an unstaggered maser and IF equalizer provided an effective net gain of 34.5 db at the band edges. This gain was sufficient to allow feeding a mixer directly from the maser output without degradation of the receiver noise temperature. The mixer had a noise temperature of approximately 4300°K which, reflected back to the maser input through 34.5 db of gain, appears as 1.5°K.

Equalized receivers were employed at Andover, Maine, and Pleumeur-

Bodou, France, and will be provided for the German installation. The performance obtained was satisfactory in every respect.

## V. MASER TERMINALS AND AUXILIARY STRUCTURE

In all previous masers, the largest contributor to the noise temperature has been the loss in the input transmission line. These, in the past, have been constructed of thin wall, stainless-steel coaxial cables in order to minimize heat conduction from their room temperature access to 4.2°K. A thin copper plating was employed to minimize electrical losses. (A delicate balance between electrical and thermal conductivity is required.) Masers using coaxial cables have had typical over-all noise temperatures of 10°K, of which only 2°K was inherent in the masers themselves. Waveguide, which intrinsically has lower loss than coaxial cable, was used for the input lead of the Telstar masers in an effort to obtain the lowest possible noise temperature. This waveguide was constructed of 0.020-inch thick seamless stainless steel and internally plated with 0.0002 inch of copper. The room temperature loss of such guide is approximately 0.1 db in the lengths required. The waveguides used in the final assemblies were selected for low-noise performance from many which had been initially prepared. This was accomplished by connecting the various waveguides, shorted at the far end, to an operating maser and noting the maser noise output.[6]

The waveguide extends from room temperature to well below the normal liquid helium level in the dewar. A transition to 0.140-inch diameter solid coaxial cable is employed (Fig. 13) and the center conductor of this cable is extended into the maser proper where it forms the final match to the comb structure (Fig. 3). Coaxial cable is permissible below the helium level, since the noise contributed by a given loss at 4.2°K is a factor of 70 less than would arise if the same loss were present at room temperature. The success of the arrangement can be judged by the measured noise temperature of these masers, approximately 3.5°K.

A new technique was employed to measure the noise temperature of these masers. The ratio of the noise power output of the maser with a matched load connected to its input to the noise power output with a short circuit at the input was determined. Since noise power is directly proportional to noise temperature, these quantities can be interchanged, provided one is consistent.

When a matched load is connected to the input of a maser whose input loss is small, the noise temperature observed at the output will be:

$$(T_{\text{out}})_1 = G(T_L + T_I + T_{\text{MF}}) \tag{9}$$

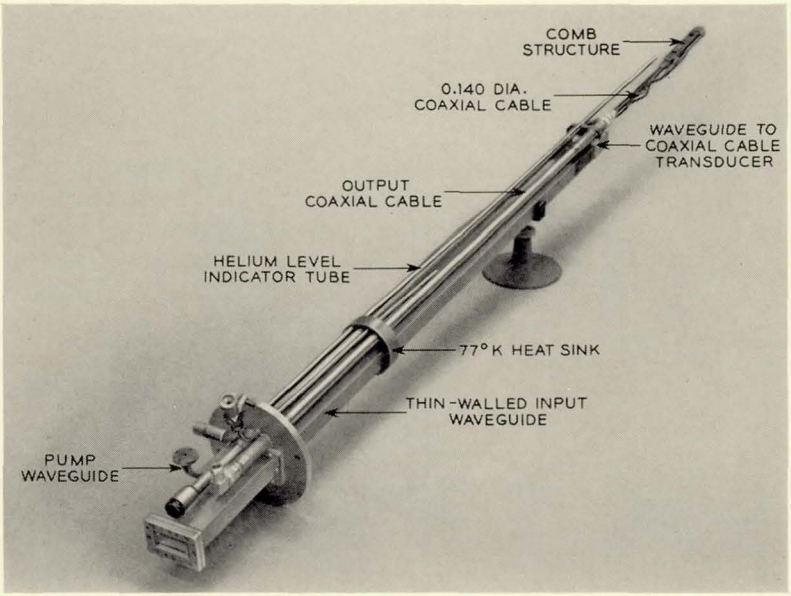


Fig. 13 — Maser head.

and when a short circuit is connected to the input, the output noise temperature is:

$$(T_{\text{out}})_2 = G(2T_I + T_S + T_{\text{MF}} + T_{\text{MR}}) \tag{10}$$

where

$G$ = power gain of the maser
$T_I$ = noise temperature due to losses in the input
$T_{\text{MF}}$ = noise temperature of the maser in the forward direction
$T_{\text{MR}}$ = temperature of the noise power emitted by the maser in the reverse direction
$T_L$ = temperature of the matched load, and
$T_S$ = noise temperature due to losses in the movable short.

The origin of (9) is clear, the noise contributed by the load and input losses being directly additive with forward-traveling maser noise. When the short is in position, the noise power generated by the input lead traveling away from the maser, as well as the noise power emitted in the reverse direction by the maser itself, are reflected, rather than absorbed, and therefore also contribute to the noise observed in the maser output. For this reason, the input noise appears doubly weighted, and the maser

reverse noise enters in (10). An observable quantity is the ratio of (9) to (10), i.e.

$$\frac{(T_{\text{out}})_1}{(T_{\text{out}})_2} = \frac{T_L + T_I + T_{\text{MF}}}{2T_I + T_S + T_{\text{MF}} + T_{\text{MR}}} . \tag{11}$$

The noise temperature of the maser, referred to the input terminals, is equal to $T_I + T_{\text{MF}}$ . $T_L$ is just equal to room temperature, approximately 300°K. $T_{\text{MF}}$ and $T_{\text{MR}}$ can be calculated from the theory of the traveling-wave maser and are typically 1.5°K and 6.5°K, respectively.

The one remaining parameter to be evaluated in (11) is $T_S$ . This can be determined by any one of a number of standard techniques, and is typically found to be of the order of 1°K. Therefore, $T_I$ can be calculated from the ratio and the maser noise temperature determined.

If the situation were as ideal as has been presented, the measurement of maser noise temperature would be well in hand. However, in practice the ratio of the maser noise outputs is found to vary as the position of the short circuit is changed. This is due to noise coherence effects which occur because of a limited bandwidth detection system and to small mismatches in the system. A detailed analysis of these effects by W. J. Tabor, which will be published separately, shows that the correct value for the noise temperature can be calculated, if one substitutes the average value of the ratio of observed noise powers into (11). This technique, which employs standard microwave components, i.e., a matched termination and a movable short in contrast to refrigerated loads, is capable of good accuracy. The range of uncertainty in the measurement of these masers was ±0.5°K.

The maser output is coaxial, since the noise contribution due to loss following the maser gain is negligible. The pump line is thin-walled WR28 waveguide. Fig. 13 is a photograph of the maser "head" which illustrates the various connections.

Fig. 14 shows the entire assembly except for the microwave pump source. The dc magnetic field is supplied by a 450-pound Alnico magnet, which allows the tuning of the maser over the entire structure passband by means of movable iron shunts. The dewar is of the standard type for liquid helium except for one innovation. A 77° heat station, in the form of a copper ring thermally tied to the liquid nitrogen jacket, was incorporated 10 inches below the room temperature flange (top). Its purpose is twofold: to reduce the thermal gradient to the liquid helium along the maser head, and to reduce the waveguide temperature in as short a length as possible in order to minimize thermal noise generation. With one filling of liquid helium (10 liters) the maser could be kept in opera-

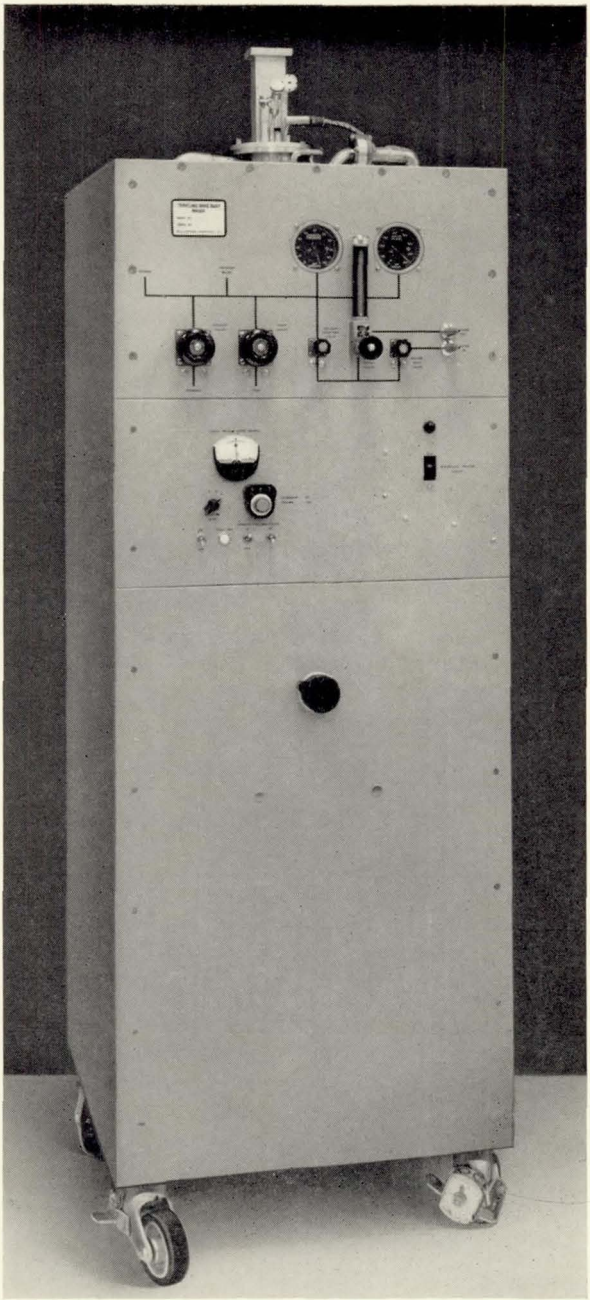

Fig. 14 — Complete maser package.

tion for approximately 20 hours. Refilling could be accomplished without disturbing maser performance.

## VI. SUMMARY

The performance of the masers is given by the following data:

| | |
|---|---|
| Center frequency: | 4170 mc |
| Effective instantaneous bandwidth: | 25 mc |
| Effective gain: | Approx. 34.5 db (equalized receiver) 28 db (magnetically staggered) |
| Pump frequency: | 30,175 mc |
| Pump power: | 70 mw |
| Magnetic field: | Approx. 3300 gauss |
| Over-all noise temperature: | 3.5°K |
| Bath temperature: | 4.2°K |
| *Liquid helium consumption:* | Approx. $\frac{1}{2}$ *liter/hr* |
| Helium capacity: | 10 liters |
| Power output at 1-db gain compression: | −38 dbm. |

The effective noise temperature, 3.5°K, of these amplifiers is almost a factor of 3 less than previously attained. Indeed, it is so low as to closely approximate the minimum noise temperature of the atmosphere itself. It therefore appears that the ultimate useful amplifier sensitivity has been achieved for application in terrestrial receivers.

## VII. ACKNOWLEDGMENTS

The authors wish to acknowledge the role played by H. E. D. Scovil in the development of these masers. The importance of his insight and continued guidance cannot be overemphasized.

We are indebted to E. O. Schulz-DuBois and E. D. Reed for reading this manuscript and making valuable suggestions. We would like to thank P. J. Pantano for his valuable assistance in the mechanical design and microwave measurements; his enthusiastic efforts in the early stages of this program were invaluable.

The authors also wish to show appreciation to certain members of the group for access to unpublished data: namely, S. Harris and R. W. DeGrasse, for calculations involving the comb bandpass cutoff, and to F. W. Ostermayer for design equations used in broadbanding.

APPENDIX

*Formulas for the Calculation of $\chi''$*

The tensor components of the susceptibility can be calculated from the following formulas

$$\chi_{xx}'' = \frac{\pi g^2 \beta^2}{\mu_0 h} g(f - f_0)(\rho_{-\frac{3}{2}} - \rho_{-\frac{1}{2}}) \mid \langle -\tfrac{1}{2} \mid S_x \mid -\tfrac{3}{2} \rangle \mid^2 \tag{12}$$

$$\chi_{xy}'' = \frac{\pi g^2 \beta^2}{\mu_0 h} g(f - f_0)(\rho_{-\frac{3}{2}} - \rho_{-\frac{1}{2}}) \langle -\tfrac{1}{2} \mid S_x \mid -\tfrac{3}{2} \rangle \langle -\tfrac{1}{2} \mid S_y \mid -\tfrac{3}{2} \rangle \tag{13}$$

etc., where $\mu_0$ is the permeability of free space, $h$ is Planck's constant, $g$ is the spectroscopic splitting factor, $\beta$ is the Bohr electronic magneton, $\rho_i$ is the density of spins in the energy level $i$, and $g(f - f_0)$ is a normalized line shape function; i.e.,

$$\int g(f - f_0)\, df = 1.$$

All the units are expressed in mks units. If emu units are used, $\mu_0$ must be replaced by $1/4\pi$.

In the case of ruby for operation at $\theta = 90°$, the transition probability between levels $-\frac{1}{2}$, $-\frac{3}{2}$ contain only $S_x$ and $S_y$ terms with $S_z = 0$, where the $Z$ direction is parallel to the dc magnetic field and the $X$ axis is parallel to the $C$ axis of the ruby. Therefore, the susceptibility tensor for this case consists only of terms $\chi_{xx}''$, $\chi_{xy}''$ and $\chi_{yy}''$. The values of the matrix elements can be computed from the data given by Schulz-DuBois.[7]

REFERENCES


1. DeGrasse, R. W., Schulz-DuBois, E. O., and Scovil, H. E. D., B.S.T.J., **38**, March, 1959, p. 305.
2. Geusic, J. E., private communication.
3. DeGrasse, R. W., Kostelnick, J. J., and Scovil, H. E. D., B.S.T.J., **40**, July, 1961, p. 1117.
4. Ostermayer, F. W., unpublished work.
5. Chen, F. S., Schulz-DuBois, E. O., and Tabor, W. J., to be published.
6. DeGrasse, R. W., Hogg, D. C., and Scovil, H. E. D., private communication.
7. Schulz-DuBois, E. O., B.S.T.J., **38**, January, 1959. p. 217.

# 4-gc Parametric Amplifier for Satellite Communication Ground Station Receiver

By M. UENOHARA, M. CHRUNEY, K. M. EISELE, D. C. HANSON, and A. L. STILLWELL

(Manuscript received March 19, 1963)

*This paper describes the design and performance of a 4-gc parametric amplifier which meets the stringent requirements of a satellite ground station receiver. It consists of two cascaded stages of similar design: the first of these is operated at liquid nitrogen temperature and the second at room temperature. One 23-gc pump source is used for both amplifier stages. The combination of the two amplifier stages provides 38-db over-all gain, 45°K over-all system input noise temperature, 60-mc bandwidth, 0.1-db short-term gain stability and 0.3-db long-term gain stability. A carefully designed cryogenic system maintains the amplifier refrigerated with only infrequent refilling of the dewar, i.e., once every 10 days.*

## I. INTRODUCTION

High sensitivity, stability and reliability are important requirements for a satellite communication ground station receiver. The maser has come to be considered the ideal preamplifier for satellite communication due to its superlative low-noise performance, and it is indeed ideal for cases where its cost and maintenance requirements are not of major concern. However, for lighter traffic routes where cheaper terminals are required, it is desirable to have a less expensive, more compact, and more easily maintained microwave preamplifier. This has motivated the development of the variable capacitance parametric amplifier described in this paper.

A block diagram of the parametric receiver is shown in Fig. 1. The receiver consists of four major sections: a circulator type parametric amplifier, an extremely stable 23-gc pump source, an efficient cryogenic system, and a control system. The first-stage amplifier is operated at liquid nitrogen temperature. The varactor diode mount, circulator,



In its Telstar 1, Vol. 3 Jun. 1963 P 1887-1908 refs (See N64-11079 02-01)

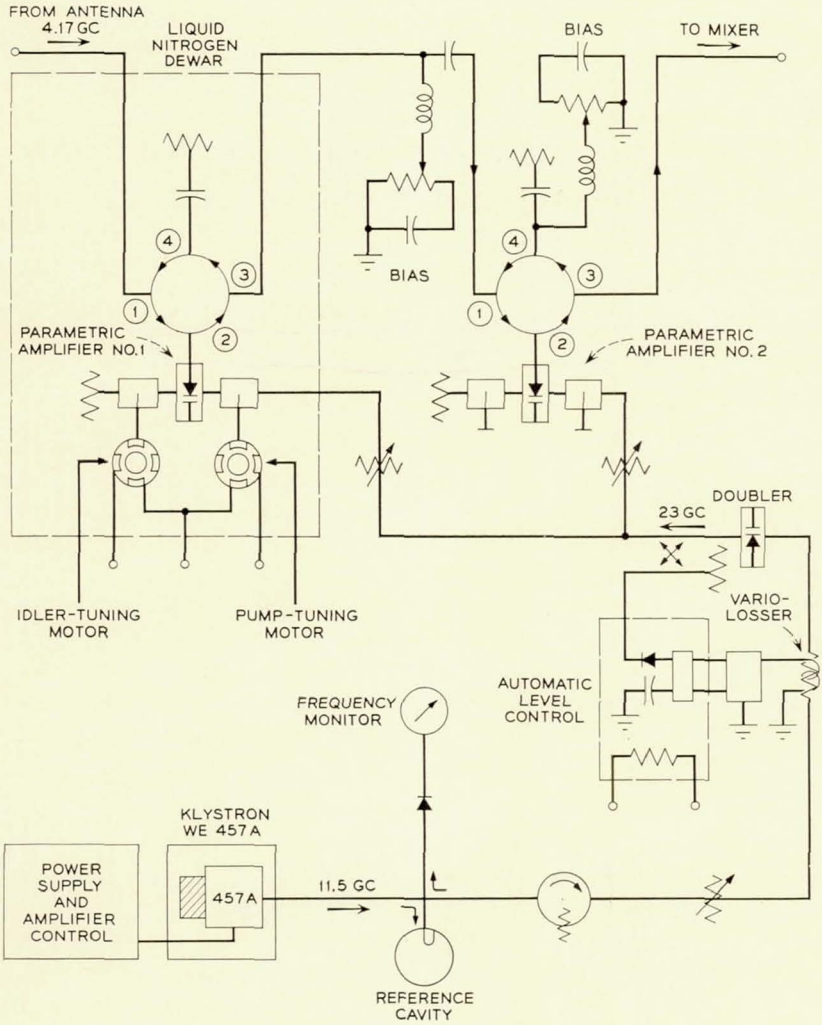


Fig. 1 — Block diagram of parametric receiver.

K-band termination for the external idler load, and two stepping motors for tuning the idler and pump circuits are all completely enclosed in a sealed copper can immersed in a liquid nitrogen dewar. This refrigerated amplifier is followed by a room temperature amplifier of the same design. Since the regenerative reflection mode of operation is used, there is no frequency conversion from input to output. The same 23-gc pump source supplies power to both amplifiers.

The gain stability of the parametric amplifier is largely dependent upon the stability of pump power level and frequency. Therefore, considerable effort has been spent to develop a pump source that would satisfy the most exacting requirements. The 23-gc source is derived from an X-band frequency-stabilized klystron of proven reliability (Western Electric 457A)[1] and a varactor frequency doubler.[2] An automatic level control is used to maintain a constant output power.

An efficient cryogenic system is required for operational simplicity and satisfactory amplifier performance. Such a system has been designed to maintain the amplifier at liquid nitrogen temperature. The dewar contains about 10 liters of liquid nitrogen and lasts more than ten days. This corresponds to an evaporation rate of 40 cc per hour or a heat inflow of 1.8 watts.

The two-stage amplifier provides a gain of 38 db at 4.17 gc with a minimum bandwidth of 60 mc. Over the entire band the effective system input noise temperature is less than 45°K. An input signal of −43 dbm produces 1-db gain compression when the small-signal gain is 38 db. Short-term gain fluctuations are less than 0.1 db and long-term gain variations are less than 0.3 db over periods of months. The amplifiers were installed in the ground station receivers at Andover and Holmdel and have been checked out to be satisfactory.

## II. DESIGN CONSIDERATIONS

### 2.1 *Parametric Amplifier*

#### 2.1.1 *Varactor Diode Considerations*

There are several factors which governed the choice of the varactor diode for the 4.17-gc refrigerated parametric amplifier. These include:

(a) A capacitive impedance of the same order as the circulator.[3]

(b) High dynamic quality factor[4] ($\tilde{Q}$) given by

$$\tilde{Q} = \frac{S_1}{2\omega R_S} = \frac{\text{Total reactance variation}}{4R_S}$$

where $S_1$ is the Fourier coefficient of the first-order term in the pumped variable elastance and $R_S$ is the spreading resistance of the diode.

(c) Crystal suitability for operation at liquid nitrogen temperature.[5] The spreading resistance should decrease or at least remain constant down to liquid nitrogen temperature. To simplify amplifier design and adjustment, a small decrease in junction capacitance from room temperature to liquid nitrogen temperature is desirable.

(d) A self-resonant frequency of the diode higher than an idler frequency is preferred.

At the time this amplifier was designed no diode was available which would meet all these requirements. Since a gallium arsenide diode satisfied all conditions but the last, which was not essential, it was chosen for this application. It was originally developed by W. M. Sharpless[6] and was further developed by N. C. Vanderwal. The recent encapsulation of the sealed diode is shown in Fig. 2.

Typical data for the diode are tabulated in Table I.

The spreading resistance decreases about 10 per cent from room temperature to liquid nitrogen temperature, and the junction capacitance changes only 5 per cent. Representative impedance loci of the diode at 300°K and 77°K (measured at 5.85 gc) are plotted in Fig. 3. The normal bias voltage for operation at liquid nitrogen temperature is −1.1 volts.

### 2.1.2 *Amplifier Design Considerations*

The main objective of the amplifier design was to achieve the best possible noise performance with moderate bandwidth (i.e., 25-mc minimum, 50-mc desired) and thus satisfy the system requirement with the available diode described in the previous section. The amplifier was required to have stable and reliable performance.

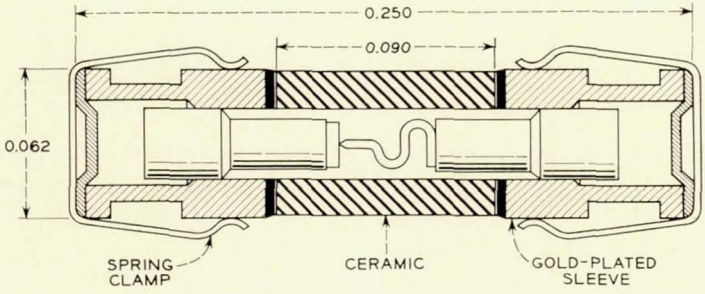


Fig. 2 — Encapsulation of sealed diode.

TABLE I

| | |
|---|---|
| Static capacitance ($C_0$) at zero bias | 0.37–0.46 pf (includes about 0.07 pf package capacitance) |
| Series inductance ($L_s$) | ≈1.2 nh |
| Self-resonant frequency ($f_{res}$) | 7.3–8.4 gc |
| Dynamic quality factor ($Q$) | 9.0–14 at 4.17 gc |
| Reverse breakdown voltage ($V_b$) | 5.0–6.0 volts (at 1 $\mu a$ current) |

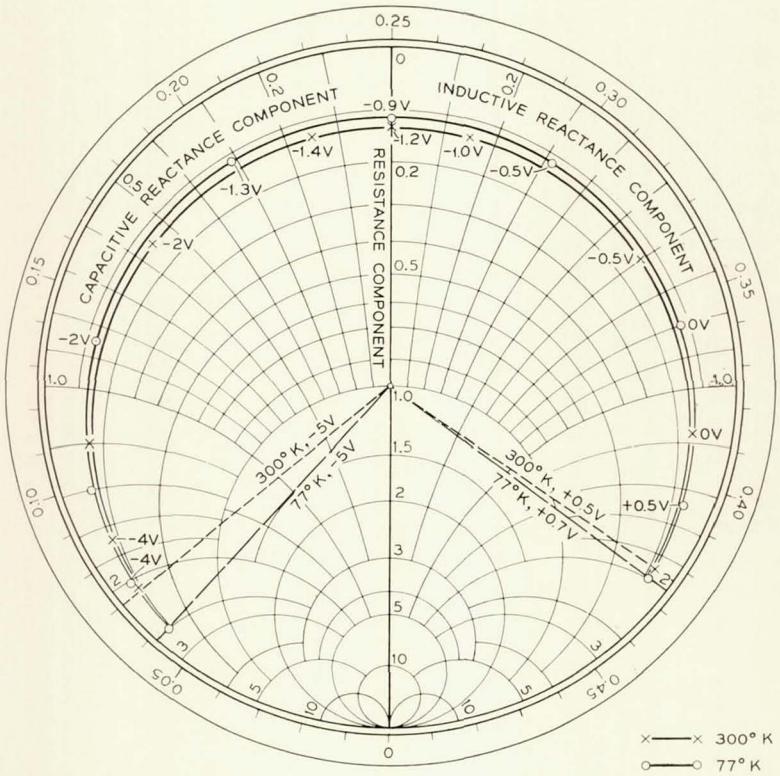


Fig. 3 — Impedance loci of input circuit at 300°K and 77°K (measured at 5.85 gc). Dynamic quality factor is 7.8 at 300°K and 9.3 at 77°K.

To achieve optimum performance, many factors, including the pump source, circuit elements and the cryogenic system, were carefully investigated. The detailed design considerations of the pump source and the cryogenic system are described in the following sections; however, selection of the pump frequency is discussed here since it primarily determines the circuit design of the amplifier.

The optimum ratio of idler frequency ($f_2$) to signal frequency ($f_1$) for best noise performance[3] is

$$\frac{f_2}{f_1} = \sqrt{1 + \frac{\tilde{Q}_1^2}{1 + \frac{R_L}{R_S}}} - 1 \qquad (1)$$

where $\tilde{Q}_1$ is the dynamic quality factor of the input circuit and $R_L/R_S$ is the external idler loading factor. Assuming the external idler loading

factor $R_L/R_S = 0.8$, which is discussed later, and using a diode whose dynamic quality factor at the signal frequency is 10, the optimum pump frequency is 31.6 gc. Unfortunately, a reflex klystron with the desired reliability was not available near this frequency. In addition, most klystrons which provide more than 100 mw of power at K-band need very high voltage supplies. Another factor was that none of these tubes provide satisfactory frequency stability without an elaborate scheme to compensate for any large environmental temperature variation and for mechanical vibration. However, a Western Electric 457A klystron (available from 10.7 to 11.7 gc) has high frequency stability with a simple closed vapor-phase cooling system.[1] Typically, the frequency variation is less than 2 mc from $-20°$F to $+120°$F ambient temperature. This klystron provides more than 500 mw power at 11.5 gc with about 500 volts cavity voltage. With a varactor frequency doubler,[2] this klystron can generate about 100 mw of power at 23 gc even after taking an additional 2-db loss for an automatic level control. The increase in noise temperature due to the utilization of a 23-gc pump source instead of a 31-gc pump source is calculated from the following equation;[3] the effective input noise temperature for a reflection type amplifier

$$T_e = \left(1 - \frac{1}{G_{11}}\right) \frac{1 + \left(\frac{f_1}{f_2}\right)^2 \frac{\tilde{Q}_1^2}{1 + \frac{R_L}{R_S}}}{\left(\frac{f_1}{f_2}\right) \frac{\tilde{Q}_1^2}{1 + \frac{R_L}{R_S}} - 1} \cdot T \tag{2}$$

where $G_{11}$ is a reflection power gain and $T$ is the amplifier temperature. From (2), we obtain that the noise temperature degradation is only 1.5°K. Because of the reasons just described, a 23-gc pump was selected for this amplifier. This produces a center-band idler frequency of 18.83 gc. Fig. 4 shows curves of the effective input noise temperature of the amplifier at liquid nitrogen temperature for $f_2/f_1 = 4.52$. Curves are plotted as a function of external idler loading factor $(R_L/R_S)$ for given values of input dynamic quality factor $\tilde{Q}_1$.

To achieve the noise performance shown in Fig. 4, the input circuit must be designed properly. The maximum normalized generator impedance $(R_g/R_S)$ which provides 20 db of reflection gain for a given $\tilde{Q}_1$ and $R_L/R_S$ is calculated[3] and plotted as a function of $R_L/R_S$ in Fig. 5.

The first and second-stage amplifiers utilize the same design, a design

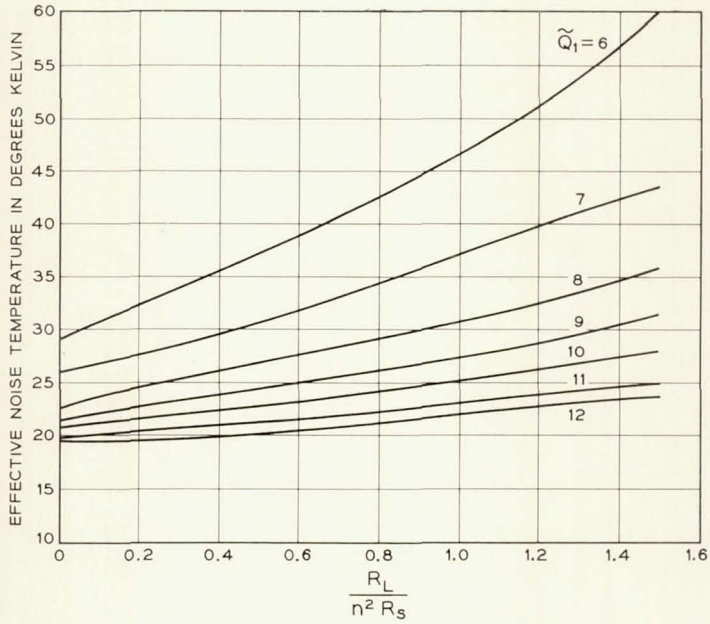


Fig. 4 — Effective input noise temperature of amplifier at liquid nitrogen temperature and room temperature as a function of external idler loading factor $(R_L/R_S)$ for various $\tilde{Q}$.

which is similar to a 6-gc amplifier previously reported.[7] Fig. 6 shows a photograph of the amplifier mount with a four-port circulator. The input circuit is a 50-ohm coaxial line and the pump and idler circuits are in RG 66/U waveguide which houses a gallium arsenide point-contact diode at the end of the input center conductor. Since the diode sustains at least three frequencies (i.e., signal, idler and pump), filters must be arranged properly to eliminate unwanted interference among the three circuits. These filters are located as close as possible to the diode to minimize energy storage at the idler frequency. The input circuit contains two coaxial chokes for the pump and idler frequencies and a coaxial capacitor which is used to adjust the input coupling to the predetermined value of $R_g/R_S$ and to tune the circuit at a desired bias voltage. These chokes and the rest of the mount are brazed into one piece for mechanical rigidity and electrical stability. The coaxial capacitor is movable along the center conductor to tune the circuit at a desired bias voltage. The input coupling is adjusted by using a different diameter coaxial capacitor.

One of the major design objectives was to increase the bandwidth

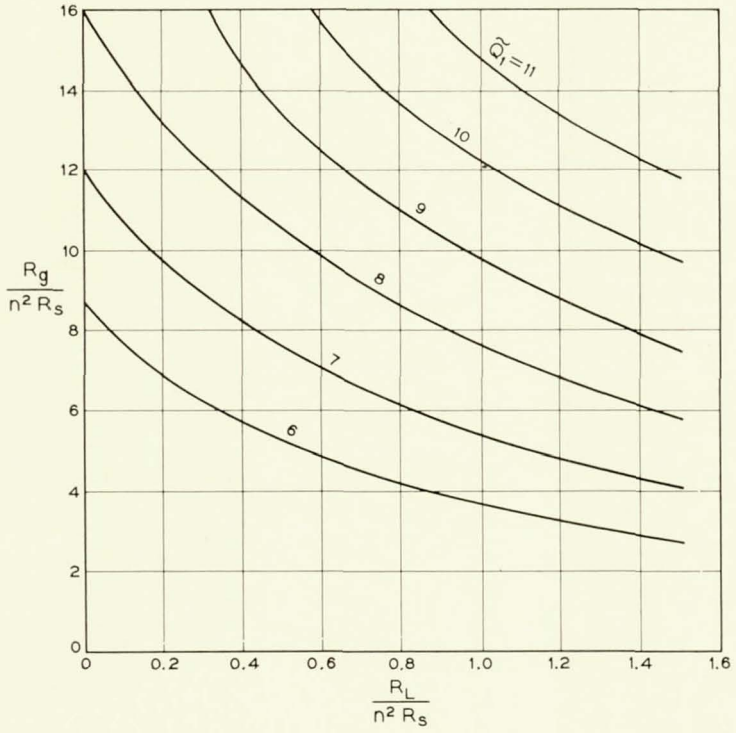


Fig. 5 — Normalized generator impedance $R_g/R_S$ required for 20-db regenerative gain as a function of external idler loading factor $R_L/R_S$ for given values of input circuit dynamic quality-factor $\tilde{Q}$.

without sacrificing noise performance. Since the self-resonant frequency of the diode is approximately 8 gc, it is unavoidable that an idler frequency much higher than the self-resonant frequency must be used. This resulted in an idler circuit of very high $Q$ and complicated impedance. It was found that the 3-db bandwidth with 20-db center-band gain was less than 20 mc when there was no external idler loading or compensation circuit. Since the input circuit was broad enough, a compensation circuit was inserted in the idler circuit to improve the bandwidth. When the idler circuit $Q$ is sufficiently high, the bandwidth can be improved by external idler loading. The optimum idler loading factor $(R_L/R_S)_{\text{opt}}$ for the case where the idler frequency is above the self-resonant frequency $f_{\text{res}}$ of the diode is given in terms of $\tilde{Q}_1$, $f_1/f_2$ and $f_{\text{res}}/f_1$ as follows[8]

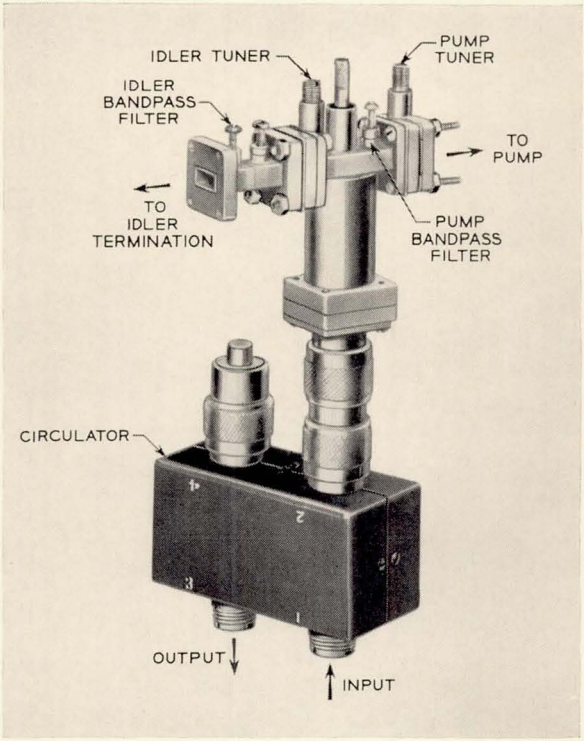


Fig. 6 — Photograph of 4.17-gc parametric amplifier and refrigerated circulator.

$$\left(\frac{R_L}{R_S}\right)_{opt} \approx \tilde{Q}_1^2 \left(\frac{f_1}{f_2}\right)\left[\frac{1}{1+\sqrt{1+\tilde{Q}_1^2\left(\frac{f_{res}}{f_1}\right)^2\left(\frac{f_1}{f_2}\right)}}\right] - 1 . \quad (3)$$

For the case where $\tilde{Q}_1 = 10$, $f_1/f_2 = 0.22$ and $f_{res}/f_1 = 1.9$, this equation shows that $(R_L/R_S)_{opt} = 1.15$. According to the curves in Fig. 4, the noise degradation caused by this external load is about 5°K; a suitable compromise between optimum gain-bandwidth and optimum noise performance is $R_L/R_S = 0.8$. This reduces the noise degradation to about 3°K. As a compensation circuit, a two-cavity bandpass filter was added adjacent to the inductive iris which tunes the idler circuit at the prescribed diode bias voltage. This iris also determines the coupling between the diode and the external idler load. The electrical separation between the iris and the filter and the filter impedance characteristic were properly adjusted for the maximum bandwidth. A Teflon tuner

was located in the idler resonant cavity to compensate for the approximate 20 per cent change in circuit impedance from room temperature to liquid nitrogen temperature due to the reduction in junction capacitance and cavity volume.

The pump filter was built in the mount as close as possible to the diode to minimize idler frequency energy storage in the idler cavity. A Teflon tuner, an inductive iris adjacent to the amplifier, and a screw in the pump filter are used for critical matched tuning and compensation from room temperature to liquid nitrogen temperature operation.

The bias voltage of the diode was applied through the third or fourth port of the four-port circulator. Any loss and instability usually caused by the bias supply circuit in the diode mount were completely eliminated.

A circulator operated at liquid nitrogen temperature (Raytheon CCL-12) was specially designed for the refrigerated first-stage amplifier. It was designed to have a maximum insertion loss from port 1 to port 2 of 0.2 db and isolation of at least 30 db. The room temperature circulator for the second-stage amplifier is the broadband Melabs X-626. Its characteristics at room temperature are similar to those of the CCL-12 at liquid nitrogen temperature.

The main design features of the amplifier are given in Table II.

### 2.2 *Pump Source*

The design of parametric amplifiers usually calls for high stability in both the frequency and amplitude of the pump source. The troubles often ascribed to parametric amplifiers, such as frequent failure and high cost, can largely be attributed to unsatisfactory pump sources. Therefore, considerable effort was devoted to obtain the simplest pump source that would satisfy the exacting requirements.

For frequency stabilization and compactness an all solid-state source is most attractive. This would consist of a transistorized crystal oscillator at a relatively low frequency with power amplification and subse-

TABLE II

| | |
|---|---|
| Input and output frequency | 4.17 gc ± 30 mc |
| Pump frequency | ≈23 gc |
| Dynamic quality factor $\tilde{Q}$ (including the circuit loss) | 10 at 4.17 gc, 2.3 at 18.83 gc |
| Normalized generator impedance ($R_g/R_S$) | 13.0 |
| Normalized idler impedance ($R_L/R_S$) | 0.8 |
| Gain | 20 db |
| Estimated noise temperature from (2) (amplifier alone) | 94°K at 300°K<br>25°K at 77°K |

quent multiplication by varactor diodes. While technically possible, such a device was not available in time for this project. Therefore, the WE 457A klystron was used as an 11.5-gc source to drive the varactor frequency doubler,[2] which produced the required 23-gc pump power.

For the automatic level control (ALC) the classical feedback approach has been used. A block diagram of the ALC arrangement is shown in Fig. 7. The output of the klystron is fed into the doubler through a Faraday rotational variolosser.[9] A small fraction of the 23-gc output is detected by a 1N26 crystal in the sampling port of a cross guide coupler. This output is compared with a reference voltage, amplified by a transistorized differential amplifier, and is fed to the variolosser. In this way the difference between the sampling voltage and the reference voltage is kept close to a preset constant value, and hence the 23-gc power output level is stabilized to better than 0.5 per cent over long time periods. Since the sensing diode characteristic is influenced by a large temperature change, this diode and the first stage of the differential amplifier are mounted in a small oven.

The second design, shown in Fig. 8, omitted the variolosser and operated directly on the doubler bias to control the output power. Although the performance was generally satisfactory, it demonstrated the need for an additional control factor. For feedback stability reasons, it is necessary to place a limit on the bias. However, this limit varies with input power to the doubler diode; hence, some additional circuitry is added to automatically set the maximum bias consistent with the input power.

The varactor frequency doubler from 11.5 gc to 23 gc used for this pump source can generate more than 200 mw of power at 23 gc with as low as 3.7-db conversion loss. The instantaneous 3-db bandwidth is about 300 mc, and no spurious oscillation is observable except at a bias

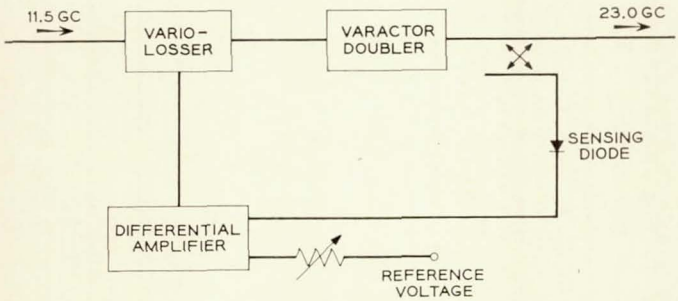


Fig. 7 — Block diagram of ALC arrangement. Power level is controlled by variolosser.

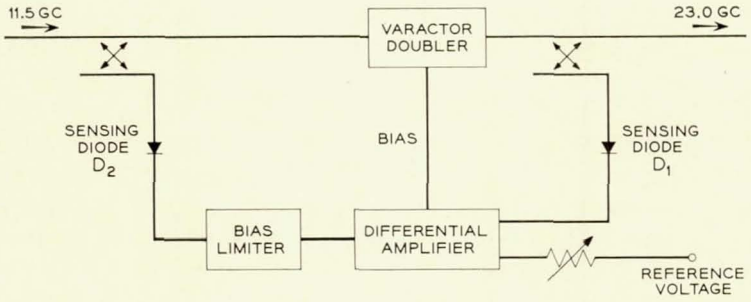


Fig. 8 — Block diagram of varactor diode bias-controlled ALC arrangement.

voltage which is much higher than the optimum. The varactor diode used is the epitaxial silicon mesa diode developed at Bell Telephone Laboratories. The diode has a cutoff frequency as high as 300 gc at −2.5 volts bias and a 25 volts average reverse breakdown voltage.

### 2.3 *Cryogenic System*

It was necessary for simple maintenance and satisfactory amplifier performance to design an efficient cryogenic system. Noise considerations dictate that not only the diode but also the total structure of the first-stage amplifier, including the circulator and the idler load, should be refrigerated. Immersing the whole amplifier in liquid nitrogen is a convenient way of refrigerating. However, it is very difficult to seal all parts of such a complex geometry in order to avoid liquid nitrogen leakage, which produces erratic electrical performance. Therefore, the whole unit is enclosed in a tight cylindrical copper vessel which is then immersed in liquid nitrogen. The walls of this vessel will assume a temperature of 77°K and cool the whole interior by conduction and radiation.

In order to achieve a long operating time with each filling of the dewar, the heat input must be minimized through the proper use of materials of low thermal conductivity. The design must make full use of the cryogenic value of the refrigerant. One liter of liquid nitrogen can absorb 38,600 cal. as heat of vaporization, and in addition the nitrogen gas which is produced can absorb 39,000 cal. when brought from 77°K to 273°K. If an arrangement can be made so that the nitrogen gas leaves the dewar with a temperature equal to that of ice, for instance, then the cryogenic value of one liter of liquid nitrogen is 77,600 cal. Furthermore, if the nitrogen gas escapes at room temperature there will be no condensation or freeze-out of moisture at the lid of the dewar, where many

electrical connections are located. A long operating time between refills can be obtained by immersing the amplifier deeply into the coolant; on the other hand, the input transmission line to the amplifier must be short to keep its loss and the corresponding noise contribution down. This imposes some restrictions on the cryogenic design. Fig. 9 shows a drawing of the cryostat. A commercial Linde Dewar featuring "Super Insulation" was chosen. It has a necktube of 5.5 inches diameter and holds 13.5 liters of liquid nitrogen. Part of this volume is taken up by the amplifier chamber, so that about 10 liters of liquid nitrogen are available for refrigeration. After immersion of the copper vessel the necktube is closed off by a lid consisting of a grooved Teflon plug, to the bottom of

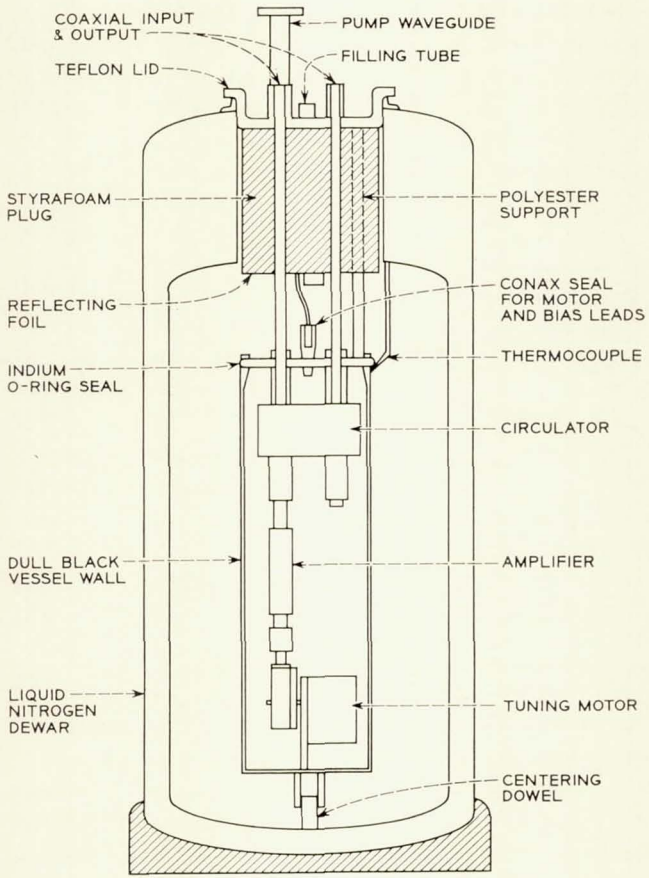


Fig. 9 — Cryostat for parametric amplifier.

which is glued a styrofoam cylinder 4 inches deep and $\frac{1}{8}$ inch smaller in diameter than the necktube. This arrangement forces the nitrogen gas to rise along the wall of the necktube and thereby cools it. The pump waveguide, two coaxial lines, a Teflon filling tube, and two polyester support rods (which add mechanical strength to the structure) pass through this lid down to the top of the amplifier chamber. The 11-inch input and output coaxial lines are made of 5-mil wall stainless steel tubes with 0.5-mil copper clad interior. Thin-wall stainless steel waveguide with silver plated interior is used for the pump waveguide. These transmission lines are vacuum sealed at the neck of the dewar (where the temperature is higher than the dew point) to prevent moisture condensation. The top of the copper chamber is sealed vacuum tight by an indium O-ring and the lower end extends almost to the bottom of the dewar, where it is held centered by a dowel pin. After all the parts are assembled, the copper chamber is tested on a helium leak tester for perfect sealing. The inside pressure of the chamber is left at atmospheric pressure to improve the speed of cooling.

With one filling of the dewar the amplifier was held for 10.5 days at liquid nitrogen temperature. This corresponds to an evaporation rate of 40 cc per hour or a heat inflow of 1.8 watts. Vertical temperature profiles which have been measured in the dewar reveal that the temperature of the gas above the liquid level stays within 2° of 77°K. This explains the constancy of the amplifier temperature over such a long time. The dewar can be refilled with liquid nitrogen without interrupting the performance of the parametric receiver.

For remote tuning of the idler and pump circuits, two tuning motors are mounted on the bottom of the copper vessel. Motors which are designed to be run at liquid nitrogen temperature must have a high starting torque, slow speed, and bearings which will not seize when the materials contract upon cooling. A stepping motor with 100 steps per revolution has been found to be the most reliable device to satisfy these requirements. The motors are operated by a transistorized multivibrator.

### 2.4 *Package*

One of the advantages of a parametric amplifier over a maser can be its compactness; however, its size is largely dependent upon the package design. Since the amplifier is highly susceptible to impedance variations and pump fluctuations, the package has to be designed not only for compactness but also to minimize any electrical malfunctions due to mechanical vibrations. Easier maintenance is also an important consideration for the package design.

Three different types of the package were constructed. Each of the first two amplifiers was packaged in a large 28 inch × 26 inch × 72 inch cabinet which can directly replace the maser cabinet and match mechanically to the horn antenna. This package was designed for operational convenience, reliability, simple maintenance and appearance. The front and back views of the amplifier are shown in Figs. 10 and 11. The dewar containing the refrigerated amplifier is in a frame at the top of the rack, with the input waveguide above the cabinet at a total height of 78 inches. The cabinet has four leveling jacks to enable an exact match to the antenna. The room temperature amplifier is mounted on

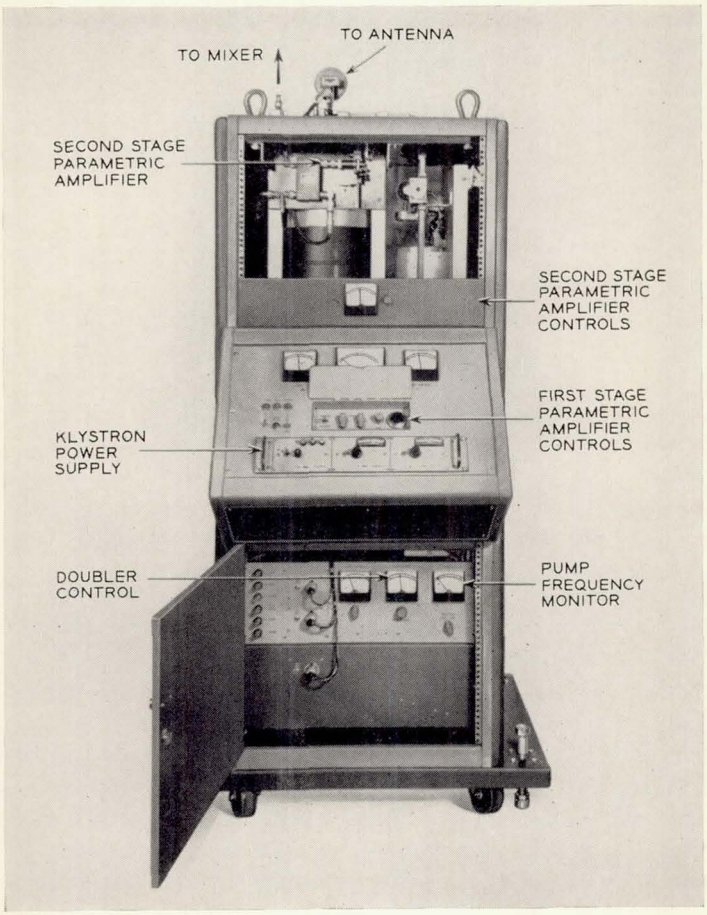


Fig. 10 — Front view of large amplifier package.

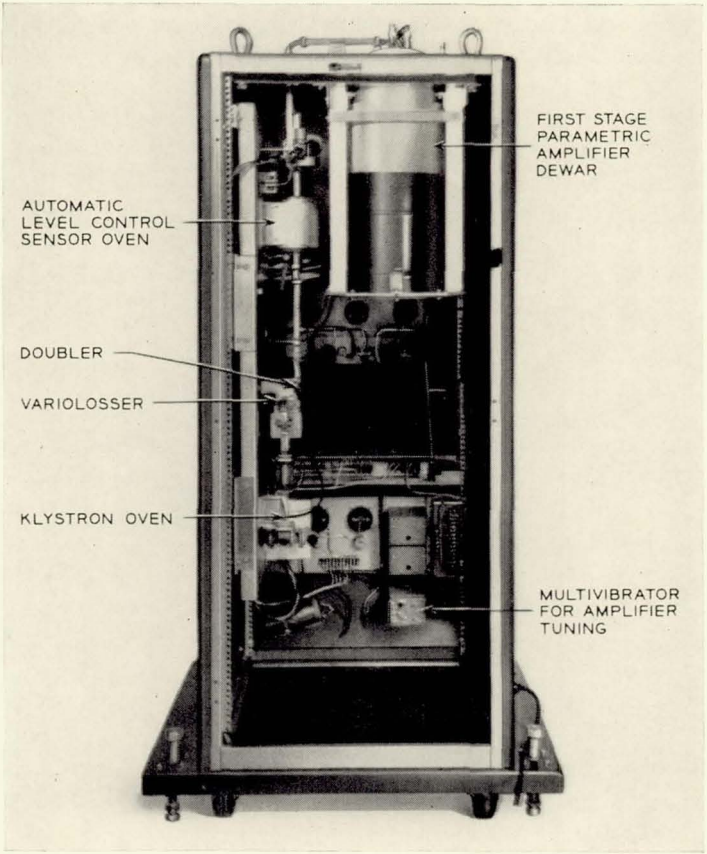


Fig. 11 — Back view of large amplifier package.

the dewar frame to minimize the interconnecting transmission line length and can be seen from the front of the rack with the top panel removed. The bias and pump power controls for the room temperature amplifier are located on the top control panel, and the controls for the liquid nitrogen temperature amplifier and the ALC are located in the recessed middle control panel. This section is usually covered and protected from accidental handling. The entire pump supply is mounted on a flat aluminum chassis which is fastened on the left side frame structure. The length of pump waveguides and the number of flange connections from the pump power sampling point to the amplifiers are minimized to maintain constant pump power levels against mechanical vibrations. The pump power level can be controlled by the motor-

driven waveguide attenuators from the front panel. One can see that the cabinet is only partially occupied.

To utilize full advantage of the parametric amplifier, a compact package was designed. This package consists of two cabinets: a control cabinet (17 inches × 18 inches × 10 inches) and an amplifier cabinet (14 inches × 14 inches × 32 inches), both shown in Fig. 12. The separation thus allowed the amplifier to be installed directly at the antenna output and the controls to be located at a convenient operating location. In this compact model, the doubler bias-controlled ALC is installed to ease the package design. Fig. 13 shows the amplifier and pump arrangement.

## III. PERFORMANCE

Five parametric receivers were built: two were housed in large cabinets, two in compact cabinets, and one in a special cabinet for a sky

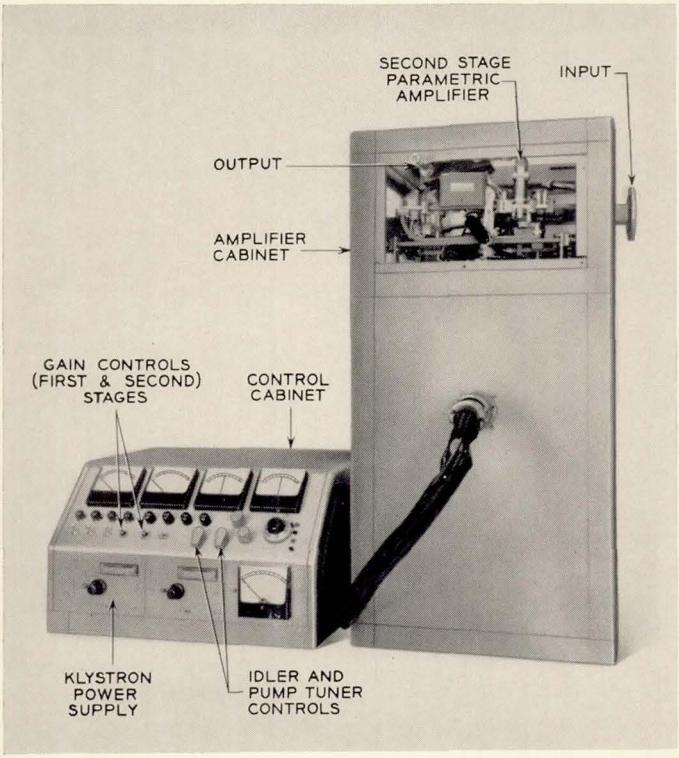


Fig. 12 — Photograph of compact package.

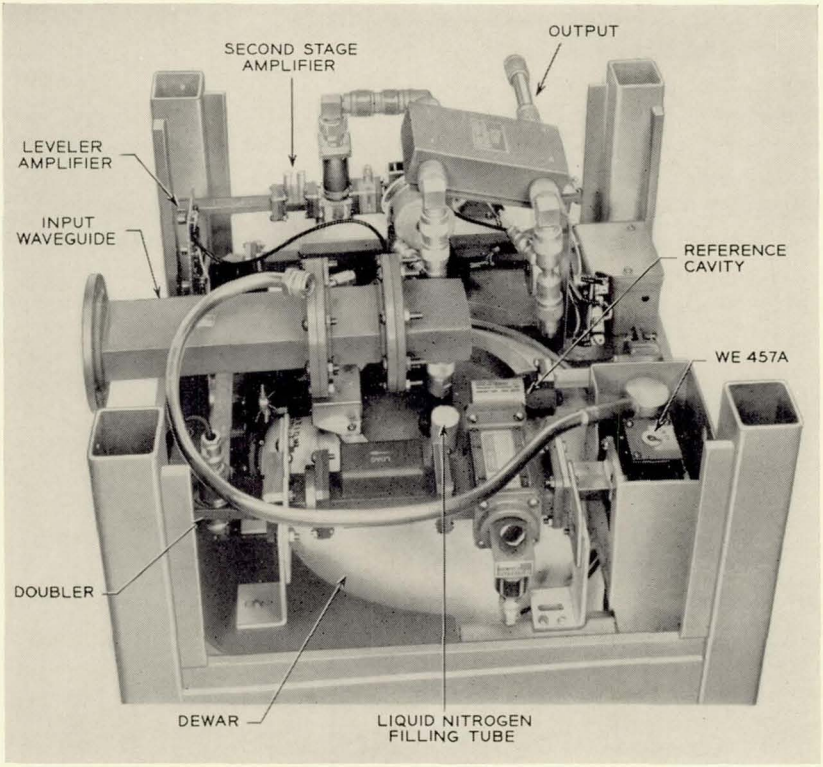


Fig. 13 — Photograph of amplifier and pump arrangement of compact package.

temperature measurement. The average values for the performance of these amplifiers are listed in Table III.

By December 1, 1962, amplifier no. 1 had been operated continuously for 6000 hours (since March 20, 1962) without any failure or degradation.

A representative gain-frequency band characteristic is shown in Fig. 14. Fig. 15 shows the recorded data on amplifier stability over a two-day period. The bottom $f_p$ curve shows the pump frequency deviation from 23 gc. One inch on the original recording paper corresponds to about 200 kc deviation. The second curve from the bottom (gain) shows the gain of the refrigerated amplifier. One inch corresponds to 1-db change in gain. The $P_{\text{pump}}$ curve indicates the pump power level. The scale is 0.25 db per 0.5 inch. Since the signal generator and the test receiver used for the stability tests did not themselves have absolute gain stability, both input and output signal level were detected by crystal detectors and were recorded simultaneously. The second ($P_{\text{in}}$)

TABLE III

| | |
|---|---|
| Gain | 38 db (first stage 20 db, second stage 18 db) |
| Bandwidth | 60 mc to 3-db points |
| Noise temperature | <45°K |
| First stage | <43°K |
| Contribution from second stage + mixer | <2°K |
| Gain stability | |
| Short-term | <0.1 db |
| Long-term | <0.3 db |
| Gain compression | 1 db down at −5 dbm output |
| 23-gc pump power required | ≈20 mw for each stage |
| Pump stability | |
| Frequency | Short-term <100 kc<br>Long-term <2 mc |
| Power | <0.02 db |
| Dewar — nitrogen service | Once a week (nitrogen lasts about 10 days) |

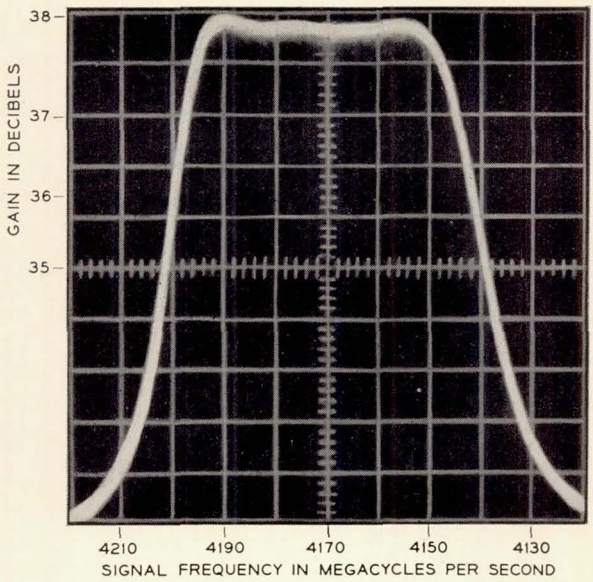


Fig. 14 — Gain-frequency band characteristic of parametric amplifier no. 2.

and third ($P_{out}$ − 21 db) curves show these outputs. The controls were adjusted so that the separation between the two curves was 1 db when the gain of the amplifier was 20 db; the gain fluctuations were then deduced from the separation of these curves. The speed of the recorder was two inches per hour.

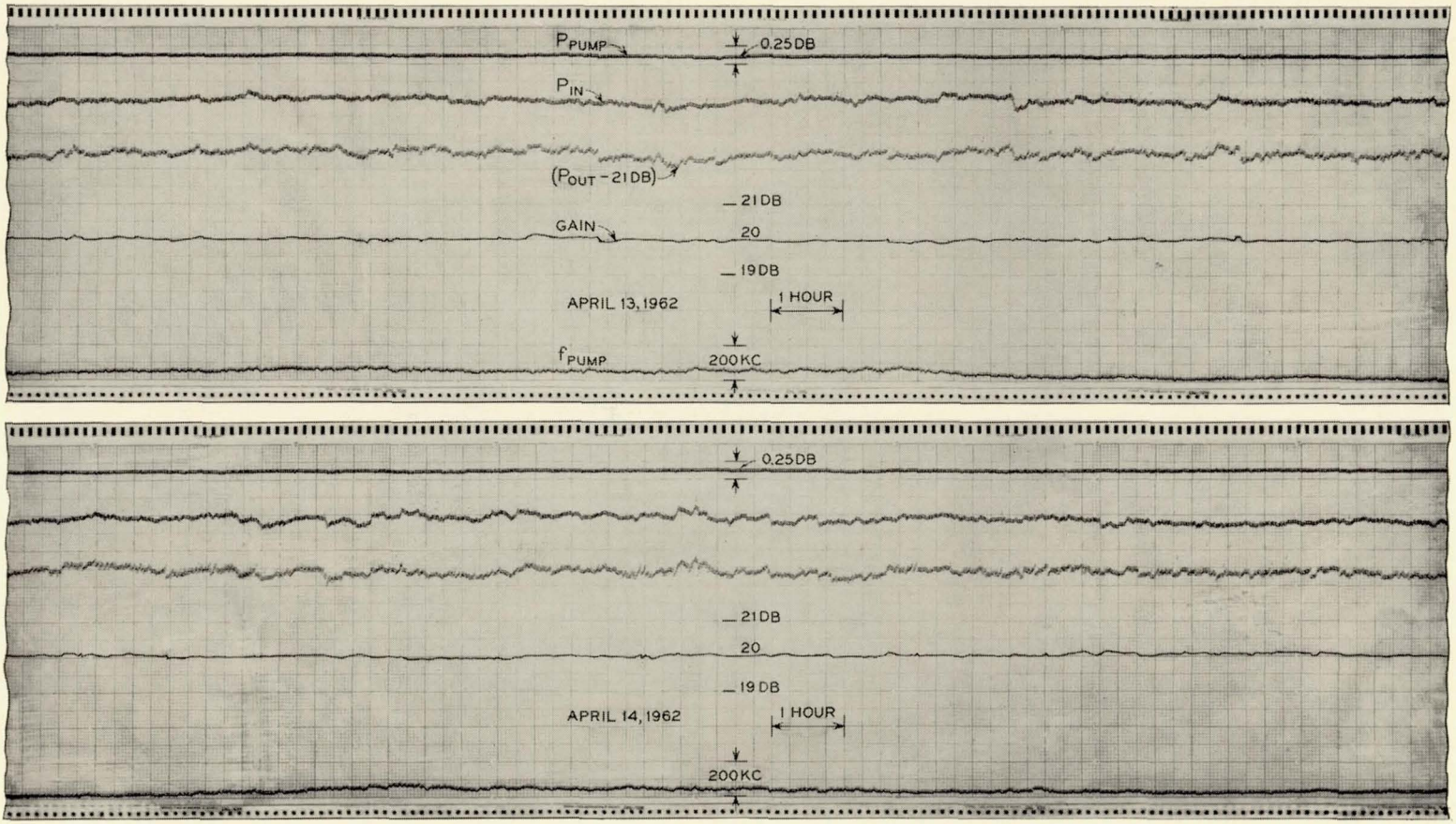


Fig. 15 — Recorded graph of amplifier stability. Pump line shows the pump power level; $P_{in}$, signal input; $P_{out}$ − 21 db, 21 db below amplifier output; $f_{pump}$ the pump frequency deviation from 23 gc.

The amplifiers were installed in the satellite ground stations both at Andover, Maine, and Holmdel, New Jersey, and were checked out as functioning satisfactorily. The complete system noise temperature of the receiver at the Andover station with the parametric amplifier was about 80°K when the antenna was directed at the zenith. This noise temperature includes about 28°K of noise from the sky, the radome, the antenna and the diplexer, and some noise from the 2.5-foot long waveguide which connects the amplifier to the diplexer.

## IV. CONCLUSION

The noise temperature of the receiver with the parametric preamplifier is 2.5 times that with the maser. However, the parametric amplifier is much cheaper to operate. The results of laboratory and field tests demonstrate that the parametric receiver meets the stringent requirements of a satellite ground station receiver. The stability performance of the amplifier also proves that a carefully engineered parametric amplifier is as stable as conventional microwave amplifiers.

The amplifier and its associated devices have been designed for high sensitivity, stability, and reliability. To assure this performance, the bandwidth was sacrificed and in many places a conservative design has been adopted. With an improved diode—in particular, one in a more suitable package—and a completely transistorized pump source, the amplifier can be considerably simplified and made very compact without any degradation in its performance and with an improved bandwidth.

## V. ACKNOWLEDGMENTS

During the course of this study many members of Bell Laboratories contributed valuable knowledge and skills. Unfortunately it is impractical to name them all here, but the authors are deeply grateful to them all. N. C. Vanderwal supplied the gallium arsenide diodes; R. L. Rulison developed the silicon epitaxial diodes; C. E. Barnes supplied the ferrite variolossers; and E. E. Prince did the initial package design. The authors wish to acknowledge their major contributions.

Acknowledgment is also made to K. D. Bowers for stimulating discussions and helpful criticism in the study of this project.

## REFERENCES

1. Gucker, G. C., Long-Term Frequency Stability of a Reflex Klystron Without Use of External Cavities, B.S.T.J., **41**, May 1962, pp. 945–958.
2. Uenohara, M., Rulison, R. L., Bricker, C. H., Varactor Frequency Doubler from 11.5 to 23 gc, Proc. I.R.E, **50**, December, 1962, p. 2486.

3. Uenohara, M., Seidel, H., 961-mc Lower Sideband Up-Converter for Satellite-Tracking Radar, B.S.T.J., **40**, July, 1961, pp. 1183–1205.
4. Kurokawa, K., Uenohara, M., Minimum Noise Figure of the Variable-Capacitance Amplifier, B.S.T.J., **40**, May, 1961, pp. 694–722.
5. Uenohara, M., Extremely Low-Noise Variable-Capacitance Parametric Amplifier, Proc. of International Congress on Microwave Tubes in Munich, Germany, 22, 1961 Monograph 4031, pp. 334–337.
6. Sharpless, W. M., Gallium-Arsenide Point-Contact Diodes, I.R.E. Transactions on Microwave Theory and Techniques, **MTT-9**, January, 1961, pp. 6–10.
7. Uenohara, M., An Extremely Low-Noise 6-gc Nondegenerate Parametric Amplifier, Proc. I.R.E., **50**, February, 1962, p. 208.
8. DeJager, J. T., private communication.
9. Barnes, C. F., Broadband Isolators and Variable Attenuators for Millimeter Wavelengths, I.R.E. Trans. on Microwave Theory and Techniques, **MTT-9**, November, 1961, pp. 519–523.

# Contributors to this Issue

J. V. Anders, B.E.E., 1953, University of Florida; Western Electric Co., 1953–1961; Bell Telephone Laboratories, 1961—. He has been engaged in guided missile systems test and evaluations programs and radar circuit design. He worked on the development of tracking receivers for the Telstar project and is presently engaged in the design of solid-state radar circuits. Member, IEEE, American Rocket Society, and American Ordnance Association.

John T. Bangert, B.S.E.E., 1942, University of Michigan; M.S.E.E., 1947, Stevens Institute; Bell Telephone Laboratories, 1942—. Mr. Bangert was first engaged in design of special circuits for military radar, investigation of fundamental problems in transmission theory, and exploration of new techniques for network analysis and synthesis in the time and frequency domain. Later he headed groups responsible for waveguide systems analysis, microwave network design and the application of analog and digital computers to the design of transmission systems. Since March, 1962, Mr. Bangert has been Director of the Transmission Technology Laboratory. Member, IEEE, Sigma Xi, Tau Beta Pi, Eta Kappa Nu, and Phi Kappa Phi.

Simon B. Bennett, B.E.E., 1959, City College of New York; M.E.E., 1961, New York University; Bell Telephone Laboratories, 1959—. He has been engaged in the study of noise in FM transmission systems and has participated in planning and performing the communications system tests for the Telstar and Relay projects. Member, IEEE, Tau Beta Pi and Eta Kappa Nu.

R. B. Blackman, A.B., 1926, California Institute of Technology; Bell Telephone Laboratories, 1926—. Mr. Blackman was first engaged in physical research in hearing, acoustics, and electromechanical filters. He later worked in applied mathematical research, specializing in linear networks and feedback amplifiers. Since 1940, he had been engaged in the development of data-smoothing and prediction techniques for anti-aircraft fire-control computers, air-to-ground bombing computers,

guided-missile computers and satellite launching computers. Member, IEEE and Tau Beta Pi.

R. W. Blackmore, B.S.M.E., 1940, Case Institute of Technology; Bell Telephone Laboratories, 1941—. He has engaged in mechanical design work on missile guidance systems, optical equipment for evaluating tracking performance of radar antennas, and flight control instruments. On the Telstar project he performed engineering liaison work with subcontractors and various Laboratories groups involved in the mechanical design, fabrication, erection, and alignment of the horn-reflector antenna. He is presently engaged in design and cost studies for future antennas. Member, Tau Beta Pi.

J. D. Bode, Ph.D., 1952, University of Pittsburgh; Bell Telephone Laboratories, 1960–63. Mr. Bode was first engaged in electroplating magnetic materials for the ESS semipermanent Twistor Memory Store. This was followed by work on the Telstar satellite project, which included the antireflection coating of the solar cells and their sapphire covers and work on the thermal control bellows. He was later involved in development work on long-wavelength sensitive photocathodes for laser applications. Member, American Chemical Society, Electrochemical Society, A.A.A.S., Electron Microscope Society of America, Faraday Society, Optical Society of America and Sigma Xi.

Max G. Bodmer, Dipl. El. Ing., 1946, Federal Institute of Technology, Zurich, Switzerland; Eng. D., 1950, Johns Hopkins University; Bell Telephone Laboratories, 1951—. Mr. Bodmer has specialized in the design and development of traveling-wave tubes, including exploratory development of TWT's, life studies for systems TWT's, the design of a high-power CW TWT for X-band, and the design and development of high-reliability long-life TWT's for satellite use. Member, IEEE and AIAA.

David C. Bomberger, B.S.E.E., 1934, and M.S.E.E., 1936, Lehigh University; Bell Telephone Laboratories, 1936—. He has worked on transmission measurements of coaxial cables, the design of broadband feedback amplifiers, the development of electromechanical gun director systems, and the analysis and simulation of complex dynamic systems. As Head, Power Systems Engineering Department, he was responsible for engineering the spacecraft power supply. Member, IEEE, Tau Beta Pi, Phi Beta Kappa; associate member, Sigma Xi.

STEPHEN J. BROLIN, B.S.E.E., 1957, M.S.E.E., 1959, New York University; Bell Telephone Laboratories, 1957—. He first worked on regulated power supplies for an experimental electronic telephone central office, and has since designed power supplies for a military project, a carrier system, and the Telstar project. He is currently working on power supplies for microwave radio relay systems. Member, IEEE, Tau Beta Pi, and Eta Kappa Nu.

W. L. BROWN, B.S., 1945, Duke University; A.M., 1947, Ph.D., 1951, Harvard University; Bell Telephone Laboratories 1950—. Mr. Brown has been engaged in research on the physical properties of semiconductor surfaces and the nature of defects produced in semiconductors by high energy radiation. He has recently been responsible for radiation experiments aboard the Telstar satellite. Fellow of American Physical Society, Sigma Xi and Phi Beta Kappa.

T. M. BUCK, B.S., 1942, Muskingum College; M.S., 1948, and Ph.D., 1950, University of Pittsburgh; Bell Telephone Laboratories, 1952—. He has been engaged in studies of the chemical and surface properties of semiconductor materials and devices. More recently, he has been responsible for development of the silicon p-n junction particle detectors for the Telstar satellite. Member, Electrochemical Society, Sigma Xi, Phi Lambda Upsilon, and Sigma Pi Sigma.

C. PAUL CARLSON, B.S. in E.E., 1926, University of Michigan; Bell Telephone Laboratories, 1926—. Until World War II he was engaged in equipment development of long-distance signaling, telephone repeaters, line balancing apparatus and transmission testing equipment. During the war he worked on radar test set development and has since been concerned with test sets, microwave radio, TASI, and undersea repeaters for transatlantic telephone cables. He presently supervises a group engaged in equipment design for the Andover, Maine, earth station. Registered Professional Engineer, State of New York.

J. G. CHAFFEE, S.B., 1923, Massachusetts Institute of Technology; Western Electric Co., 1923–25; Bell Telephone Laboratories, 1925—. He first engaged in short-wave transmission studies; this was followed by participation in the first ship-to-shore radiotelephone commercial installation. He then made extensive studies of frequency modulation and invented the FM-with-feedback receiver. During World War II he engaged in radar and guided-missile projects. Following this he spent the

next 15 years in studies for microwave radio relay systems. Since the inception of the Telstar project he has worked on circuit design, principally the design of the FMFB receiver for the ground station. Fellow of IEEE.

Roger C. Chapman, Jr., B.S.E.E., 1954, University of Vermont; Bell Telephone Laboratories, 1954—. Mr. Chapman was first engaged in the study of pulse code modulation systems and pulse transmission. He developed circuits for regenerative repeaters, particularly the retiming and reshaping circuits. In 1961, he started work on command circuit design for the Telstar project, and later became supervisor of a group responsible for the command and telemetry portion of the ground station. Currently, Mr. Chapman is supervisor of a systems analysis group responsible for the Telstar systems tests and for analysis and system studies of possible future satellite communications systems. Member, IEEE; associate member, Sigma Xi.

Michael Chruney, B.S.E.E., 1948, and M.S.E.E., 1949, Pennsylvania State College; Bell Telephone Laboratories, 1949—. He has engaged in the design and development of beam devices such as the barrier-grid storage tube and the flying-spot scanner for the memory of an experimental electronic central office. He contributed to the microwave printed hybrids used in the Telstar satellite and the parametric amplifier used as a standby receiver at the Andover earth station. Member, IEEE.

A. J. Claus, B.S. in E.E. and M.E., 1956, University of Ghent, Belgium; Ph.D., 1961, University of Michigan; Bell Telephone Laboratories, 1961—. He has worked on orbit determination for the Telstar satellite and tracking studies for the Apollo project.

Robert J. Collier, B.S., 1950, M.S., 1951, and Ph.D., 1954, Yale University; Bell Telephone Laboratories, 1954—. He has been engaged in the development of microwave electron tubes, including the coaxial magnetron, the forward-wave crossed-field amplifier, and the traveling-wave tube for the Telstar transmitter. He presently heads a group which is designing high-power traveling-wave tubes for pulsed radar. Member, American Physical Society, Sigma Xi and Phi Beta Kappa.

R. L. Comstock, B.S., 1956, and M.S., 1957, University of California; Ph.D., 1962, Stanford University; Bell Telephone Laboratories, 1957–58,

1961—. He has been concerned with the development of microwave solid-state devices, including isolators, power limiters and magnetoelastic devices. Member, IEEE, Eta Kappa Nu, Sigma Xi, and Tau Beta Pi.

J. S. Cook, B.E.E. and M.S., 1952, Ohio State University; Bell Telephone Laboratories, 1952—. He has engaged in microwave electron device research, including low-noise studies, coupled microwave circuits, electrostatic electron beam (slalom) focusing, and parametric amplification. He took part in the development of the autotrack system for the horn-reflector antennas used at Andover and Pleumeur-Bodou, France. He is presently engaged in studying special radar and communications antennas. Senior member, IEEE.

Arthur B. Crawford, B.S. in E.E., 1928, Ohio State University; Bell Telephone Laboratories, 1928—. Mr. Crawford has specialized in radio research, including work with measuring techniques, propagation, and antenna studies in the ultra-short-wave and microwave areas. He designed the horn-reflector antenna used in the Project Echo passive satellite communications experiments. As Head, Radio Research Department, he is in charge of a group which was responsible for transmission studies for the Telstar project. Fellow, IEEE; member, Eta Kappa Nu, Pi Mu Epsilon, Sigma Xi and Tau Beta Pi.

George F. Critchlow, B.E.E., 1942, and B.M.E., 1943, Cornell University; Bell Telephone Laboratories, 1943 —. He has been engaged in the development of precision impedance and transmission equipment and in the supervision of groups responsible for this work. He is presently head of a group which designs solid-state circuits for communications satellites. Member, IEEE, Eta Kappa Nu, Phi Kappa Phi and Tau Beta Pi.

C. Chapin Cutler, B.S., 1937, Worcester Polytechnic Institute; Bell Telephone Laboratories, 1937—. He has made significant contributions in the areas of microwave antennas, microwave tubes, and new radar and communication systems. As Director, Electronic Systems Research, he heads a group which has worked on communications engineering for both the Project Echo and Project Telstar satellite communications experiments. Fellow, IEEE.

Donald B. Cuttriss, B.S. in E.E., 1959, Newark College of Engineering; M.S. in E.E., 1961, New York University; Bell Telephone Labora-

tories, 1951—. Until 1959 Mr. Cuttriss worked on design and development of laminated-core inductors and semiconductor field-effect devices. In 1959 he transferred to semiconductor device development and was concerned with the development of diffused-base germanium transistors. Since 1960 he has been engaged in the evaluation of solar cell performance, particularly in the design and evaluation of solar power plants for communication satellites. Member, Tau Beta Pi.

J. B. D'Albora, Jr., B.S. in E.E., 1934, Massachusetts Institute of Technology; Research Assistant, M.I.T., 1935–40; Senior Radio Inspector for Inspector of Naval Material, N.Y.C., 1940–41; Western Electric Company, 1941–45; Bell Telephone Laboratories, 1945—. His early assignments at the Laboratories included development of shipborne fire control equipment and search radar for the DEW Line. In 1956 he was assigned responsibility for the ground guidance equipment for the Titan ICBM at Cape Canaveral, and since 1961 he has been in charge of the Cape Canaveral Laboratory as Resident Technical Director. Senior member, IEEE; member, American Rocket Society.

Claude G. Davis, B.S. in E.E., 1950, Case Institute of Technology; M.S. in Mathematics, 1960, Stevens Institute of Technology; Bell Telephone Laboratories, 1950—. He has specialized in transmission systems development, including the development of armorless submarine cable for a transoceanic telephone system, a PCM system for exchange trunks, PCM repeaters for an experimental waveguide transmission system, the Time Assignment Speech Interpolation (TASI) system, and satellite repeater design and data analysis. He is currently responsible for development of customer radio systems. Member, Eta Kappa Nu and IEEE.

W. A. Dean, Bell Telephone Laboratories, 1955—. He has worked on solid-state microwave device development, including devices for tropospheric scatter systems, Project Echo, and the Telstar project. He is presently engaged in circulator development for a carrier transmission system.

T. B. Delchamps, B.S.M.E., 1945, University of New Hampshire; B.S.M.E., 1947, Lehigh University; Bell Telephone Laboratories, 1959—. Mr. Delchamps is presently Head, Environmental Engineering Department of the Reliability Engineering Center.

Alton C. Dickieson studied electrical engineering at Brooklyn Poly-

technic Institute and joined the Western Electric Company Engineering Department in 1923. At Bell Laboratories, Mr. Dickieson's responsibilities have included long-distance communications systems; military telephone, sonar and torpedo-guidance systems during World War II; and transmission and radio systems engineering. In 1951 he became Director of Transmission Systems Development and subsequently directed the planning for the communication and detection systems used in the first Distant Early Warning stations. He became Executive Director of the transmission division in 1961, in which position he has general responsibility for the Telstar experiment. Naval Ordnance Development Award, 1945; Gen. H. H. Arnold Trophy of the Air Force Association (with Dr. J. R. Pierce), 1962; General Hoyt S. Vandenberg Award of the Arnold Air Society, 1963 (with Dr. J. R. Pierce); Fellow, IEEE.

J. C. Dolling, B.S. Eng., 1949, and M.S.M.E., 1952, Technical University of Hanover, Germany; Ph.D., Eng., 1955, Technical University of Brunswick, Germany; Weserhuette AG, Oeynhausen, Germany, Chief Development Engineer, 1954–56; Wuelfel AG, Hanover, Germany, Assistant to Vice-President, 1956–58; Bell Telephone Laboratories, 1958—. He has been engaged in electromechanical development of military radar and space communication antennas, including structural, mechanical, and system analyses for military projects. He was responsible for preliminary design of and engineering guidance on the Telstar horn-reflector antenna, and presently is developing this antenna for commercial use. Member of A.S.M.E. and German Engineers Association (VDI).

K. M. Eisele, Dipl. Phys., 1954, Institute of Technology, Stuttgart, Germany; M.A., 1955, and Ph.D., 1958, University of Toronto; Bell Telephone Laboratories, 1960—. He has been engaged in studies of low-noise performance in parametric amplifiers through cryogenic techniques and thermoelectric cooling. He is presently working on the noise performance figures of varactor diodes, determined independently of the system in which the diode is used.

Roy E. Elicker, B.S., 1950, and M.S., 1951, Michigan State University; Bell Telephone Laboratories, 1951—. He was first engaged in studies of low-temperature extrusion of aluminum as a sheath for cable. He then worked on development of a cooling system for an airborne bombing and radar system, after which he was concerned with the design and development of forward-scatter tropospheric antennas for early-

warning systems. He is currently engaged in development of communications structures and equipment resistant to nuclear blast effects. Member, Pi Mu Epsilon, Pi Tau Sigma, and Phi Lambda Tau.

RUDOLF S. ENGELBRECHT, B.S.E.E., 1951, and M.E.E., 1953, Georgia Institute of Technology; Bell Telephone Laboratories, 1953—. He was first engaged in the design of exploratory low-noise microwave receivers and parametric amplifiers for military projects. He presently supervises a group concerned with parametric device studies. Member, IEEE, Tau Beta Pi, and Eta Kappa Nu.

DAVID FELDMAN, B.S.E.E., 1947, M.S.E.E., 1949, Newark College of Engineering; Assistant Professor of Electrical Engineering, 1949–1954, Cooper Union School of Engineering; Bell Telephone Laboratories, 1956—. He was first engaged in the design of magnetic amplifiers and transistorized regulator circuits for military systems and later supervised activities in the field of energy conversion. He was responsible for the initial design of the Telstar spacecraft power supply and for development of the nickel-cadmium storage battery. Currently he is Head, Transmission Component Department, responsible for the design and development of reliable passive components for satellite and submarine cable systems. Member, A.A.S.E. and IEEE.

J. D. GABBE, B.A., 1950, New York University; M.S., 1951, University of Illinois; Ph.D, 1957, New York University; Bell Telephone Laboratories, 1956—. Mr. Gabbe was first associated with video telephone studies. At present, he is engaged in research on the earth's radiation belts.

ADOLF J. GIGER, Diploma in Electrical Engineering, 1950, and Doctor of Electrical Engineering, 1956, Swiss Federal Institute of Technology; Bell Telephone Laboratories, 1956—. Mr. Giger heads a group working on development of ground receivers for satellite communications systems. His earlier work was in development of circuits for the TH microwave transmission system. Senior member, IEEE.

JOHN A. GITHENS, B.S.E.E., 1951, Drexel Institute of Technology; Bell Telephone Laboratories, 1951—. He has been engaged primarily in computer research, including design of solid-state circuits, computer systems, and logical design. He took part in the design and develop-

ment of Tradic and Leprechaun, early transistorized computers. He later supervised logical design of the data conversion unit used for antenna steering on Project Echo. On the Telstar project, he was responsible for the digital control portion of the antenna pointing system. Member IEEE, Eta Kappa Nu, Tau Beta Pi, and Phi Kappa Phi.

HERMANN K. GUMMEL, Dip. Phys., 1952, Philipps University (Germany); M.S., 1952, and Ph.D., 1957, Syracuse University; Bell Telephone Laboratories, 1956—. His work has been in research and development of semiconductor devices. Member, American Physical Society and Sigma Xi.

EDWIN G. HALLINE, B.S.E.E., 1953, Bucknell University; Bell Telephone Laboratories, 1953—. He has primarily been concerned with computer programming for military research and development projects, including work with the Leprechaun computer for TRADIC and work on Project Mercury. He supervised the computer programming group on the Telstar project and is presently working on the Apollo project for Bellcomm, Inc. Member, IEEE and Tau Beta Pi.

D. C. HANSON, B.S. in E.E., 1959, University of Wisconsin; M.S. in E.E., 1961, New York University; Bell Telephone Laboratories, 1959—. He has been engaged in military system analysis, transistor circuit design for a Vocoder, the design and analysis of varactor diode amplifiers for the Telstar ground station receiver, the TD-3 radio relay system, and a parametric amplifier operating at liquid helium temperature. Member, Pi Kappa Delta, Tau Beta Pi, Eta Kappa Nu, and IEEE.

EARL T. HARKLESS, M.S., 1949, Case Institute of Technology; Bell Telephone Laboratories, 1949—. He has been engaged in the development of transmission systems, including the TH and TJ microwave radio relay systems, and the L3 coaxial cable system. He has worked on the exploratory development of millimeter-wave networks. On Project Telstar, he contributed to the antenna system design. Member, IEEE, Sigma Xi, and Tau Beta Pi.

RICHARD W. HATCH, B.S. in E.E., 1952, Northeastern University; M.S., 1958, Stevens Institute of Technology; Bell Telephone Laboratories, 1952—. For several years he worked on design of FM terminals for the TH microwave system. In 1961–62 he supervised a group working on systems analysis for a satellite communications system. Presently he is

Head, Transmission Studies Department, concerned with studies of objectives and maintenance of facilities for long-distance telephone transmission. Member, IEEE, Eta Kappa Nu, and Tau Beta Pi.

PAUL T. HAURY, B.E., 1941, Vanderbilt University; Bell Telephone Laboratories, 1942—. His first assignment was with the trial installation group preparing models of radar test equipment. Later he designed airborne and portable radar equipment, and after the war turned to equipment engineering related to carrier telephone systems. He worked on submarine cable systems for military communications from 1951 to 1956, and in 1957 he became supervisor of a group engaged in design of TH microwave equipment. Since early 1961 he has supervised mechanical design and construction work on electronic assemblies for satellite repeaters.

GEORGE D. HELM, B.S.E.E., 1947, Rensselaer Polytechnic Institute; M.S., 1955, Northeastern University; Bell Telephone Laboratories, 1956—. He first worked on long-range search radar, automatic data processing, and missile integration in connection with the SAGE system. More recently, he has worked on high-power microwave amplifiers for Telstar and other projects. Member, IEEE and Sigma Xi.

EDWARD F. HIGGINS, JR., B.S.E.E., 1961, Newark College of Engineering; Bell Telephone Laboratories, 1953—. He was first engaged in test and evaluation of missile ground guidance equipment and later worked on the development and evaluation of guided-missile systems. On the Telstar project, he was involved with system performance of the precision tracker receiver. At present he is concerned with the development of radio guidance systems.

J. NED HINES, B.S.E.E., 1943, University of Connecticut; M.Sc., 1949, Ohio State University; Bell Telephone Laboratories, 1958—. His first assignment was work on the design, construction and testing of an electronically scanned array. On the Telstar project he worked on the autotrack system and on measurements of the horn-reflector antennas at Andover and Pleumeur-Bodou. He is presently concerned with the design of a low-noise antenna for satellite communications systems. Member, IEEE and Sigma Xi.

WILLIAM C. HITTINGER, B.S. in Metallurgical Engineering, 1944, Lehigh University; Western Electric Co., 1946–52; National Union

Radio Corp., 1952–54; Bell Telephone Laboratories, 1954—. While with the Western Electric Co., Mr. Hittinger was concerned with the specification, testing and application of electron tube and semiconductor materials. After two years as Production Manager with the National Union Radio Corp., he joined Bell Laboratories, where he was initially engaged in exploratory and final development of semiconductor devices. He was appointed Director of Development at the Allentown, Pa., Laboratory in 1960, and Executive Director, Semiconductor Device and Electron Tube Division in 1962. Member, IEEE, Amer. Inst. of Mining, Metallurgical and Petroleum Engineers, Omicron Delta Kappa.

DANIEL F. HOTH, B.S. in M.E., 1935, Stevens Institute of Technology; Bell Telephone Laboratories, 1936—. Mr. Hoth was first concerned with studies of local plant transmission; he later engaged in the study and planning of development projects for wire and radio systems, engineering of initial Distant Early Warning (DEW) Line installations, and long-range planning studies for transmission systems. As Director, Transmission Studies Center, his responsibilities include engineering studies of satellite communication systems. Senior member, IEEE; member, Sigma Phi Epsilon.

PETER HRYCAK, B.S., 1954, M.S., 1955, and Ph.D., 1960, University of Minnesota; Instructor, Mechanical Engineering Dept. of University of Minnesota, 1955–60; Bell Telephone Laboratories, 1960—. He has worked on low-temperature refrigeration problems, thermal design and thermal testing of the Telstar satellite. Member, American Institute of Aeronautics and Astronautics.

P. T. HUTCHISON, B.S., 1944, Mississippi State University; M.S., 1947, California Institute of Technology; Ph.D., 1960, Georgia Institute of Technology; Bell Telephone Laboratories, 1960—. Mr. Hutchison was first engaged in development work on microwave reflectometers used in TH radio test equipment. He has done development work on the microwave portion of the 4-gc ground receiver used in the Telstar experiment. Later he was responsible for electrical aspects of the microwave repeater in the Telstar satellite. Currently, he is responsible for development work on microwave antennas and microwave circuitry to be used in future communications satellites. Member, IEEE and Sigma Xi.

MORIMI IWAMA, B.S., 1954, M.S., 1955, and Ph.D., 1960, University

of California; Bell Telephone Laboratories, 1961—. He has been engaged in the design of automatic control systems for satellite communication systems and was responsible for the design of the antenna servo for the Telstar project. Member IEEE, Tau Beta Pi and Sigma Xi.

WILLIAM C. JAKES, JR., B.S. in E.E., 1944; M.S. in E.E., 1947; Ph.D., 1949, Northwestern University; Bell Telephone Laboratories, 1949—. Mr. Jakes has been engaged in research in microwave radio antennas and microwave propagation. He was project engineer in charge of the Bell Laboratories team participating in the Project Echo passive satellite communication tests. During the Telstar system tests he has been test conductor at the Holmdel, N.J., satellite communication station. He is presently head of the Mobile Radio Research Department. Member, Eta Kappa Nu, Pi Mu Epsilon, and Sigma Xi; Fellow, IEEE.

GENE C. JONASSON, B.S.E.E., 1961, University of Washington; Western Electric Co., 1961—. He has been engaged in the development of environmental test specifications and in the environmental testing and evaluation of the Telstar satellite. He has also analyzed data received from the Telstar satellite and evaluated its performance in space. Member, IEEE.

H. P. KELLY, B.S.E.E., 1937, M.S.E.E., 1938, Virginia Polytechnic Institute; Bell Telephone Laboratories, 1943—. Mr. Kelly was first engaged in the design and development of military radio equipment. Later he was responsible for the design of transmission test equipment for telephone carrier systems and the development of video and microwave radio systems. At present he is Head of the Ground Station Design Department, responsible for planning, design, and coordination of construction of the satellite ground station near Andover, Maine. Member, IEEE, Tau Beta Pi and Phi Kappa Phi.

W. J. KINDERMANN, A.B., 1933, Columbia College; B.S., 1934, and M.E., 1935, Columbia University School of Engineering; New York Telephone Co., 1935–1941; Bell Telephone Laboratories, 1941—. He was first responsible for the design and construction of precision potentiometers employed in analog computers for missile guidance systems and flight instrumentation equipment. He later supervised work on data take-off devices for the Command Guidance system and Project Echo antennas. On the Telstar project, he performed liaison work with contractors on horn-reflector antenna mechanical design and supervised

work on data take-off devices, drives and electromechanical equipment for both the Andover and Pleumeur-Bodou antennas.

JOHN P. KINZER, M.E., 1925, Stevens Institute of Technology; B.C.E., 1933, Polytechnic Institute of Brooklyn; Bell Telephone Laboratories, 1925—. Except for an initial two years spent on loudspeakers for the first sound movies, and the four war years on radar test sets, he has been concerned with long-haul transmission systems. His work has included the development of two-wire and four-wire voice and program repeaters and the negative-feedback repeater used in cable carrier systems. Following the war, he was engaged in systems studies, first on the L1 and L3 coaxial systems and, more recently, on the TH microwave radio relay system. Since early 1961, he has been participating in the planning and analysis of the communications tests for the Telstar system. Senior member, IEEE.

A. ROBERT KOLDING, B.S.E.E., 1941, Polytechnic Institute of Brooklyn; Bell Telephone Laboratories, 1930—. Mr. Kolding first worked on the exploratory development of cable transmission of television, which later evolved into television transmission over the L1 system. During World War II he worked on the development and field evaluation of airborne radar bombing systems. He returned to television systems after the war, taking part in the development of the L3 coaxial system, the A2A local television system, and terminals for the TH microwave system. He supervised a development group on the TASI system. At present, he is supervisor of the Telstar Launch Operations Group. Member, IEEE, Eta Kappa Nu.

RUDOLF KOMPFNER, Diplom. Ingenieur, Technische Hochschule, Vienna, 1933; Ph.D., Oxford, 1951; Bell Telephone Laboratories, 1951—. Dr. Kompfner invented the traveling-wave tube while at Birmingham University during World War II. At Bell Laboratories, he has specialized in microwave electronics, work which has more recently been enlarged to include research on quantum electronics and satellite communications. Director of Electronics Research, 1955; Director of Electronics and Radio Research, 1957; Associate Executive Director, Research, Communications Systems Research Division, 1962. Fellow I.R.E., 1950; Duddell Medal, Physical Society, 1955; A.I.E.E. David Sarnoff Award, 1960; Franklin Institute Stuart Ballentine medal, 1960.

D. E. KOONTZ, B.S. in Chemistry, 1945, Youngstown University;

M.S. in Chemistry, 1948, Ph.D. in Chemistry, 1951, University of Pittsburgh; Bell Telephone Laboratories, 1952—. Mr. Koontz was first engaged in studies of electron tube materials and processing. For the Telstar project, he was responsible for the selection and application of materials for the space vehicle and their evaluation in simulated space environments. He is presently Head of the Electron Device Technology Department, responsible for chemicals and materials associated with the development of electron devices. Member, American Chemical Society, Sigma Xi and Phi Lambda Upsilon; Chairman of Committee F1-X of the American Society for Testing Materials.

Ronald W. Kordos, B.E.E., 1957, University of Detroit; M.S.E.E., 1959, Northeastern University; Bell Telephone Laboratories, 1957—. He has engaged in the design of microwave ferrite devices, including field-displacement and resonance isolators for several microwave radio relay systems. At present he is working on circulator development for a military radar system. Member, IEEE, Tau Beta Pi, and Eta Kappa Nu.

Joseph P. Laico, M.E., 1933, Brooklyn Polytechnic Institute; Bell Telephone Laboratories, 1929—. He has been engaged in the mechanical design and development of electron tubes from early amplifiers through magnetrons, klystrons, and traveling-wave tubes used in radar, coaxial cable, radio relay, missile guidance, and the Telstar satellite. He is presently engaged in the design and development of high-power traveling-wave tubes for use in a radar system.

Tingye Li, B.Sc., 1953, University of Witwatersrand (South Africa); M.S., 1955, and Ph.D., 1958, Northwestern University: Bell Telephone Laboratories, 1957—. He has been engaged in studies of microwave antennas and microwave propagation. Recently he has been primarily concerned with work on optical masers. Member, IEEE, Eta Kappa Nu, and Sigma Xi.

Robert Lowell, B.S.E.E., 1948, New York University; M.S.E.E., 1951, University of Maryland; M.S. (Applied Math), 1959, Stevens Institute of Technology; Bell Telephone Laboratories, 1953—. Mr. Lowell was first engaged in military systems studies. At present, he supervises a group in the military antenna and microwave research department. Member, IEEE.

John C. Lozier, A.B., 1934, Columbia University; Bell Telephone

Laboratories, 1936—. He was first concerned with the theoretical aspects of toll transmission systems, feedback amplifiers and control systems. On the Telstar project he headed a group which designed and developed the control system for the antennas. He presently supervises research and exploratory development work on military guidance and control systems. Senior member, IEEE.

A. A. LUNDSTROM, B.S.E.E., 1928, Oregon State University; Pacific Telephone and Telegraph Co., 1928–29; Oregon State University faculty, 1929–30; Bell Telephone Laboratories, 1930—. He first engaged in research on telephone transmission and signaling systems, including the first nationwide dialing system. He has since done research and development on radar, computer, and control systems. On the Telstar project he headed a group responsible for research and development work on the antenna direction systems. He is presently Head, Digital Technique Research, and is concerned with guidance and control system analyses and cryogenic digital techniques. Member, IEEE, Eta Kappa Nu, Tau Beta Pi, and Phi Kappa Phi.

CHARLES MAGGS, B.S. in M.E., 1941, New York University; Bell Telephone Laboratories, 1928—. He has chiefly been engaged in the design of electron tubes, including early magnetrons and klystrons and the close-spaced triode. More recently he has worked on magnetrons and supervised a group working on beam-deflection tubes. He headed a group which worked on the frame and solar power plant for the Telstar satellite and presently supervises a mechanical engineering group developing millimeter-wave power amplifiers and microwave printed circuits.

HENRY MANN, B.A., 1950, Brooklyn College; M.S. in E.E., 1955, Columbia University; Bell Telephone Laboratories, 1954—. His work has included the design of the synchronizing circuits, the demultiplex gate, and portions of the encoder for the experimental pulse code modulation system. He also engaged in the development of a system for the transmission of two PCM groups over short-haul microwave carrier circuits. He was responsible for the design and production of a command decoder for an experimental active satellite communications system. At the present time he supervises a group responsible for the design of an improved single-frequency signaling unit. Member, IEEE and Pi Mu Epsilon.

H. I. MAUNSELL, B.S., 1950, University of the Witwatersrand; Bell

Telephone Laboratories, 1957—. For several years he worked on the terminal equipment, test sets and protection switching circuits for the TH microwave radio relay system. In late 1960, he became concerned with communication circuits for the Telstar satellite, and he is presently responsible for transmitter design for the satellite system ground station. Member, IEEE.

JOHN S. MAYO, B.S. in E.E., 1952, M.S. in E.E., 1953, Ph.D. in E.E., 1955, North Carolina State College; Bell Telephone Laboratories, 1955—. He was first engaged in computer research, including studies relating to the use of digital computers for measurement and automatic tracking of pulsed radar range information, and in military weapons control systems. His recent work has involved the development of line repeaters for an exchange carrier PCM system, and high-speed PCM terminals for an experimental transmission system. He has been in charge of the PCM terminal department since December, 1960. Member, IEEE and Sigma XI.

ROBERT J. MCCUNE, B.S.E., 1948, U.S. Coast Guard Academy; Bell Telephone Laboratories, 1954—. He was first engaged in military systems engineering, concerned with operational studies and planning for SAGE and related air defense systems. In 1961–62 he worked on operational planning for the acquisition, tracking, and command complex of the Telstar ground station, and supervised a group responsible for design and operation of the control console, including provision of operations procedures and training of the operations team. He has since been engaged in special operations studies for Bellcomm, Inc., of communication and tracking system requirements for the Apollo project. Member, IEEE.

B. A. MCLEOD, B.S.E.E., 1954, Northeastern University; Bell Telephone Laboratories, 1954—. He first worked on the development of transmission systems, including test set development for the TH microwave radio relay system. He engaged in early studies for the TASI system and worked on TASI development until 1961, when he became associated with the launch operations group for the Telstar project. Member Tau Beta Pi, Eta Kappa Nu.

L. V. MEDFORD, Pell Telephone Laboratories, 1955—. At Pell Laboratories Mr. Medford has participated in the study of adsorption of gases on metal and semiconductor surfaces by use of the photoelectric effect.

Early in 1961 he began development of space radiation instrumentation for the Telstar project, followed by a similar and concurrent undertaking for the NASA Project Relay. Later he participated in the development of radiation instrumentation for the Explorer XV satellite and was active in the launch operations for Project Relay. At present, Mr. Medford is studying development problems related to future space radiation experiments.

G. L. MILLER, B.Sc. (Physics), 1949, M.Sc. (Mathematics) 1952 and Ph.D. (Physics), 1957, University of London; Brookhaven National Laboratories, 1957—. Since his association with Brookhaven Laboratories, he has been engaged in the study and development of nuclear instrumentation.

LOUIS F. MOOSE, B.S.E.E., 1940, University of California; Bell Telephone Laboratories, 1945—. After graduate study at the University of California and Massachusetts Institute of Technology, Mr. Moose joined the Laboratories and worked on microwave tubes for radio relay and radar applications, and semiconductor diodes for microwave usages. Currently, he is engaged in the final design of alloy transistors and applied mechanics at the Allentown Laboratory. Member, IEEE, Tau Beta Pi, Sigma Xi and Eta Kappa Nu.

J. L. MURRAY, B.E.E., 1955, Rensselaer Polytechnic Institute; Bell Telephone Laboratories, 1955—. He has specialized in missile electronics, including design of pulse logic circuitry, and has designed experiments to characterize the system aspects of several radars for a guided missile system. On the Telstar project, he supervised a group responsible for electronic design of the precision tracker. Since then, he has supervised a group responsible for the electronic design of a solid-state missile guidance radar transmitter and receiver. He presently supervises a group responsible for electronic design of the Nike Sprint missile-borne guidance transmitter and receiver. Member, IEEE.

R. J. NIELSEN, Bell Telephone Laboratories, 1941—. At Bell Telephone Laboratories, he was first engaged in design drafting of automatic central office equipment. He has also been concerned with the study of metal-ceramic sealing and other special problems in connection with the mechanical design of electron tubes. During this time he also studied at the University of Idaho and Fairleigh-Dickinson University. From 1960 to the present, Mr. Nielsen has worked on the Telstar project and

is now engaged in the mechanical design of special microwave oscillator tubes.

J. A. Norton, B.A.Sc., 1957, University of Toronto; A.M., 1959, Princeton University; Bell Telephone Laboratories, 1960—. He has been engaged in the design of antenna control systems on the Echo and Telstar projects. He is also engaged in research in the stochastic aspects of nonlinear computer-controlled systems. Member, IEEE and Sigma Xi.

Edward G. Olsen, Bell Telephone Laboratories, 1927—. He has specialized in the mechanical design and development of electron devices, including devices used in early radio transmission, special research structures, and traveling-wave tube amplifiers for microwave radio relay and guided-missile systems. On the Telstar project he was concerned with the mechanical design and development of the traveling-wave tube amplifier for the spacecraft repeater.

E. F. O'Neill, B.S. and M.S. in Electrical Engineering, 1940 and 1941, Columbia University; Bell Telephone Laboratories, 1941—. Mr. O'Neill's early work was in the development of radar transmitters and of amplifiers and regulators for cable and radio-relay systems. Beginning in 1956 he headed a group responsible for the development of the Time Assignment Speech Interpolation (TASI) system terminals. Mr. O'Neill is Director, Satellite Communications Laboratory at Bell Laboratories, and is Project Manager for the Telstar experimental system. Member, Tau Beta Pi and Sigma Xi.

S. Pardee, Jr., A.B., 1939, Harvard University; M.S. in E.E., 1960, Stevens Institute of Technology; Bell Telephone Laboratories, 1946—. He has been engaged in the design and development of military electronic equipment, fire control radar, and missile guidance systems. At present, he is working on a military communications system. Member, IEEE.

D. Stewart Peck, M.S. in E.E., 1940, University of Michigan; Bell Telephone Laboratories 1947—. Mr. Peck has been concerned in the design for production of gas-filled electron tubes such as rectifiers, thyratrons and cold-cathode tubes. More recently, he has been in charge of work on reliability studies, applications engineering, and specifications for electron devices. On the Telstar project Mr. Peck's department has been generally responsible for the specification, aging and selection

programs for semiconductor components used in the satellite. Member, IEEE, American Standards Association, Tau Beta Pi, Eta Kappa Nu, Sigma Xi and Phi Kappa Phi.

T. R. PETERS, B.S.E.E., 1955, Virginia Military Institute; Bell Telephone Laboratories, 1955—. He has participated in the systems and logic design of a military special-purpose digital computer, studies of logic connectives for integrated circuits, and cryogenic logic studies. On the Telstar project he was involved in the system and logic design for the antenna pointing system and later was concerned with development, installation and maintenance of the digital equipment at Andover, Maine. He is currently working on studies for a military digital computer.

E. JARED REID, B.S., 1956, Trinity College; B.S.E.E., 1957, Rensselaer Polytechnic Institute; M.E.E., 1959, New York University; Bell Telephone Laboratories, 1957—. He was first engaged in development work on the TASI system, and took part in final field tests of TASI installations in the U.S. and overseas. He subsequently worked on the development of the Telstar satellite electronics system.

WILLIAM C. RIDGWAY, III, B.S.E., 1957, Princeton University; M.E.E., 1959, New York University; Ph.D., 1962, Stanford University; Bell Telephone Laboratories, 1957—. He has worked chiefly in the field of data processing, first for the Nike Zeus anti-missile system and more recently for the Telstar project. Member, A.C.M., IEEE, Phi Beta Kappa, Sigma Xi.

W. ROSENZWEIG, B.S., 1950, Rutgers University; M.S., 1952, University of Rochester; Ph.D., 1960, Columbia University. Brookhaven National Laboratory, 1951–1953; Radiological Research Laboratory, Columbia University, 1953–1960; Bell Telephone Laboratories, 1960—. At Bell Laboratories, Mr. Rosenzweig has been mainly engaged in studies of radiation damage to semiconductors. Member, American Physical Society, Radiation Research Society, Sigma Xi and Phi Beta Kappa.

A. THOMAS ROSS, B.S.E.E., 1939, Lafayette College; Bell Telephone Laboratories, 1946—. Mr. Ross was first engaged in the field of high-altitude bombing systems. Subsequently he worked on the development and testing of a high-powered, tunable magnetron. Prior to his work on

the Telstar project, he was concerned with the development of tubes for broadband submarine telephone cable systems. He is currently engaged in the development of parametric amplifiers. Senior member, IEEE.

R. E. SAGEMAN, B.E.E., 1944, and M.E.E., 1948, Renssalaer Polytechnic Institute; Long Lines Department of the American Telephone and Telegraph Co., 1948—. He has engaged in plant engineering for the overseas radiotelephone division and statistical analyses for the accounting and traffic operations departments. He has been Director of Electronic Data Processing Activities for the Long Lines Department and Satellite Projects Engineer, responsible for coordinating the activities of the Long Lines Department in the Telstar and Relay projects. He is presently Service Engineer, Southeastern Area, Long Lines. Member, Eta Kappa Nu, Tau Beta Pi, and Sigma Xi.

FRED J. SCHAEFER, B.E.E., 1950, Syracuse University; Bell Telephone Laboratories, 1951—. His early assignments included circuit design and field evaluation of a target designation system; operations and system planning for the DEW Line project, including evaluation of the VHF scatter system. He later supervised groups working on circuit design and performance analysis of missile systems, and is presently supervisor of a group developing missile guidance radar. He supervised a group responsible for the design of the Telstar precision tracker. Member, IEEE, Tau Beta Pi, and Eta Kappa Nu.

R. H. SHENNUM, B.S. in E.E., 1944, and M.S. in E.E., 1948, Montana State College; Ph.D., 1954, California Institute of Technology; Bell Telephone Laboratories, 1954—. He first worked on the design of microwave parts for the TJ microwave system. Later, he was responsible for companding, signaling, and voice-frequency development and field experiments for the T1 carrier system (PCM). As Head, Satellite Design Department, he was responsible for the development of the electronic circuits for the Telstar satellite. Mr. Shennum was also responsible for the assembly of the spacecraft and final testing at the Hillside, N. J., laboratory. Member, IEEE, Sigma Xi, Tau Beta Pi, and Phi Kappa Phi.

JOHN T. SIBILIA, B.S. in Physics, 1955, Rutgers University; M.A., 1957, and Ph.D., 1962, Princeton University; Bell Telephone Laboratories, 1960—. He has been engaged in maser development, including studies of the use of rutile for a 10-kmc maser. He presently supervises

a group responsible for the development of masers for the Telstar project and military projects.

D. H. SMITH, B.S.E.E., 1944, University of Minnesota; M.S. in Industrial Management, 1961, Stevens Institute of Technology; Bell Telephone Laboratories, 1947—. He has been engaged in development work on voltage regulating apparatus, including rectifiers and regulated exciters, and advance engineering and development of power systems, including long-range planning. From 1952 to 1961 he supervised a group concerned with power systems engineering. In 1961, as Head, Reserve Power Systems Department, he became responsible for development work on power systems, which included the power generating and reserve power systems at the Andover earth station, and for development of the timing mechanism to shut off the beacon transmitter in the Telstar satellite. Member, IEEE and its Subcommittee on Definitions, Magnetic Amplifier Committee; Chairman of American Standards Association Sectional Committee C85 on terminology for automatic control.

KENNETH D. SMITH, M.A. in Physics, 1930, Dartmouth College; Bell Telephone Laboratories, 1930—. He has worked on high-frequency test equipment, coaxial cable system development, proximity fuses, radar bombing equipment, and microwave radio relay systems. Since 1951, he has been engaged in semiconductor device development, including high-frequency transistors, power rectifiers, voltage limiters, and the Bell Solar Battery. He currently supervises a group concerned with high-frequency transistor development. Senior member, IEEE.

FRIEDOLF M. SMITS, Dipl. Phys., 1950, Dr. rer. nat., 1950, University of Freiburg, Germany; research associate, Physikalisches Institut, University of Freiburg, 1950–54; Bell Telephone Laboratories, 1954–62. Mr. Smits went to the Sandia Corporation in May 1962. His work at Bell Telephone Laboratories included studies of solid-state diffusion in germanium and silicon, device feasibility, and process studies, as well as the development of UHF semiconductor devices. He supervised a group that conducted radiation damage studies on components, particularly solar cells, used in the Telstar satellite. Member of the American Physical Society and the German Physical Society.

R. V. SPERRY, B.S.E.E., 1949, M.S.E.E., 1951, West Virginia University; Bell Telephone Laboratories, 1952—. Mr. Sperry was first engaged in the development of transmission networks for coaxial, radio

and military systems. He has worked on repeater development for an exploratory waveguide transmission system and on the antennas and several circuits used on the Telstar satellite. At present, Mr. Sperry supervises a group working on the development of repeaters for a high-speed PCM coaxial cable system. Member, Eta Kappa Nu, Pi Tau Sigma, and Tau Beta Pi.

JOHN W. STAFFORD, B.S.A.E., 1954, Massachusetts Institute of Technology; M.S.A.M.; 1959, Brooklyn Polytechnic Institute; Bell Telephone Laboratories, 1961—. Mr. Stafford participated in the mechanical design and testing of the Telstar satellite. He is now engaged in development studies of an orientation system for communications satellites. Member of American Institute of Aeronautics and Astronautics.

ALBERT L. STILLWELL, B.A., 1925, M.A., 1928, Gonville and Caius College, Cambridge, England; Bell Telephone Laboratories, 1927—. His early assignments included the design of filters, special networks, and the first three-stage cathode feedback amplifier for coaxial transmission. After wartime activity in the development of proximity fuses and radar, he worked on television transmission apparatus. Later he developed special circuits for the research department and is presently in a group concerned with the design of solid-state microwave circuits. Senior member, IEEE.

KURT M. STRINY, B.S.M.E., 1953, and M.S., 1961, Newark College of Engineering; Bell Telephone Laboratories, 1956—. He has been engaged in the mechanical design and development of electron tubes such as the coaxial magnetron and low-noise traveling-wave tubes. He is currently working on high-power traveling-wave tubes used for the Telstar ground transmitter and other applications. Member A.S.M.E.

R. A. SWIFT, B.S. in E.E., 1943, Union College; Bell Telephone Laboratories, 1946—. He has been engaged in mechanical and equipment design aspects of system design, and was responsible for mechanical design and evaluation of missile-borne guidance equipment for the Titan and Thor-Delta Missiles. On the Telstar project he was responsible for the formation and conduct of the design, qualification, and acceptance test program for the satellite. Member, IEEE.

WILLIAM J. TABOR, B.S. in Chemistry, 1953, Renssalaer Polytechnic Institute; A.M. (Physics) and Ph.D. (Chemical Physics), 1954 and 1957, Harvard University; Bell Telephone Laboratories, 1959—. Since

coming to the Laboratories, he has engaged in research and development work on microwave masers, including the maser for the Telstar ground station receiver.

E. W. THOMAS, Bell Telephone Laboratories, 1961—. He has contributed to the design and development of radiation experiments for the Telstar experimental communications satellite and other satellite programs. Following the Telstar satellite launch, he assisted in interpretation of the radiation data. He is currently conducting experiments to aid in more precise understanding of the Telstar results as well as results of other satellite radiation experiments.

LEROY C. TILLOTSON, B.S.E.E., 1938, University of Idaho; M.S.E.E., 1940, University of Missouri; Bell Telephone Laboratories, 1941—. Mr. Tillotson's early work included design of filters and networks; he has since been concerned with microwave radio relay systems. From June, 1958, to July, 1959, he served as a member of technical staff of the Advanced Research Projects Agency division of the Institute for Defense Analyses. As Assistant Director, Radio and Electronics Research, and Head, Radio Systems Research Department, he has been active in planning the communications aspects of Project Telstar. Senior member, IEEE; member, Sigma Xi.

DAVID E. TRUCKSESS, B.S.E.E., 1926, Pennsylvania State University; Bell Telephone Laboratories, 1926—. He has worked in the field of regulation for motor generators and rectifiers. During World War II, he supervised a group which designed power supplies for military systems. He is presently Head, Power Conversion Department, and is concerned with the development of power facilities for submarine cable systems, microwave communications systems, PBX equipment, and military sonar systems. Fellow and Deputy Director of Technical Operations, IEEE; member, N.S.P.E.

RICHARD H. TURRIN, B.S.E.E., 1956, Newark College of Engineering; M.S.E.E., 1960, New York University; Bell Telephone Laboratories, 1956—. He has been chiefly concerned with propagation and antenna work at micro and millimeter wavelengths. He participated in the design of the Telstar ground-station antennas. Member, IEEE, Eta Kappa Nu and Tau Beta Pi.

MICHIYUKI UENOHARA, B.E., 1949, Nihon University (Japan); M.S., 1953, and Ph.D., 1956, Ohio State University; D.E., Tohoku University

(Japan), 1958; Bell Telephone Laboratories, 1957—. He has been engaged in exploratory studies of microwave variable reactance amplifiers, Esaki diode amplifiers, and related devices. He was also engaged in microwave tube research at Nihon University from 1949 to 1952, and taught there in 1957. Member, American Physical Society, IEEE, Institute of Electrical Communication Engineers (Japan), Eta Kappa Nu, Pi Mu Epsilon, Sigma Xi, and R.E.S.A.

Burton A. Unger, B.S.M.E., 1954, Purdue University; M.S.M.E., 1960, Newark College of Engineering; Bell Telephone Laboratories, 1960—. Mr. Unger participated in the thermal test program of the Telstar satellite. He is now engaged in development studies of orientation systems for communication satellites.

H. Nelson Upthegrove, B.S., 1945, U.S. Naval Academy; S.B., 1948, Massachusetts Institute of Technology; Ph.D., 1954, California Institute of Technology; Bell Telephone Laboratories, 1953—. Mr. Upthegrove served in the U.S. Navy, 1945–49, and was a Teaching Fellow in engineering at Cal. Tech., 1949–53. At the Laboratories, he was first engaged in submarine cable development and later in the planning and acquisition of new cable ships and equipment. On the Telstar project, he was Head of the Satellite Launch Operations Department, responsible for integration of the satellite and the Delta launch vehicle. He is presently Head of the Missile and Tracking Department. Member, IEEE, Sigma Xi, and Tau Beta Pi.

Paul W. Ussery, B.S. in Physics, 1951, Upsala College; M.S.E.E., 1956, Newark College of Engineering; Bell Telephone Laboratories, 1957—. He has engaged in the development of regulated power supplies for an experimental electronic switching system, solid-state inverters and regulators, microwave radio relay systems and missile guidance equipment. He worked on the design of the Telstar spacecraft power supply system and is presently engaged in development work on thermoelectric regulators and power supplies for radio relay systems. Member, IEEE and Sigma Pi Sigma.

L. J. Varnerin, S.B., 1947, Ph.D., 1949, Massachusetts Institute of Technology; Bell Telephone Laboratories, 1957—. He has been engaged in the development of components and solid-state devices, and was first concerned with the development of very high frequency germanium transistors, field-effect devices, thin film components and circuits. He is

presently Head, Solid-State Microwave Device Department, concerned with the development of microwave ferrite, magnetoelastic and optical devices. Fellow, American Physical Society; senior member, IEEE.

EDWARD J. WALSH, Bell Telephone Laboratories, 1928—. He has chiefly been engaged in the mechanical design of electron tube structures and enclosures, including the design during World War II of proximity fuse tubes and the thermally tuned klystron, and later of the frame-grid tube used in microwave radio relay systems. More recently he has supervised a group responsible for mechanical design of electron tubes for a submarine cable system; he is presently in charge of a group working on structures for the gaseous optical maser, photomultipliers, and other electron devices.

IRWIN WELBER, B.S.E.E., 1948, Union College; M.E.E., 1950, Rensselaer Polytechnic Institute; Bell Telephone Laboratories, 1950—. Mr. Welber has worked on the design and analysis of long-haul microwave radio relay circuits and the Time Assignment Speech Interpolation (TASI) switching system. As Head, Ground Station Design Department, he has been responsible for over-all systems analysis, ground communications equipment and technical planning with foreign participants for the Telstar project. Member, IEEE, and Sigma Xi.

PAUL R. WICKLIFFE, JR., B.S.E.E., 1949, Purdue University; S.M., 1951, Massachusetts Institute of Technology; Bell Telephone Laboratories, 1951—. He was first concerned with development of antennas and traveling-wave tube amplifiers for the TH microwave system. He later worked on a narrow-band radio system for order wire and alarms. In 1961 he became supervisor of a group engaged in the design of the ground transmitter for the Telstar project. Member, IEEE, Eta Kappa Nu, and Tau Beta Pi.

FRANCIS J. WITT, B.S.E.E., 1953, M.S.E.E., 1955, Johns Hopkins University; Bell Telephone Laboratories, 1954–55, 1957—. At Bell Laboratories, he has engaged in active and sampled-data network exploratory research and in solid-state circuit development for short-haul carrier systems. Later he was in charge of a group responsible for the development of some of the solid-state circuits in the Telstar experimental communications satellite. At present he is concerned with the development of digital processing circuitry for a high-speed PCM transmission system. Member, IEEE, Tau Beta Pi and Sigma Xi.

ALBERT M. WITTENBERG, B.S. in Physics, 1949, Union College; Ph.D., 1955, Johns Hopkins University; Bell Telephone Laboratories, 1955—. His early work at the Laboratories concerned the development of gas tube devices for switching applications. He later engaged in studies on photoconductive and electroluminescent materials. At present he is involved in developing techniques for space simulations, and is also concerned with the effects of space environment on the thermal and mechanical properties of satellites and satellite materials. Member, American Physical Society, Sigma Xi and Institute of Environmental Sciences.

K. B. WOODARD, B.S. in M.E., 1943, Georgia Institute of Technology; Bell Telephone Laboratories, 1946—. He has been engaged in the mechanical design and testing of components and structures for guided missile systems, including the antennas for the Nike Zeus system. For the Telstar project, he was responsible for mechanical design of the precision tracker antenna and the large air-supported structures and slip rings for the horn-reflector antenna. Member, A.S.M.E., Pi Tau Sigma, and American Rocket Society.

M. C. WOOLEY, B.S. in E.E., 1929, Ohio Northern University; Bell Telephone Laboratories, 1929—. He has been engaged in the design and development of inductors and capacitors, including capacitors for the Havana-Key West submarine cable. He has worked on fundamental development of capacitor materials and processes and presently supervises a group responsible for development capacitors and resistors for ultra-high reliability applications such as the Telstar experiment. Member, Nu Theta Kappa.

# Index to *Telstar* Issue

## A



## B



## C

## R



## S

## T



## U

## V



## W



## Y